Engineering Doctorate in Non-Destructive Evaluation

Thesis

The Development and Implementation of Advanced Ultrasonic Phased Array Technology

Jonathan Russell

UK Research Centre in NDE, Imperial College, London

Abstract

Ultrasonic inspection is the primary technique for the detection of planar flaws within the nuclear industry. Current inspections are typically limited to the application of rigid wedge, single element transducers to components with regular surface geometry. This thesis addresses some of the limitations of this approach and develops new methods and techniques that are suitable for application in an industrial environment.

Inspection modelling is a cost effective technique for inspection design and qualification; it can be used to aid understanding of the inspection process, and provides valuable insight into inspection data interpretation. In this work semi-analytical and numerical modelling tools have been used to accurately and efficiently simulate the ultrasonic inspection of large complex components.

Modelling tools have also been applied to aid in the design of a membrane coupled conformable phased array device. The membrane coupled array is a low-cost, robust device that uses a conventional phased array coupled to the outer surface of the component under test via a water path encapsulated by low-loss membrane. Early design of this device was performed by Long and Cawley at Imperial College, London. The work reviewed in this thesis discussed the further development of this membrane coupled device and its application for the inspection of a specific target application component.

The target application is a safety critical, thick-walled stainless steel section of pipe-work that contains an austenitic weld. The current inspection of this component is carried out by first removing the component weld cap and then mechanically raster scanning a large number of rigid wedge single element transducers. Weld cap removal is an expensive time consuming task that can lead to excessive wall thinning and the exposure of small surface breaking defects. The motivation for this work is to provide complete inspection of the weld and heat affected zone with the weld cap in place. It is also designed to improve inspection speed and accuracy, and to reduce the amount of user intervention required to complete the inspection in a hostile environment.

Inspection results from the 2nd and 3rd generation membrane coupled device on multiple test-pieces representative of the target application are presented. These results demonstrate that the membrane coupled device can be used to detect defects in locations that cannot be inspected using conventional techniques. The amount of scanning required can be significantly reduced, simplifying the inspection and helping to improve inspection speed by over 60% in comparison to the single element approach.

Acknowledgements

I would like to thank my supervisor, Peter Cawley for his help and guidance. The level of support that he has provided during my studies has been exceptional and I am very grateful.

My thanks also go to others within the Imperial College NDT group, particularly Mike Lowe and Rob Long whose assistance in this project has been invaluable. I am thankful to Daniel Hesse, Mickael Drozdz and Prabhu Rajagopal for introducing me to finite element modelling and their patience in answering my many questions.

I am grateful to Rolls-Royce for supporting this work and providing an environment in which I could learn and develop my knowledge of NDE. I am especially thankful to Noel Habgood, Lionel Reyes and the following members of the NDE research team – Chris Greener, Martin Mienczakowski, Dave Duxbury, Chris Reed and Iain Baillie.

I would also like to acknowledge the assistance that I have received from individuals within the RCNDE. There are too many to name them all but I'd like to thank everyone involved in the provision of the EngD scheme. I am also grateful to my fellow Research Engineers for their support and for making the various training courses so enjoyable.

I thank my friends and family for their encouragement and patience. Particularly, I want to thank Cathy, without whose support and understanding this would not have been possible.

Table of Contents

Figures

Tables

1. Introduction

The Engineering and Physical Sciences Research Council (EPSRC) established the Engineering Doctorate (EngD) scheme in 1992. The Scheme was established to address a belief held by industry, that an alternative research degree to the traditional PhD was required to better prepare researchers for a career in industry. The EngD is a 4 year research degree, which is awarded for industrially relevant research at a level equivalent to a PhD. The research component of the degree is complemented by a number of technical and management courses. The program of training is designed to allow the Research Engineer (RE) to develop the necessary skills to function as an innovative NDE engineer in the future. The UK Research Centre in Non-Destructive Evaluation (RCNDE) was established in 2003 as a focal point for research in Non-Destructive Evaluation (NDE) within the UK. The RCNDE then launched the EngD program in NDE in 2005; I am one of the first cohort of RE's to participate in the programme.

Rolls-Royce is a world-leading supplier of power solutions. The organization is made up of five individual business units, civil aerospace, defence aerospace, marine, energy and nuclear. Rolls-Royce is a strong supporter of the EngD scheme and has provided industrial sponsorship to a large number of EngD students since the inception of the programme. Rolls-Royce is a full industrial member of the RCNDE, and is currently supporting multiple RE's in NDE. My EngD is industrially supported by Rolls-Royce Submarines, which is part of the nuclear business unit. Rolls-Royce Submarines is the delegated UK technical authority (TA) for the Nuclear Steam Raising Plant (NSRP) on all Royal Navy submarines.

My EngD research is part of the Nuclear Propulsion Critical Technology (NPCT) project. This is a major Ministry of Defence (MoD) funded research initiative within Rolls-Royce Submarines to research technologies that are essential to the future needs of the naval submarine fleet. The key aims of the overall research project are to improve safety, reduce costs, and maximise availability of the submarine fleet. In the advanced NDE NPCT project Rolls-Royce are working with three RCNDE member Universities - Imperial College, University of Bristol and University of Strathclyde. The advanced NDE NPCT project develops conformable phased array devices

designed to improve the inspection of the NSRP components with irregular surface geometry. This includes a membrane coupled phased array device and a flexible matrix phased array device. The overall project includes the development of advanced post processing algorithms intended to improve inspection speed, versatility and defect characterisation. Research is also ongoing to develop novel modelling techniques to improve inspection planning, qualification and data interpretation.

As part of the technical authority role Rolls-Royce is responsible for ensuring the safe operation of the NSRP. A major part of this role is the development and deployment of a wide range of NDE based inspections. In-service inspection (ISI) of NSRP components can be particularly challenging. Access constraints present a major difficulty within the submarine environment. Inspections must typically be carried out from the component outer surface only. Also as space on a submarine is very restricted, the area around the component under test during the inspection process is limited. Inspections must be performed in a potentially high radiation area; it is necessary to limit the exposure of personnel to harmful ionising radiation. Therefore automated inspection techniques are developed wherever practically possible and all realistic measures are taken to ensure that radiation dose levels are as low as reasonable practicable (ALARP). The use of automated inspection also helps to ensure that the high integrity testing is performed in as a short time period as possible and that an auditable inspection record can be maintained.

A number of components within the NSRP have a complex geometry which can make inspection even more challenging. Components are designed to fit into a relatively small space, and typically large, regular surfaces are not available as a platform to complete inspection. Many components have some form of irregular surface finish; this can be relatively minor irregularities such slight changes in the surface profile of a forging or more dramatic such as the presence of an undressed weld cap or a change in component cross-section. The conformable phased array technology under development in the advanced NDE NPCT project is specifically designed to address this inspection requirement. The membrane coupled phased array uses a commercial array which is then coupled to the outer surface of the component under test via a water path encapsulated in a low loss rubber membrane. The main focus of my EngD

is the development of a full inspection capability based on this technology and its transfer from academia into Rolls-Royce.

1.1. Role within Rolls-Royce

My role within the advanced NDE NPCT project has evolved during the four years of my EngD degree. The overall aim of my work has been to introduce the membrane coupled phased array inspection capability into Rolls-Royce. However, I have been involved in a range of additional tasks and have also gradually assumed greater responsibility for my own work and that of others. My initial involvement in the project was to complete a range of finite element (FE) modelling tasks; which will be discussed in greater technical detail in chapter 4. Inspection modelling is routinely carried out by engineers within the Rolls-Royce NDE teams. However, previously this has been limited to the use of simple spreadsheet based models and basic commercial NDE simulation packages. The spreadsheet based models are limited in terms of their functionality and cannot be widely used. The commercial packages are suitable for use in many inspection scenarios but can have limited accuracy. FE modelling offers a means to accurately simulate a broader range of inspections than can be achieved with these commercial packages. However, FE modelling is highly computationally intensive and it can be rather complex to accurately generate appropriate models. Prior to the completion of my research these techniques had not been applied to industrially significant inspection problems within Rolls-Royce.

The development of FE modelling techniques and their application within Rolls-Royce was the primary objective of my research over approximately the first year of my EngD. Nearing the end of this period a target application was selected for the membrane coupled phased array; due to security restrictions it is not possible to provide details of this component and its function in the NSRP. In this report the component will be referred to as the target application. Details of the work performed on the initial development of two flat plate, non-welded test-pieces is described in chapter 3. Upgrades made to the membrane device design based on the results of this initial testing are then reviewed in chapter 5. Results obtained using this modified design on two flat plate, welded test-pieces are then discussed in chapter 6. When the target application was selected, the development of the membrane coupled device could become much more focused towards specific Rolls-Royce requirements. The

further development and the transfer of this technology became the primary focus of my research. My role was to design the inspection of the target application; this involved the design of suitable test-pieces and development of a primary detection technique for each of the artificial defects within the test-pieces. I carried out experimental testing on the test-pieces using single element, conventional phased array transducers and the membrane coupled device. I also simulated a subset of these tests using FE modelling the results of which are discussed in chapter 4.

During my doctorate I have gradually taken on greater responsibility for the overall planning and execution of the entire advanced NDE NPCT project. Initially I assumed responsibility for the organisation of quarterly review meetings with the three Universities. At these meetings the university representatives provide a presentation of the work that they have performed during the previous 3 months. I arrange and then chair the meetings; I also produce minutes from the meetings and provide these to all invitees as a permanent record of the discussion. As I took greater responsibility for the project and as the technologies under development became more mature I also introduced an interim meeting with each of the universities. Typically I visit each individual university four times a year; these meetings are held approximately six weeks after each of the main review meetings. The focus of these meetings is to allow me to gain a greater appreciation of the research work taking place and to provide more focussed support to the university based researchers. These meetings have proved to be a useful tool to ensure that the research remains suitably focussed on industrially relevant problems and that specific problems are addressed quickly.

The flexible matrix array, which is under development at the University of Strathclyde is a relatively immature technology and significant further development will be required before this technology can be deployed on the NSRP. Although I am involved in the development of this device it is not part of my EngD research and will not be reviewed in detail in this document. Likewise much of the research work being carried out at the University of Bristol to develop advanced full matrix capture (FMC) based inspection algorithms including autofocus is not part of my doctorate research and will not be discussed here.

In addition to the increased responsibility for coordinating the advanced NDE NPCT project I have also gradually become more involved determining overall NDE research areas. I have been involved in a number of activities within this role. In order to develop a coherent NDE strategy across the whole of Rolls-Royce, NDE Panel meetings are held where stakeholders from across the business attend. When required I have acted as a secretary at these meetings and published minutes, I have also presented results from my research at this forum. One aspect of these meetings is to discuss specific research areas with applicability across Rolls-Royce and how to most appropriately attract Rolls-Royce funding for this research.

Over the past two years I have provided input into the NDE section of the high-level component and structural integrity research and technology (R&T) strategy document. This document has been developed to ensure that the research work within Rolls-Royce Submarines is suitably coordinated and funded. Through the development of this strategy document it has been possible to identify a number of areas where specific research is needed to address future NDE requirements. More recently I have also been responsible for producing some supporting documentation, briefly describing all of the current and future research areas to be addressed through the NDE R&T strategy. This document is used as a basis for discussing research areas both within and outside the NDE teams.

The main R&T strategy document is updated on an annual basis; based on the result of this process future research work to be addressed through the R&T programme is identified. Research work can be funded through the MoD or directly through Rolls-Royce. In each case in order to obtain funding for a project a proposal document and a range of associated documentation such as project plans and costs must be produced. For the past two years I have produced the bid proposal for the advanced NDE NPCT project which includes all of the University research projects discussed previously. As part of this process I have been responsible for clearly defining the long-term objectives of all four of these tasks and demonstrating how these address the needs of the submarine programme. In the final year of my doctorate my involvement in the bid process increased and along with Chris Greener (NDE research, team leader) I was involved in generating the bids for all MoD funded research work in 2009/2010. The overall research work is a major activity costing

well in excess of £1million per annum and involving all six members of the NDE research team as well as a number of third party academic and industrial partners.

Each research task funded through the NPCT project must provide a range of tangible benefits and these are reported to the MoD in an appropriate manner. In the advanced NDE NPCT project a detailed report on progress is provided to the MoD on a regular basis throughout the year. I am responsible for generating the progress report related to the advanced array inspection project and I have represented the NDE teams at review meetings with the Rolls-Royce project manager for over two years. I am also responsible for generating an annual progress report related to the project which has been the main annual deliverable associated with this work.

Rolls-Royce submarines subcontract NPCT funded research to a number of different organisations, including other industrial companies as well as academic institutions. In April 08 the Support and Development (S&D) OBU which includes the NDE research team started to subcontract some work to Serco Technical Assurance Services (Serco TAS) (Risley, UK). I am responsible for supervising some aspects of the work performed by Serco TAS under this contract. In this role regularly meet face-to-face with Serco TAS representatives to monitor their progress. I also represent Rolls-Royce on the Inspection Modelling Working Group (IMWG). This is a sub-group established by Serco TAS specifically to address inspection modelling requirements. The IMWG includes users of different modelling platforms from Serco TAS, Rolls-Royce and external experts (Dr R Chapman - British Energy and Prof M. Lowe - Imperial College). I am the representative from the Rolls-Royce S&D OBU and I am responsible for ensuring that the IMWG is addressing the needs of the entire Rolls-Royce department.

The objective of the advanced NDE project is to develop new tools and capabilities that can improve the inspection of NSRP components. In order to understand the requirements of the new technology in this type of application it is important to have an appreciation of the environment in which they are likely to be used. I have spent time working on a submarine completing existing inspections which has given me an insight into the unique challenges that the inspection engineers face. This has

involved completing a number of specific training courses designed to ensure that I can support the inspection in a safe manner.

The EngD is designed to prepare the RE for a senior career in industry, and the combination of technical courses, focused research and industrial experience is well suited to achieving this aim. My research has allowed me to develop a detailed knowledge of ultrasonic inspection and particularly the use of phased arrays. In recognition of this expertise I was asked by Rolls-Royce Aerospace to represent this part of this business in an RCNDE targeted project with University of Bristol, University of Strathclyde and a range of other industrial sponsors. The targeted project is intended to develop the use of 2D ultrasonic phased arrays for NDE applications. This is outside the scope of my EngD but provides an opportunity to gain an understanding of this area. It also gives me an insight into the main NDE drivers for Rolls-Royce Aerospace.

The advanced NDE NPCT project has progressed well and it has been identified as an area that Rolls-Royce would like to support in the future. The scope of this project is also increasing as more of the research topics become further developed and more mature. In order to continue to develop the different research areas and to continue the strong relationship between Rolls-Royce submarines and the RCNDE universities, Rolls-Royce have decided to support another EngD RE. I was the primary Rolls-Royce contact for the recruitment of the next RE, gathering and assessing applications and interviewing the student who was offered the position. The second RE started his studies in October 2008; I was responsible for outlining the content of his research and have acted as his industrial supervisor on his EngD studies. In addition to my mentoring role with the second Rolls-Royce NDE RE I am also responsible for mentoring Rolls-Royce apprentices as they spend time with the NDE research team. I am also increasingly involved in the direction of work through other researchers within the NDE research team. In order to embed the technologies developed through the advanced NDE NPCT project within Rolls-Royce these capabilities must be transferred to others within the organisation. As the individual responsible for the advanced NDE project I must ensure that this transfer process is successful. This will become increasingly important as the technologies become more mature.

As stated above, in addition to the MoD funded projects, some research work is directly funded through Rolls-Royce. I am responsible for the only project that we currently have funded through this route. This is an RCNDE targeted research project to "Array imaging of inhomogeneous steel welds by measurement of weld material maps". This is a three year research project in collaboration with Imperial College London, University of Manchester and E.On. It is likely that the second RE now working on the advanced NDE NPCT project will also support some aspects of this RCNDE project.

My role within Rolls-Royce is clearly beyond the scope of the typical EngD RE role. I am responsible for a range of activities throughout Rolls-Royce, many of which are beyond the scope of my doctorate. In recognition of the significant additional responsibility that I have taken on during my studies I was offered a position of full-time employment in October 2008. I accepted this offer and during the final 12 months of my doctorate have worked directly for Rolls-Royce. I have taken on many of the additional tasks discussed above as part of this role.

1.2. Outline of Thesis

This thesis presents the development of the membrane coupled phased array inspection capability. The aim of this development activity is to provide an improved inspection capability for the NDE of components with complex surface geometry typically found within the nuclear industry. The membrane coupled phased array uses a commercially available linear phased array. The array is then coupled to the surface of the component under test via a water path that is encapsulated by a polyurethane membrane with properties that are well matched acoustically to water.

Chapter 2 provides an overview of ultrasonic inspection techniques. The chapter begins with the physical principles of this approach and discusses conventional single element, rigid wedge inspection techniques. Phased array design and usage is then discussed and the benefits of this approach over single element transducer inspection are highlighted. Two different phased array transducers that are designed to improve the inspection of components with an irregular surface geometry are then introduced. The second of these devices is the membrane coupled phased array device; the focus

of this thesis is the development of inspection techniques for defect detection using this device, defect sizing is not considered.

In order to develop the conformable membrane coupled phased array for use within Rolls-Royce Submarines a specific target application has been selected. The target application component and the inspection of two flat plate, non-welded test-pieces designed to replicate the target application component are described in chapter 3. These test-pieces do not contain an actual weld but do have a representative weld cap. Inspection results comparing the defect detection performance of a rigid wedge phased array transducer to the 2nd generation membrane coupled phased array device are presented and the performance benefits of the flexible array discussed.

In chapter 4 the two primary modelling techniques used in this investigation are described. Simulation of the target application inspection was carried out using the CIVA model and using FE modelling. Results from both modelling approaches are presented and compared to experimental data gathered from the single element transducer inspection of the flat plate, non-welded test-pieces.

Development of the 3rd generation membrane coupled phased array transducer is described in chapter 5. In comparison to the 2nd generation design this device provides a reduced level of internal noise and improved beam forming characteristics. The 3rd generation device also incorporates an integrated irrigation system which is required for the deployment of this transducer in a commercial inspection.

Results from the inspection of two flat plate, welded test-pieces using the 3rd generation membrane coupled device are presented in chapter 6. These test-pieces contain a weld and weld cap representative of the actual target application component and 14 different artificial defects. Each defect is inspected using multiple techniques from both directions either side of the weld. All defects can be positively detected by at least one of the inspection techniques used.

The internal noise signal that limited the performance of the second generation membrane coupled device is still evident in the 3rd generation device. This limits the through weld inspection capability of the 3rd generation membrane coupled device. A

twin crystal membrane coupled device, designed to eliminate this issue and improve the inspection of some challenging defects is reviewed and assessed in chapter 7. Preliminary results obtained using the twin crystal device are presented, which demonstrate that the internal noise signal has been eliminated and that improved inspection performance is possible by using this device.

The main conclusions of this thesis and ideas for future work are presented in chapter 8.

2. Ultrasonic Inspection

Ultrasonic testing (UT) is a well-established Non-Destructive Evaluation (NDE) method using high frequency acoustic energy, usually in the range 1-5MHz, to conduct measurements (Birks & Green, 1991). It is a highly versatile method of testing and can be used in a number of different situations including flaw detection/evaluation, dimensional measurements, and material characterization (Mitsui Babcock, 2005).

Ultrasonic inspection is one of the major NDE techniques used within the nuclear industry and represents the biggest area of NDE research and development within Rolls-Royce Submarines. In this chapter, the basic principles of bulk wave ultrasonic inspection are reviewed, along with the use of phased array inspection techniques and the use of flexible arrays for the inspection of components with irregular surface geometry. This is not an exhaustive review of all uses of ultrasonic inspection, but focuses on the techniques and the applications of these techniques that are relevant to the nuclear industry.

2.1. Background

Ultrasonic energy is commonly introduced into the material using a piezoelectric transducer. Piezoelectric materials produce an electrical charge when subjected to a mechanical stress, equally when electrically excited these materials become stressed (Auld, 1973; Cheeke, 2002). The direct piezoelectric effect occurs stress is applied to the piezoelectric material. In this situation bound electric charges appear at opposing surfaces of the medium, causing a difference in potential across the medium. The direct piezoelectric effect is always accompanied by the indirect, or converse piezoelectric effect. The indirect piezoelectric effect corresponds to the induced stress in a material when subjected to an applied voltage.

Ultrasonic transducers used in NDE are typically produced to behave as an oscillating piston. In a simple contact transducer operating in transmission an electrical pulse is sent to the transducer. This produces motion in the piezoelectric element, via the indirect piezoelectric effect which then generates an acoustic wave in the component under test. The acoustic wave then propagates through the material under test.

Waves returning to the transducer cause a potential drop across the transducer through the direct piezoelectric effect. This voltage is then detected and interpretation of these signals is used to infer information related to the component being inspected.

The ultrasonic energy produced by the transducer propagates through the material under test until there is a change in acoustic impedance. Acoustic impedance is the product of the velocity of sound within a material and the density of that material. When the wave encounters an interface between two different media, reflection and transmission of the wave occurs. When calculating the behaviour of the wave at the interface between the two media the boundary conditions must be satisfied. At the interface the two boundaries are connected and hence there is continuity of the normal and tangential components of displacement and stress. The simple case of a pressure wave traveling in the positive x-direction at normal incidence to an infinite interface at x=0 between two media is shown in the schematic diagram in Fig 2-1.

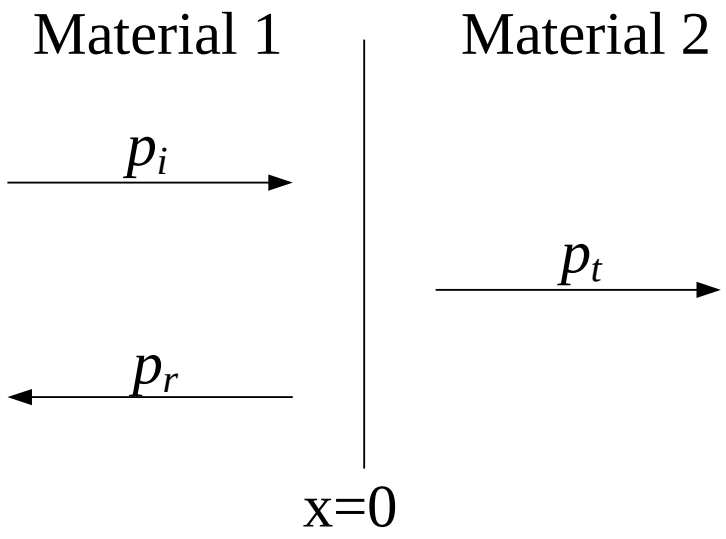

Figure 2-1 Schematic diagram of a wave at normal incidence to an interface between two media.

The three waves shown in Fig 2-1 can be represented as:

$$\begin{aligned} p_i &= A_i \exp i(\omega t - k_1 x) \\ p_r &= A_r \exp i(\omega t + k_1 x) \\ p_t &= A_t \exp i(\omega t - k_2 x) \end{aligned} \qquad (2.1)$$

Where p = Pressure
A = Amplitude
ω = Angular frequency
t = Time
k = Wavenumber
T_p = Transmission coefficient for pressure
R_p = Reflection coefficient for pressure

As discussed above, there must be continuity of displacement (velocity) and stress (pressure), therefore at the boundary it follows that:

$$p_i + p_r = p_t \qquad (2.2)$$

$$P_i + P_r = P_t \qquad (2.3)$$

Equations (2.2) and (2.3) can be solved to give the pressure transmission and reflection coefficients for normal incidence:

$$\frac{P_t}{P_i} = T_P = \frac{2Z_2}{Z_1 + Z_2} \qquad (2.4)$$

$$\frac{P_r}{P_i} = R_P = \frac{Z_2 - Z_1}{Z_1 + Z_2} \qquad (2.5)$$

Where Z_1 = Impedance of material 1
Z_2 = Impedance of material 2

Therefore from the definition of acoustic intensity:

$$I = \frac{p^2}{2Z} \qquad (2.6)$$

It follows that the energy transmission and reflection coefficients for normal incidence are given by equations (2.7) and (2.8) respectively. In each case the phase of the wave is given by the sign of the coefficient:

$$T_E = \frac{4Z_1Z_2}{(Z_1 + Z_2)^2} \qquad (2.7)$$

$$R_E = \left(\frac{Z_2 - Z_1}{Z_2 + Z_1} \right)^2 \qquad (2.8)$$

The transmission and reflection coefficients will also vary with the angle of incidence and depending on whether the two materials are liquids or solids. All of these cases are covered by standard texts on ultrasonic waves such as Cheeke (2002), Auld (1973b) and Schmerr (1998).

The difference in acoustic impedance between a solid and air is very large; therefore if the wave encounters a crack filled with air almost all of the wave energy will be reflected. In this scenario, the phase of the reflected wave will also be reversed in comparison to the incident wave. The presence of a defect can be detected by either the increase in the reflected signal or the reduction in the transmitted signal. Since the velocity of sound within the material is known the time taken for the transmitted signal to propagate through the material and reflect from the defect back to the receiver can be used to calculate the defect position. By studying the nature of the signal it is often possible to infer further information concerning the type of defect present.

Ultrasonic inspection is essentially a point technique; only the region in the immediate vicinity of the transducer is irradiated with ultrasonic energy. Therefore the transducer must be scanned over the surface of the specimen under test. This procedure can be automated or performed manually. Automated scanning provides an accurate permanent record of the defect but it is time consuming and expensive. It is also very challenging on curved or complex geometries. Manual scanning is faster and more flexible but no permanent record of the scanning is available and the inspection reliability is highly dependent on human factors (Lemaitre et al, 1996). In

the majority of inspections carried out by Rolls-Royce Submarines and within the nuclear industry generally the benefits of completing a high integrity automated inspection outweigh the cost implications. This approach has been adopted to generate the experimental data reviewed later in this document.

Under most circumstances a coupling medium is also required between the transducer and the component. As previously mentioned there is a large acoustic impedance mismatch between the solid and air. This allows defects to be detected within the solid material but reduces transmission between the transducer and the component under test. This air gap must generally be eliminated to effectively couple the transducer to the component. This can be achieved by immersing the component in a water tank. However, this is usually unsuitable for particularly bulky specimens or when the specimen cannot be moved. Alternatively a coupling medium, usually a gel or water, can be used. Lack of coupling is a common cause of poor results and care must be taken to ensure good ultrasonic contact is maintained throughout the test.

Ultrasonic energy can travel through a material in a number of different ways. The main wave modes relevant to this testing will be discussed. If we first consider a 1-dimensional case for a small element of length, l, and density, ρ, undergoing an elongation of ∂u due to an external force, F in the positive x-direction. The external stress is given by equation (2.9), where A represents the area of the element:

$$p = \frac{F}{A} \qquad (2.9)$$

Hooke's law can be written as:

$$p = E\varepsilon \qquad (2.10)$$

Where E = Young's Modulus

ε = Strain

Assuming small strains only, then:

$$\varepsilon = \frac{\partial u}{l} = \frac{\partial u}{\partial x} \qquad (2.11)$$

Newton's second law can be written as:

$$\frac{\partial p}{\partial x} = \rho \frac{\partial^2 u}{\partial t^2} \qquad (2.12)$$

The 1-dimensional wave equation is then obtained by combining Hooke's law with equation (2.12):

$$\frac{\partial^2 u}{\partial x^2} = \frac{\rho}{E} \frac{\partial^2 u}{\partial t^2} \qquad (2.13)$$

The velocity of the wave is given by:

$$c = \sqrt{\frac{E}{\rho}} \qquad (2.14)$$

By substituting equation (2.14) into equation (2.13), we can rewrite the wave equation as:

$$\frac{\partial^2 u}{\partial x^2} = \frac{1}{c^2} \frac{\partial^2 u}{\partial t^2} \qquad (2.15)$$

It is possible to show that this result can be then be extended to 3-dimensions, this is provided in standard texts (Cheeke, 2002; Schmerr, 1998) and shown in vector notation in equation (2.16)

$$\mu \nabla^2 \mathbf{u} + (\lambda + \mu) \nabla (\nabla \bullet \mathbf{u}) = \rho \frac{\partial^2 \mathbf{u}}{\partial t^2} \qquad (2.16)$$

Liquids cannot support shear stresses and therefore only support longitudinal or compression waves and the bulk modulus of the material should be considered, whereas solids offer elastic resistance to shearing forces, therefore, solids can support both longitudinal and shear or transverse waves. In solids, the compression modulus of the material, which is a combination of the bulk modulus and the shear modulus, is used. In longitudinal wave propagation the particle displacement is in the same plane as the direction of wave propagation. In shear waves the particle displacement is perpendicular to the direction of the wave propagation and can occur in two orthogonal polarizations. Solids can support both vertically and horizontally polarized shear waves. However, due to their mode of operation, piezoelectric transducers typically are used to produce vertically polarized shear waves only and this type of wave has been used throughout the experimental work detailed in this thesis.

Separation of the longitudinal and transverse wave modes can be achieved by the Helmholtz decomposition (Lowe, 1992). The displacement vector is decomposed into a scalar function Θ to represent the longitudinal wave, and a vector function $\boldsymbol{\psi}$, to represent the shear wave.

$$\mathbf{u} = \nabla\Theta + \nabla \times \boldsymbol{\psi} \qquad (2.17)$$

The 3-D wave equation in (2.16) can then be satisfied if the functions Θ and $\boldsymbol{\psi}$ satisfy the following equations:

$$\nabla^2\Theta - \frac{1}{c_L}\frac{\partial^2\Theta}{\partial t^2} = 0$$

$$\nabla^2\boldsymbol{\psi} - \frac{1}{c_S}\frac{\partial^2\boldsymbol{\psi}}{\partial t^2} = 0 \qquad (2.18)$$

which have two distinct wave speeds, which can be described in terms of the Lamé constants: λ' and μ:

$$c_L = \sqrt{\frac{\lambda'+2\mu}{\rho}} \qquad (2.19)$$

$$c_S = \sqrt{\frac{\mu}{\rho}} \qquad (2.20)$$

The Lamé constants are related to Young's modulus, *E*, and Poisson's ratio, *v* by the following equations:

$$\lambda' = \frac{E\upsilon}{(1+\upsilon)(1-2\upsilon)} \qquad (2.21)$$

and $$\mu = \frac{E}{1(1+\nu)} \qquad (2.21)$$

When propagating at a sufficient distance from the material boundaries that no interaction between the wave and material boundaries occurs, both shear and longitudinal waves act as in an infinite medium and are known collectively as bulk waves.

Solid materials also support Rayleigh waves which travel along the surface of the solid. Rayleigh waves propagate with a mixture of longitudinal and shear wave motion. Therefore, the particle motion of a Rayleigh wave is elliptical, with the major axis of particle displacement perpendicular to the direction of propagation. Rayleigh waves are constrained to exist in only 2-dimensions and only extend a distance approximately equal to one wavelength into the material. Rayleigh waves follow the surface geometry of a part; the waves can travel long distances but are damped by surface roughness and by any moisture that is present on the material surface (Auld, 1973b; Cheeke, 2002; Krautkramer & Krautkramer, 1983; Schmerr, 1998).

Ultrasonic waves obey Snell's law at a material interface. Snell's law is provided in equation (2.22).

$$\frac{\sin\theta_1}{\sin\theta_2} = \frac{v_1}{v_2} \qquad (2.22)$$

Where θ_1 = Angle in material 1

θ_2 = Angle in material 2

v_1 = Propagation velocity in material 1

v_2 = Propagation velocity in material 2

The angle of refraction within a given material is different for each of the different types of wave modes that propagate through a material. This is because each of the different wave modes propagates with a different velocity through the material. Therefore different modes can be excited within a component by changing the angle of incidence of the transducer. This is shown the schematic diagram in Fig 2-2 for an inspection in immersion where the incident angle is given by θ_i, and the angle of the longitudinal and shear waves are θ_l and θ_s respectively. The generation of a shear wave within a solid from an incident longitudinal wave is known as refractive mode conversion. In immersion testing this is achieved by simply moving the transducer relative to the component. In contact testing a wedge of material (typically Perspex or similar) is introduced between the transducer and the component. The relative intensity of the different wave modes within a solid is dependent on the angle of incidence. The incidence angle of the transducer can be optimized to detect a certain type and position of the defect.

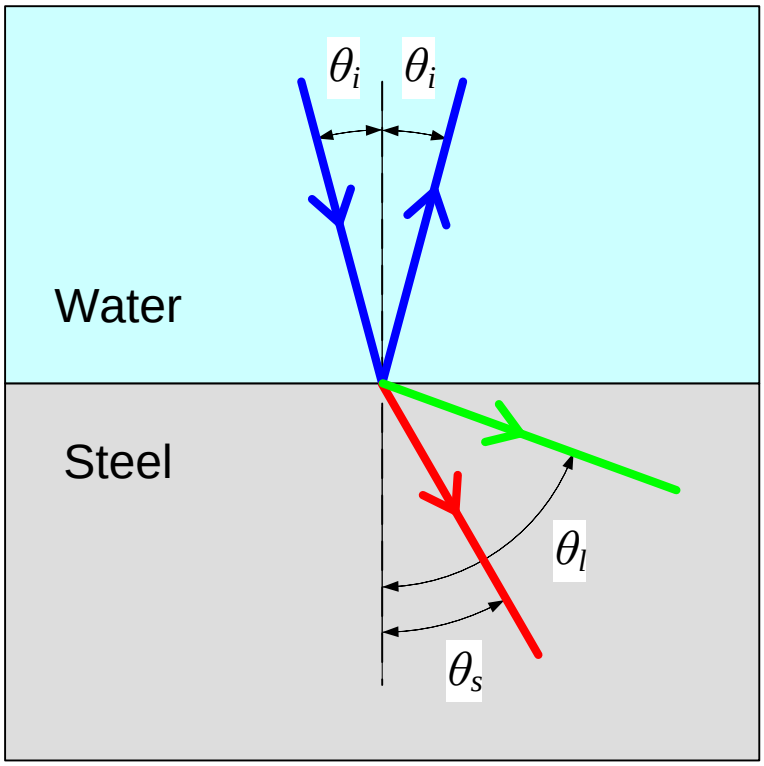

Figure 2-2 Schematic diagram of refraction at a boundary between water and steel.

If the angle of the incident longitudinal wave is gradually increased the angle of the refracted longitudinal wave also gradually increases. At a certain angle, known as the first critical angle, the angle of the refraction of this wave is equal to 90º. At this incident angle only a bulk shear wave is generated in the material. If the angle of incidence is increased further the refracted shear wave will also eventually reach 90º, this point is known as the second critical angle. As the refraction angle is increased further still the Rayleigh wave angle is reached, at this point there is only a surface wave generated within the material. The first and second critical angles can be readily calculated from equation (2.22). At an angle just below the first critical angle a creep wave or subsurface longitudinal wave is generated in the material.

Within the solid test medium, reflective mode conversion can occur at the boundary of the component. If a longitudinal wave is incident on a boundary at a given angle of incidence then a longitudinal wave will be reflected at an angle equal to the angle of incidence; a shear wave will also be generated at a different angle. As in the refracted case the relative intensity of the two reflected waves will depend on the angle of incidence. The same phenomenon occurs for an incident shear, both shear and

compression waves being reflected from the surface at different angles and intensities. The reflection coefficients for longitudinal and shear waves at the boundary between steel and air is provided in Fig 2-3. These reflection coefficients have been calculated using the software package Spectrum. The case for an incident longitudinal wave is shown in Fig2-3a and that for an incident shear wave is provided in Fig 2-3b.

a.)

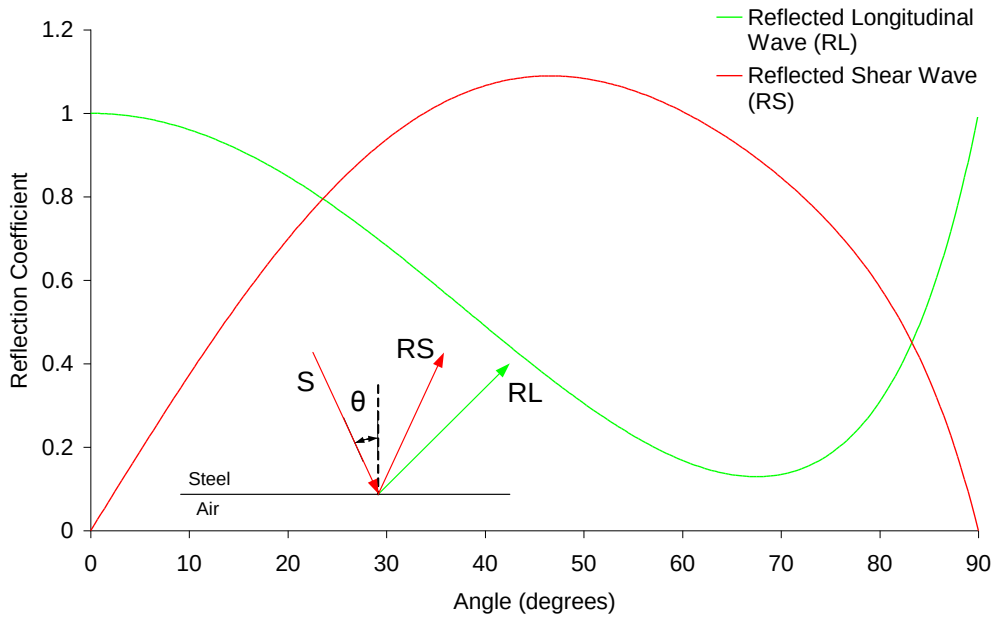

b.)

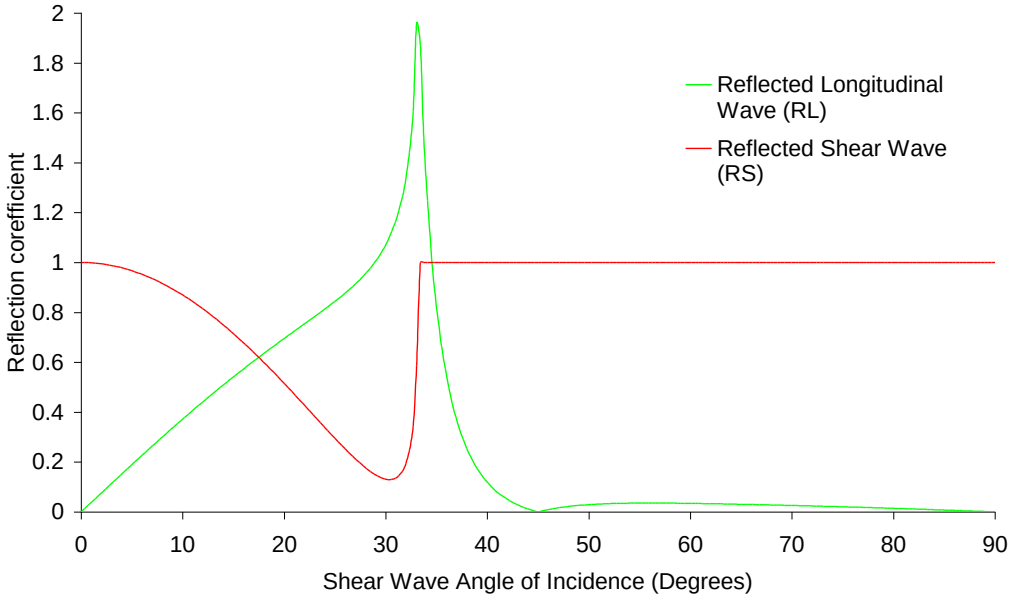

Figure 2-3 The reflection coefficients for longitudinal and shear waves at the boundary between steel and air, a.) for an incident longitudinal wave and b.) for an incident shear wave.

Further information on ultrasonic wave propagation and testing is provided in standard reference textbooks (Birks & Green, 1991; Drury; 1983; Henneke et al, 1991; Krautkramer & Krautkramer, 1983).

2.2. Ultrasonic Phased Arrays

Historically ultrasonic inspection has been performed using individual transducers; these have been reviewed in a range of texts (Krautkramer & Krautkramer, 1983; Birks & Green, 1991). A single transducer can be used to complete testing in pulse-echo where the transducer is used as both a transmitter and receiver. Pitch-catch and through transmission inspections have also been developed where separate transmitter and receiver probes are used. In each of these techniques fixed angle transducers are used, which insonify a limited inspection volume within the component under test. All of these are point techniques and the probes must be mechanically scanned to build up an image of the component. If defects can occur at different orientations, as is commonly the case in metallic structures, then the inspection must be repeated with a number of different angle probes.

Phased arrays are arrangements of small individual transducers, which are referred to as the elements of the array. The arrangement of the elements within the array controls its basic operation. Linear arrays, shown in Fig 2-4a, are also referred to as 1D arrays; this type of array allows beam steering and focusing anywhere within a 2D imaging plane. Planar or mosaic arrays, shown in Fig 2-4b, contain a number of elements that are arranged in a 2D grid, some work has been done on the optimization of the grid configuration (Martinez et al, 2003; Norton, 1992; Mondal et al, 2005). This type of array allows beam steering and focusing anywhere in a 3D inspection volume. Annular arrays, shown in Fig 2-4c, are circular, these arrays do not allow beam steering but they do provide variable focal depth capability. Different array designs are reviewed in detail elsewhere (Drinkwater & Wilcox, 2006; Shung, 2002).

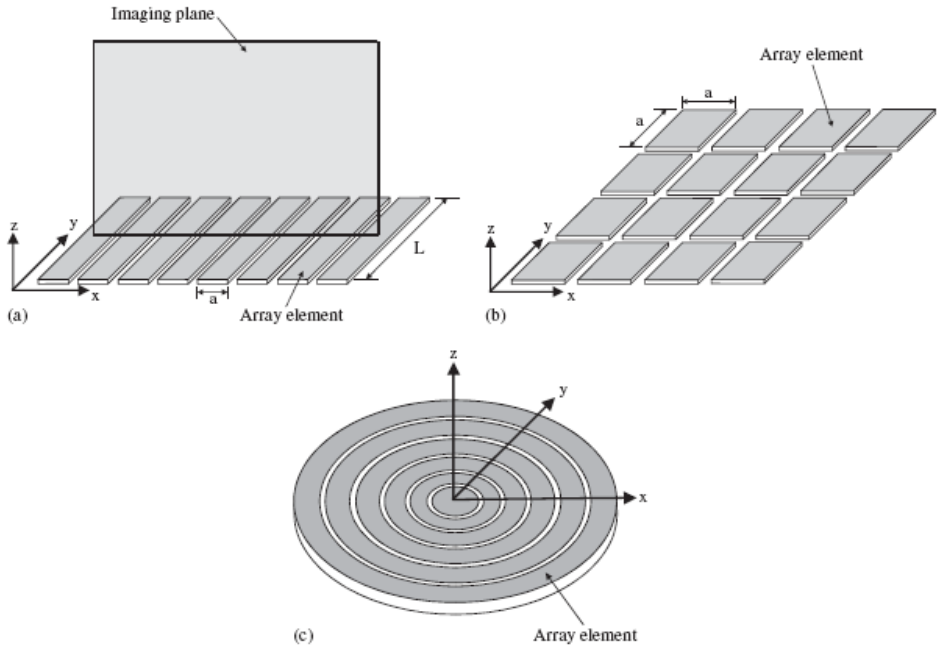

Figure 2-4 Common array transducer configurations: (a) linear array, (b) 2D array and (c) annular array, figure taken from (Drinkwater & Wilcox, 2006).

The manufacture and operation of 2D arrays is relatively complex, thus increasing cost and difficulty of production. Also limitations in array controller technology and computing power mean that the size of arrays is currently limited to a relatively small number of elements. Therefore, although some applications have been reported (Casula et al, 2005; Akhnak et al, 2002), they are yet to find widespread use in industry. In many inspections defects can occur at a range of angles. Beam steering is therefore important and so annular arrays find limited application. At the current time linear arrays are by far the most commonly used in industrial NDE.

Linear arrays typically contain a number of rectangular array elements arranged side by side. Elements within the array are normally relatively long and narrow so that they behave approximately like line sources. A perfect line source would generate a semi-cylindrical wavefront. However, the element has a finite width, this reduces the amount of beam spread and hence the width of the beam generated. The length of the element, the y-dimension in Fig 2-4, is significantly greater than the wavelength thus minimizing acoustic beam-spread in this dimension.

Elements within the transducer array are typically made from a similar piezocomposite material to their modern single element counterparts. Each element

in the phased array is electrically isolated from its neighbours. This is achieved by connecting each element with an individual electrical delay line; these delay lines are then all connected to a multiplexer. This allows each element to be independently addressed, providing beam steering and focusing in both transmission and reception. As the ultrasound is generated in the same way as for single element probes, similar requirements exist to couple the ultrasound into the component. Testing must once again be performed using some form of suitable coupling medium to prevent large interface reflections.

The beam profile generated by a single element probe is controlled by the mechanical design of the probe. The field generated by the probe is fixed and cannot be changed. Phased array transducers are much more flexible, and they can typically be used to mimic the fields generated from a range of different single element probes. This flexibility means that a wide range of testing regimes can be implemented with a single phased array transducer. Individual elements or a group of elements (termed the aperture) can be fired in-phase with one another to generate a plane wave within a component. Alternatively different delays can be applied to each element to steer or focus the beam. A different set of delay laws (or focal laws) is required for each different test case.

The array operation is shown for the simple case of beam steering in the schematic diagram provided in Fig 2-5. In order to generate the plane wavefront indicated by the solid blue line in Fig 2-5 the timing delays applied to two adjacent elements must be suitably controlled to ensure that constructive interference occurs along this line. The signal from the first element must travel a distance *a* calculated from equation (2.23) before the second element is fired. The time delay *t*, required for a wave to travel this distance at a velocity c, within the test medium is then found from equation (2.24)

$$a = p\cos\theta \qquad (2.23)$$

$$t = \frac{p\cos\theta}{c} \qquad (2.24)$$

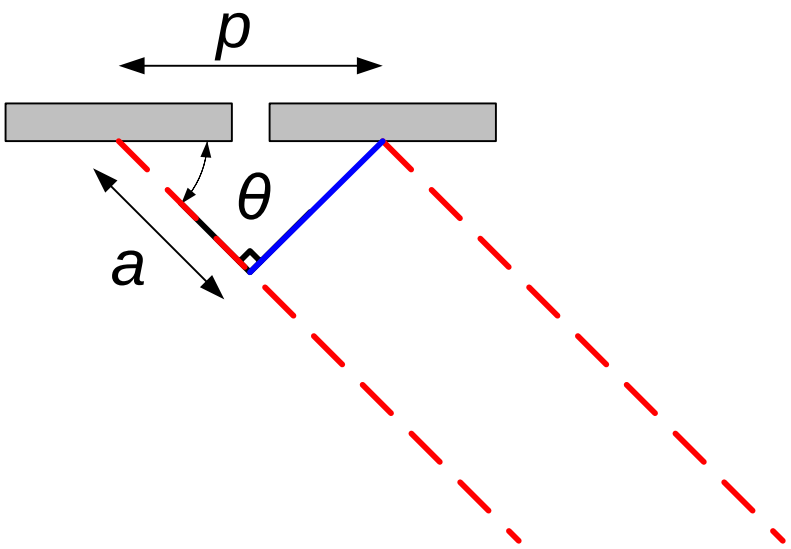

Figure 2-5 Schematic diagram of the required time delays to generate an angled beam using a phased array.

To allow a phased array to be used to detect small scattering objects in pulse-echo mode, a sharp, narrow pulse of ultrasonic energy is required in the time domain. To achieve this desired output, a wide bandwidth transducer is typically used, containing a large range of frequencies. The ultrasonic output of the array is controlled through the transducer design and control of the electrical signal used to excite the transducer. The individual elements within the phased array transducer operate in the thickness mode. Therefore individual elements are prepared so that the thickness of the element corresponds to half the ultrasonic wavelength of the desired operation. Therefore the fundamental operating frequency, f_0, of the phased array is given by equation (2.26). The drive signal used to generate the ultrasonic signal should be well matched to both the centre frequency and the bandwidth of the array to ensure efficient ultrasonic wave generation and optimum performance.

$$f_0 = \frac{c}{2d} \qquad (2.26)$$

Where c = Velocity

d = Thickness

One potential issue found when using phased array transducers is the appearance of grating lobes. These can occur in arrays with regularly spaced elements and are due to constructive interference between the signals transmitted from each element. Grating lobes are a characteristic of any phased array transducer and depend on element pitch, frequency and bandwidth (RD Tech, 2004). The angle at which the grating lobes exist is given by equation (2.27) (Wooh & Shi, 1999).

$$\theta_{grating} = \sin^{-1}\left(\sin\theta_{steering} - \frac{m\lambda}{p}\right) \qquad (2.27)$$

Where $\theta_{steering}$ = Array steering angle (in radians)

m = Integer (±1, ±2, …)

λ = Wavelength

p = Element pitch

The critical element pitch to ensure that no grating lobes exist is then given by equation (2.28). In order to eliminate grating lobes under all operational conditions an element pitch of $\leq\lambda/2$ must be adopted.

$$p_{critical} = \frac{\lambda}{1+\sin(\theta_{steering})_{\max}} \qquad (2.28)$$

The effect of grating lobes can be clearly seen in the CIVA screen shots shown in Fig 2-6. In Fig 2-5 a 2MHz centre frequency, 64 element contact phased array transducer on a stainless steel load is simulated. The longitudinal wavelength (λ_L) in stainless steel at the centre frequency of the transducer is approximately 2.9mm and the shear wavelength (λ_S) is 1.5mm. In all of the simulations suitable delay laws are selected to generate a 45° shear wave in the stainless steel component, which represents a challenging inspection for this type of transducer. In Fig 2-6a an element pitch of 1.5mm or λ_S is simulated; and a grating lobe is clearly observed. The image in Fig 2-6b shows the performance of an array with an element pitch of 0.75mm or $\lambda_s/2$, this array meets the critical element pitch requirement and no grating lobes are observed.

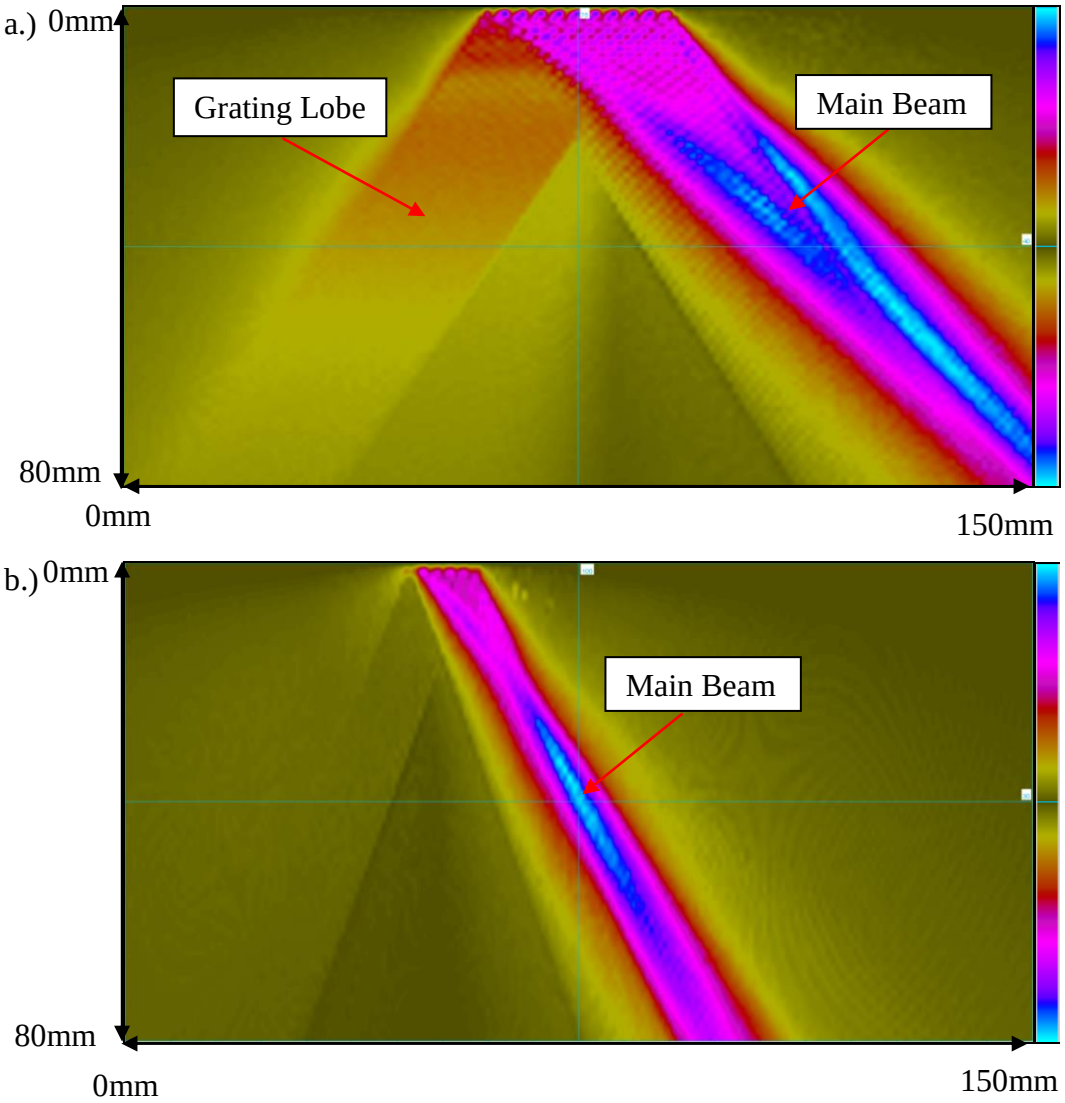

Figure 2-6 CIVA beam plots for a 2MHz centre frequency contact array on a stainless steel block producing a 45° shear wave with an element pitch of a.) 1.5mm and b.) 0.75mm. Both images are shown with a dynamic range of 40dB.

When using single element transducers the probes must be mechanically scanned across the surface of the component to provide complete test coverage. Mechanical scanning of a component is a laborious and time-consuming task. The accuracy and repeatability of the scanning process can be improved through automation. Data collection and storage can also be automated, which improves the overall reliability of the inspection procedure. However, the scanning process must still be carried out for each scan angle and the overall time requirement remains high. The scanning process can be made significantly faster and more flexible by using a phased array transducer. Scanning can be performed electronically by sequentially addressing different

elements with a set of delay laws. Electronic scanning is only limited by the pulse repetition frequency (PRF) associated with the inspection. The PRF is the maximum rate at which consecutive excitation pulses can be generated. Because of this, electronic scanning is typically an order of magnitude faster than mechanical scanning (RD Tech, 2004).

Phased array transducers can also be used to inspect components in ways that are not typically possible using standard single element transducers. Applying a set of delay laws to an aperture generates a beam at a given angle. By updating the delay laws the angle of the beam generated can be modified, this process can be repeated to complete an angular sweep, or a sector scan. An example of a sector scan is shown in Fig 2-4 for the inspection of three SDH defects (Long & Cawley, 2006). This is particularly useful if defects can occur over a range of angles within the component. However, the phased array must be mechanically raster scanned so that each region of the component is insonified by beams at a range of different angles. This approach ensures that defects with different tilts can be detected. If only a particular region of the component is of interest then inspection performance can be further improved by modifying the delay laws further to provide some focusing.

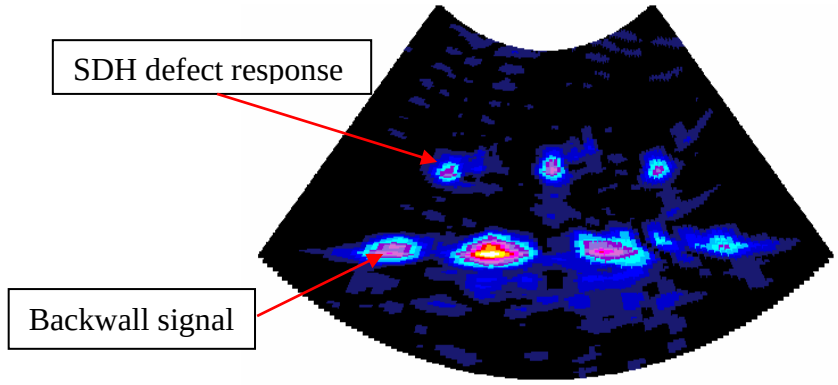

Figure 2-7 Sector scan of three side drilled hole (SDH) defects, figure taken from (Long & Cawley, 2006).

The beam characteristics of phased array transducers are dependent on a number of parameters. Each of these parameters must be carefully controlled in order to optimize the performance of the array in a given application. Wooh and Shi (1999) and Azar et al (1998) have reviewed the influence of each of these parameters. This demonstrates that control of element width, inter-element spacing and number of

array elements is essential. These parameters are typically controlled during array manufacture and cannot be adjusted at a later time. The practical uses of any array are therefore limited; given these limitations array manufacturers have developed guidelines for use of their product (RD Tech, 2004). When high angled beams are required it is typically recommended to angle the transducer relative to the component test surface in the same manner as used for single element transducers.

There are similar practical restrictions to beam focusing. As with single element transducers there is a near field length associated with a phased array transducer. The near field length for a circular transducer can be found from the relationship shown in equation (2.29), this simplifies when the aperture diameter is much greater than the wavelength of operation (Krautkramer & Krautkramer, 1983). It is only possible to focus at distances less than this near field length. It is possible to increase the potential focal length of the array by using a larger aperture or larger array but due to access restrictions this is not always possible in practice. The maximum size of the array is also limited by the number of channels that can be addressed by the phased array controller and the element pitch.

$$z = \frac{D^2 - \lambda^2}{4\lambda}$$
$$z \approx \frac{D^2}{4\lambda} \qquad (2.29)$$

Where z = Near field length
D = Aperture diameter
λ = Wavelength

Typically phased arrays are used to replicate single element transducer inspection procedures. A set of fixed delay laws are used to replicate each angle beam and a specific acoustic parameter is recorded at each measurement position. A trained NDT practitioner monitors the data recording process in real time. Although faster than the equivalent single element transducer inspection this approach remains slow and must be repeated for each desired parameter. In addition, using an ultrasonic phased array in this way does not exploit the full potential of the array technology. Holmes et al

(2005) have reported a new approach to industrial array inspections, which uses a technique known as Full Matrix Capture (FMC). This approach has been used in the seismic field for some time (Berkhout, 1986) but until recent research work it has not been used in the NDE field.

When operating in FMC mode the full matrix of time domain signals (A-Scans) from each transmitter-receiver pair within the array is captured and stored. All data processing can then be performed offline in post processing. By using this approach it is only necessary to capture a single set of data, different algorithms can then be applied to this data set in order to simulate each different test mode. This approach also future proofs the inspection; as more advanced algorithms are developed they can be applied to the same data set.

As part of this research activity algorithms have been developed that emulate conventional phased array testing (Long et al, 2008). However, additional algorithms that can only be practically implemented in post processing have also been developed. The first of these is the total focusing method (TFM), in this technique the inspection volume is discretized into a grid with a given resolution, the FMC data is then processed to provide an effective focus at every point within the inspection volume (Holmes et al, 2005). This could be achieved using a conventional approach but the delay law calculation and the acquisition of data would be extremely time consuming. One potential drawback of the FMC technique is degradation in the signal to random noise ratio (SNR) due to the low acoustic power of the transmit signal for each transmitter-receiver pair. Experimental work is ongoing within the Advanced NDE NPCT project to quantify this effect and understand the potential benefits of averaging to reduce this issue (Duxbury, 2009).

The TFM approach is particularly appropriate for small point like reflectors and has been shown to out-perform other approaches in this type of inspection (Holmes et al, 2005). The TFM has been developed further into the vector TFM (VTFM) algorithm (Wilcox et al, 2007). This allows the angular reflectivity characteristics of any point in the inspection volume to be investigated. This provides valuable insight into the orientation of any defect within the inspection volume and assists with defect characterization. Another algorithm that has been developed using FMC data that

cannot be implemented using single element transducers is the Almost Total Focusing Method (ATFM) (Long et al, 2008). The ATFM technique provides a fully-focused B-Scan image from an aperture within the array. Hunter et al (2009) have demonstrated that for the inspection of planar defects occurring over a limited range of angles the ATFM algorithm provides an improved inspection capability in comparison to the TFM technique.

2.3. Inspection of Components with Irregular Surface Geometry

In industrial situations non-destructive inspections must often be performed on components with complex geometries. In the target application, discussed in greater detail in chapter 3, a circumferential pipe weld is to be inspected. In this type of component defects may occur that are associated with the welding procedure. These defects typically occur at a range of angles and have significant through-wall extent. Inspection for this type of defect is usually carried out using fixed angle, rigid wedge coupled transducers. A series of scans are performed using probes with different angles optimized for the detection of different defects. As previously mentioned phased array probes could be used to reduce the amount of axial scanning and the number of different probes required. This would improve the speed, and potentially the reproducibility of the inspection. However, phased array transducers typically have a significantly larger footprint than single element transducers. Maintaining a uniform couplant layer between a rigid phased array and the component under test can therefore be challenging, especially on rough or irregular surfaces.

When inspecting pipe welds of the type in the target application some inspection techniques require the transducer to be placed above the weld itself. It is not possible to effectively couple rigid, wedge-coupled transducers to this region due to the curved nature of the weld cap. Typically, inspection coverage is achieved by removing the weld cap from the weld region. Weld cap removal is an expensive, time-consuming task that can compromise the integrity of safety critical pipe-work. In some cases it is also possible that even when the weld cap has been removed that the inspection surface is not completely flat due to material distortion caused as part of the weld process. The optimum inspection would use a conformable phased array; this would

deliver the benefits derived from a phased array inspection without the need to remove the weld cap. The phased array delay laws would need to be updated to account for changes in the beam steering and focusing due to the presence of the weld cap. It has been shown that severe degradation in inspection performance occurs if delay laws are not correctly updated to accommodate irregular surface profiles (Long & Cawley, 2006; Roy et al, 2002).

One approach developed by the Commissariat à l'Energie Atomique (the French atomic energy commission) (CEA List, Saclay, France) uses a flexible contact array (Chatillon et al, 2000); this is shown in Fig 2-5. In this device 28 array elements with a centre-to-centre separation (pitch) of 1.4mm are arranged along two flexible wires. The individual elements are then able to conform in the vertical direction to an irregular profile. However, issues have been encountered with the degree of flexibility that can be achieved using this device (Hunter et al, 2009; EPRI, 2004). The location of the elements is measured using 7 linear profilometers positioned along the length of the array. The delay laws for each individual element are updated based on the surface profile measurements from the profilometers.

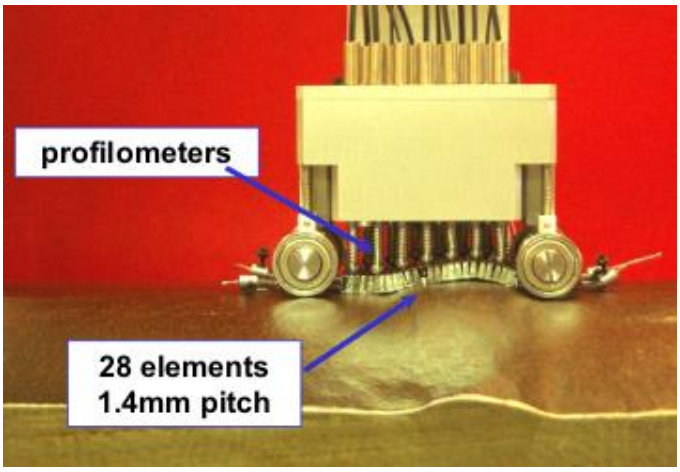

Figure 2-8 CEA flexible contact array (Chatillon et al, 2000).

The measurement of the surface profile of the component under test using the profilometer technology from the CEA is patented. Imasonic (Besançon, France) have recently obtained an exclusive licence for the use of this patent, which allows Imasonic to design and manufacture the flexible contact transducers. Imasonic have

improved the robustness of the transducer and made it more suitable for industrial application. It is also now possible to readily replace elements if damage does occur during operation. Arrays with centre frequency of 2 and 4MHz are now available with up to 32 elements.

(a) (b)

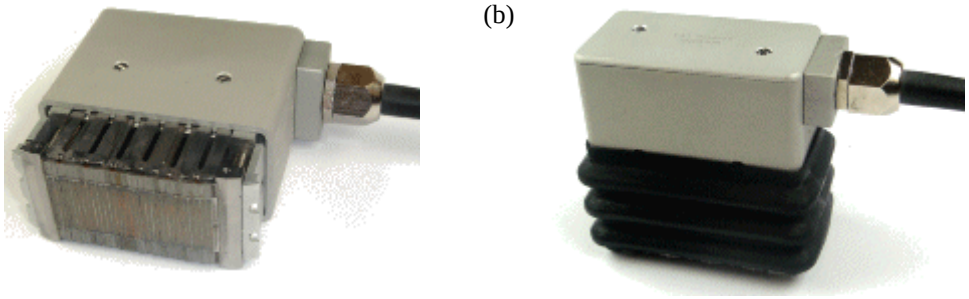

Figure 2-9 Commercially available flexible arrays produced by Imasonic (Besançon, France).

An alternative approach using a membrane coupled phased array device has been developed and was originally reported by Long and Cawley (2006). The development of the membrane coupled phased array has been supported by Rolls-Royce and the further development of this device along with its transfer to Rolls-Royce has formed a significant part of my EngD research. In the membrane coupled device a standard ultrasonic phased array is used but the rigid wedge is replaced by a water filled standoff encapsulated within a low-loss rubber membrane. A schematic diagram of the first generation membrane device is shown in Fig 2-7(b). In this approach the surface profile is measured using the phased array itself, the delay laws are then updated to accommodate the varying geometry. Long and Cawley have shown that the delay law calculation using this approach is slightly more complex but that the probe is significantly cheaper and more robust than the CEA/Imasonic flexible probe (Long & Cawley, 2006).

(a) 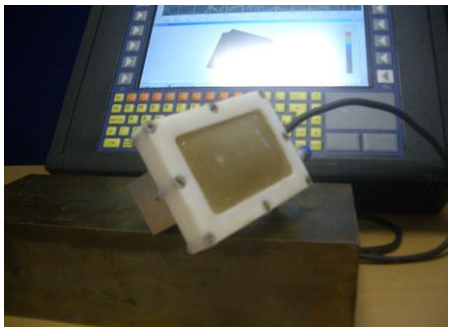

(b) 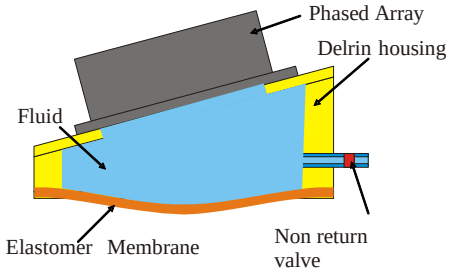

Figure 2-10 1st generation membrane coupled phased array device a. photograph and b. device schematic diagram (Long & Cawley, 2006).

The membrane probe developed by Long and Cawley was designed to operate using FMC data acquisition. When using the membrane coupled device a surface profile measurement of the component under test must first be performed. This test is done using the membrane probe itself. The surface profile can strongly influence the nature of the ultrasonic beam pattern within the component. It is then possible to apply each of the algorithms referenced above to the matrix of data obtained. The delay laws used to generate each beam type must be updated to accommodate the nature of the surface profile. The performance of a first generation membrane probe has been demonstrated on a range of machined samples provided by Rolls-Royce (Long et al, 2007c).

The first generation membrane probe device contained a constant volume of water. This approach ensures that there are no air bubbles within the water standoff and no water movement to disrupt the transmission of ultrasonic energy. However, using this approach the membrane cavity seal must be very high quality to prevent leakage of water. When scanning the device on a pipe the force required to ensure good coupling between the transducer and the component would vary depending on the orientation of the transducer relative to the pipe. This would become an issue on a horizontally oriented pipe when the transducer is scanning upside down. If the membrane was highly pressurised it would also not be possible to maintain the angle of the transducer relative to the component when scanning on and off the weld cap. This approach has therefore not been used in the 2nd generation device. The 2nd generation membrane probe (Long & Cawley, 2006; Long et al, 2007b), shown in Fig 2-8 has been designed to maintain a constant water pressure within the standoff; a

header tank arrangement is used to achieve this. The 2nd generation membrane device uses a linear 80 element, 1.25mm pitch, 2MHz centre frequency transducer. The bespoke transducer design from Imasonic was modified to include an extended flange, which was used to improve the seal between the array and the probe housing, and ensure no leakage from the device during operation.

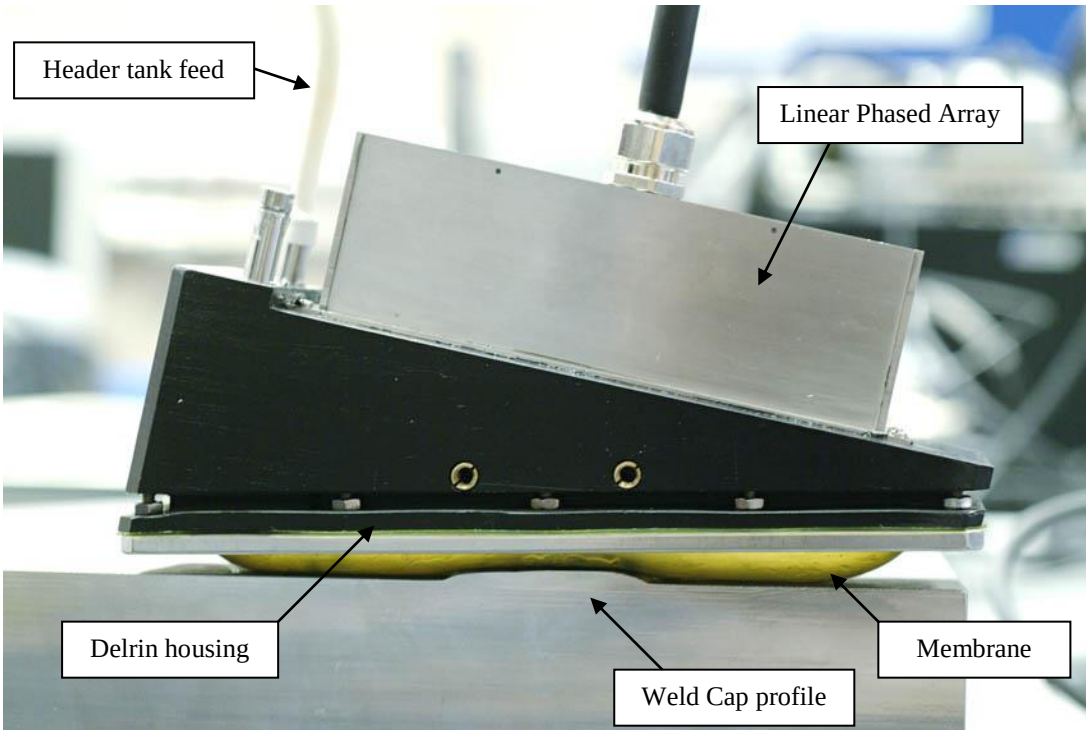

Figure 2-11 Second generation membrane probe (Long et al, 2007b).

The membrane used in the first generation membrane probe was a low-loss rubber, sold commercially for use in ultrasonic wheel probes. The rubber was only available in a limited range of thicknesses, none of which were ideal for the membrane probe application. In the second-generation probe a polyurethane membrane is used; this material can be cast into thin sheets of the desired thickness. The housing has also been updated and improved to make the device more robust and to make changing the membrane faster and more straightforward. Subsequent testing of the membrane coupled device concept has been carried out on a specific target application, which is discussed in chapter 3.

2.4. Summary

Ultrasonic inspection is a very well established NDE technique and is widely used for a variety of measurements throughout industry. Typically existing inspection techniques use rigid wedge single element transducers to produce a fixed angle and focal depth ultrasonic beam. This is a point technique and the transducer must be laboriously mechanically scanned over the component surface to build up an image of the component volume. This scanning process must be performed with range of different angled probes to provide information on defects with a range of orientations.

Ultrasonic phased array probes contain a number of individual transducer elements, each of which is connected to an electrical delay line. By controlling the time delay of the electrical signal to the individual elements it is possible to replicate the performance of many different single element transducers using a single phased array probe. It is also possible to generate an ultrasonic beam from an aperture within the array and then electronically scan the component. This approach offers significant improvements in terms of speed over conventional single element transducer inspection. An alternative approach to phased array inspection is to use FMC data acquisition. In this technique all of the possible inspection data from each transmitter-receiver pair within the array is captured. Different beam forming algorithms can then be applied to the dataset in post-processing. This approach allows the use of inspection methods that cannot be applied using conventional techniques and provides a mechanism to future-proof an inspection against further algorithm development.

Phased array transducers are typically much larger than single element transducers; this allows a large area of the component under test to be scanned electronically from a single transducer position. However, in order to provide a high quality inspection the entire footprint of the array must be in intimate contact with the component under test. This becomes very challenging on components with irregular surfaces. A typical inspection problem that must be addressed by engineers at Rolls-Royce is the inspection of welded components where the weld cap has not been removed. It is not possible to scan rigid wedge-coupled transducers over this weld cap region. There are two main alternatives to address this inspection requirement. The first is a flexible contact array developed by the CEA and Imasonic. This device is commercially

available but issues have been encountered with the degree of flexibility that can be achieved, the robustness of the transducer and its price. The alternative approach is the membrane coupled phased array; this low cost, robust device uses a conventional linear array which is coupled to the surface of the component under test via a water path encapsulated in a low loss polyurethane membrane. This thesis focuses on work carried out on the development of this membrane coupled device.

3. Flat Plate, Non-Welded Test-Piece Inspection

The membrane coupled phased array device is being developed to address the requirement to allow detailed inspection of any component with complex surface geometry. Early development work was based on very generic inspection requirements; this allowed the basic principles of operation to be understood but in order to develop the capability further more focused research was required. A typical inspection that must commonly be addressed by Rolls-Royce is the inspection of welded components that contain a convex weld cap. The target application for the development of the membrane coupled phased array is a large bore pipe weld which is representative of this issue. A diagram of the target application component is shown in Fig 3-1. An inspection is required to detect and characterise a range of potential defects in a circumferential weld and the associated Heat Affected Zone (HAZ) within the pipe. Due to access constraints the inspection must be performed from the outside of the pipe only. There is an elbow in the pipe that has a variable radius of curvature making inspection from this surface very difficult; scanning is therefore carried out from a straight section of pipe on one side of the weld only.

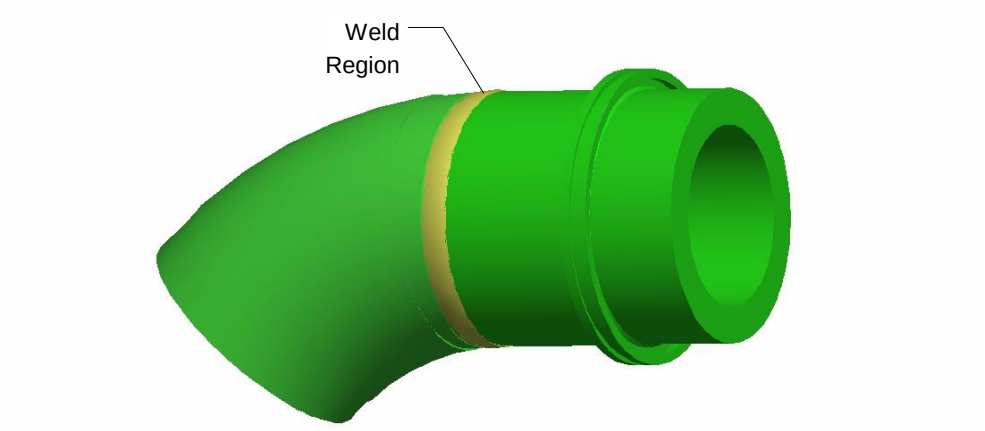

Figure 3-1 Diagram of the target application component.

Inspection of the target application component is currently performed using conventional single element transducer technology by a third party organisation. The first stage in the inspection process is to manually remove the weld cap so that rigid wedge technology can be used. This is an expensive and time-consuming task; it has also been found that due to weld shrinkage that even when the weld cap is removed

the top surface of the component is still slightly irregular. This prevents complete test coverage and increases the time and cost associated with the inspection. Once the weld cap has been removed the current inspection is then performed using a large number of different single element probes to generate beams with a range of angles and focal lengths.

The time and cost associated with completing the inspection of the target application could potentially be improved by using a conventional rigid wedge phased array. This would allow multiple beams to be generated using a single phased array probe. Electronic scanning could also be used in place of some mechanical axial scanning to increase inspection speed. However, the weld cap would still need to be removed to allow inspection coverage. The larger footprint associated with the conventional phased array would make it more challenging to maintain a uniform couplant layer due to weld shrinkage. Therefore in order to achieve the benefits associated with phased array inspection but maintain, and ideally improve, the inspection coverage with the weld cap in place the membrane coupled phased array has been developed. The target of this work is also to minimise the amount of mechanical axial scanning required to complete the inspection; this will improve inspection speed and potentially reduce manipulator complexity. To achieve this aim a large footprint phased array transducer is used.

In this chapter the inspection development process will be reviewed, this includes the design and manufacture of suitable flat plate, non-welded test-pieces. These test-pieces did not contain an actual weld but did have weld metal deposited on their surfaces to produce a weld cap representative of that found in the target application. During the early phase of development the non-welded test-pieces were used as this eliminated many of the additional challenges caused by the presence of austenitic weld material. However, because these test-pieces did contain a representative weld cap it allowed the mechanical challenges of conforming to the complex geometry of the component to be addressed in isolation. A detailed review of the inspection techniques used to detect each of the defects embedded into the flat plate, non-welded test-pieces will then be carried out. A comparison between the performance of the membrane coupled device and conventional inspection techniques is then provided in section 3.4.

3.1. Test-Piece Development

Development of the 2nd generation membrane coupled device was performed by producing inspection procedures to achieve complete inspection of the target application component. I started this development process by completing a thorough review of the current inspection procedure used on the target application and on similar inspections (Rolls-Royce, 2001a; Rolls-Royce 2002b). In the current inspection the weld cap must be removed in order to provide the required test coverage (Rolls-Royce, 2001b). Removal of the weld cap is a time consuming, manual process which can also impact the structural integrity of the component. Removal of the weld cap can expose small buried flaws which subsequently must be removed by further grinding. Weld metal is also typically softer than the parent material leading to a potential risk of undercut and an unacceptable reduction in component wall thickness. Weld cap removal when the component is already in service can be even more difficult due to reduced access to the component. It is therefore desirable to test the components in service with the weld cap in place.

As shown in Fig 3-1 the target application is a stainless steel section of pipe-work that contains an austenitic weld with a convex weld cap. The presence of the austenitic weld introduces two main areas of complexity in terms of the ultrasonic inspection. The first challenge is associated with the irregular surface geometry of the component under test and the second issue is related to the grain structure within the weld. Therefore in order to simplify the inspection development process two flat plate non-welded test-pieces were produced. These test-pieces were manufactured from a single plate of stainless steel with a wall thickness of greater than 50mm. The wall thickness of the flat plate test-pieces was selected to replicate that of the actual target application component. Unfortunately, due to security restrictions associated with this development work it is not possible to provide further details of the component geometry. Specifically it is not possible to provide the exact wall thickness or diameter of the pipe-work. Weld metal was deposited onto the surface of the two flat plates to produce an undressed weld cap representative of that found in the target application. A tungsten inert gas (TIG) welding process was used that is representative of the actual weld procedure (BAE Systems, 1986). Two test-pieces were produced so that each individual test-piece could be manually moved. The

target application pipe surfaces are assumed to have internal and external surfaces machined concentrically and to have a surface roughness of 6.4μm or better. The flat plate, non-welded test pieces will be machined to a similar surface roughness.

The goal of this inspection is to reliably detect and size all the defects described in the defect description document (Rolls-Royce, 2006c) with the undressed weld-cap in place. The defect description document describes nine different defect types including both planar and volumetric defects of different sizes. The two flat plate non-welded test-pieces have been designed to include examples of the worse case planar defects considered credible based on the defect description document.

The amplitude of the ultrasonic response from planar defects is highly dependent upon the angle at which ultrasound impinges upon the defect. Therefore in order to accurately detect planar defects the ultrasonic technique must be carefully controlled. Detection of the volumetric defects such as porosity and inclusions is generally simpler because the ultrasonic beam to defect orientation is much less critical. However, volumetric defects such as porosity are often small, also in the case of inclusions there is only a small change in acoustic impedance between the defect and the parent material, therefore the amount of ultrasonic energy reflected from the defect can be limited. In both cases this leads to a defect signal with low amplitude. These are fundamental limitations of ultrasonic inspection and are not specific to the membrane coupled device. This issue is not being specifically addressed at this stage in the development of the conformable array. It is also not possible to intentionally embed volumetric defects into the non-welded test-pieces and this type of defect has not been included in the test-pieces developed at this stage. Planar defects with significant through wall dimensions are considered to be a greater risk from a structural integrity standpoint. Therefore only planar defects are included in the two flat plate, non-welded test-pieces.

All of the defects included in the test-pieces are described in Table 3-1. The postulated shape of all defects is elliptical with a 2:1 aspect ratio (length to through-wall extent) and it is assumed that elliptical flaws have their major axis parallel to the direction of the weld (Rolls-Royce, 2006c). The through-wall extent of the defects is based on the approximate height of two weld beads. Based on the

welding procedure document (BAE Systems, 1986) two weld beads equates to approximately 3-4.2mm. The choice of 4mm as the target through-wall defect size is therefore somewhat arbitrary but is chosen to provide a challenging target for the ultrasonic phased array system. Schematic diagrams of the six different defects are provided in Fig 3-2, defects 1-3 are contained within evaluation block 1 (Rolls-Royce, 2006a) and defects 4-6 are contained in evaluation block 2 (Rolls-Royce, 2006b). In both test-pieces the defects are separated from the side-wall of the test-piece by at least 60mm, each defect is then also separated from its nearest neighbour by 60mm. This approach ensures that each defect can be imaged individually which simplifies the data interpretation process. A photograph of the two test-pieces is shown in Fig 3-3. Defects 1, 2 5 and 6 are elliptical with a size of 4mm x 8mm and have been produced by electro-discharge machining (EDM). In the case of the two mid-weld defects artificial flat bottomed hole (FBH) defects were drilled into the test pieces with a diameter of 5.6mm. This approach produces a defect with a comparable cross sectional area to the elliptical 4mm x 8mm defects. This drill hole is indicated by the dotted line in Fig 3-2c and 3-2d.

Table 3-1 Defect Description for flat plate, welded test-pieces

Defect Number	Type of Defect	Location	Tilt	Skew
1	Lack of root fusion	Centreline of simulated weld region - inner surface breaking	0°	0°
2	Lack of sidewall fusion	Along lower simulated weld fusion face - inner surface breaking	25°	0°
3	Lack of sidewall fusion	Along lower simulated weld fusion face - at highest point of 25° prep angle from inner surface	25°	0°
4	Lack of sidewall fusion	Along upper simulated weld fusion face - at lowest point of 10° prep angle from outer surface	10°	0°
5	Lack of sidewall fusion	Along upper weld fusion face - outer surface breaking	10°	0°
6	Structurally significant planar defect derived from LEFM[1]	Centreline of simulated weld - under weld cap with ligament of 2-5mm to outer surface	0°	0°

Notes

1. LEFM – Linear Elastic Fracture Mechanics

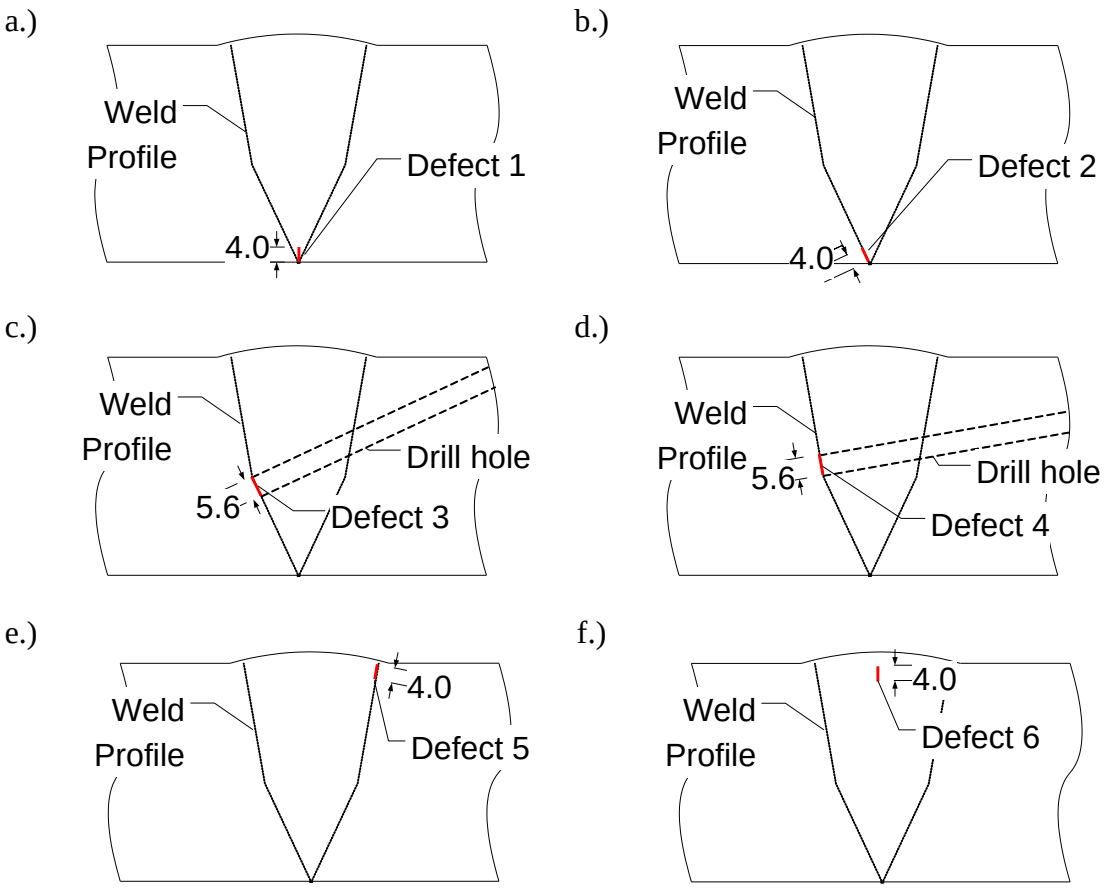

Figure 3-2 Schematic diagram of defects contained in the conformable phased array non-welded evaluation blocks, a.) defect 1, b.) defect 2, c.) defect 3, d.) defect 4, e.) defect 5, f.) defect 6.

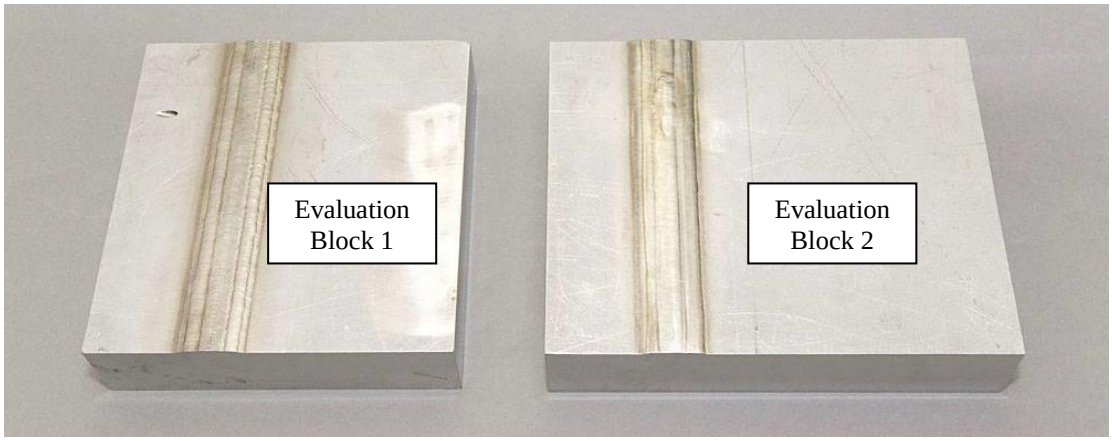

Figure 3-3 Photograph of the two flat plate, non-welded test-pieces.

Each of the defects described in Table 3-1 was artificially introduced into the non-welded test-pieces during manufacture. Defects 1-4 and 6 were introduced prior to adding the weld cap, in the case of defects 1-4 this approach made manipulation of the test-pieces more straightforward, whereas defect 6 had to be added before welding to

produce the required ligament. Defect 5 was embedded after the artificial weld cap had been deposited to ensure that the defect occurred at the weld toe. All of the EDM work and the deposition of the weld cap were performed by Rolls-Royce personnel.

The width of the surface breaking flaws is the separation ("gape") between the flaw faces. It is assumed that these faces are not under any significant compressive stress; this assumption is valid given the manufacturing process. When developing the test-pieces to demonstrate the techniques described in this document a best endeavour attempt was made to accurately produce these flaws with a gape as described in the defect description document (Rolls-Royce, 2006c). However, the actual gape of each defect within the test-pieces is dictated by the machining technique used. The gape of the defects produced by EDM is likely to be approximately 300µm for all of the defects. Mid-wall defects in non-welded components can only be produced by drilling a FBH at a suitable angle. However, by using this technique the gape of the flaw will no longer be representative of the actual defect. More realistic embedded defects will be used in the manufacture of flat plate welded test-pieces. The inspection of these welded test-pieces is discussed in Chapter 6.

The defect description document (Rolls-Royce, 2006c) states that all defects will have a roughness of 13-37µm. Surface roughness tends to reduce the amplitude of any specular reflection but can also improve defect detection when insonified at oblique incidence. This is because the defect has facets at a range of different angles, some of which may be orientated favourably for detection. Surface roughness only causes a significant reduction in the surface reflectivity if the roughness is greater than approximately 10% of the wavelength (Ogilvy, 1991). Even when considering the maximum frequency content, and hence minimum wavelength, of the ultrasonic pulse used in the inspection the maximum surface roughness is expected to be 2.5% of the longitudinal wavelength and 5% of the shear wavelength. Therefore the expected defects can be considered ultrasonically smooth and the artificial defects included in the test-pieces can be considered representative.

Flaws occurring in the actual target application can occur at a range of tilts and skews. If the major axis of the flaw is taken to lie in the plane of the flaw, such that it is parallel to the direction of the weld, the tilt is then measured as a rotation of the flaw

about its major axis. Skew is measured as a rotation of the major axis about the local surface normal. A longitudinal (circumferential) flaw is taken to have 0º skew. The orientation of all of the flaws in the non-welded test pieces is accurately known. Although the exact tilt and skew of the six defects in the flat plate test piece are known the inspection techniques developed must be capable of dealing with a variety of defect orientations. Defects have been produced within the flat plate, non-welded test-pieces at a range of tilts but all defects have a nominal skew of 0˚. This approach was used because it is postulated that all possible defects within the target application component will occur along the weld and the defect skew will not vary. Consideration of defects with different skew angles is therefore not included in this thesis. When using transducers with a finite aperture size to detect real planar defects of finite size and imperfect smoothness a specular reflection will occur over a small range of angles. Toft (Toft, 1987) has shown experimentally that defect misorientation of about 15º tilt or skew gives a defect response within 6dB of the response obtained from a defect with perfect orientation. Scanning at additional angles was therefore not performed on the flat plate, non-welded test-pieces. One of the benefits of the phased array test approach is that scanning at more angles can easily be incorporated with minimal increase in time and without adding any additional scanning requirements or capital cost to the inspection, particularly if FMC data acquisition is used. The use of FMC data acquisition was discussed in detail in chapter 2. However, scanning additional angles using a single element test approach necessitates the use of additional scan for each new test angle and the purchase of a new wedge to generate each of the different angles.

3.2. Technique Description

At the start of the inspection development process I identified a primary detection technique for each of the defects present within the flat plate, non-welded test-pieces. The focus of this work is to develop the membrane coupled device inspection capability and defect sizing has not been considered as part of this activity. These detection techniques represent a subset of the range of techniques employed in the current single element transducer inspection. The primary detection technique for each of the critical defects was chosen with two major considerations in mind. The test pieces used do not contain an actual weld, therefore any inspection techniques that traverse the weld region were not considered. Secondly the test pieces have been

designed to allow single sided access; this is equivalent to the inspection of straight pipe to elbow welds. Therefore all testing of the flat plate, non-welded test-pieces was performed from one side of the simulated weld region only. No testing was carried out from left to right on the test-pieces shown in Fig 3-3. Despite the test-pieces not containing an anisotropic austenitic weld, the goal of this testing was to develop inspection techniques that could in the long-term be applied to welded structures. Shear waves are very highly attenuated and scattered by austenitic weld material and are therefore not typically used for stainless steel weld inspection. The primary detection techniques were selected with this inspection limitation in mind so that longitudinal wave inspections have been used where possible.

The primary detection methods used to detect defects 1-6 in the flat plate, non-welded test-pieces essentially represent three different ultrasonic inspection techniques. These techniques are described below:

1. Corner echo
2. Transverse-Longitudinal (TL) skip
3. Transverse-Longitudinal-Longitudinal (TLL) skip

3.2.1. Corner Echo

Surface breaking defects oriented normal to the component surface are typically detected using the corner echo technique. Ordinarily a 45º shear wave is used as this gives the strongest indication from this type of interaction (Krautkramer & Krautkramer, 1983); this type of inspection is shown in the schematic diagram in Fig 3-4. The shear wave is not expected to traverse any weld material in this type of inspection technique, so attenuation and scattering of the shear wave is not an issue.

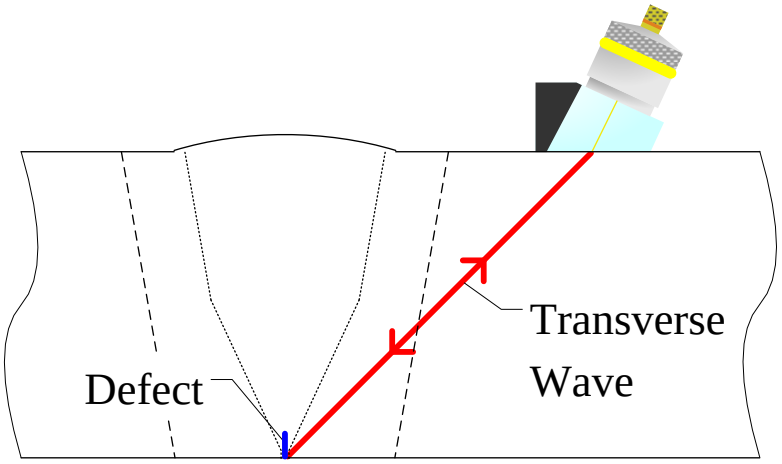

Figure 3-4 Schematic diagram of corner echo technique.

3.2.2. Transverse-Longitudinal (TL) Skip

The Transverse-Longitudinal (TL) mode conversion skip technique is a type of indirect specular reflection. The technique involves a beam of ultrasound insonifying the defect specularly after a reflection with a surface within the component. In this situation a reflection occurs at the backwall of the component; this represents the inner diameter of the target application pipe-work. This technique is analogous to the full-skip inspection commonly applied in shear wave inspection of ferritic welds where a transverse-transverse inspection technique is employed (British Standards Institution, 1998b).

Due to the orientation of the defects to be detected it is necessary to use a high angle ultrasonic beam to achieve a normal incidence specular reflection. A longitudinal wave is used to minimise the potential effects of scattering and beam steering when considering an actual welded component. Access is limited to the outer surface of the component only; therefore a suitably angled longitudinal wave can be generated using two different techniques. The first is to use a high angled longitudinal wave transducer positioned appropriately so that the longitudinal leg reflects from the backwall and impinges specularly on the defect. This technique is ineffective due to high mode conversion losses at the backwall reflection and a very broad beam width. As a consequence of generating an angled longitudinal beam, an associated angled shear wave is also generated. The second inspection technique uses this angled shear

wave, upon reflection from the backwall the shear wave mode converts into both an angled compression wave and an angled shear wave. The compression wave generated through this mode-conversion is at the same angle as the original compression wave produced by the transducer.

The amplitude of this mode-converted longitudinal wave is appreciable. The reflection coefficient for shear and longitudinal waves at a boundary between steel and a vacuum for an incident shear wave are provided in Fig 2-3b and is reproduced in Fig 3-5. The diagram in Fig 3-5 shows how the amplitude of the reflected shear and longitudinal wave varies at a steel/air interface for different angles of incident shear wave. As the angle of the incident shear wave is increased the amplitude of the reflected shear wave rapidly decreases, whilst the amplitude of the mode-converted compression wave undergoes a corresponding increase in amplitude. Due to the high amplitude of the mode-converted longitudinal wave it can be used for defect detection. The mode-converted longitudinal wave is specularly reflected from the defect, a further mode-conversion into a shear wave then occurs at the backwall and the transducer records a signal from the shear wave. This technique is used for the detection of a range of defects; it is shown in the schematic diagram in Fig 3-6.

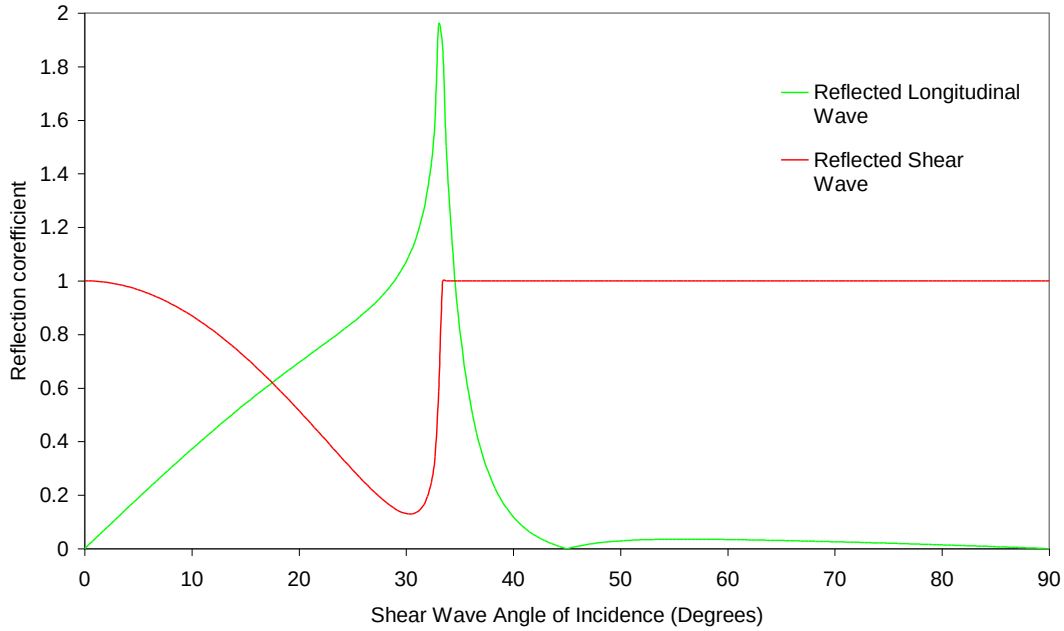

Figure 3-5 Schematic diagram of the amplitude variation of the shear(S) and mode-converted longitudinal (C) waves reflected at a steel/air interface when a incident shear wave at angle β strikes the boundary.

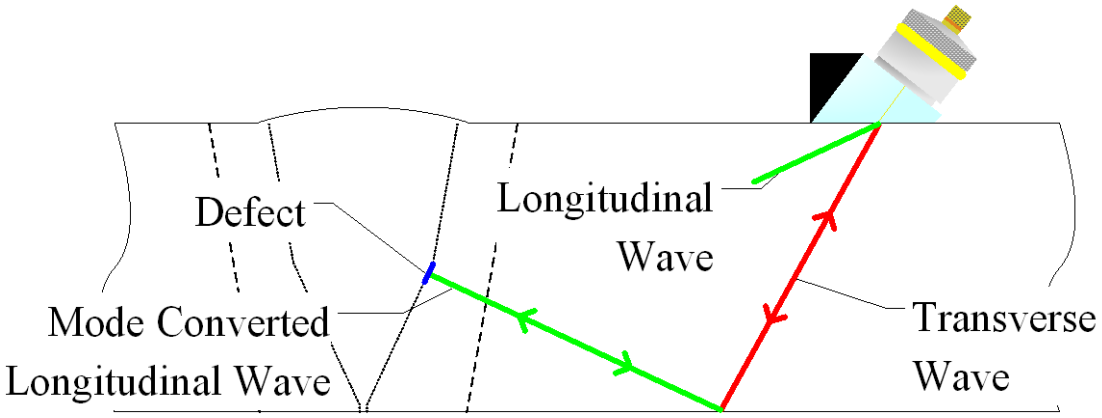

Figure 3-6 Schematic diagram of the Transverse-Longitudinal (TL) skip inspection technique.

3.2.3. Transverse-Longitudinal-Longitudinal (TLL) Skip

There is a requirement to detect planar defects of through-wall orientation (0º tilt) and defect at tilts of ± 10º relative to the through-wall orientation. These types of defects give low signals at the highest practicable direct beam angle of approximately 70º. An alternative technique to generate a reliable specular reflection is therefore

required. A Transverse-Longitudinal-Longitudinal (TLL) skip technique can be used to provide a suitable defect response. Using this technique two high angle compression probes are used in a pitch-catch arrangement. The transmitting probe generates a compression wave and an associated transverse wave. When the transverse wave interacts with the backwall it generates a mode-converted compression wave and a reflected transverse wave. The mode-converted compression wave can then be reflected from a through-wall orientated defect and detected using the receiving probe. This detection technique is shown in the schematic diagram in Fig 3-7. By controlling the separation between the transmitting and receiving probes it is possible to change the depth of optimum sensitivity. Therefore the separation used must be optimised to ensure that each different defect is detected.

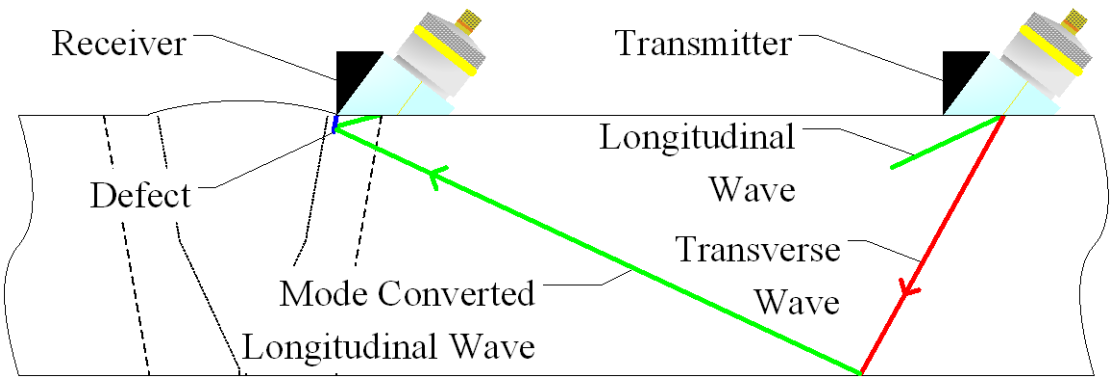

Figure 3-7 Schematic diagram of the Transverse-Longitudinal-Longitudinal (TLL) skip inspection technique.

The TLL skip technique is a more general description of the self-tandem (ST) technique. The ST technique is simply the TLL with zero probe separation; this is shown in Fig 3-8. It is possible that in some scenarios it would be possible to use the TLL technique as ST. This would be dependent on defect through wall position and probe size.

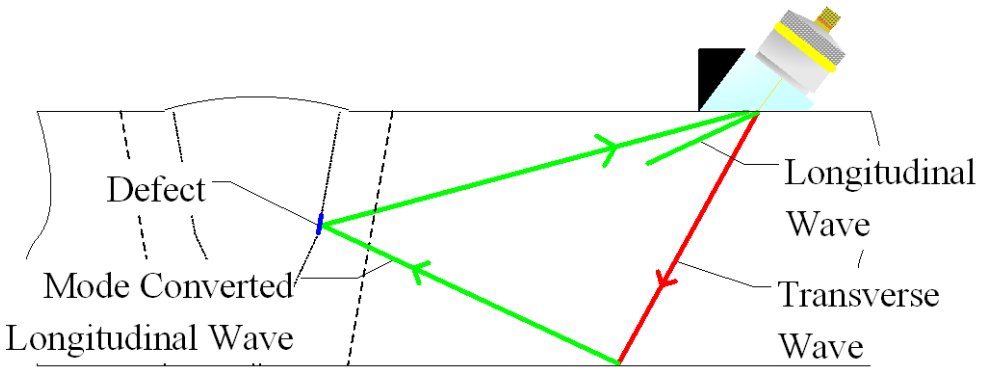

Figure 3-8 Schematic diagram of the self tandem inspection technique.

A summary of the primary detection technique used to detect each of the six defects in the flat plate, non-welded test-pieces for each of these is provided in Table 3-2. Defect 1 is detected from the corner echo response using a 45º shear wave. The inspection of defect 2 and 3 is performed using the same 65º longitudinal wave TL mode conversion technique. Defect 4 is detected using a 65º longitudinal wave TLL mode conversion technique, there is a small separation between the optimum position of the transmit and receive paths but typically a self tandem approach can be used. The inspection of defects 5 and 6 is again performed using a single technique, for these two defects a pitch-catch TLL mode conversion approach is used. A rigid wedge 48 element phased array transducer is used as a transmitter. The 80 element membrane transducer, discussed in chapter 2, is positioned over the weld cap and is used as a receiver only. All experimental testing has been carried out using a Peak NDT (Derby, UK) MicroPulse 5PA phased array controller with 128 parallel channels. The pitch-catch configuration used to detect defects 5 and 6 is the largest number of elements that can be addressed using this equipment. The size of the two flat plate, non-welded test-pieces has been designed to ensure that the primary detection technique for each of six defects can be suitably deployed. The length of evaluation block 2 is therefore greater than evaluation block 1 to accommodate the phased array pitch-catch arrangement. This difference in the size of the two test-pieces is clear from the photograph in Fig 3-3.

Table 3-2 Defect Description for first stage of membrane coupled phased array device inspection development (OD – Outer Diameter).

Defect	Description	Tilt°	Primary Detection Technique
1	Lack of root fusion	0	Corner echo using 45° shear
2	Lack of sidewall fusion	25	Transverse – longitudinal (TL) using 65° compression
3	Lack of sidewall fusion	25	Transverse – longitudinal (TL) using 65° compression
4	Lack of sidewall fusion	10	Self tandem, transverse – longitudinal - longitudinal (TLL) using 65º compression
5	Lack of sidewall fusion	0	Pitch-catch, transverse – longitudinal - longitudinal (TLL) using 65° compression
6	Structurally significant planar defect derived from LEFM[1]	0	Pitch-catch, transverse – longitudinal - longitudinal (TLL) using 65° compression

Notes

1. LEFM – Linear Elastic Fracture Mechanics

3.3. Inspection Development

The current inspection of the target application component is performed using 15 different single element transducers in five different probe pans (Rolls-Royce, 2002b). When completing this inspection a large amount of mechanical raster scanning must typically be performed to provide maximum coverage of the inspection volume. The scanning speed using this approach is limited which leads to a long inspection time. When completing a phased array inspection it is possible to replicate the single element transducer performance by exciting an aperture within the array and electronically scanning this aperture along the array. As discussed in chapter 2 this approach is typically 10 times faster than mechanical raster scanning (RD Tech, 2004). It is also possible to use different delay laws to steer the beam generated by the transducer over a range of angles. This allows multiple different single element transducers to be replaced with a single phased array probe. Ideally all of the single element transducers would be replaced by a single phased array probe. This is

impractical for an inspection as complex as that required on the target application but would be possible in some circumstances. The focus for this development work is to reduce the number of phased array probes required as far as possible and to simplify the inspection procedure. The 80 element, 2nd generation membrane probe, which has been discussed in chapter 2, was therefore designed with a large footprint to minimize the amount of axial scanning required.

The inspection of the flat plate, non-welded test-pieces was performed using different phased array based approaches. Multiple phases of testing were performed, but in each case data was collected using FMC with a 128 channel Peak NDT MicroPulse 5PA. Testing was primarily performed with a 2MHz centre frequency, 1.25mm pitch, 48 element, linear phased array with a Perspex rigid wedge and the 80 element, 2nd generation membrane coupled device. In both the Perspex wedge and the 2nd generation membrane coupled device the wedge angle was controlled to produce a longitudinal wave with a natural angle of 65º in stainless steel. A photograph of both probes is shown in Fig 3-9.

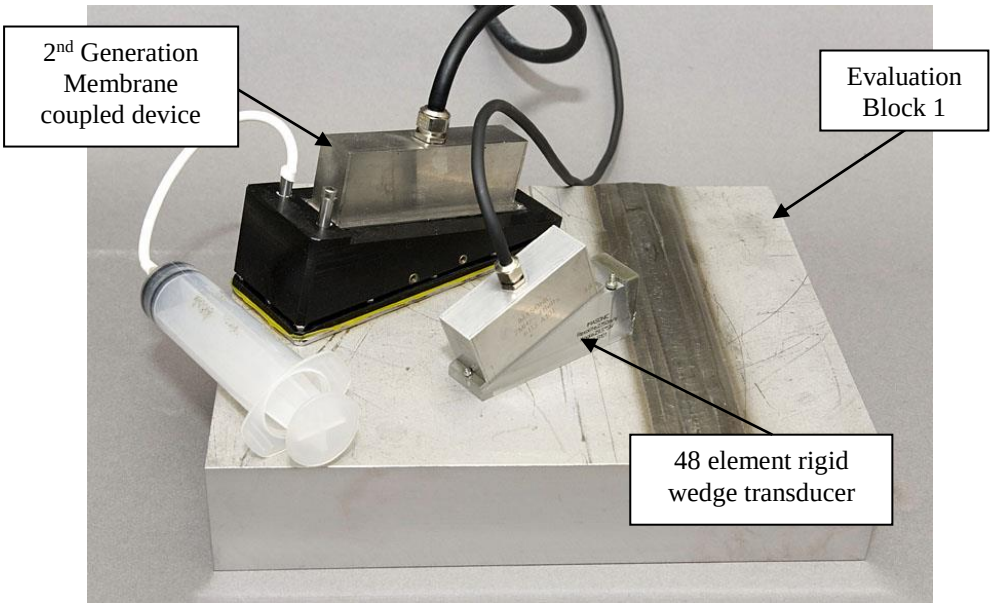

Figure 3-9 Photograph of the 2nd generation membrane coupled device and the 48 element rigid wedge linear phased array.

The rigid Perspex wedge contains irrigation channels but suitable fixtures to connect to these channels were not available. The 2nd generation membrane coupled device also does not provide any means of irrigation. Therefore all inspection testing with

both probes was carried out in contact immersion. In this type of inspection the component is placed in an immersion bath with sufficient water to just submerge the component. This approach eliminates issues related to variable coupling between the transducer and the component under test. This technique still involves use of the membrane material itself and allows appraisal of the performance of membrane device but is not fully representative of the way the device will be used on an actual application. The inspection was performed in an automated x-y scanning frame using a custom jig mechanism. The jig was specifically designed for development of the membrane probe inspection capability and offers a high degree of flexibility in terms of controlling the transducer position and height. Lionel Reyes (Rolls-Royce, Senior Design Engineer) assisted in producing the final design for this scanning mechanism.

The ride height of the membrane coupled device, defined as the distance between the base of the metal picture frame and the flat plate outer surface must be controlled to accommodate the weld cap. In the target application the weld cap is not expected to exceed 4mm in height relative to the parent material. A ride height of 6mm is therefore selected to ensure sufficient clearance between the probe and the component.

As discussed previously the 2nd generation probe uses a constant pressure design, however, it is not possible to rely on the pressure within the membrane cavity to support the weight of the transducer and the jig assembly. An alternative approach is therefore required to ensure that a constant ride height is maintained. Ideally the scanning frame assembly would include the capability to control this ride height and allow the membrane device to be fixed a set distance away from the component under test. This approach will be adopted when a bespoke pipe-manipulator is designed. However, this is not possible using the current x-y scanning frame and an alternative technique is required. In the x-y scanning frame a weight is used to force the transducer into contact with the component. In order to prevent the metal picture frame contacting with the component a second, rigid wedge transducer is used to control the ride height. This configuration is shown in the photograph in Fig 3-10. The membrane device jig assembly ensures that the height of the membrane device can be accurately controlled.

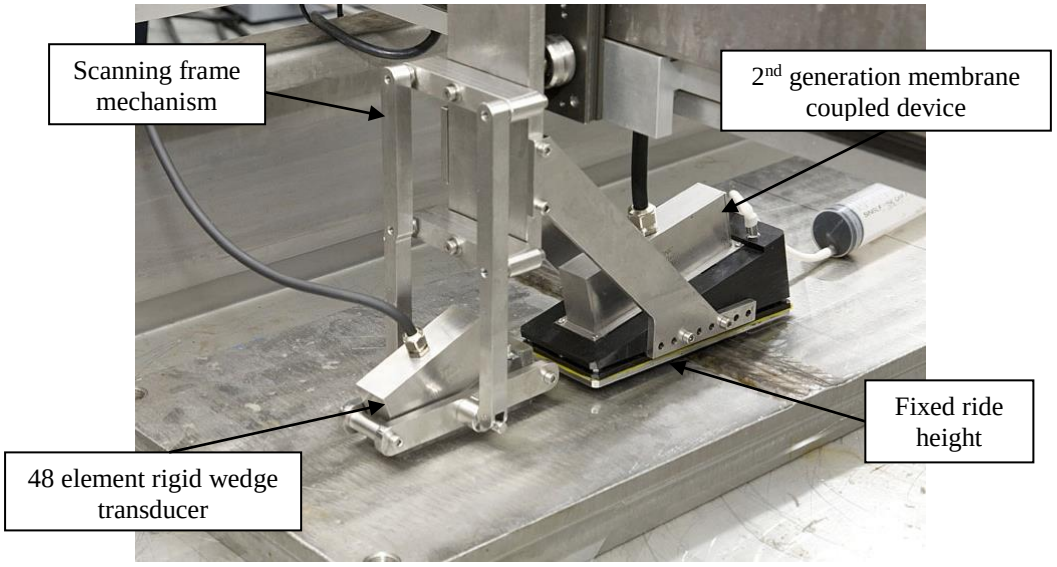

Figure 3-10 Photograph of the 2nd generation membrane coupled device inspection showing the scanning frame configuration.

As discussed the inspection techniques used to detect defects 2 and 3 is identical. In order to optimize the technique for the detection of each defect the transducer position relative to the centre of the weld must be changed. However, by using a large phased array transducer in the membrane coupled device it is possible to minimize the amount of transducer movement required. Results from the inspection of defect 2 only will be discussed in this thesis. The inspection of defects 5 and 6 is also the same and only results from the inspection of defect 6 are included in this thesis. Both of these defects represent a major challenge when using the primary detection technique with conventional rigid wedge transducers. However, when using conventional probe technology defect 5 can be detected by using a full skip corner echo technique. This technique is shown in the schematic diagram in Fig 3-11. Defect 6 cannot be detected using this technique because it is inappropriately positioned to provide a corner echo. Without the removal of the weld cap it is not possible to detect defect 6 using conventional rigid wedge transducers. However, it is possible to detect this defect using the 2nd generation membrane device and results from this inspection will be presented.

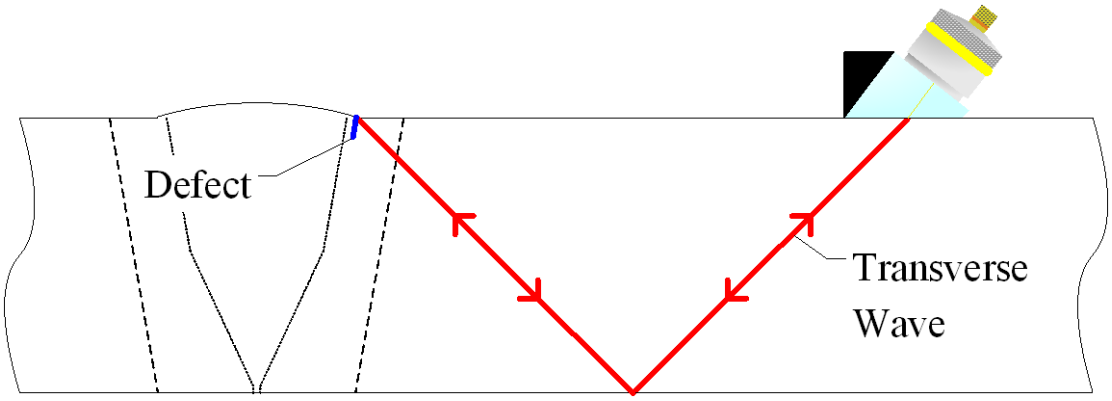

Figure 3-11 Schematic diagram of the Transverse-Transverse (TT) full-skip inspection technique.

When using conventional single element transducers the probe must be mechanically scanned to achieve the maximum coverage of the inspection volume. By using a phased array it is possible to achieve coverage from a single transducer position. In both cases when displaying the experimental results obtained from an inspection it is necessary to be able to correctly position the ultrasonic responses within the inspection volume. In conventional ultrasonic testing the index point of the transducer is typically used, where the index point refers to the centre of the ultrasonic beam. The index point of the transducer is found experimentally during calibration (British Standards Institution, 2001). When using FMC based inspection all possible inspection data is collected in a single acquisition and an image of the inspection volume is produced in post-processing. It is not possible to measure the index point for the ultrasonic beam during the data collection phase. Therefore an alternative reference point is required that can be easily measured by the operator when setting up the inspection. The back of the probe housing is used as this reference point. The offset between the back of this housing and the index point of the actual beam generated is then calculated so that the ultrasonic signals are suitably positioned.

3.4. Experimental Results

The performance of the 2nd generation membrane coupled device can be quantified by comparing the results obtained for the inspection of the two flat plate, non-welded test-pieces to those achieved using conventional rigid wedge technology. In order to make a direct comparison between the two different approaches a calibration procedure is required. FMC data acquisition is relatively immature technology, so no standards exist governing the use of this approach and a recognised calibration routine

does not yet exist. Rolls-Royce is keen to address this limitation and I am leading the project to develop a full calibration routine. This work is being performed in collaboration with researchers at Imperial College, University of Bristol and engineers at Serco TAS. However, this development activity is ongoing and has not yet been finalised. An alternative approach to calibration has therefore been adopted in this work.

A fixed gain of 45dB has been used to collect all FMC data with the 2nd generation membrane coupled device. This gain is selected as it provides a good defect response from a single element without saturating the single element signal from reflectors within the test-piece. The front wall echo does saturate but this is gated out in the time domain when processing the FMC data and does not affect the accuracy of the results. A baseline comparison between the membrane device results and those obtained from the 48 element rigid wedge transducer is then made using the response from a single 3mm diameter SDH defect. Calibration testing was performed on a stainless steel test-piece containing a range of SDH defects. This test-piece was selected because it had approximately the same material properties as the two flat plate, non-welded test-pieces and a similar wall thickness. A schematic diagram of the test-piece and the experimental set-up using the membrane device is shown in Fig 3-12. In each case the transducer is positioned so that the centre of the array is positioned appropriately to provide an optimum response from the 35mm deep SDH defect with a direct 65º longitudinal wave. This SDH defect was selected because it is relatively isolated from the other features within the block and hence could be used as a single reference point for the calibration. The full matrix of A-Scan data was acquired using both transducers and processed using the Imperial College FMC processing software. For each transducer the FMC data is processed to produce an unfocused direct 65º longitudinal wave inspection of the test-piece using a 10 element (12.5mm) aperture. The first step in the calibration procedure was to acquire and process the 2nd generation membrane probe data with a fixed gain of 45.0dB. The data was processed and the 35mm deep SDH response was recorded as shown in Table 3-3. The relative amplitude of the signal is automatically calculated by the FMC post processing software. The SNR is measured by gradually reducing the dynamic range of the image until the background noise is removed; this approach is representative of that used elsewhere within industry. An iterative approach was then

used to set the gain when completing the SDH test-piece inspection using the 48 element rigid wedge transducer. By using this approach it was found that approximately the same amplitude SDH response could be obtained when using a gain of 43.25dB with the 48 element array. The amplitude and SNR of the 35 mm deep SDH signal is again shown in Table 3-3. All subsequent testing with the 48 element array was therefore performed using a gain of 43.25dB.

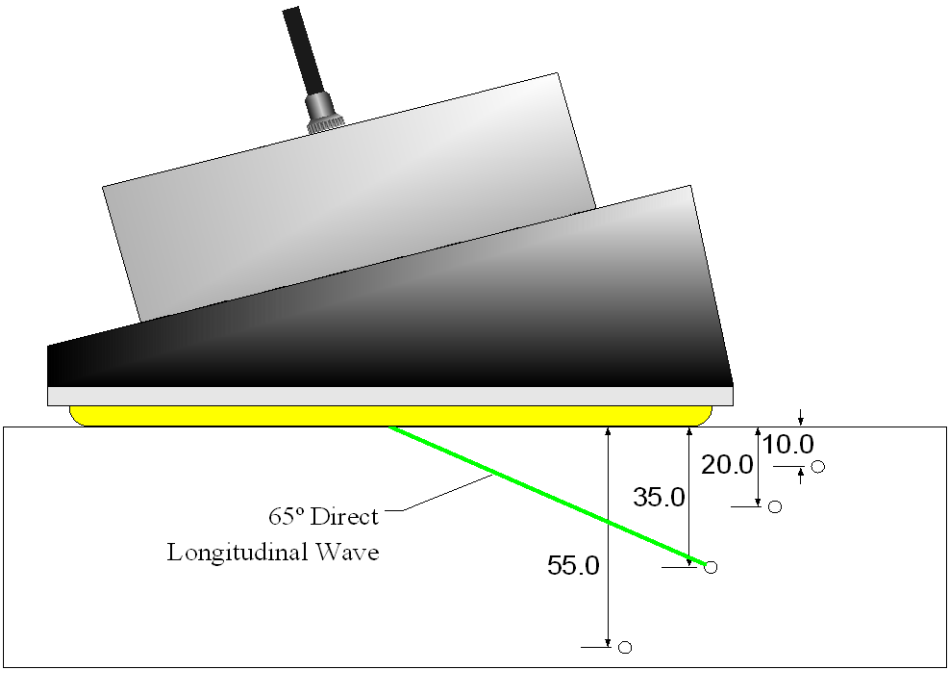

Figure 3-12 Schematic diagram of the flat plate non-welded test-piece calibration set-up.

Table 3-3 SDH calibration experimental data obtained using the 2nd generation membrane device with 45dB gain and the 48 element rigid wedge phased array with 43.25dB gain.

Transducer	Aperture Size (Elements)	Beam Steering	
		SNR (dB)	Max Amplitude (A.U.)
2nd generation membrane	10	20	12
48 element rigid wedge	10	17	12

This approach to calibration ensures that if each of the two arrays is in a suitable position to ensure that the centre of the array insonifies the defect then the flaw

response measured will be is approximately equal. However, the results indicate there is likely to be some difference in the response from different regions of the array. Table 3-3 shows that the SNR of the response from the 35mm deep SDH defect is slightly worse when using the 48 element rigid Perspex wedge array than the 2nd generation membrane coupled array. However, the level of difference between the two devices is relatively small and this is not considered to be an issue. The region of the test-piece that is insonified using the 48 element device from a single position is significantly less than when using the 2nd generation membrane device. This is because the overall size of the rigid wedge array is less than that of the 2nd generation device. Correct positioning of the 48 element rigid wedge array is therefore more critical than for the 2nd generation device.

All experimental testing with the membrane coupled device and the rigid wedge array was completed with between 4 and 8 averages. This approach was taken to reduce the level of incoherent noise, thus improving SNR without excessively increasing the time required to complete the measurements. Testing was completed at a 25 MHz sampling rate, which is well in excess of the Nyquist frequency for the array signal.

A comparison of the results obtained using both transducers for the four defects considered are discussed below. As stated previously the acquisition and processing of FMC data is relatively immature and when this testing was carried out it was not possible to capture and process encoded scan data. Commercially available phased array controllers are not designed to perform this type of inspection, bespoke software is required to acquire this type of data and process it. This requirement is being addressed in the next phase of this project and will be used in the future. At this stage in development it is only possible to collect inspection data from a single probe position. However, this is not a significant limitation in this study and meaningful comparison between the performance of the 2nd generation membrane device and conventional technology can still be made. The use of a large footprint array also allows coverage of much of the inspection volume from a single transducer position and scanning the transducer is less critical.

In the comparison of results discussed below, each transducer is positioned in approximately the correct position so that energy from the centre of the array

impinges on the defect. Small variations in the position of the array relative to the component under test is the main source of error within the experimental measurement and this contributes to the predicted variation of up to ±1 dB in the results. The FMC data is then acquired and suitably processed using the Imperial College FMC post-processing suite. A direct comparison can then be made between the two B-Scans obtained. This approach does not allow a comparison of the defect length sizing (circumferential extent) using the two different transducers. However length sizing is typically carried out using the 6dB drop technique (British Standards Institution, 2008) and is dependent on the lateral beam width. The width of the array element is the same in both transducers and hence the beam width is comparable. The defect length measured using both transducers will therefore be very similar.

In order to make meaningful comparison between the two different transducers the FMC data has been processed in a number of different ways. Initial comparison is made using a 10 element or 12.5mm aperture with both a focused and an unfocused beam. When completing a focused inspection, a single focal depth is used corresponding to the centre of the defect. A phased array can only be used to focus a beam within the near field of the array aperture used for the inspection. For inspections with a long path length such as many of those performed in testing the flat plate, non-welded test-pieces a large aperture must be used to provide effective focusing. A second comparison is therefore made using an aperture of 24 elements or 30mm. This aperture size is limited by the overall size of the rigid wedge transducer and is selected as a compromise between increasing the focal range of the array being used and limiting the B-Scan width from a single transducer position.

A comparison was carried out of the maximum amplitude of each defect signal and of the localised SNR around the defect. The value of the maximum amplitude signal is automatically provided by the post processing software, this gives a measure of the relative beam intensity at different steering angles and hence a measure of inspection quality. It is important when completing this comparison that the maximum signal in the image is due to the defect signal and not a spurious signal. In order to achieve this it is necessary at times to consider a smaller image region. The signal to noise ratio for each inspection is assessed by eye from the images generated. This approach is somewhat subjective but is in line with that used currently when interpretation

engineers use platforms such as the British Energy (British Energy Group PLC, East Kilbride, UK), Graphical User Interface Data Evaluation (GUIDE) and is accepted within the broader nuclear industry. Also I am a qualified Level II GUIDE user and have received training in this interpretation process.

3.4.1. Defect 1

Defect 1 is inspected using a 45º shear wave corner echo technique; this technique is shown using the two different transducers in the schematic diagram provided in Fig 3-13. In order to generate this beam angle suitable delay laws must be generated to steer the ultrasonic beam away from the natural angle of the transducer. When using this approach it can be seen from the results in Table 3-4 that both transducers can be used to detect the defect using both aperture sizes considered. However, there is a major difference between the amplitude of the response using the two different transducers. The relative time delay between the firing of adjacent elements in the two probes is different because of the disparity in ultrasonic velocity in the two different wedge materials used. This gives rise to differences in the amplitude of the beam and leads to the variation in the amplitude of the response. The improved defect SNR that is achieved when using the 48 element transducer is due to a reduction in the background noise within the rigid wedge design. When the aperture size is increased the amount of energy impinging upon the defect also increased, this leads to a higher amplitude response. There is an improvement in the performance of the inspection when using a focused beam with the larger aperture using both transducers. This is because the larger aperture allows effective focusing at the depth of the defect. The use of single depth focusing with the 24 element aperture at the centre of the defect (corresponding to 56mm depth) improves the SNR performance of the 2nd generation transducer so that the performance is comparable to the rigid wedge transducer.

a.)

b.)

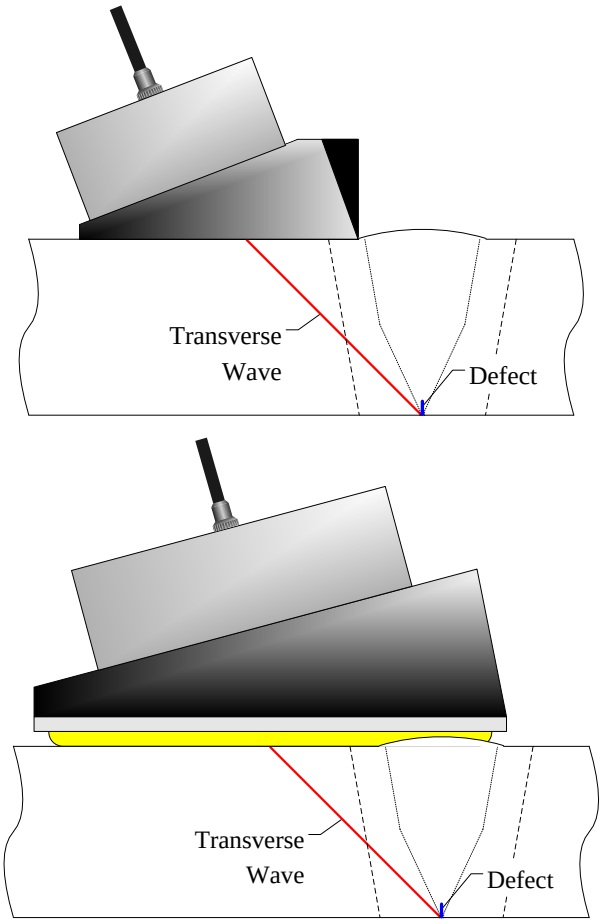

Figure 3-13 Schematic diagram of the inspection of defect 1 using a.) the 48 element rigid wedge phased array and b.) the 2nd generation membrane coupled device.

Table 3-4 Experimental results for the inspection of defect 1.

Transducer	Aperture Size (elements)	Beam Steering		56mm focal length	
		SNR (dB ± 1 dB)	Max Amplitude (A.U.)	SNR (dB ± 1 dB)	Max Amplitude (A.U.)
2nd generation membrane	10	23	147	24	159
2nd generation membrane	24	25	326	31	645
48 element rigid wedge	10	28	74	29	85
48 element rigid wedge	24	28	192	31	321

3.4.2. Defect 2

Defect 2 is detected using a TL mode conversion technique with a 65º longitudinal wave. This technique is also used for the detection of defect 3; however, the detection of defect 2 is more challenging because of the presence of the weld cap. A schematic diagram of the inspection technique used to detect defect 2 is shown in Fig 3-14. The presence of the weld cap is a particular issue when using the rigid wedge transducer. The image provided in Fig 3-14a indicates that only energy from elements at the very front of the array impinges upon the defect. When using the rigid wedge array the amount of energy reaching the defect is very low and hence the defect cannot be detected. Defect detection could be improved if it was possible to position the array closer to the defect location. This loss of inspection coverage is a major limitation of the rigid wedge design and provides motivation for the development of the membrane device. As shown in Fig 3-14b when using the 2nd generation membrane coupled device the membrane can conform to the surface geometry of the component under test. This allows the device to be optimally positioned for detection of the defect.

a.)

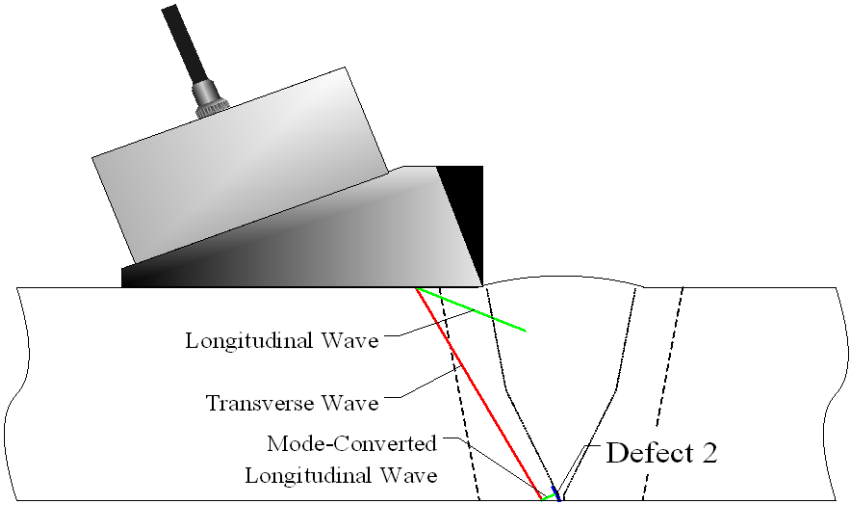

b.)

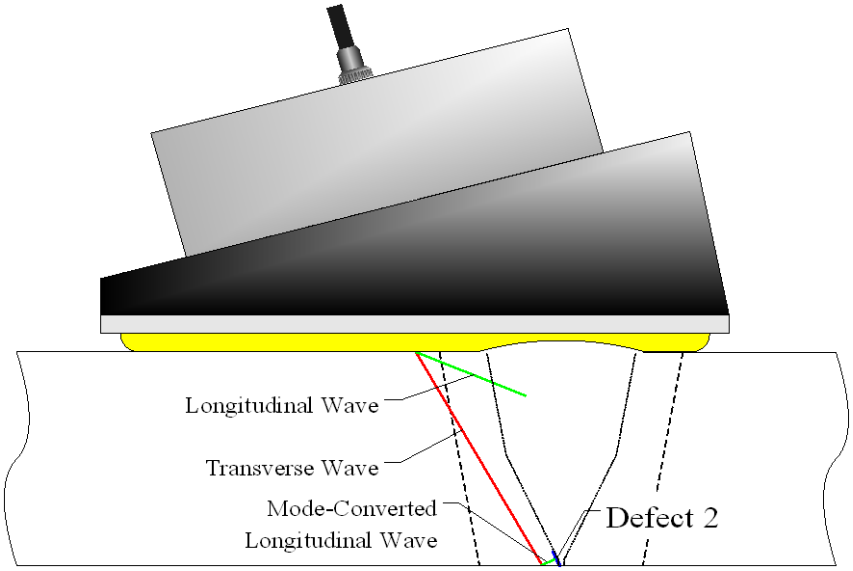

Figure 3-14 Schematic diagram of the inspection of defect 2 using a.) the 48 element rigid wedge phased array and b.) the 2nd generation membrane coupled device.

The B-Scan obtained from the inspection of defect 2 using the two different transducers is provided in Fig 3-15. The data shown in Fig 3-15 has been produced without using any focusing with a 10 element aperture. The data in Fig 3-15a shows the null defect case using the rigid wedge transducer. This data is taken away from the defect 2 position to demonstrate the level of background noise. The image in Fig 3-15b shows the B-Scan obtained from the inspection of defect 2 using the rigid wedge transducer. A comparison of Fig 3-15a and 3-15b indicates that it is not possible to detect defect 2 using the rigid wedge, 48 element transducer. There are some minor differences between the two images but these cannot be reliably attributed to the presence of the defect. It is also important to note that the null defect data was taken with the transducer positioned away from the weld cap. Therefore any

signals due to weld cap interactions are omitted from the image. The B-Scan obtained using the 2nd generation membrane coupled device is provided in Fig 3-15c. The optimum positioning of the defect signal within the B-Scan is possible because the membrane device is positioned over the weld cap. The image provided in Fig 3-15c has then been produced by using delay laws that compensate for the irregular surface geometry if the flat plate, non-welded test-piece. The other signal that is clearly evident in Fig 3-15c is an internal noise band. The noise band signal is well removed from the signals of interest in the inspection of defect 2. However, in the inspection of some defects this is not the case and the presence of this band of noise is an issue with the 2nd generation membrane coupled device. The origin of this noise and the work performed to reduce the effect of this noise will be discussed in detail in chapter 5.

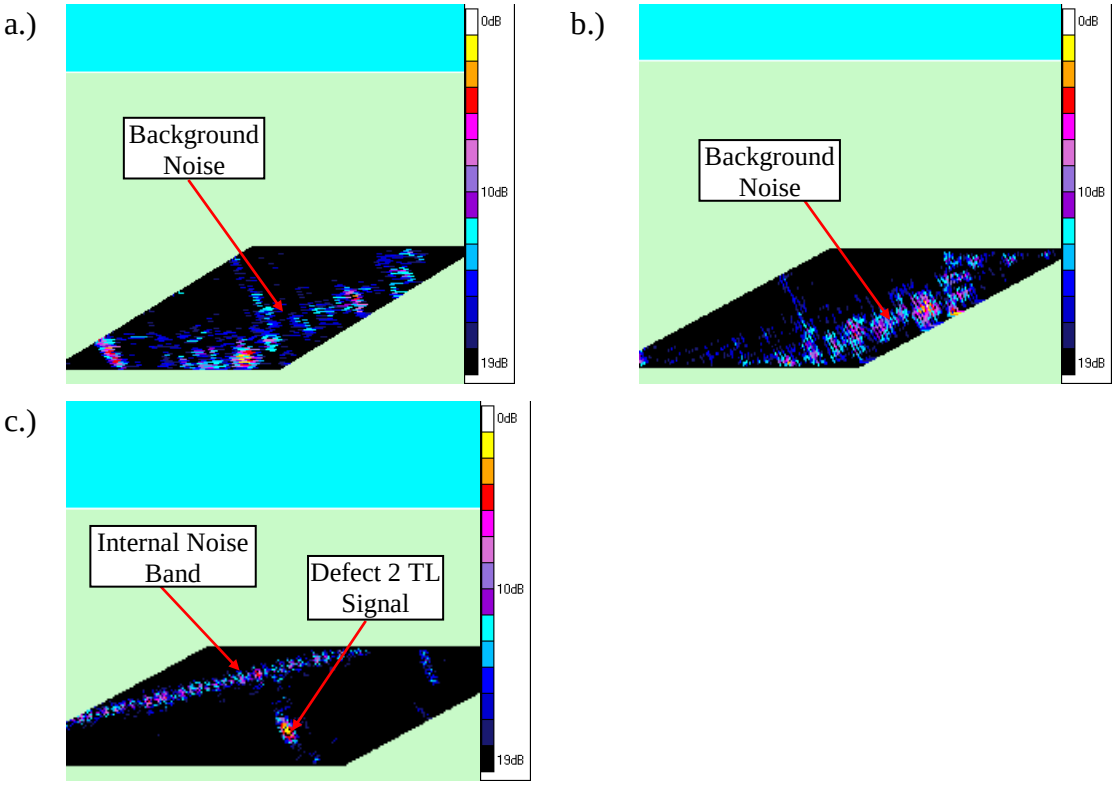

Figure 3-15 B-Scan image produced from a. the null defect inspection, and b.) the inspection of defect 2 using the 48 element rigid wedge phased array and c.) using the 2nd generation membrane coupled device.

The inspection performance of the 48 element rigid wedge phased array and the 2nd generation membrane coupled device for the inspection of defect 2 is provided in Table 3-5. Comparison of the membrane device results from defect 2 in Table 3-5

and those from defect 1 shown in Table 3-4 demonstrate that the amplitude of the defect 2 signal is approximately a factor of 3 lower than that from defect 1. The inspection mechanism used to detect the two defects is different and hence the amplitude of the response also varies. The SNR for defect 2 has been calculated ignoring the presence of the internal noise signal. Although defect 2 is still clearly observed against the background material noise the SNR is less than that achieved with defect 1.

Table 3-5 Experimental results for the inspection of defect 2.

Transducer	Aperture Size (elements)	Beam Steering		56mm focal length	
		SNR (dB ± 1 dB)	Max Amplitude (A.U.)	SNR (dB ± 1 dB)	Max Amplitude (A.U.)
2nd generation membrane	10	14*	52	16*	57
2nd generation membrane	24	15*	105	17*	185
48 element rigid wedge	10	-	-	-	-
48 element rigid wedge	24	-	-	-	-

Notes

* Defect SNR is calculated ignoring the effects of the internal noise signal.

3.4.3. Defect 4

The inspection of defect 4 is relatively challenging due to the position and the orientation of the defect. A self tandem TLL technique is employed to detect the defect using a 65º longitudinal wave. The results obtained in this inspection using both the 48 element rigid wedge transducer and the 2nd generation membrane coupled device are provided in Table 3-6. Despite the challenges associated with this inspection it is possible to reliably detect the defect using both transducers with each

of the two aperture sizes considered. The path length associated with this inspection is relatively long. The maximum focal length of an inspection is governed by the near field and hence size of the array aperture used for the inspection. Therefore focusing has very little effect in the inspection performance using both the rigid wedge phased array and the 2nd generation membrane coupled device when using a 10 element aperture. This is because the path length is beyond the near field length of the aperture and focusing is not possible. When using a larger aperture size of 24 elements the SNR of the defect response is improved using both probes when focused inspection is used. The 2nd generation membrane coupled device again provides better inspection performance than the 48 element rigid wedge transducer. The larger footprint associated with the membrane coupled device also allows the entire defect to be imaged and characterised even when using larger aperture sizes. The amplitude of the response in each case is much lower than that obtained from either defect 1 or 2. This is because the path length of the defect 4 inspection is relatively long and the beam is broad when it impinges upon the defect.

Table 3-6 Experimental results for the inspection of defect 4.

Transducer	Aperture Size (elements)	Beam Steering		30mm focal length	
		SNR (dB ± 1 dB)	Max Amplitude (A.U.)	SNR (dB ± 1 dB)	Max Amplitude (A.U.)
2nd generation membrane	10	16*	20	16*	20
2nd generation membrane	24	16*	39	19*	52
48 element rigid wedge	10	9	6	9	6
48 element rigid wedge	24	10	7	15	26

Notes

* Defect SNR is calculated ignoring the effects of the internal noise signal.

The internal noise signal observed in the inspection of defect 2 using the 2nd generation membrane coupled device is again present, as shown in the B-Scan data provided in Fig 3-16. The data shown in Fig 3-16 provides a comparison of the performance using the two different transducers, in each case the B-Scan has been generated using a 10 element aperture with a 30mm focal depth. When using the 48 element rigid wedge transducer some background noise is present, however, the most prominent feature within the B-Scan is due to the defect. The comparison provided in Table 3-6 demonstrates that if this internal noise is ignored that the 2nd generation membrane device performs well in comparison to the 48 element rigid wedge device. However, in the 2nd generation membrane coupled device inspection the internal noise signal occurs at a higher amplitude than the defect signal. The internal noise signal is approximately 11dB higher amplitude than the defect signal. The defect SNR has been estimated by ignoring this high amplitude noise signal. Therefore the data is displayed on a 0-29dB dynamic range in Fig 3-15 but the defect SNR is only 18dB. This approach is only possible because the defect signal and the internal noise signal do not occur at the same location in the B-Scan. However, if these two signals did overlap it may not be possible to detect the presence of the defect.

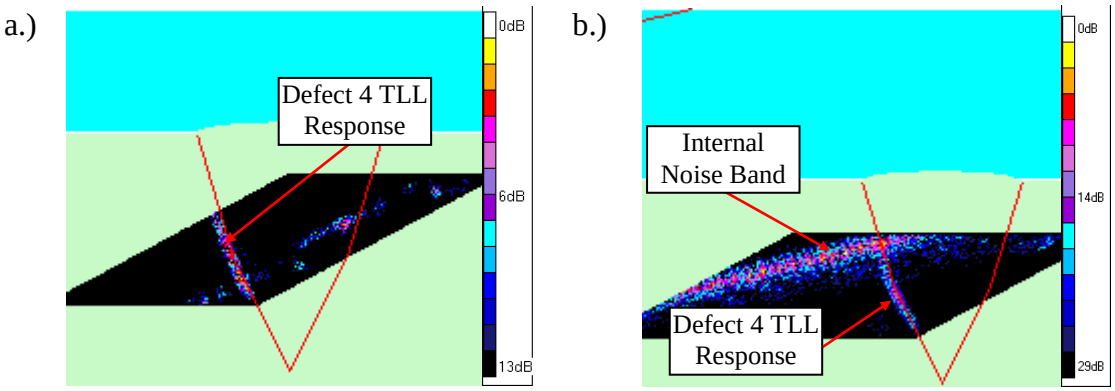

Figure 3-16 The B-Scan image obtained from the inspection of defect 4 using a.) the 48 element rigid wedge transducer and b.) the 2nd generation membrane coupled device. In the membrane transducer inspection the internal noise signal is the highest amplitude signal and corrupts the image obtained, the SNR has been calculated ignoring this effect.

3.4.4. Defect 6

When testing with rigid transducer wedges it is only possible to scan the transducer up to, but not over, the weld cap and maintain coupling. It is therefore not possible to detect defect 6 with the weld cap in place using a rigid transducer. However, by using the membrane coupled device it is possible to scan the entire length of the test piece. This is shown in the schematic diagram provided in Fig 3-17.

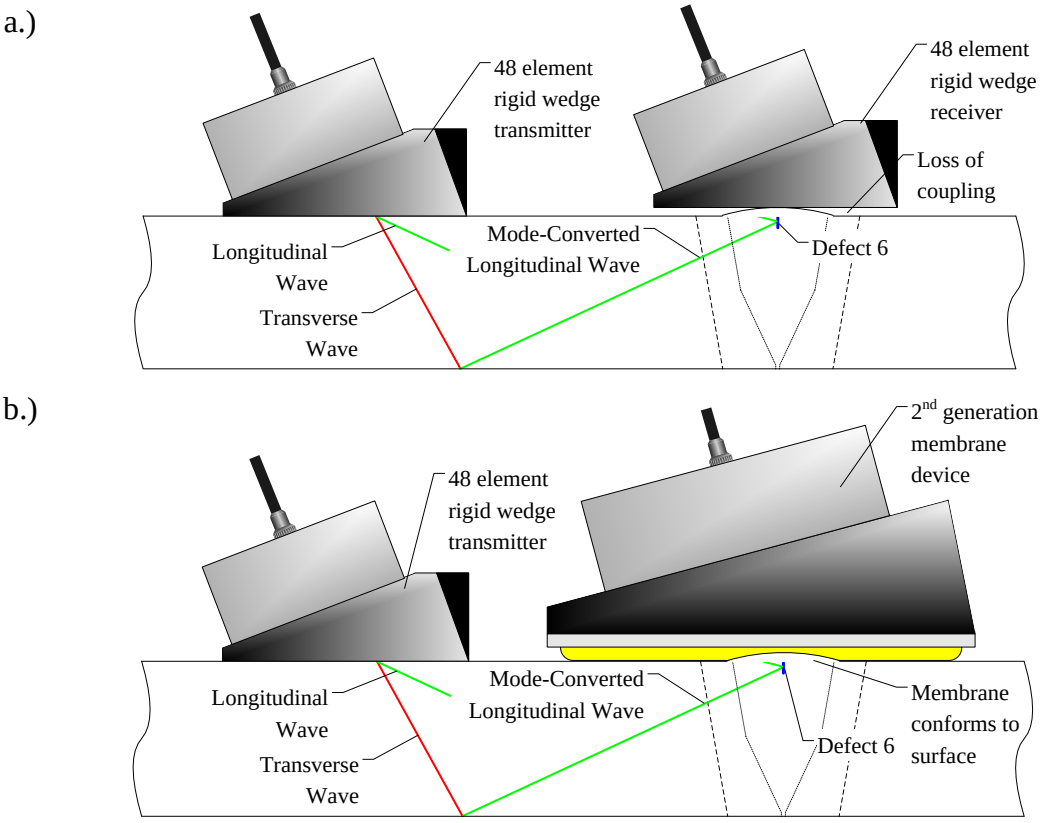

Figure 3-17 Schematic diagram of the inspection of defect 6 using a.) rigid wedge phased array transducers in transmission and reception, and b.) a rigid wedge transmitter probe and the 2nd generation membrane coupled device as a receiver.

The inspection results obtained from defect 6 using the rigid wedge transducer and using the 2nd generation membrane device is provided in Table 3-7. In each case the 48 element rigid wedge transducer is used to transmit an unfocused plane wave. The use of focused delay laws in reception once again provides a significant improvement in inspection performance and it is only possible to detect the defect when using the membrane device with suitable delay laws to focus at the outer surface of the

component under test. The delay laws used have been corrected to compensate for the irregular surface profile of the test-piece. A B-Scan of the inspection of defect 6 is shown in Fig 3-18(a) using an aperture of 10 elements. Interpretation of this B-Scan signal is difficult because of the high amplitude weld toe signal. However, comparison between the B-Scan of defect 6 with a defect free case shown in Fig 3.18(b) clearly demonstrates the presence of a defect signal. The amplitude of the weld toe signal is higher than that obtained from the defect, so the data is shown on a 0-24dB dynamic range but the defect SNR is only 10dB. This SNR is lower than ideal but it is acceptable in an industrial inspection when a priori knowledge of the weld toe signal is available.

Table 3-7 Experimental results for the inspection of defect 6.

Transducer	Aperture Size (elements)	Beam Steering		0mm focal length	
		SNR (dB ± 1 dB)	Max Amplitude (A.U.)	SNR (dB ± 1 dB)	Max Amplitude (A.U.)
2nd generation membrane	10	-	-	10*	29
2nd generation membrane	24	-	-	11*	56
48 element rigid wedge	10	-	-	-	-
48 element rigid wedge	24	-	-	-	-

Notes

* Defect SNR is calculated ignoring the effects of the weld toe signal.

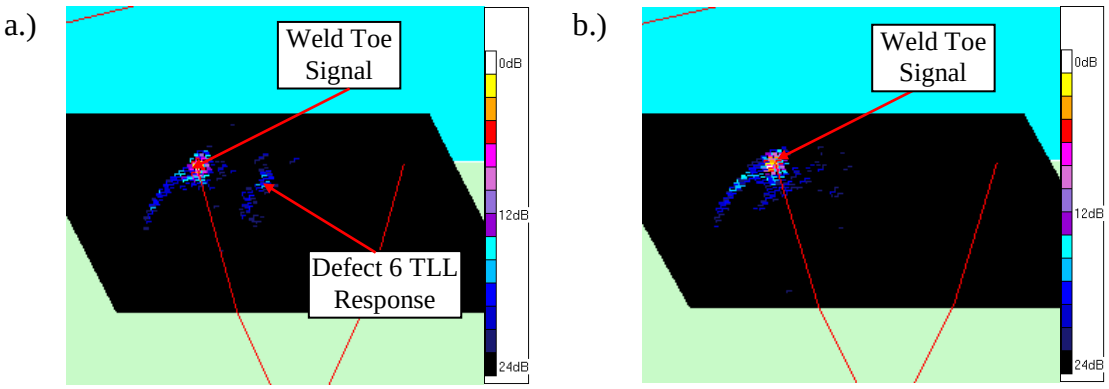

Figure 3-18 Comparison of the response from a.) defect 6 and b.) a defect free region. The top surface of the parent plate of the test-piece occurs at 0mm depth so that the weld cap material is deposited above this level and the defect signal appears partially above the component.

3.5. Summary

A specific target application was selected to provide an industrial focus for the development of the conformable membrane coupled phased array device. This target application is a section of large bore stainless steel pipe-work that contains an austenitic weld. This is a typical component inspected within the nuclear industry and is a specific component of interest to Rolls-Royce submarines. In the current inspection of this component a large number of rigid wedge single element transducers are mechanically raster scanned over the component. In order to maximise the coverage of the current inspection the weld cap must be removed. Weld cap removal is a time consuming mechanical process that can damage the structural integrity of the component. The overall inspection process is slow, the inspection techniques used are limited and coverage of the inspection volume is restricted. The goal of the membrane coupled device development activity is to improve the inspection of this component.

Two flat plate, non-welded test-pieces that are representative of the target application component were designed and manufactured. These test-pieces do not contain an actual weld but do have a weld cap that is designed to mimic the weld cap on the actual target application component. The absence of an austenitic weld simplifies the inspection process by eliminating signal scattering and refraction effects due to the weld material. A phased array inspection of these two test-pieces has been designed and the performance of a 48 element rigid wedge phased array transducer and the 80

element 2nd generation membrane coupled device is compared and assessed. The performance of the two different approaches is compared on four different defects. Both the rigid wedge transducer and the 2nd generation membrane coupled device were successfully used to detect defects 1 and 4 and the performance of both transducers is comparable but the membrane device slightly outperforms the rigid wedge device. Defects 2 and 6 could only be detected using the membrane device because of the presence of the weld cap. When using the rigid wedge transducer coupling cannot be maintained between the transducer and the component in the weld cap region.

Unfortunately when using the membrane coupled device a prominent internal noise signal was also observed. This internal noise signal was an issue in the detection of defect 4 and to a lesser extent the inspection of defect 2. In the inspection of defect 2 this noise signal was at a lower amplitude than the defect response and occurred away from the defect region. However, in the inspection of defect 4, the defect response occurs at a point in the B-Scan that is much closer to this noise signal. In addition the signal from defect 4 is relatively low amplitude and the noise signal is more prominent within the B-Scan. Although the 2nd generation membrane coupled device can be successfully used in inspection of defects that cannot be detected using conventional transducer technology this noise signal is a limitation in the performance. The source of this noise signal must be understood and actions taken to reduce and ideally eliminate its effect. This activity and the subsequent design of a 3rd generation membrane coupled device is documented in chapter 5.

4. Ultrasonic Inspection Modelling

The non-destructive inspection of safety critical components is carried out to ensure that the components are fit for purpose. Before an inspection can be performed it must be suitably qualified; this provides an assurance that an inspection will meet its objectives. Inspection Qualification (IQ) within Rolls-Royce Submarines is performed in line with European Network for Inspection and Qualification (ENIQ) (JRC Petten, 2007). ENIQ documentation provides information on the way in which different aspects of a qualification can be developed and implemented.

Using ENIQ methodology an inspection system must be designed specifically to find the type and size of significant defects in the component under test. The capability of the inspection technique to detect these defects must then be demonstrated. This capability has traditionally been demonstrated theoretically using simple trigonometric models and then supported with a significant body of experimental data. However, in order to demonstrate inspection capability on all types of defects of different sizes and orientations the expense and time required in this approach becomes prohibitive. By simulating an inspection, the cost associated with the development of expensive samples and the time and cost of experimental testing can both be reduced. The desirability of using suitable models in IQ has been recognised by ENIQ and it has published guidelines on their use (JRC Petten, 1999). The performance of any model used in the IQ process must be validated against experimental data to ensure its accuracy. It is therefore expected that modelling will only form part of the process of generating the technical justification for an inspection.

Modelling can also be used as an alternative to round robin testing such as the European Programme for the Inspection of Steel Components (PISC II) (Lemaitre et al, 1996) to understand the performance capability and limitations of an inspection (Schmitz et al, 1995). Once an appropriate model framework has been developed then defects of different sizes and orientations can be introduced at any position within the model. The flexibility of this approach also allows the introduction of a combination of defects so that complex defect interaction can be investigated.

There are a wide range of different approaches that can be adopted to solve the inspection modelling requirement. Historically Rolls-Royce has relied on the basic spreadsheet based trigonometric models. However, through the Advanced NDE NPCT project and a Nuclear Technology and Sustainability (NTS) project, which is designed to develop an IQ framework for phased array inspection (Shipp et al, 2008; Rolls-Royce, 2009) Rolls-Royce engineers have started to implement a much broader range of modelling techniques. The use of these models is still not widespread and through my EngD studies I have been heavily involved in promoting the use of the different modelling techniques within Rolls-Royce. The two inspection models discussed below do not represent an exhaustive list of all of the modelling packages available or used within industry. This review is limited to the main models that I have implemented as part of my research and it represents the two models that I have demonstrated within Rolls-Royce. In section 4.1 I will discuss the CIVA modelling package. In section 4.2 I will then review the use of finite element (FE) analysis for modelling ultrasonic inspection. In section 4.2 I will also review the specific FE development work that I carried out to address the needs of this project to allow the simulation of the flat plate, non welded test-piece inspections. Then in section 4.3 I will demonstrate the use of both packages and present modelling results obtained to simulate the detection of defects within the target application component. I will also comment on the applicability of each of the two approaches for industrial application.

4.1. CIVA

CIVA is a semi-analytical model developed by CEA in France and marketed by CEDRAT (Meylan, France) The software is used by a range of industrial and academic groups as a rapid inspection planning and data interpretation model. CIVA contains ultrasonic, electromagnetic and radiographic inspection models. However, my work has focused on ultrasonic inspection and this review is limited to the ultrasonic inspection module within the CIVA platform. In CIVA the probe beam model is based on a wave theory developed by Deschamps (Deschamps, 1972). The transducer is discretized into a number of point sources, each source is assumed to radiate a hemispherical wavelet of energy. The beam propagation and defect interaction is then estimated using the pencil method (Gengembre & Lhemery, 2000). A pencil is a collection of rays emanating from the point source and diverging slightly, the wavefront produced is then characterized using matrix representation. In

this approach the propagation of the rays emitted by the source and centered on the geometrical path linking the source and the computation point are considered. This approach allows CIVA to simulate the effects of reflection and refraction through multiple material layers with arbitrary geometry. It is therefore possible to simulate ultrasonic beam propagation into complex geometrical structures such as the target application. The pencil approach also makes it possible to simulate the beam produced by an arbitrary transducer. It is therefore possible to simulate single element transducers as well as 1D and 2D phased arrays. This functionality has been used extensively to simulate the membrane coupled device performance and assist in the development of this transducer.

CIVA also contains a number of flaw/beam interaction models. The ultrasonic beam is calculated based on the pencil method; it is then assumed that the interaction between the beam and the defect can be simulated as the sum of several separate echoes corresponding to the different possible ultrasonic paths (Calmon et al, 1998). Depending on the inspection situation to be simulated CIVA uses the Kirchhoff approximation, the Geometrical Theory of Diffraction (GTD) or the Born approximation (Calmon et al, 2004). The Kirchhoff approximation is based on Huygens principle and the field scattered from a defect is calculated by summing the responses from a large number of point sources positioned on the surface of the defect (Kirchoff, 1891). GTD is a ray theory originally developed for optics by Keller (Keller, 1957); which was later applied to elastodynamics by Achenbach and Gautesen (Achenbach & Gautesen, 1977). The theory provides a correction to geometrical elastodynamics to predict the response from a defect due to rays diffracting from the edge of the defect as well as that due to the specular surface reflection. Both the Kirchoff theory and GTD are high frequency approximations and should not be used for predicting the response from defects smaller than approximately two ultrasonic wavelengths (Chapman, 1990). Also in both cases the approximations should only be used in the far-field of the defect. The Kirchhoff approximation is used to simulate the response from component boundaries and calibration reflectors such as side drilled holes and flat bottomed holes. Depending on the exact inspection scenario GTD or the Kirchhoff approximation are used to predict the response from cracks. Typically Kirchhoff is preferred for normal or near-normal incidence and GTD is used for off-specular directions.

A slightly modified form of the low frequency Born approximation (Gubernatis & Domany, 1977) has been included into the CIVA platform relatively recently to predict the response of solid inclusions (Darmon et al, 2003). The use of this type of approximation is valid for weak scatterers such as inclusions where energy is reflected from the front and back surface of the defect. Although it is possible that this type of defect may occur with the target application component weld (Rolls-Royce, 2006c) it is considered less critical than the planar flaws included in the test-pieces developed.

The Kirchhoff approximation and GTD have been extensively validated against exact theoretical solutions and experimental results by the Central Electricity generating Board (Chapman, 1984; Chapman, 1990). This work demonstrated a good level of agreement and highlighted the range of validity of both approaches. The low frequency Born approximation has been validated against analytical solutions (Ying & Truell, 1956) and experiment for alumina inclusions in steel (Darmon et al, 2003). The CEA also has its own validation centre, which has a substantial ongoing programme of validation work and regularly participates in model benchmarking exercises (Cinquin et al, 2006; Lonné et al, 2006). In general, CEA have reported good agreement with experiment and the CIVA platform has outperformed other modelling packages available.

4.2. Finite Element Modelling

The range of inspection scenarios that can be simulated using commercially available software is fundamentally limited by the range of validity of the approximations underpinning the model. An alternative to these analytical models is to use a numerical approach, such as the finite difference (FD) or finite element (FE) methods. Numerical inspection modelling can be used in a much wider range of scenarios to provide an accurate simulation of the inspection. The early part of my EngD was focused on the development of the FE modelling techniques to simulate a range of different ultrasonic inspection scenarios. The focus of this work was to develop my understanding of the experimental and simulation techniques and to demonstrate the application of FE modelling in an industrial context. I performed a range of modelling tasks including the development of an inner diameter creep wave model for the inspection of a narrow bore section of pipework and a SDH response model. This

modelling work was performed using FE simulations because the most up to date version of CIVA available at that time did not account for creep wave behaviour. The creep wave response was critical in both of the small bore pipe and SDH defect inspection and was a significant restriction in terms of CIVA modelling. These models are included in my 6-month, 12-month and 24-month reports (Russell, 2006a; Russell, 2006b; Russell, 2007b) but are not relevant to this thesis and will not be included in this discussion.

In the finite element method (FEM) a structure is divided into a number of small pieces, these pieces are known as elements. Individual elements are linked at their boundaries by nodes; typically nodes exist at the corner of elements but nodes can also be introduced on the element edges or at their centre. The pattern of the elements within the model is known as the mesh. Each element is sufficiently small that its individual behaviour can be calculated using relatively straightforward analysis. By combining the behaviour of all of the elements within the structure it is possible to approximate the overall behaviour of the structure. Therefore complex problems with no analytical solution can be solved using this approach. The FEM does not provide an exact solution, but through careful control of the material properties, the applied loads and the pattern of the mesh it is possible to extract accurate solutions using the method (Lowe & Hansen, 2008).

The FE modelling technique can be highly computationally intensive. The structure must be broken down into a number of small elements. In the simulation of ultrasonic inspection the maximum element size that can be used is limited by the shortest wavelength of inspection. The Rayleigh wavelength must therefore be considered at the highest frequency of interest within the model (Kishore et al, 2000; Pavlakovic, 1998). To ensure model accuracy the required mesh density estimates range between 8 and 20 nodes per wavelength (Schmid, 1997; Alleyne, 1991; Ansys, 1992). The time step used within the model is also critical to maintain stability. The exact criterion has been expressed in different ways by other authors (Alleyne, 1991; Kishore et al, 2000; Pavlakovic, 1998; Drozdz, 2008). However, it is essentially necessary to ensure that energy cannot propagate across an entire element within the model in a single time period. The maximum time step that is allowed within the model is therefore governed by the fastest wave within model.

In realistic structures the number of elements required to generate an accurate model can rapidly become prohibitive and a series of approximations must be made to limit the overall model size. All of the models discussed in this thesis are 2-dimensional and assume plane strain conditions. This approximation is valid as the thickness of the component is large in comparison to the beam width. However, the widths of the defects contained in the target application test-pieces are comparable to the width of the ultrasonic beam, which reduces the accuracy of the approach. In order to limit the shortest wavelength in the model to the Rayleigh wavelength in stainless steel the transducer is omitted. The transducer used in this type of inspection uses a Perspex wedge; ultrasound propagates in Perspex with a short wavelength. In order to accurately model the actual transducer wedge the element density would need to be increased which in turn would increase the overall complexity of the model. The transducer input is therefore simulated using Huygens' principle. The wavefront was generated by applying a load to individual nodes on the upper surface of the model. This is shown for a small number of nodes within the FE model in the schematic diagram provided in Fig 4-1; the length of the arrow indicates the relative time delay between each adjacent node. The load applied was modelled using a 5-cycle Hanning-windowed toneburst, as shown in Fig 4-2 for a 2.25MHz transducer. These tonebursts were delayed relative to one another in time giving rise to the angled wavefront. In each model the time delays used were controlled to simulate the different angles required.

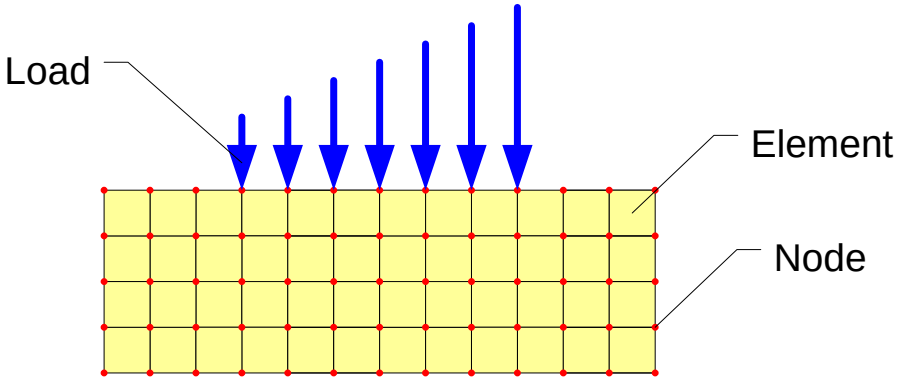

Figure 4-1 Schematic diagram of the excitation method used in the FE models.

a.)

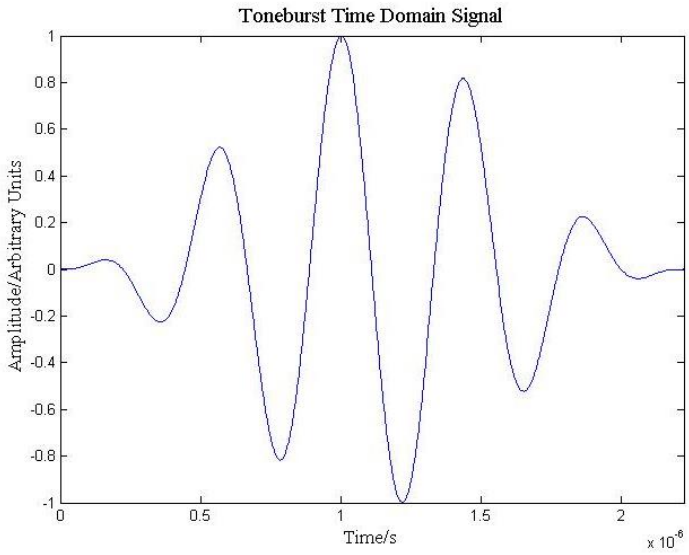

b.)

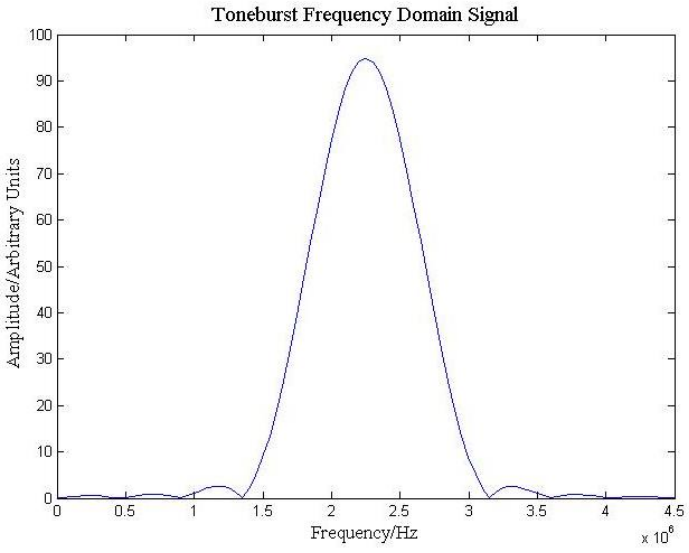

Figure 4-2 The 5-cycle Hanning-windowed toneburst with centre frequency of 2.25MHz used for nodal excitation of the target application model a) time domain, b) frequency domain.

To reduce the model size further only a section of the component is simulated. Unfortunately this approach introduces artificial boundaries into the model. Some signals of interest from the scatterer can be corrupted by reflections from these artificial boundaries and a sufficiently large model must be generated to eliminate this issue. Despite the use of all of these approximations it was not possible to accurately simulate the inspection of the target application using this conventional approach. It was not possible to increase the overall size of the model sufficiently and the boundary reflections occurred at a similar time period to some of the signals of interest from the defect, so an alternative modelling approach was required. The approach used in this work was the Absorbing Layers using Increasing Damping (ALID) technique. This approach can be implemented around the model boundaries in the time domain within ABAQUS (Drozdz et al, 2005; Drozdz et al, 2006; Drozdz, 2008; Liu & Quek Jerry, 2003). The absorbing region is made of a material that has the same properties as those within the main body of the model apart from having a gradually increasing damping.

A harmonic plane wave travelling in the x-direction can be defined as:

$$A(x,t) = A_0 \exp(-i\omega t + ikx) \qquad (4\text{-}1)$$

Where A = Amplitude

A_0 = initial amplitude

k = Wave number

ω = Frequency

t = Time

When considered in the frequency domain the ALID technique uses the concept of a complex compression modulus (or just shear modulus for shear waves) or density. If either of these quantities are complex then this leads to a complex wave number. Equation (4-1) then becomes:

$$A = A_0 \exp[-i\omega t + (ik^{'}x - k^{''}x)] \qquad (4\text{-}2)$$

where k' = Real wave number

k'' = Imaginary wave number

The imaginary part, k'' represents the viscoelastic material properties which is responsible for the decay of the wave in the absorbing layer (Drozdz et al, 2006; Ansys, 1992).

The absorbing region is then defined as a series of layers; as the distance between the layer and the model boundary is increased the damping parameter is also increased. This change in the wave number between the area of study and the absorbing layer causes a change in impedance, which can cause some reflections. In order to minimise these reflections the change in damping between each layer must be kept small. To enable the dissipation of sufficient energy within the absorbing region and prevent significant reflections from the model boundary re-entering the region of interest it may be necessary to use a relatively large number of layers. Although small spurious reflections can still occur, these can be controlled to acceptable levels. In this work a reflection of less than -60dB or 0.1% of the incident energy pulse is considered acceptable.

Typically when using FE models to simulate ultrasonic inspection a uniform linear quadrilateral mesh is used, and I had adopted this approach in the development of some early models. The conventional use of the ALID absorbing regions also depends on this type of deployment. However, the target application component contains a curved weld cap and a range of defects at different angles. The uniform linear quadrilateral mesh does not readily conform to this complex geometry. One solution to address this limitation is to use a very fine mesh and a "staircase" approach around the weld cap and defect regions (Rajagopal et al, 2008). However, this approach would significantly increase the computational complexity of the model and prevent the simulation of the target application. In order to simulate the inspection of the target application component I adopted a quadratic triangular element mesh. A schematic diagram of the boundary between the main model and the ALID region is shown in Fig 4-3; this shows a comparison of the typical usage and the modified usage of the ALID region.

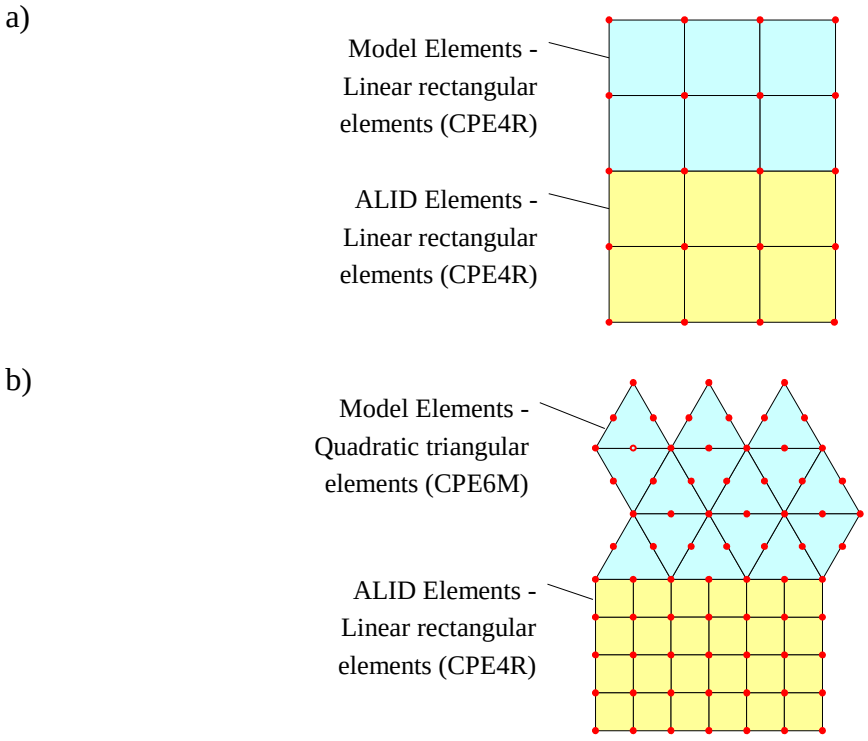

Figure 4-3 Schematic diagram of ALID usage, a) conventional usage with linear quadrilateral mesh, b) modified usage with quadratic triangular mesh.

Since the completion of my initial research, further work has been performed by Drozdz et al (2007) and Rajagopal et al (2008) to improve this approach. In my initial research the transition between the quadratic triangular elements in the main section of the model and the linear quadratic elements in the absorbing boundary led to some spurious reflections. Although these reflections were very low level they were still present. Subsequent research has developed an approach to generate ALID absorbing regions using automatically generated quadratic triangular elements. This eliminates the transition between two different element types and hence reduces the amplitude of the boundary reflection. It also allows further automation of the model production and hence improves model development speed. The work by both Drozdz et al and Rajagopal et al is also funded through the NPCT project and I have provided some assistance in the development of this approach. This research is also generating a set of user guidelines for the development of accurate FE models using automatically generated triangular mesh elements. In the longer term this will assist with the implementation of FE modelling capability within Rolls-Royce Submarines.

4.3. Target Application Modelling

The inspection of the target application component was simulated using both CIVA and FE modelling techniques. The approximations discussed in section 4.2 were used to produce FE models for the inspection of the target application component. In each case a 2D plane strain model is produced. The transducer has been omitted and the ultrasonic energy is simulated by using a series of time delayed 5-cycle Hanning tonebursts, as shown in Fig 4-2. In this approach the probe is modelled using a simple piston transducer approximation which is a reasonable representation of the single element inspection of the target application component or an aperture in a contact array. This approach can also be used to represent an inspection performed using a single aperture within a wedge coupled phased array. However, due to beam spread in the wedge the performance of different apertures within an array of this type is not identical. Simulation of the entire membrane coupled device inspection in FE would be very time-consuming. A separate simulation for each aperture within the array would need to be run which would require a substantial amount of computation time on specialist computer facilities. FE simulation of a scanned single element inspection to build up a B-Scan image of the inspection volume would require a similar time investment. This is impractical in an industrial environment and remains a major limitation of the FE modelling technique. The CIVA modelling package can be used to simulate this type of scenario and phased array or scanned single element transducer inspection can be simulated. However, the motivation of this work was to demonstrate the use of CIVA and FE modelling within the industrial context, to compare the performance of each simulation technique and to provide a better understanding of the inspection techniques being used.

To simplify the FE modelling, and to allow comparison between experimental and both sets of simulated results, all comparisons were carried out with the transducer in a single position. The transducer position corresponded to the theoretical optimum location, based on a geometrical study, for maximum defect response for each of the flaws embedded in the flat plate, non-welded test-pieces. A comparison was then made between the A-Scan response obtained using the three different techniques. The transducer used experimentally is a Krautkramer MSWQC ½" diameter circular single element probe, the same size transducer was also simulated using the CIVA

model. As discussed previously the FE models were simplified by using a 2D approximation, the width of the element corresponds to the diameter of the transducer. However, the FE model does not take into account the overall shape of the transducer, this is a potential source of error in the FE model.

In the FE models produced as part of this work around 16 nodes per wavelength have been used, which satisfies the maximum node spacing criteria discussed in section 4.2. However, Rajagopal et al (2008) have subsequently performed a more detailed study of modelling accuracy using this type of mesh. This work concluded that it is possible to achieve a negligible error in the displacement field from the defect with a mesh density of 20 nodes per wavelength. However, a mesh density of at least 30 nodes per wavelength is required to ensure a wave propagation velocity error of less than 1%. In a recent modelling study by Velichko et al (2009) a mesh density of 40 nodes per wavelength were used to reduce errors further in the predicted defect response. Based on the study performed by Rajagopal et al (2008) the FE models generated to simulate the inspection of the target application will suffer from a velocity error of approximately 2% due to the coarseness of the mess used. Unfortunately, it is not possible to simulate the inspection of the two flat plate, non-welded test-pieces using a significantly finer mesh because of the geometrical size of the component. When completing FE modelling of this type of component a compromise must be reached between model size and accuracy. The target application component is unexceptional in terms of its geometrical size and much larger components are routinely inspected within the nuclear industry. The limitation in terms of modelling accuracy for the inspection of large components is a major drawback. FE modelling is unlikely to be widely adopted within the nuclear industry until these limitations can be overcome. Current NPCT research in collaboration with Imperial College is addressing this limitation and a hybrid ray-tracing/FE model is under development. I manage this project on behalf of Rolls-Royce and I will be directly involved in the transfer of this technology into Rolls-Royce when it reaches a mature level of development.

It is possible to significantly reduce the geometrical size of the FE models by using ALID absorbing regions. The modified ALID usage described in section 4.2 and shown in the schematic diagram in Fig 4-3 was used in all of the models generated.

In fact in many cases it is only actually possible to generate the desired FE model by using absorbing regions. In each of the models, 300 layers have been used within the ALID regions. The reductions in the model size that can be achieved by using ALID absorbing regions are significant, and these are summarised for each defect model in Table 4-1.

Table 4-1 Summary of the reduction in the overall model size when using ALID absorbing regions for FE models to simulate the single element transducer inspection of defects 1-6.

Inspection	Size Reduction (%)	Approximate Final Model Size (million elements)
Defect 1	45	2.6
Defect 2	41	2.2
Defect 3	50	3.3
Defect 4	27	3.6
Defect 5	60	5.7
Defect 6	65	5.2

When generating FE models using Abaqus CAE the coordinates of each node and each element is individually assigned and listed in the input file. This rapidly increases the size of the input file that must then be manipulated in a text editor program. It was found that standard text editors (winedt, wordpad, notepad) are not capable of handling the size of file produced using this approach for the larger models considered in this work. However, by using an upgraded PC with additional RAM and Textpad software to manipulate the text file it was possible to generate a sufficiently large model to simulate the inspection of all of the defects within the target application test-pieces. Also, despite the use of these approximations the processing times for these models remains substantial requiring a number of hours, therefore processing was typically carried out overnight. The use of absorbing regions is also essential. Without the use of ALID it would not be possible to generate a model to simulate many of the inspections performed, particularly the inspection of defects 5 and 6.

The experimental testing has been performed with a high quality transducer with a short ring down time. The experimental input pulse is clearly observed in each of the

inspections completed. This input pulse has been omitted from both the FE and CIVA modelling results provided in this thesis.

The FE model structure was generated using the Abaqus CAE with an automatically generated mesh. When simulating the inspection using CIVA the geometry of the models was generated using the built-in CIVA drawing package. In both the FE and the CIVA models the defects were included as isolated geometrical features and in each case the defect gape was 0.3mm. In these models the faces of the defect are perfectly parallel and have well defined corners. Mid-wall, non-surface breaking defects, such as defects 3 and 4, were also generated in this way. However, in the actual flat plate, non-welded test-pieces these defects are drilled as FBH defects. This difference in geometry between the experimental and simulated testing is a potential source of error in both models. In each approach to modelling the through-wall extent of the mid-wall defect is 5.6mm which accurately represents the diameter of the FBH. This defect provides an equivalent area to an 8mm x 4mm elliptical defect, which corresponds to the critical defect size in the component. This approach is taken because it is a robust and reliable means of ensuring that approximately the same proportion of the beam energy is reflected by the FBH as would be expected from the defect.

When obtaining the results experimentally and using the two different approaches to simulation, standard material property values have been used. In each case these material properties are used to calculate the propagation velocity of ultrasound in the component. This ensures that the same values have been used in all three approaches. The use of standard values and not measured results is routinely used during experimental testing and allows calibration to be performed on a standard SDH test-piece prior to testing on the actual component of interest. This approach also represents the technique typically employed within Rolls-Royce when completing simulation of an inspection. However, it is possible that the actual material properties of the calibration test-piece and the two flat plate, non-welded test-pieces are slightly different from these standard values. This discrepancy in material properties between the predicted and actual values can lead to errors in the arrival times of the defect signal.

A comparison of the results obtained experimentally and using the two different modelling techniques for defects 2, 4 and 5 is provided below. The inspection modelling results from these three defects provide an insight into the accuracy of the different simulation techniques. The amplitude of the signals obtained from all three defects are normalised to that obtained from defect 2, which represents the highest amplitude signal. This technique allows direct comparison between all three sets of results. Further details of the development work performed to produce these models and the results obtained are provided in my 24-month and 30-month reports (Russell, 2007b; Russell 2008a). These results have also been published at the 34th Annual Review of Progress in Quantitative NDE (Russell et al, 2007) and at NDT 2007, the 46th annual conference of the British Institute of Non-Destructive Testing (BINDT).

4.3.1. Defect 2

A schematic diagram of the inspection of defect 2 is shown in Fig 4-5. A comparison of the experimental and simulated results obtained from this defect is shown in Fig 4-6. The experimental calibration of the single element transducer was performed in-line with BS EN 583-2 (British Standards Institution, 2001); this calibration demonstrated that the probe angle was not exactly as expected. The wedge used in this experiment actually generated a 67º longitudinal wave. A transducer producing a 67º longitudinal wave and the associated 29.5º shear wave was simulated in all of the modelling results presented below. There is a close agreement between the three sets of results, and a strong Transverse-Longitudinal (TL) response is seen in each case. The origin of the additional, unlabeled, low amplitude signals seen in the experimental data is unclear and do not appear in the simulated data. The three sets of data have been normalised so that the TL signal has an amplitude of unity, this allows direct comparison between the responses for three different defects considered. There is a small discrepancy in the defect response arrival time prediction between the three sets of results. This leads to a difference in arrival time of the TL signal and the greater separation between the TL signal and the transverse (T) wave response in the experimental results. Some of this difference may be due to the material property values used; there is also an additional error in the FE prediction due to the relatively coarse mesh used. The amplitude of the L-wave tip diffraction signal predicted using

the FE model is very similar to that seen experimentally; however, the signal predicted using the CIVA modelling approach has a significantly lower amplitude. This is a limitation of the CIVA model prediction and demonstrates the value of the using different modelling approaches. The results provided in Table 4-2 demonstrate that there is close agreement in the predicted signal arrival times obtained using both models.

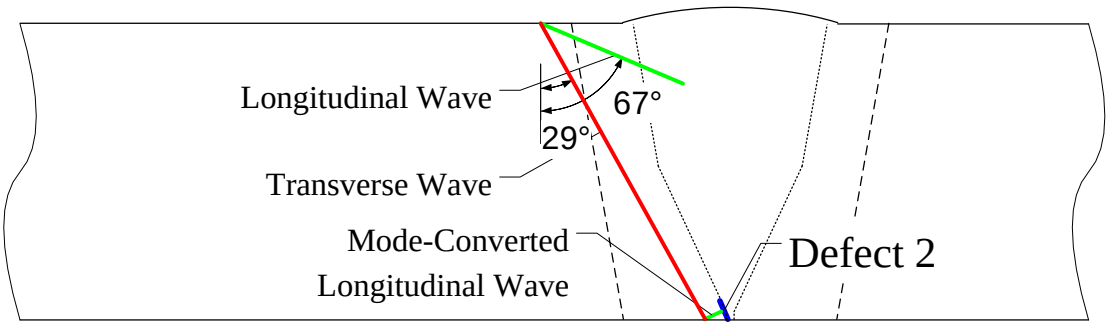

Figure 4-4 Schematic diagram of the inspection of defect 2.

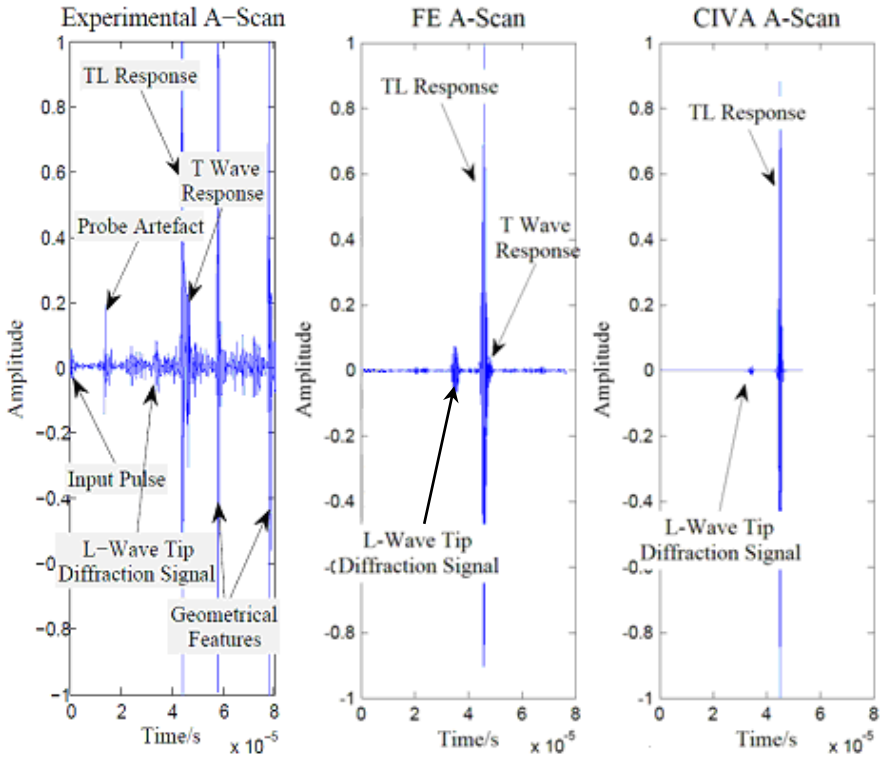

Figure 4-5 Comparison of the experimental and simulated A-Scans obtained for defect 2.

Table 4-2 Experimental and simulated TL signals obtained for the inspection of defect 2. The amplitude of each signal has been normalised to unity.

Data Source	Defect 2 Signal	
	Amplitude (A.U.)	Arrival Time (μs)
Experimental	1.00	44
FE Model	1.00	46
CIVA Model	1.00	45

4.3.2. Defect 4

The schematic diagram of the inspection of defect 4 is shown in Fig 4-7. The same 67º longitudinal wave transducer was once again used to gather these results and the simulations have been performed appropriately to model this behaviour. A prominent TLL signal is seen in both the simulated and the experimental data obtained from the inspection of defect 4, this is shown in Fig 4-8. There is once again close agreement between the positions of the TLL response in each case; this can be seen from the comparison of the results provided in Table 4-3. In all cases the amplitude of the main defect TLL response signal recorded using this technique from defect 4 is significantly lower than that measured from defect 2. This reduction in signal amplitude is attributable to the longer path length which leads to a much wider beam at the defect and also the beam offset at the transducer. The amplitude prediction of the main TLL defect response using both modelling approaches is reasonable, although both models provide a slight underestimate. The amplitude prediction of the FE model is closer to the experimental result than that achieved using the CIVA model.

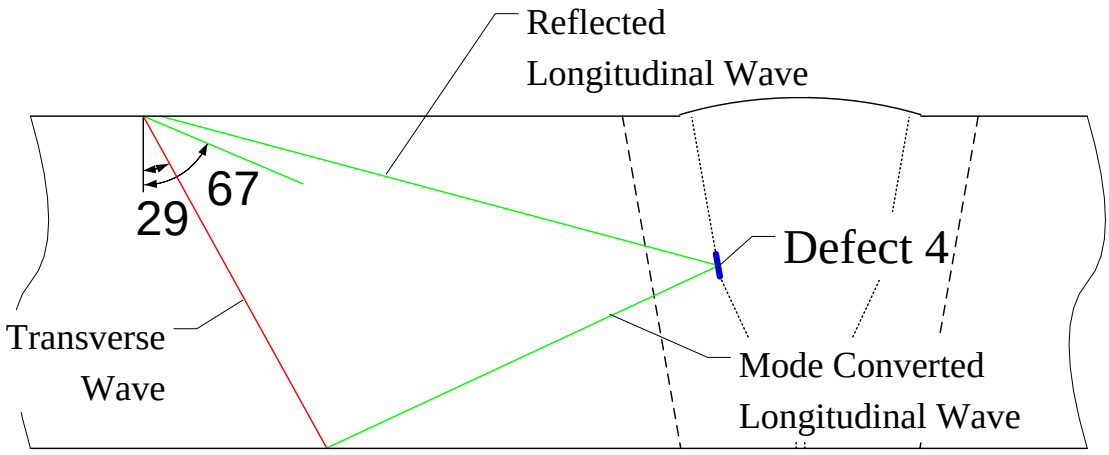

Figure 4-6 Schematic diagram of the inspection of defect 4.

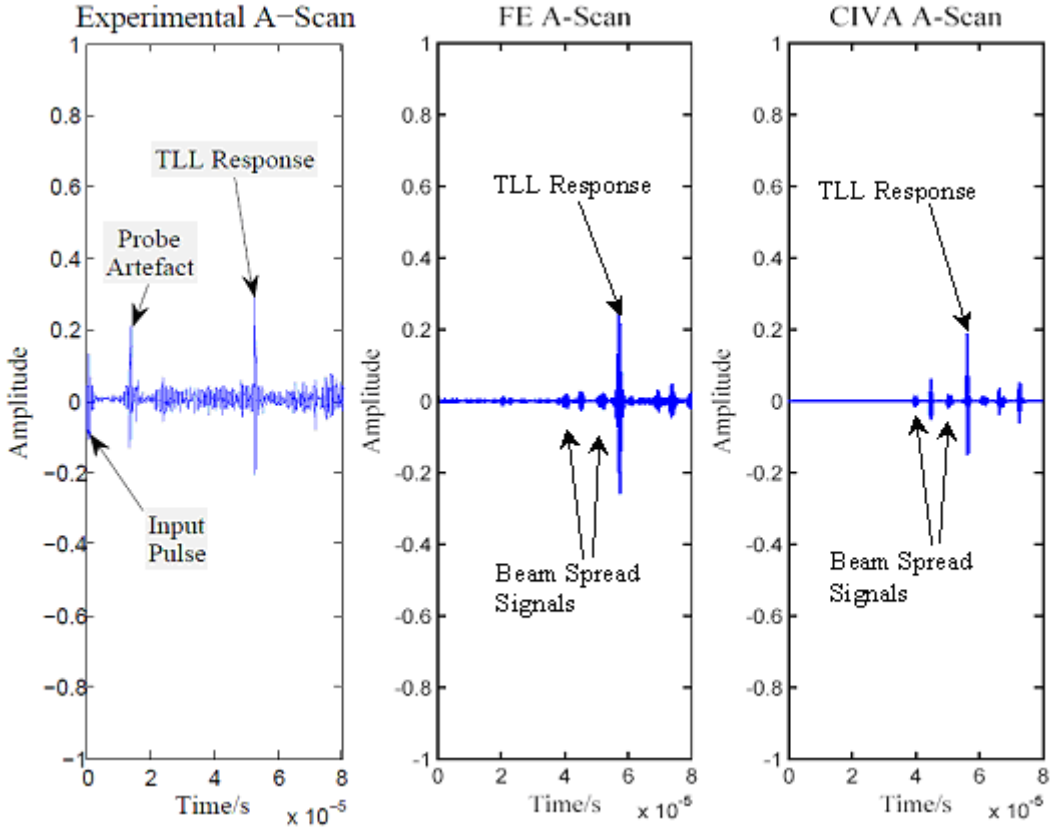

Figure 4-7 Comparison of the experimental and simulated A-Scans obtained for defect 4.

Table 4-3 Comparison of the experimental and simulated TLL signals obtained for the inspection of defect 4.

Data Source	Defect 4 Signal	
	Amplitude (A.U.)	Arrival Time (μs)
Experimental	0.29	53
FE Model	0.26	56
CIVA Model	0.19	56

In addition to the main signal predicted, a number of additional beam spread signals also occur because of additional interactions along alternative propagations paths within the component. These beam spread signals are more prominent in the simulated results than in the experimental data. In both modelling techniques background noise has not been included. The material noise in both of the flat plate, non-welded test pieces is expected to be low, but some grain scatter is inevitable and this increase in noise leads to the reduction in the experimental signal to noise ratio. The beam spread signals cannot be distinguished against this background noise in the experimental case. The discrepancy in the predicted amplitude of the beam spread signals is also linked to the approximations that have been made when producing the two modelling results. In both models the transducer has been simulated as a simple piston, this leads to off-axis beams appearing at a higher amplitude than measured in experiment.

The lower amplitude signal and the greater uncertainty in the A-Scan indicate the issues with interpreting data from this type of inspection. In the current inspection of the actual target application component this technique is used as a secondary detection technique to confirm the findings of other scans. However, these alternative techniques rely on techniques that traverse the weld material. As there is no weld present in the test-pieces used for this testing an inspection technique that traverses the weld is inappropriate. Inspection of this type of defect through the weld material will be addressed in chapter 6.

4.3.3. Defect 5

A schematic diagram of the model generated to simulate the inspection of defect 5 is shown in Fig 4-9. The experimental scanning equipment used only allows a limited number of probe offsets to be used. Experimental testing has been performed with the probe index points approximately 154 mm apart. The receiving transducer is placed as close as possible to the weld without scanning over the weld cap. This ensures that the maximum coverage is achieved without losing couplant and hence inspection performance. The probe separation in this inspection is relatively large; this increases the geometrical size of the model that is required and increases the modelling complexity. This is particularly challenging in generating the FE model and it is only possible to model this case with the use of ALID absorbing regions.

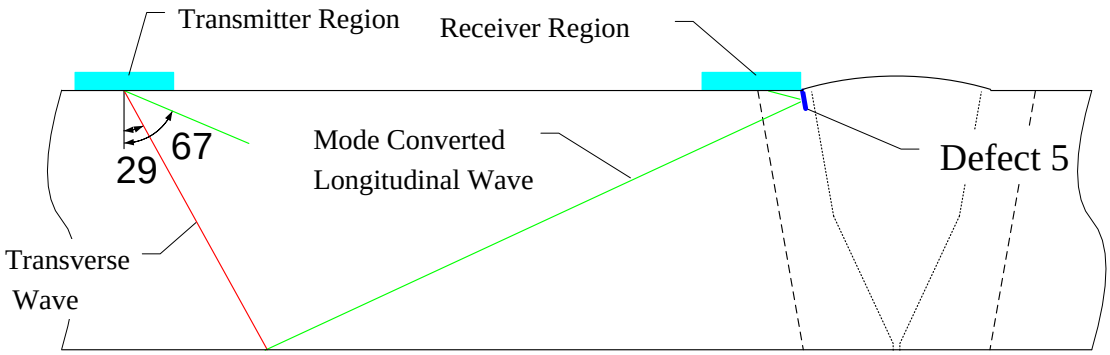

Figure 4-8 Schematic diagram of the model for defect 5 - lack of sidewall fusion defect at the OD.

The simulated A-Scans from the FE model and the CIVA model are compared to the experimental A-Scan recorded for defect 5 in Fig 4-10. Once again the amplitude of the A-Scan has been normalised to that obtained for the inspection of defect 2. The amplitude response from this type of inspection is very low and the data is therefore plotted over a reduced scale in Fig 4-10. Due to the presence of the weld cap the receiver position used in this inspection is compromised, and this leads to a low level of defect response. This type of inspection cannot be used experimentally to reliably detect flaws such as that represented by defect 5. The industrial value of this technique using standard single element transducers for the inspection of defect 5 is therefore limited. This issue is one of the motivations for development of the

membrane probe concept. The origin of the low amplitude signal that occurs at a slightly earlier time to the direct longitudinal wave response in both the FE and CIVA simulations is unclear. The signal is not observed experimentally and further study of the interaction mechanism causing this signal was not considered relevant when performing this work.

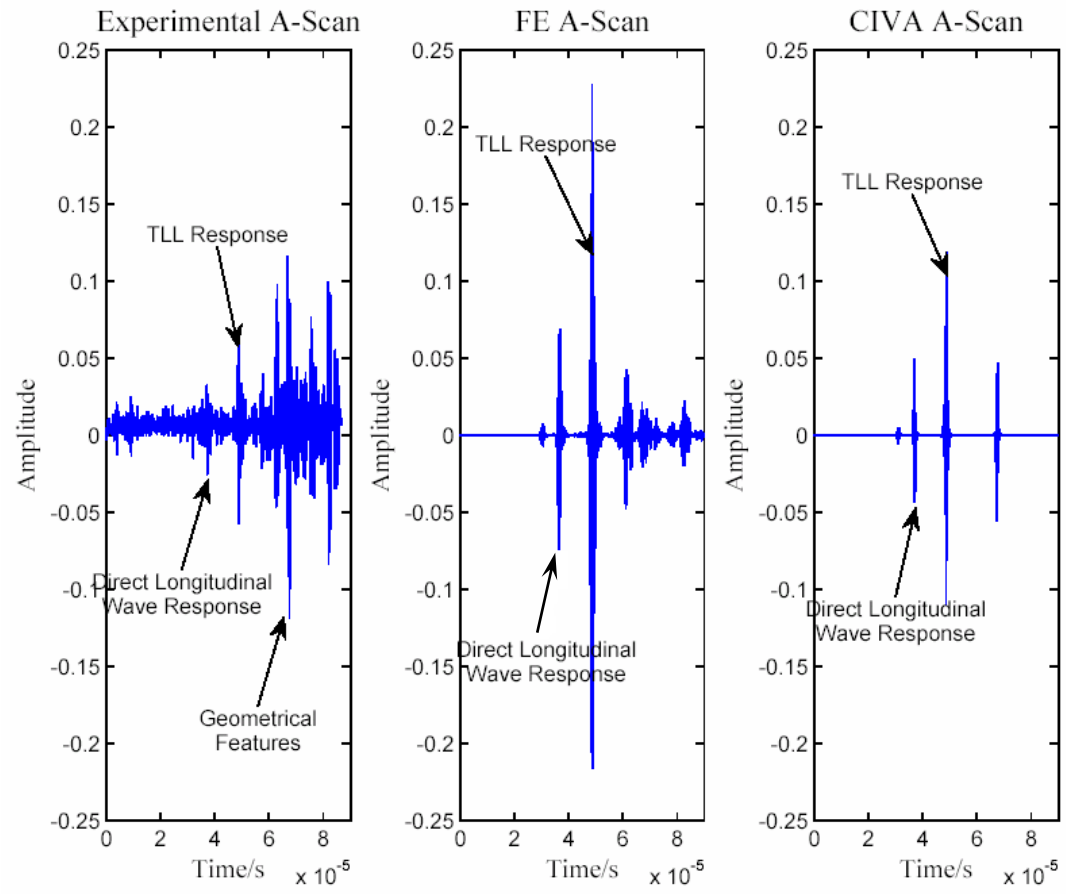

Figure 4-9 Comparison of the experimental and simulated A-Scans obtained for defect 5.

A comparison of the experimental results to the simulated results obtained using the FE model and CIVA is provided in Table 4-4. Table 4-4 demonstrates that there is a reasonable level of agreement between the simulated and the experimental results. The predicted timing of the main TLL defect response signal is very accurate in both simulations and a maximum error of 1µs is measured between the models and the experimental result. There is a discrepancy in the amplitude prediction of the main TLL response from the FE model; the amplitude prediction of the CIVA model for this wave mode is more accurate. However, the relative amplitude of the different

signals observed in the FE model is better than that obtained from the CIVA prediction. The FE model uses a 2D approximation so that the transducer and defect are both considered infinitely wide. In the CIVA model a more accurate 3D representation of the inspection is used. It is likely that this leads to differences in the prediction obtained from the two different modelling approaches.

Table 4-4 Comparison of the experimental and simulated pitch-catch TLL signals obtained for the inspection of defect 5.

Data Source	Defect 4 Signal	
	Amplitude (A.U.)	Arrival Time (μs)
Experimental	0.13	49
FE Model	0.23	48
CIVA Model	0.12	49

Once again noise has been omitted from the simulated results and a number of low amplitude signals can be clearly observed. Typically a video output can be generated from the FE model; this can be used to assist in the data interpretation process. Unfortunately this cannot be done with models of this size, and this reduces some of the benefits of the modelling process. A video cannot be generated because the size of the output file generated exceeds the maximum file size that can be processed. An investigation into the origin of the additional signals arising from the inspection has therefore been carried out using a basic time of flight calculation technique. The direct longitudinal wave response arises from an off-axis region of the longitudinal wave. The longitudinal wave is incident upon the backwall of the model; reflection at the backwall occurs and generates both a longitudinal wave and a mode converted shear wave. The mode-converted shear wave is not detected because it does not occur at a suitable angle. However, the longitudinal wave is reflected back up towards the defect and the receiver. The reflected longitudinal wave interacts with the defect and the response is detected by the receiver. This interaction is shown in the schematic diagram provided in Fig 4-11. The direct transverse wave response observed in each of the results shown in Fig 4-10 is also due to an off-axis transverse wave reflection from the backwall of the component impinging on the defect. This interaction is similar to that shown in Fig 4-11 but occurs at a later time because of the slower velocity of the transverse wave.

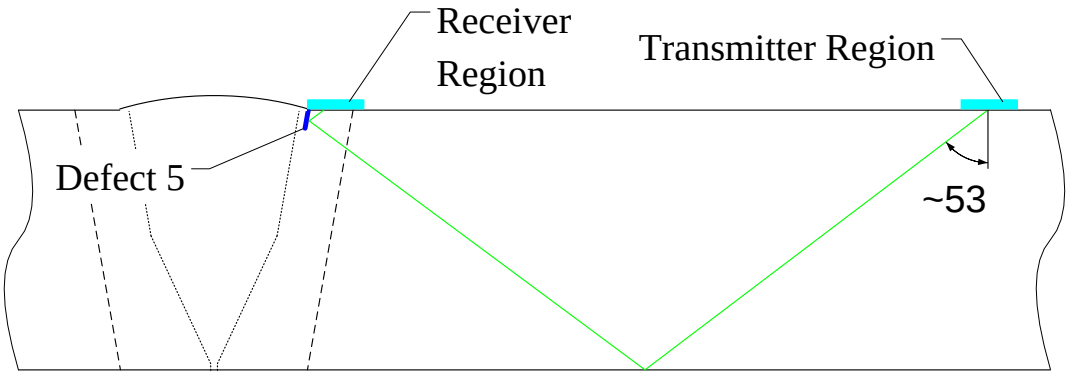

Figure 4-10 Schematic diagram of the beam spread longitudinal-longitudinal wave interaction with defect 5.

4.4. Summary

Modelling is fast, cost effective method of supporting the development of new non-destructive inspections for safety critical components found within the nuclear industry. In this chapter I have reviewed the CIVA modelling platform and the FE method applied to ultrasonic inspection. CIVA is a semi-analytical model developed by the CEA and used by a wide range of academic and industrial users. CIVA contains a beam computation model to visualise the ultrasonic field produced by a transducer and a defect response model that can be used to predict the response from different defects. CIVA incorporates a drawing package that allows the user to design different test-piece configurations and to embed complex defect shapes. The CIVA model contains the Kirchhoff approximation, the Geometrical Theory of Diffraction (GTD) and the Born approximation and automatically selects the most appropriate model for the inspection of a given defect. CIVA has been designed to provide a rapid modelling capability even in relatively complex inspection scenarios. The CIVA platform is supported by a large team of engineers and scientists and is constantly being improved. My personal experience with CIVA platform is that the functionality and usability of the platform have been enhanced significantly in recent years. However, the defect response approximations within CIVA are not suitable for use in the near field of the defect or for small defects. CIVA does not offer any warning messages when it is being used outside its range of validity and relies on the user being aware of the model's capability. Although the CIVA model is under constant development it still does not support some types of inspection.

FE modelling offers an alternative to the CIVA platform and can be used to simulate inspection techniques not supported by CIVA. FE modelling offers a potentially accurate method to simulate the inspection of small, complex defects using a wide range of different techniques. However, FE modelling is relatively complex and difficult to implement and the quality of the FE model is highly dependent on the skill of the user. Modelling complexity increases with size and this severely limits the applicability of the technique in industry. Techniques such as the use of the ALID absorbing regions help to reduce the overall model size but further research is required to develop more accessible approaches to FE modelling.

The results comparison between experimental testing and CIVA and FE simulations demonstrates a reasonable level of agreement between both types of model and experiment. However, neither of the models offers an entirely accurate simulation of the inspection, and some differences exist between the simulated and experimental results. The CIVA simulation models were more easily produced and much faster to run than the FE simulations. Given the comparable performance of the two different approaches CIVA modelling is typically considered to be more appropriate in the industrial context but care must be exercised to ensure the accuracy of the results produced.

The CEA are working to incorporate the ability to simulate the response from small and complex defects using FE within the CIVA package. In release 10 of the CIVA platform it will be possible to buy Athena which is a bespoke FE package and has been embedded into the CIVA model. Rolls-Royce is also working with the CEA and researchers at Imperial College to develop a hybrid ray-tracing/FE inspection model using Abaqus, which is a commercially available FE model. The use of this combined model will also improve the accuracy of the simulations. The ability to utilise the strengths of both modelling approaches will be very beneficial and is likely to facilitate the adoption of modelling tools within industry.

5. Membrane Coupled Device Developments

In the experimental results presented in chapter 3 there was an internal reflection that occurs within the 2nd generation membrane probe design. This internal noise signal corrupts the quality of the inspection data obtained using the 2nd generation membrane coupled device. In order to deploy the membrane coupled device in a commercial application the origin of this internal noise signal had to be fully understood and removed from the inspection image. Analysis of this signal and subsequent redesign of the 3rd generation membrane coupled device was reported in my 30 month and 36 month reports (Russell, 2008a; Russell, 2008b) and formed the basis for papers presented at the 35th Annual Review of Progress in Quantitative NDE (Russell et al, 2008) and at NDT 2008, the 47th annual conference of the British Institute of Non-Destructive Testing (BINDT). A detailed discussion of this work is provided in this chapter. Firstly, the presence of this internal noise signal within the inspection volume of interest will be presented. This will be followed by a discussion of the modelling and experimental work performed to identify the two actual sources of noise. The first noise source is due to the presence of grating lobes within the 2nd generation membrane device water path due to the large element pitch used in the array. The second source of noise, which is the most significant in the 2nd generation design and which occurs in all phased array wedges, is due to a beam spread signal within the transducer wedge. I will then discuss the optimisation of the 2nd generation, 80 element membrane coupled device and the subsequent design changes that were made in the 3rd generation 128 element device. The performance of the three different 3rd generation designs in comparison to the 2nd generation will then be compared considering the inspection of the flat plate non-welded test-pieces.

5.1. Second Generation Membrane Probe Design

In the inspection of some defects contained within the flat plate, non-welded test pieces, the internal echo signal occurs at a similar time to a signal of interest. This leads to noise being observed within the data and can prevent accurate defect detection. This was shown in the results provided previously in Chapter 3. This issue is particularly significant for defects 2, 3 and 4 where the defect signal occurs at relatively long time periods. The inspection of defect 3 in the non-welded test-pieces is shown in Fig 5-1, a schematic diagram of the TL mode conversion technique used

to detect this type of defect is shown in Fig 5-1(a) and the result obtained using this technique is shown in Fig 5-1(b).

a.)

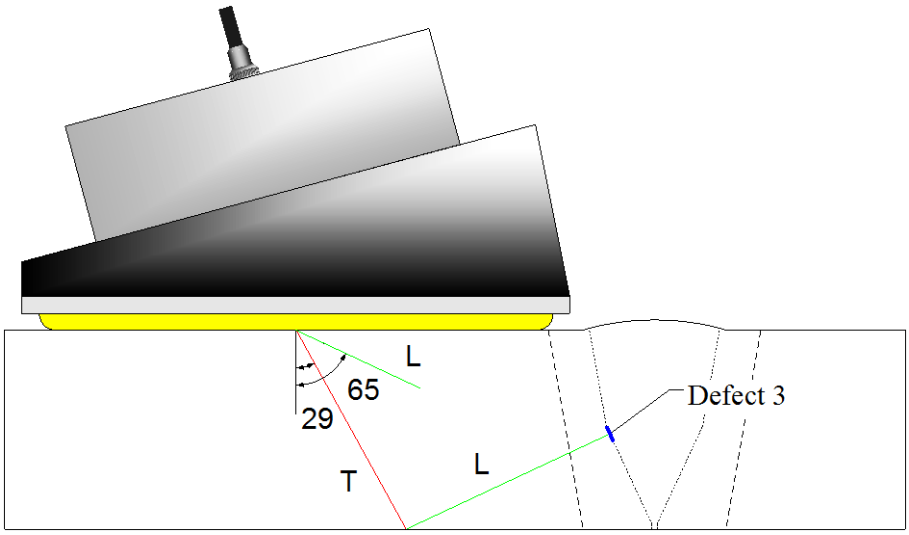

b.)

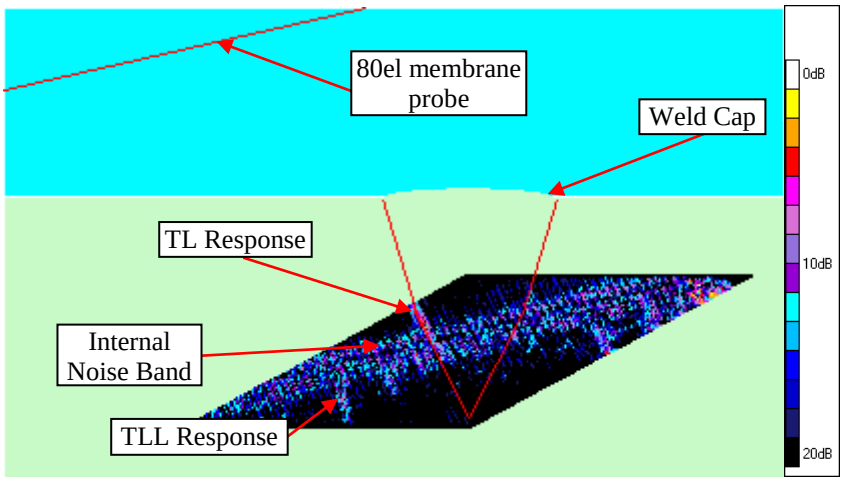

Figure 5-1a.) Schematic diagram of the inspection technique used for the detection of defect 3, b.) B-Scan recorded during the inspection of defect 3 using the membrane probe with FMC, data is post processed to simulate a 65° longitudinal wave probe.

The presence of this noise signal severely degrades the performance of the membrane coupled phased array, and reducing its effect is critical to the success of the membrane coupled device development project. Unfortunately it is not possible to simulate this reflection using CIVA; this is because CIVA was not intended for use as a transducer wedge design tool and does not simulate multiple reflections within the wedge. Modelling this reflection using a FE simulation is also not straightforward; a very fine mesh density would be required because the acoustic wavelength in water is short. It is therefore not possible to produce an accurate mesh of the entire 80 element

membrane probe housing and a reduced size probe housing must therefore be considered. In order to generate an accurate model the material properties of the medium under test must be accurately represented so that the propagation of acoustic energy can be precisely modelled. Validation of the model produced would also be required to demonstrate that it accurately represented the physical inspection. It is achievable to generate validated models of this type, but due to the time associated with this activity it is not considered viable in an industrial environment. Alternative modelling approaches were therefore considered to investigate the origin of the membrane device internal noise.

5.2. Grating Lobe Internal Noise

An initial simulation of the membrane coupled device performance was performed using QSonic. QSonic is a relatively crude model developed by Imasonic to assist with the design of phased array transducers. The model has not been extensively validated (Shipp et al, 2008) but can be used to quickly generate an approximate solution. QSonic can be used to rapidly understand the nature of the beam transmitted into the component under test and to assess whether any grating lobes are generated by the array in both the water wedge and the stainless steel component.

The software was used to investigate the presence and nature of grating lobes within the membrane coupled device. Grating lobes were discussed in chapter 2 and are a characteristic of any phased array transducer. The membrane coupled phased array can be used to generate acoustic energy over a wide range of angles. There is a large difference in the acoustic impedance of water and stainless steel. Therefore only energy produced by the membrane probe over a limited angular range can propagate into the stainless steel component. The 2nd critical angle for propagation of any ultrasound into stainless steel using the membrane coupled phased array is approximately 29^{o}. This corresponds to the absolute maximum required steering angle when using the membrane probe approach. By substituting this value into equation (2.4) an element pitch of approximately $\leq 2\lambda/3$ must be used to eliminate any grating lobes. This larger element pitch is acceptable because the overall steering range is relatively limited. In order to eliminate grating lobes under all operational conditions an element pitch of $\leq \lambda/2$ must be adopted.

The 2nd generation 80 element membrane coupled device design was selected to allow the complete inspection of the flat plate, non-welded test-pieces from the minimum number of axial transducer positions. In order to achieve this objective a comparatively large footprint device was required and a device with a relatively large element pitch was selected. The pitch of the 80 element array violates the $2\lambda/3$ rule when coupled to the water filled wedge. Equations (2.3) and (2.4) along with QSonic were used to quantify this issue and to understand whether the internal reflection observed in the testing performed using the 2nd generation device is related to the presence of a grating lobe.

In order to generate these results the probe configuration must be input to QSonic via a graphical user interface. The number of elements, the element width and pitch, the array angle and the steering angle are all required along with the ultrasonic velocity in the wedge and test material. The images in Fig 5-2 have been obtained by simulating the 2nd generation membrane coupled device using QSonic, in each case the main beam is shown in red and the grating lobes are shown in blue. In all cases a 2MHz, 80 element array with a water wedge angle of 13.5º, an element pitch of 1.25mm and element width of 1mm is modelled. In Fig 5-2a there is no beam steering and a longitudinal wave at the natural angle of the array is produced. In Fig 5-2b the beam is steered to produce a 0º longitudinal wave in stainless steel. Finally in Fig 5-2c a high angle shear wave is produced with an angle of incidence at the outer surface of 28.7º which corresponds to the shear wave critical angle between water and stainless steel. This study demonstrates that at least two grating lobes are present in the membrane device at all beam angles and that a third grating lobe is observed when steering over a large angular range. The results presented in Fig 5-2 also demonstrate that when the array is steered over large angles grating lobes can exist within the steel component. These extreme cases were not used in the inspection of the two flat plate non-welded test-pieces but are required to provide a complete inspection capability. A summary of the grating lobes and the angles at which these are generated is included in table 5-1.

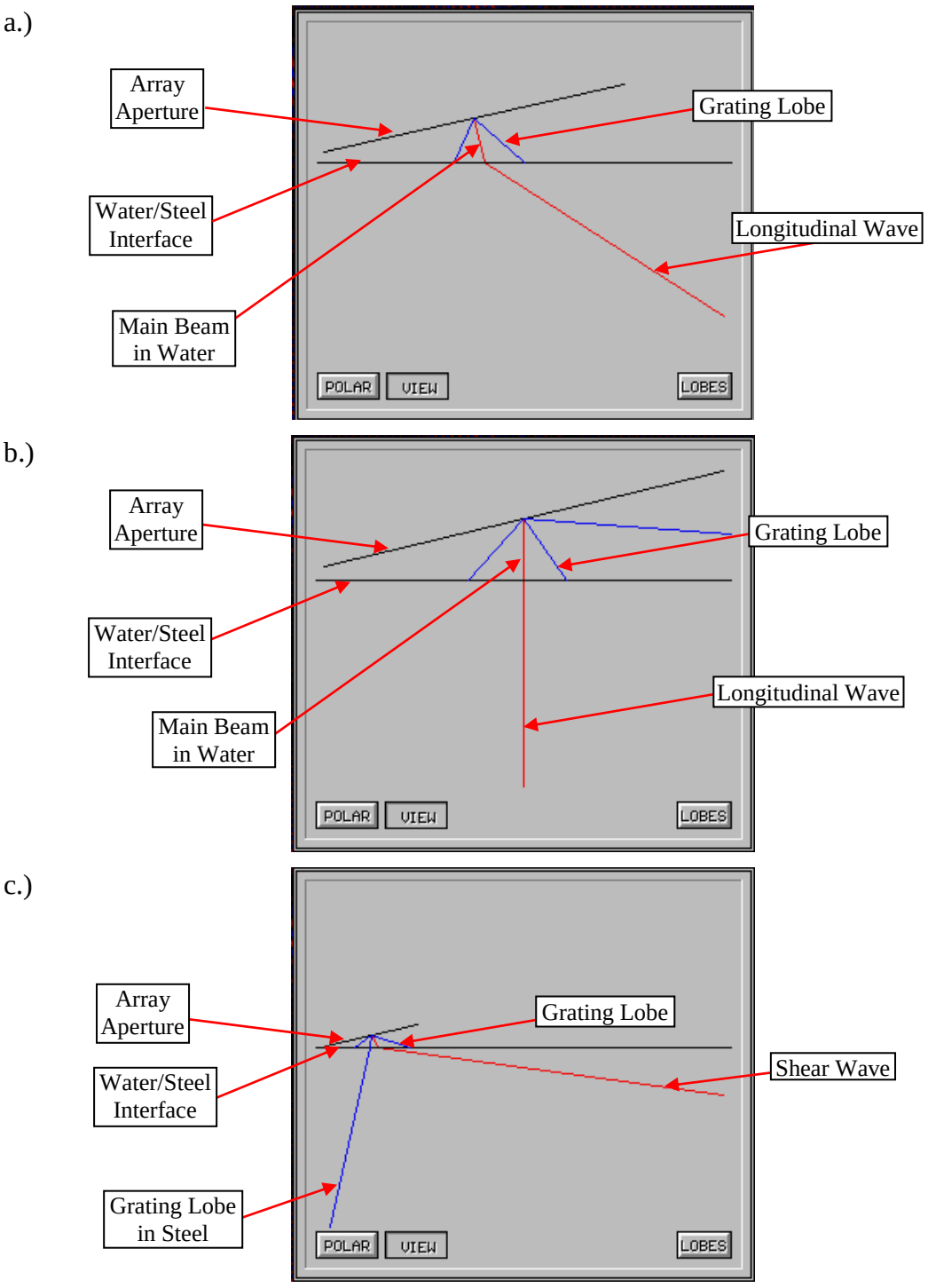

Figure 5-2 QSonic images based on current membrane probe design a.) No beam steering, b.) Steering to 0º, c.) Steering to shear wave critical angle.

Table 5-1 Summary of the results obtained from the QSonic study to investigate the grating lobes produced by the 2nd generation membrane coupled device over different steering angles.

Angle of incidence	Grating lobe angles relative to main beam in water (º)			Grating lobe angles relative to main beam in steel (º)
13.5	-22.8	49.8	-	-
0.0	-42.1	34.5	85.4	-
28.7	-5.8	-53.7	72.2	-12.0

The data obtained concerning the membrane coupled device using QSonic was then used to support a theoretical analysis. The prototype membrane coupled device was designed to generate a longitudinal wave with a natural angle of 65º in stainless steel; this beam angle is used in the majority of the flat plate, non-welded test-piece inspections. Therefore, in order to carry out the theoretical study the natural angle inspection configuration was considered, which is shown in the schematic diagram in Fig 5-3. It can be seen that in this configuration two grating lobes are generated, these occur at approximately ±36º relative to the main beam, or -23º and +50º relative to the surface normal. QSonic does not provide any information regarding the relative amplitude of the different grating lobes. However, CIVA can be used to provide this data and the relative amplitude of the three beams can be observed in the CIVA beam propagation model shown in Fig 5-4a. In this simulation an aperture of 20 elements has been used to generate the image. The CIVA plot demonstrates that the amplitude of the grating lobes is very small in comparison to the amplitude of the main beam. An echodynamic response generated along the water/steel interface in the CIVA plot is also included in Fig 5-4b. The echodynamic is a plot of the signal amplitude along this interface. Analysis of this result demonstrates that the highest amplitude grating lobe signal is approximately 19dB lower in amplitude than the main beam at the component interface.

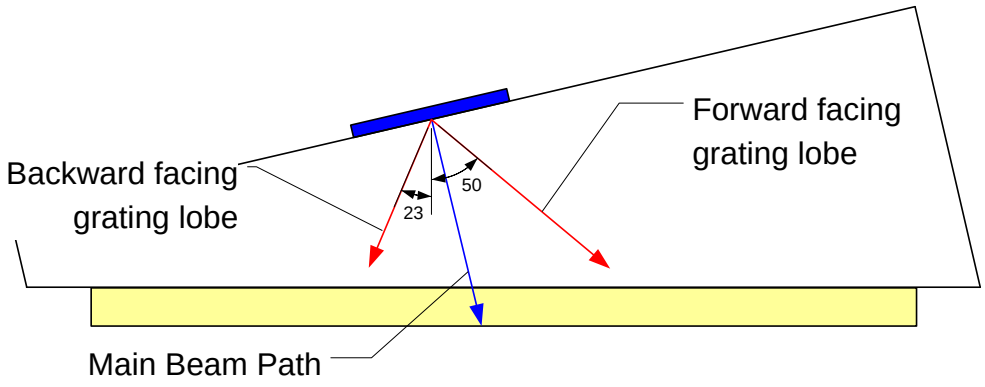

Figure 5-3 Schematic diagram of the prototype membrane coupled device, showing the main beam and the two associated grating lobes.

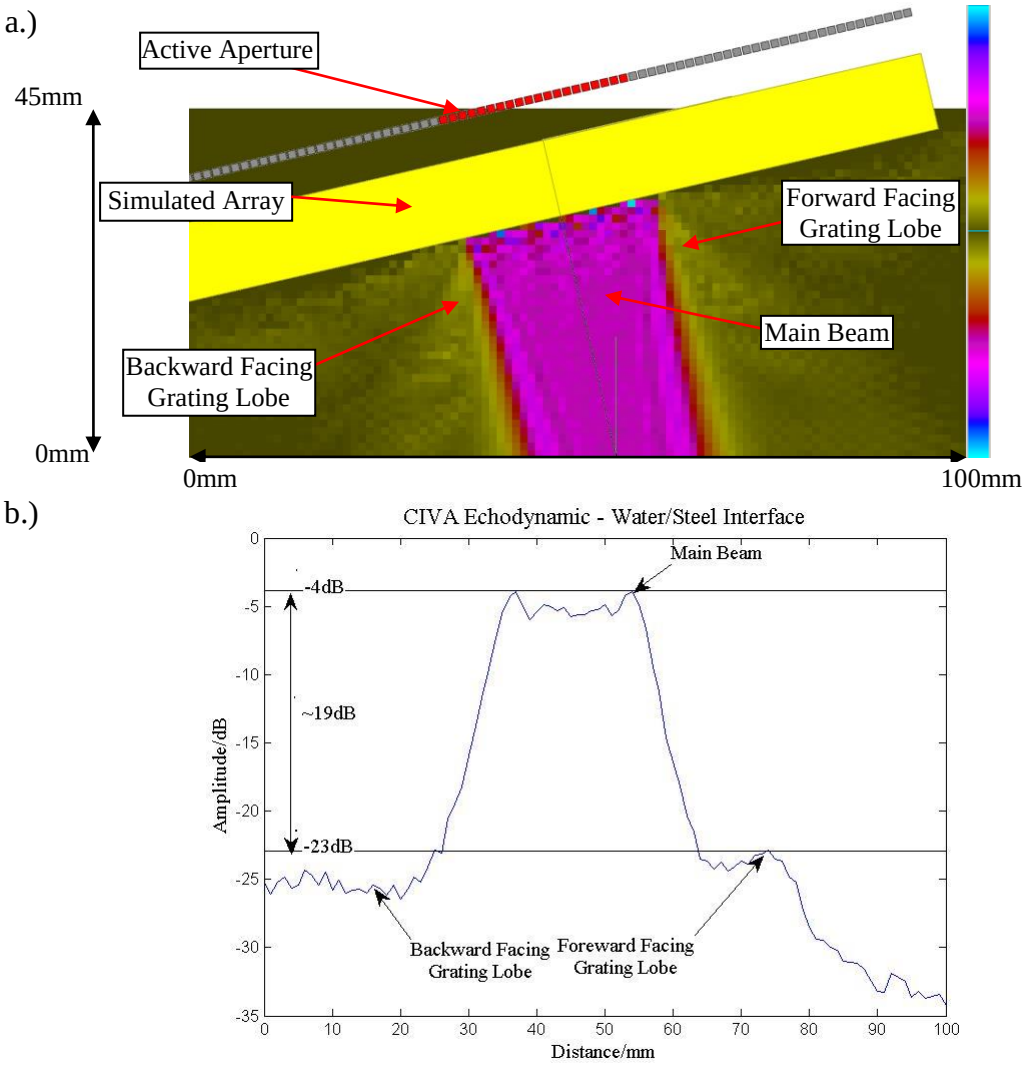

Figure 5-4 a.) CIVA beam plot obtained from a 20element aperture using the 2nd generation membrane probe demonstrating the relative amplitude of the main beam and the two grating lobes, image is shown with a dynamic range of 30dB, b.) the echodynamic response along the water/steel interface.

As the inspection angle is electronically steered, the angle of each grating lobe is fixed relative to the main beam. Therefore in the 2nd generation prototype membrane coupled device when a 65º longitudinal wave is generated in steel, the forward facing grating lobe at water occurs at 50º relative to the component surface normal. This water wedge grating lobe reflects from the outer surface of the component under test and propagates towards the front face of the wedge housing. A schematic diagram of the grating lobe path is shown in Fig 5-5. The angle of the front face of the membrane device housing has been suitably selected to minimise the amount of energy associated with this beam that is reflected back towards the active aperture. The amplitude of the beam associated with this reflection path is therefore expected to be very low. The path length of this signal is also long and varies depending on the active aperture. Therefore any signal that does return to the active aperture will occur at a delayed point in time and will not interfere with the defect signals of interest within the inspection. Due to the variable path length this reflection does not form a single well defined signal and this reflection path does not contribute to the internal noise band observed in Fig 5-1(b).

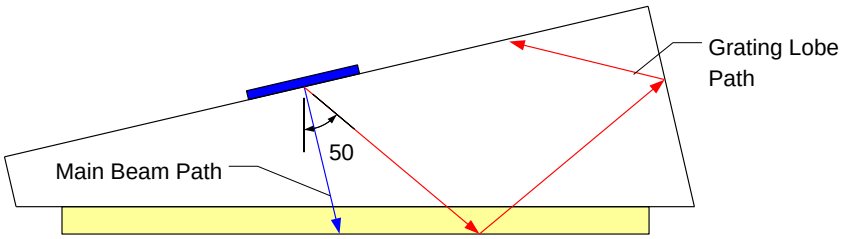

Figure 5-5 Schematic diagram of the prototype membrane coupled device, showing the forward facing grating lobe internal reflection path.

As previously stated the backward facing grating lobe occurs at -36º from the main beam, or -23º from the surface normal. The angle of the grating lobe relative to the component outer surface therefore changes depending on the inspection angle selected. A geometrical study of the grating lobe path using the 2nd generation prototype membrane coupled device was performed for different angles of incidence; schematic diagrams of the configurations considered are shown in Fig 5-6 for angles of incidence between approximately 0º and 20º. The path length is calculated for energy at the centre of the beam through measurement based on the schematic

diagrams assuming a wave velocity in water of 1483ms^{-1}. This reflection path was not considered in the design of the 2nd generation membrane coupled device and hence the probe was not designed to avoid this issue. It is clear from these figures that the path length of the grating lobe reflection changes significantly with the steering angle used. If the grating lobe reflection causes the internal noise band observed in the data then the time and hence position of the noise band would vary with changing angle of incidence. A geometrical analysis of the predicted time associated with the grating lobe noise band for each beam shown in Fig 5-6 is provided in Table 5-2. Once again this analysis has been performed assuming a 20 element aperture so that the minimum length reflection path corresponds to elements 1-20 and the maximum corresponds to elements 61-80. The effective noise path length is the difference in time between the noise path and the main beam. This corresponds to the time at which any noise would be measured experimentally.

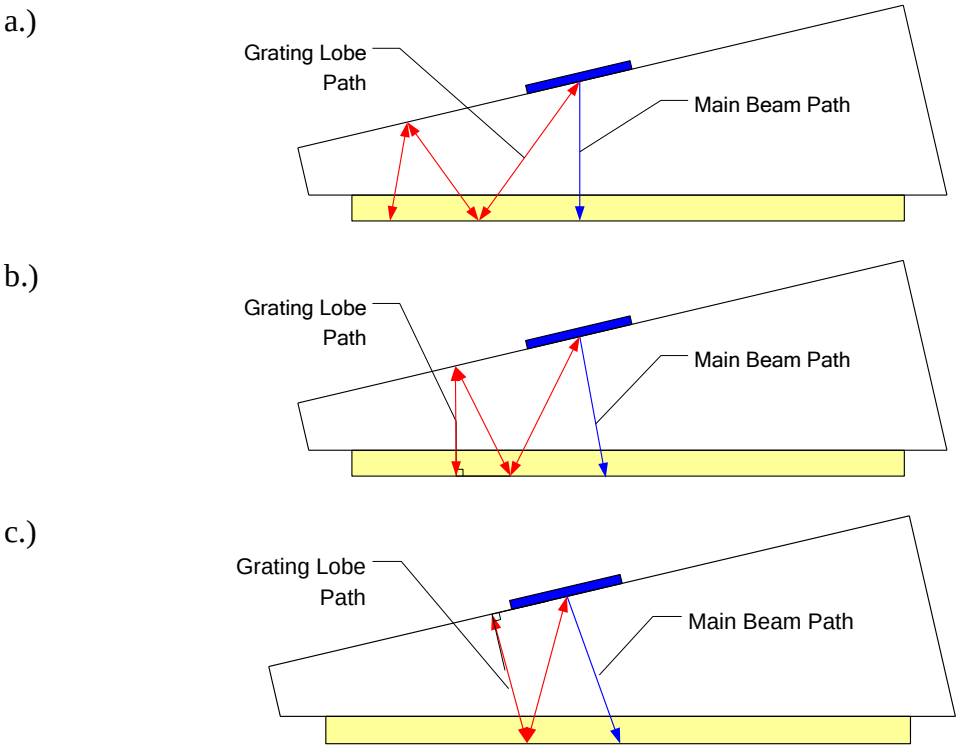

Figure 5-6 Schematic diagrams of the grating lobe reflection path occurring in the 2nd generation membrane coupled device at different angles of incidence, a.) 0º incidence angle, 0º longitudinal wave, b.) 10º incidence angle, 45º longitudinal wave, c.) 20º incidence angle, 45º shear wave.

Table 5-2 Membrane coupled device grating lobe noise band predicted through geometrical analysis.

Incident wave angle (º)	Probe Angle (º)	Main Beam Path (µs)		Grating Lobe Noise Path (µs)		Effective Noise Path (µs)	
		Min	Max	Min	Max	Min	Max
0	0 Long	31.6	55.2	90.9	160.1	59.3	104.9
10	45 Long	32.6	56.1	89.7	154.1	57.0	98.0
20	45 Shear	34.3	58.7	62.7	107.5	28.5	48.8

The amplitude of this noise signal would also vary significantly with angle; at low angles of incidence, shown in Fig 5-6(a) and Fig 5-6(b), the internal noise signal undergoes five reflections. Also shown in Fig 5-6(a) is that in the final reflection from the outer surface of the component under test is not exactly at right angles. At this point the beam is relatively broad and therefore contains energy at a range of angles, only energy at the correct angle is reflected back to the active aperture. These effects will significantly reduce the amplitude of this signal. At higher angles of incidence, as shown in Fig 5-6(c) only three reflections occur. Therefore at these angles the noise signal amplitude is expected to be higher.

The time associated with the internal noise band can be validated experimentally by altering the angle of incidence and measuring the time associated with the internal reflection. This is readily achievable using the FMC data acquisition approach because the complete matrix of data has been collected and different inspection angles can be generated in post-processing. Experimental results are shown in Fig 5-7, the images shown in Fig 5-7 have been optimised to indicate the different noise signals and hence are not shown on the same scale. In order to study this internal noise signal I identified that the Imperial College post-processing software must be updated to allow the user to directly measure the time associated with any point within the B-Scan image. Changes to this software facility were subsequently implemented by Dr Rob Long. In order to assess the variation in amplitude of the internal noise signal the functionality of the Imperial College processing software was further updated to allow this information to be extracted. Once again I identified the requirement to make these updates and they were subsequently implemented by Dr Long. The software was updated to report the maximum signal within the B-Scan image produced. This improved functionality of the FMC post processing software has been used to

generate the experimental results provided in Table 5-3. The results in Table 5-3 clearly demonstrate that the time period associated with the effective noise path is very consistent over different incident angles. In table 5-3 the amplitude of the internal noise signal is estimated by reducing the size of the B-Scan image produced by the post processing software so that only the noise signal is present. The values reported in Table 5-3 are therefore only indicative of the signal amplitude of the region of the internal noise signal imaged. The amplitude of the internal noise signal gradually decreases as the angle of the ultrasonic beam generated is increased. If the internal noise signal were due to the grating lobe signal the opposite effect would occur. As the angle of the ultrasonic beam is increased the grating lobe beams undergo less reflections and an increased amplitude signal is expected. The analysis of the time and amplitude of the internal noise signal demonstrates that the grating lobe noise band does not significantly contribute to the noise observed in the experimental data.

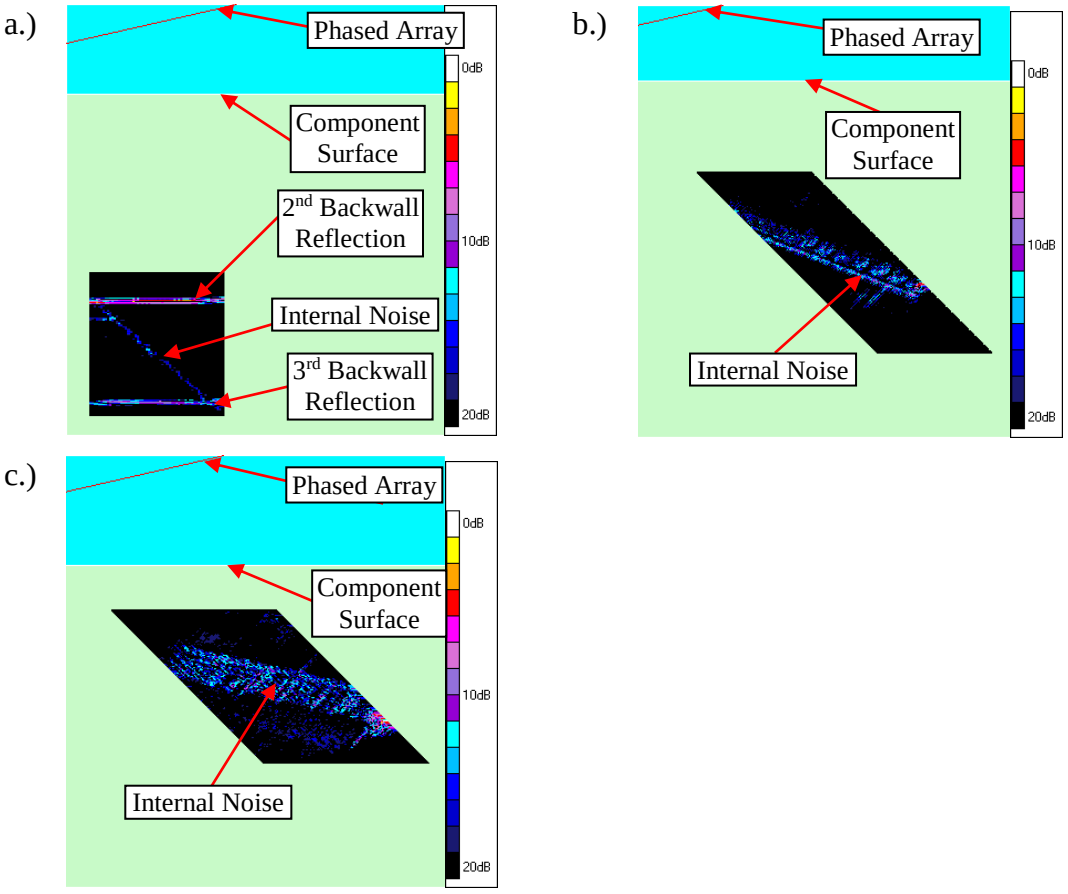

Figure 5-7 Experimental results obtained using the membrane coupled phased array device, a.) 0° incidence angle, 0° longitudinal wave, b.) 10° incidence angle, 45° longitudinal wave, c.) 20° incidence angle, 45° shear wave.

Table 5-3 2nd generation membrane coupled device internal noise band experimental results.

Incident wave angle (º)	Probe Angle (º)	Effective Noise Range (µs)		Signal Amplitude (A.U.)
		Min	Max	
0	0 Long	80	120	40
10	45 Long	80	120	19
20	45 Shear	80	120	15

5.3. Beam-Spread Internal Noise

A source of internal noise, which occurs in all phased array wedges, is due to beam spread within the wedge material. In the majority of phased array inspections an aperture within the phased array is used to generate the ultrasonic beam. The beam generated by this aperture is not perfectly collimated and some beam spread due to the effects of diffraction is observed. Some energy is generated at the correct angle to reflect from the component outer surface, back up to the phased array. It impinges normally on the phased array and then follows the same path in reverse back to the active aperture. This reflection path is shown for a simple 0˚ longitudinal wave inspection using the membrane probe in the schematic diagram in Fig 5-8. As shown in Fig 5-8 it is the beam energy that occurs at an angle equivalent to the wedge angle that contributes to this internal noise signal. The effect of the internal noise signal is highly dependent upon the aperture size used. As the aperture size is increased the beam generated becomes more collimated in nature and the amount of beam spread reduces. The amplitude of the beam spread noise signal therefore decreases and inspection performance improves. This implies that if the array design cannot be controlled to completely remove the internal noise signal from the region of interest then a large aperture should be used to mitigate the deleterious effects of the beam spread noise signal.

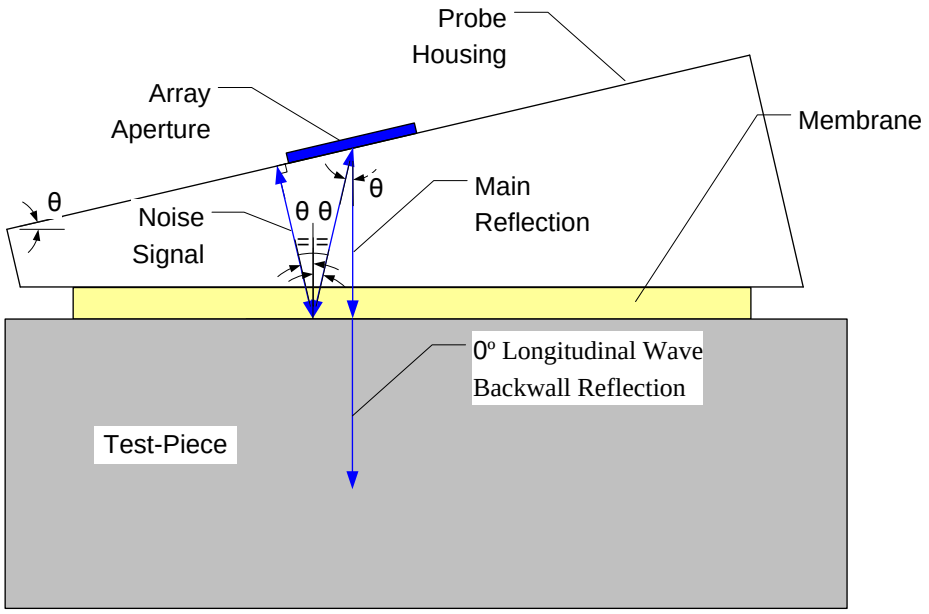

Figure 5-8. Schematic diagram of the beam spread noise signal in a simple case where the main beam is steered to normal incidence.

As stated, this beam-spread reflection occurs in all angled wedge phased arrays, this is indicated in the experimental results provided in Fig 5-9. In Fig 5-9(a) a 48 element, 1.25mm pitch linear array with a conventional rigid Perspex wedge has been used. The Perspex wedge has a 6mm first element standoff and an angle of approximately 21˚, which is used to generate a longitudinal wave with a natural angle of 65˚ in stainless steel. In Fig 5-9(b) the 80 element 2nd generation membrane probe with a 13˚ wedge angle and a 25mm first element standoff is used. The beam spread internal signal in the 48 element Perspex wedge transducer occurs between approximately 18μs and 38μs which corresponds to a region between the front wall and back wall echoes. The beam spread signal in the 2nd generation membrane coupled device occurs between approximately 80μs and 120μs which corresponds to a range between the 2nd and 3rd back wall signals. This difference in time associated with the internal beam spread noise signal is due to the higher velocity of sound in the Perspex in comparison to the water. The time measurements performed have been made directly from the highest amplitude part of the signal in B-Scan images shown in Fig 5-9. This approach is slightly subjective and the times are only approximate but it does provide an indication of the time associated with the signal. It is clear that the amplitude of the signal in Fig 5-9(b) is higher than that seen in Fig 5-9(a). A similar approach to that described in section 5.2 can be taken to assess the difference in the

amplitude of these two signals. It is found that the amplitude of the internal noise signal in the water wedge is approximately three times higher than that found in the Perspex wedge. This reduction in amplitude of the internal noise signal within the Perspex wedge in comparison to the water wedge is due to three factors. Firstly, the Perspex wedge is at a greater angle than the 2nd generation membrane coupled device and so less energy occurs at the correct angle to reflect back to the active aperture. Secondly, Perspex is more attenuative than water and hence the amplitude of the noise signal is reduced, and finally there is less of an acoustic impedance mismatch between Perspex and steel so less energy is reflected at the wedge/component interface.

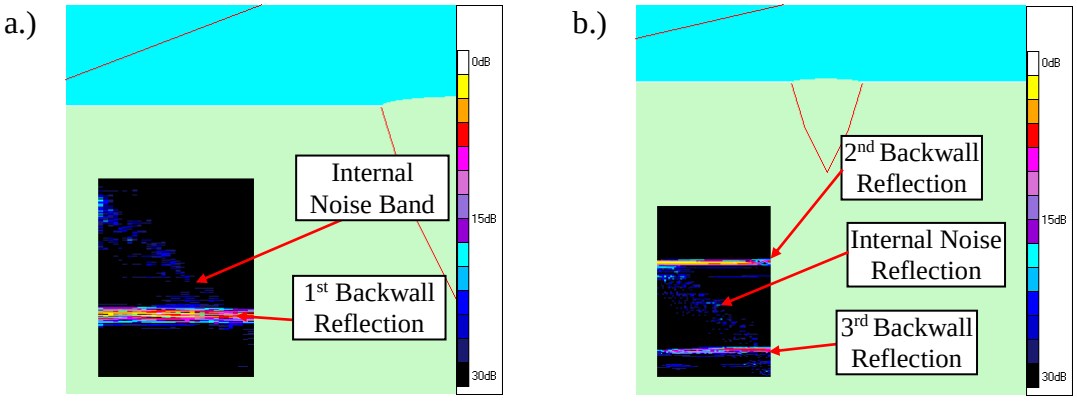

Figure 5-9. Internal beam spread noise generated in a 0° longitudinal wave inspection for the a.) conventional phased array b.) 2nd generation conformable membrane coupled device.

A range of different probe configurations have been investigated, this provides an understanding of whether this beam-spread reflection significantly contributes to the internal noise band within the membrane coupled phased array. An experimental study has been performed to assess this variation. A geometrical study has also been performed using the same principles applied in the grating lobe noise study detailed in section 5.2. Schematic diagrams have been produced for each experimental configuration measured. To facilitate the experimental study and to allow complete flexibility in terms of probe height and angle a bespoke probe jig was designed, the usage of this jig is shown in the photograph in Fig 5-10. The jig consisted of two freestanding Perspex plates, the plates were held together using four bolts, which allowed the separation between the plates to be accurately controlled. By using this jig it was possible to clamp the phased array transducer between the plates in a range of different positions relative to the component outer surface.

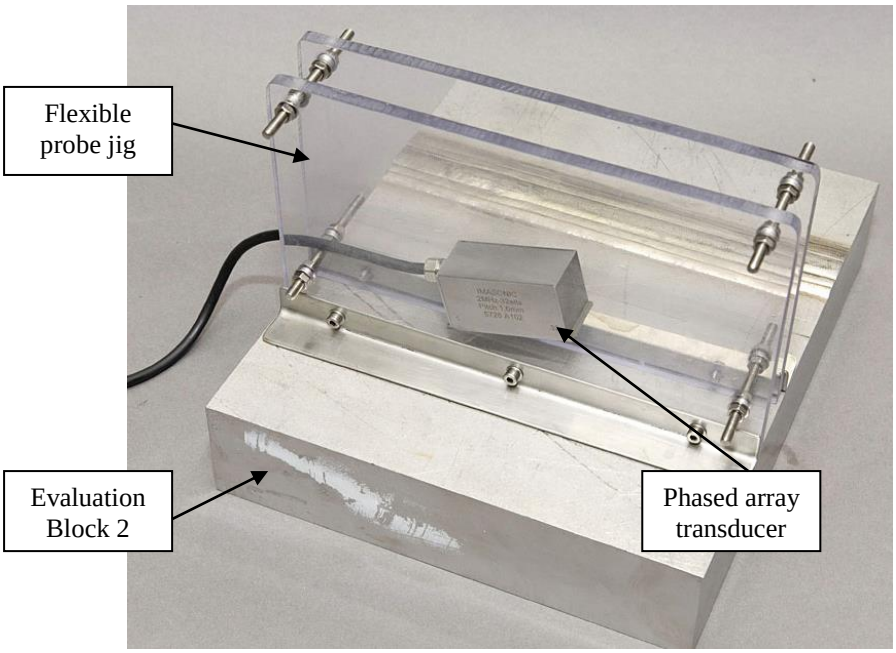

Figure 5-10 Photograph of the bespoke probe jig for internal noise signal measurements.

All experimental results have been obtained using an aperture of 20 elements, which corresponds to 25mm. As in the grating lobe internal noise study, the minimum length reflection path corresponds to elements 1-20 and the maximum corresponds to elements 61-80. The minimum and maximum experimental values have again been measured directly from the B-Scan image produced using the FMC post processing software. The theoretical beam path lengths have been predicted based on the schematic diagrams by considering energy at the centre of the beam. A comparison of the results obtained to assess the time associated with the internal noise signal using both the geometrical study and experimentally is provided in Table 5-4. In order to produce the results in Table 5-4 the gain used in the experimental set-up must be changed so that internal noise signal is at a sufficiently high level for accurate measurements to be taken. This variable gain has been compensated for when calculating the amplitude of the internal noise signal measured experimentally.

Table 5-4 A comparison of the membrane coupled device beam spread noise predicted through geometrical analysis and found experimentally.

Wedge Material	Number of Elements	Probe Angle (°)	1st Element Height (mm)	Theoretical Effective Noise path (μs)		Experimental Effective Noise path (μs)		Experimental Internal Noise Amplitude (A.U.)
				Min	Max	Min	Max	
Water	80	13	14	44	86	42	86	4.2
Water	80	13	21	62	104	60	104	4.2
Water	80	13	35	96	140	98	142	4.2
Water	80	18	21.5	62	118	64	128	3.8
Water	80	18	38.5	102	144	106	150	3.8
Water	80	5	11.0	32	50	35	54	20.9
Water	80	10	11.5	36	70	40	72	6.2
Water	80	15	12.5	40	88	46	92	3.5
Water	80	20	13.5	42	102	42	108	3.1
Water	80	25	14.0	42	112	Not visible[1]		Not visible[1]
Water	80	30	15.0	42	116	Not visible[1]		Not visible[1]
Perspex	48	21	9.0	16	38	18	38	2.9

Notes

[1] The internal noise signal is not observed even when the experimental gain used is increased.

It is clear based on the results provided in Table 5-4 that there is generally a very good agreement between the times associated with the theoretical and experimental effective noise band. This indicates that the noise signal observed during the inspection of the flat plate, non-welded test pieces is due to beam spread noise. There are some minor discrepancies between the two results; much of this is due to experimental measurement inaccuracy and the positioning of the array relative to the component surface. The amplitude of the internal reflection is also relatively low and occurs over a finite time period, as stated above there is therefore some subjectivity in the exact time associated with this noise.

The amplitude of the internal noise signal is highly dependent upon the angle of the array relative to the component outer surface. This effect is clearly seen from the

experimentally measured signal amplitude for each array configuration in Table 5-4. The results provided in Table 5-4 demonstrate that when the angle of the array is increased, the amplitude of the noise signal decreases and that when the water wedge angle is increased to 25˚ or greater that no internal noise signal is observed. Therefore at high array angles the impact of the noise band diminishes. This effect can be seen in the B-Scan image in Fig 5-11; this image has been produced using the 15mm, 30º, 80 element array configuration. The image provided in Fig 5-11 has been produced using a large dynamic range of 40dB but the internal noise signal is not discernible against the background noise.

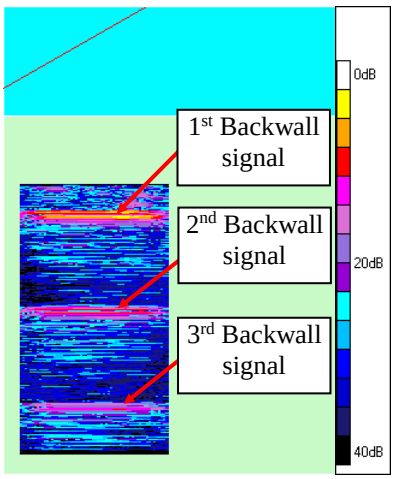

Figure 5-11 B-Scan image generated for a 0˚ longitudinal wave inspection for the 80 element, 15mm, 30º array configuration.

5.4. Optimised 80 Element Device Design

The investigations detailed above provide an insight into the use of wedge-coupled phased arrays, this improved understanding can be used to optimise the device design and improve performance of the membrane probe. As stated previously one method of reducing the amplitude of the internal noise band would be to increase the angle of the array. However, in this configuration the array must be steered over a wide angle in order to generate energy at the required beam angle. This leads to a deterioration in beam performance and decreases the effectiveness of the inspection. An alternative approach is to control the time associated with the internal noise band so that the signal occurs outside the region of interest for the inspection. There is a particular region of interest in the inspection of each of the defects present in the flat plate, non-welded test pieces. The approximate time period associated with the main defect

signal is provided for each defect in Table 5-5. The internal noise band can be moved in two ways, either by reducing or increasing the time at which the reflection occurs. In order to increase the time associated with the internal reflection the height of the array must also be increased. Unfortunately a prohibitively large device would be required to delay the noise signal sufficiently to provide a suitable inspection for all six defects. Also as the height of the array is increased the footprint must also be extended in order to avoid further internal reflections. This would be an issue in the actual target application where the large footprint would compromise performance on the elbow section of the pipe work and where access is limited. A more appropriate approach is to reduce the height of the array so that the internal reflection occurs as early as possible.

Table 5-5 Approximate time range of interest in the inspection of defects 1-6.

Defect	Approx Range of Interest (μs)	
	Min	Max
1	45	60
2	40	55
3	65	75
4	50	60
5	60	75
6	60	75

When using the membrane coupled device the minimum standoff between the first element and the component outer surface is determined by the ride-height of the array. In turn this is governed by the weld cap height that must be dealt with during the inspection. In the current application a ride-height of approximately 6mm is used to ensure that any anticipated variations in weld cap height can be accommodated. The 80 element transducer used in the current membrane probe design has a “skirt” which extends 5mm around the footprint of the array; this skirt is used to ensure that a seal can be maintained between the array and the probe housing. A schematic diagram of the probe design is shown in Fig 5-12. The skirt and the transducer ride-height requirement limits the minimum array height. When using this array, the minimum element height that can be attained is approximately 7mm. This design allows the target application weld cap, which is approximately 3-4mm in height, to be

accommodated. The optimised array configuration using this array height and a transducer angle of approximately 8º is shown in the schematic diagram in Fig 5-13.

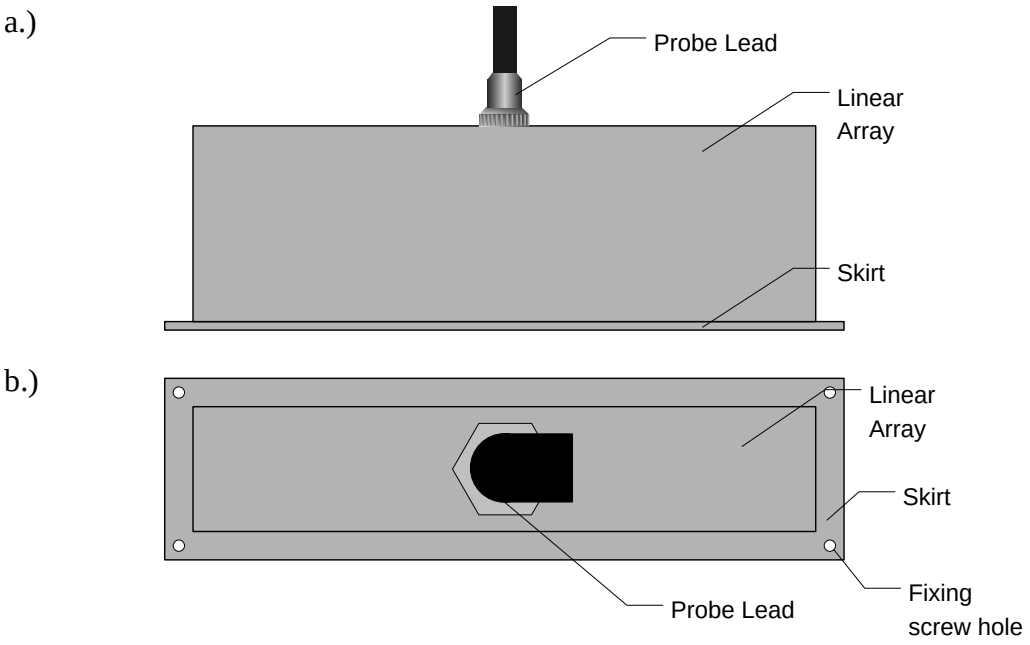

Figure 5-12 Schematic diagram of the 80 element membrane coupled device transducer a.) side view, b.) plan view.

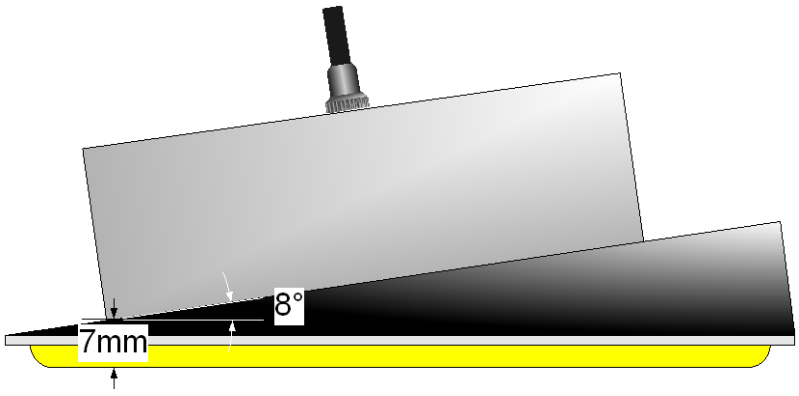

Figure 5-13. Schematic diagram of the optimised membrane coupled device housing.

In the optimised 80 element membrane coupled device design the beam spread and grating lobe noise signals still exist but occur much earlier in time, this is shown experimentally in Fig 5-14. The arrival time of the beam spread noise signal in the optimised design coincides with the first backwall signal and is comparable to that found when using the Perspex wedge, shown previously in Fig 5-9(a). In the result shown in Fig 5-14 the grating lobe noise signal is also clearly seen. In the optimised

design both of the noise signals occur before the inspection time period of interest, which allows an accurate inspection to be performed.

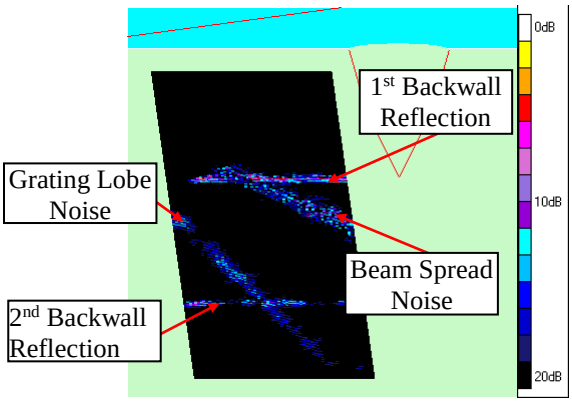

Figure 5-14. Internal noise signals in the optimised membrane coupled device.

The inspection results obtained from defect 3 using the conventional 48 element Perspex wedge transducer and the optimised 80 element membrane coupled device are shown in Fig 5-15. The result shown in Fig 5-15(b) has been obtained using the optimised membrane probe configuration; this result clearly demonstrates that the noise band has been removed from the region of interest. This result shows that through the optimisation of the design the performance of the membrane coupled device can be improved so that it is in line with conventional technology. The signal to noise ratio of the results shown in Fig 5-15(b) is comparable to that shown for the conventional array in Fig 5-15(a).

a.)

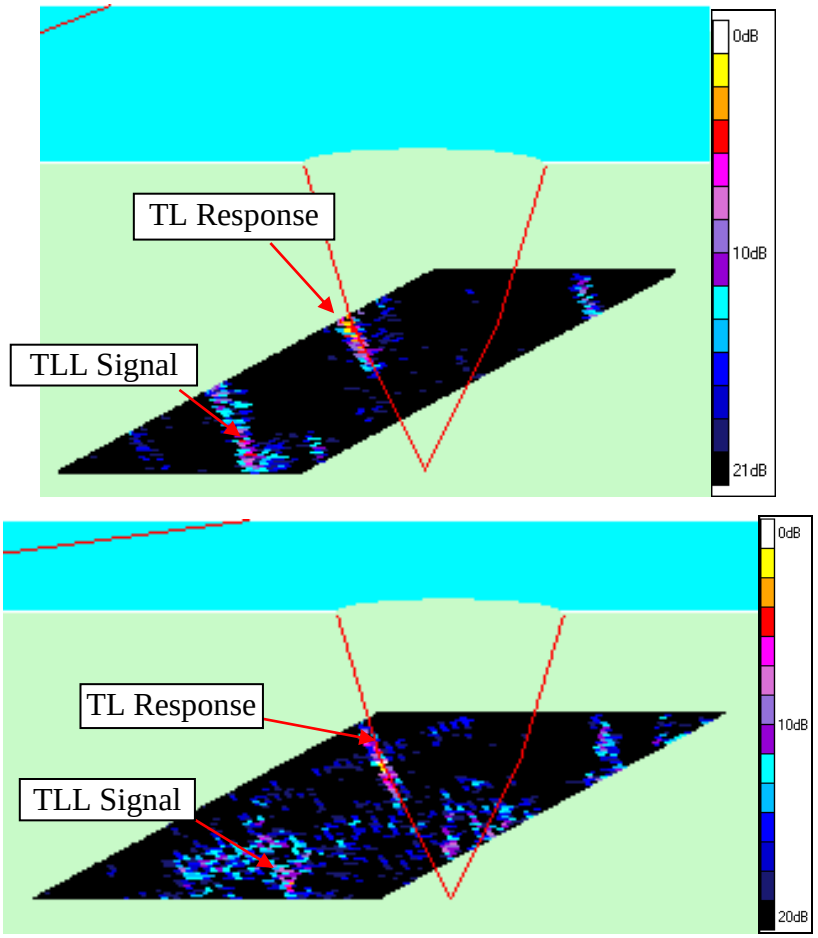

Figure 5-15. Results obtained from the inspection of defect 3 using a.) conventional phased array, b.) optimised conformable membrane coupled device.

5.5. 3rd Generation Device Design

5.5.1. Coupling

The 2nd generation membrane probe housing design did not incorporate any system for irrigation, therefore in order to ensure good coupling was constantly maintained between the probe and the component immersion testing has been used. In immersion testing the membrane is not actually required; however, testing using this approach has allowed the probe performance to be verified without the potential issue of variable coupling. Unfortunately immersion testing is typically not possible in submarine applications because in-situ testing must be performed on large components. In submarine inspections coupling is typically maintained by providing water irrigation either through the probe itself or through the probe holder assembly.

In the 3rd generation membrane coupled device design self-irrigation was investigated. The simplest mechanical solution to provide coupling would have been to puncture the membrane material itself. This technique would provide coupling to the membrane interface but would also increase the likelihood of damaging the membrane. It may also become challenging to ensure sufficient water flow to achieve coupling whilst maintaining the required membrane pressure and not introducing air into the membrane probe cavity. An alternative approach was to integrate an irrigation system into the probe housing. A separate water flow is then used to maintain membrane pressure and to provide coupling. In the 3rd generation design water is injected through the metallic base plate to maximise coupling between the membrane and the component, this is shown in the schematic diagram in Fig 5-16. In this design water will be delivered to the membrane – component interface through eight 2mm diameter tubes. Each of the housing designs discussed below use this same base-plate, this allows component re-use if required. A photograph of one of the 3rd generation membrane devices in use is provided in Fig 5-17. The main water feed into the front of the device is clearly seen being split into the eight individual feed pipes. This is a prototype design, which as will be discussed in detail below has proved successful at providing sufficient coupling between the membrane and the component under test. However, the overall size of the device is increased significantly by the inclusion of these tubes. Subsequent probe designs will incorporate irrigation channels in the delrin probe housing to reduce the overall probe size.

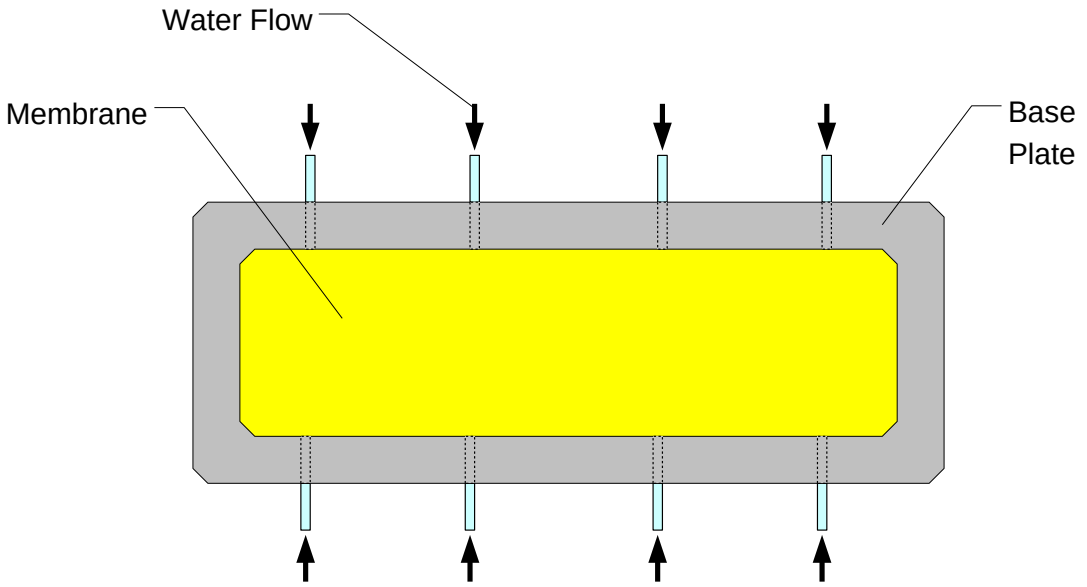

Figure 5-16 3rd generation membrane probe base plate design.

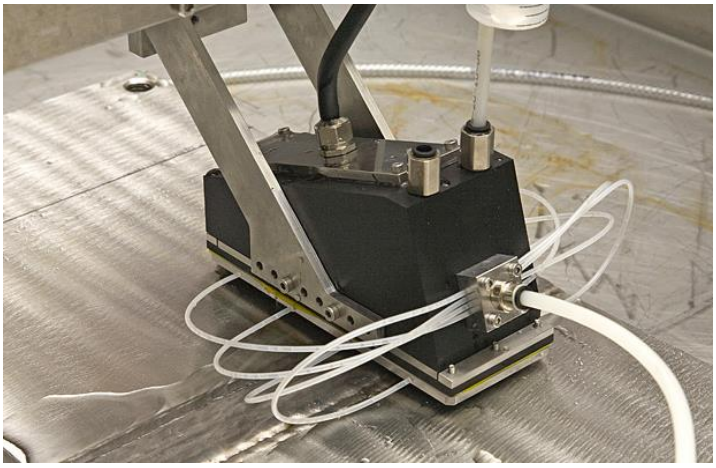

Figure 5-17 Photograph of the 3rd generation membrane coupled device showing the integrated irrigation system.

5.5.2. 3rd Generation Membrane Device Configurations

The transducer used in the non-destructive inspection of a component is optimised for the specific application. Current development of the membrane coupled phased array device is focussed on the target application inspection. The target application is a relatively large, thick walled section of pipe work. In order to minimise the amount of axial mechanical scanning required a large footprint array is used; this improves the inspection speed and can be used to provide high levels of focusing at long

distances. However, the number of array elements that can be supported is limited due to the phased array controller and the complexity of designing and manufacturing very large arrays. This trade-off leads to the element pitch used in the array exceeding the λ/2 element spacing rule and grating lobes exist which contribute to the internal noise as discussed in chapter 3. The 1.25mm element pitch used in the 2nd generation membrane coupled device design gave rise to at least two grating lobes within the probe housing at all steering angles. In this design, grating lobes can also exist within the component when generating some beam angles. Grating lobes within the component cannot reliably be compensated for in all inspection scenarios. Therefore in the 3rd generation design a smaller element pitch was selected. Analysis using QSonic indicates that no grating lobes can exist in the component if an element pitch of 0.75mm is selected. Grating lobes still exist within the water wedge but these are low amplitude and occur at an angle of approximately ±81° to the main beam, thus reducing the potential source of noise.

The phased array controller units that have been used to acquire data and to support the membrane probe development work are limited to 128 channels. This limits the active aperture of the 3rd generation device to approximately 96mm, which is comparable to the 80 element device used previously. Therefore all of the techniques that have been used to date should also be appropriate for the welded test piece inspection. The inspection of these test-pieces and the results obtained will be discussed in detail in chapter 6. This also implies that a similar approach to that discussed in chapter 3 can again be used to minimise the effect of noise in these inspections. In the 3rd generation device the transducer skirt was moved to the upper edge of the probe. This allows the first element height to be reduced as much as possible and reduces the time associated with the internal noise signals as much as possible. A schematic diagram of this probe design is shown in Fig 5-18.

a.)

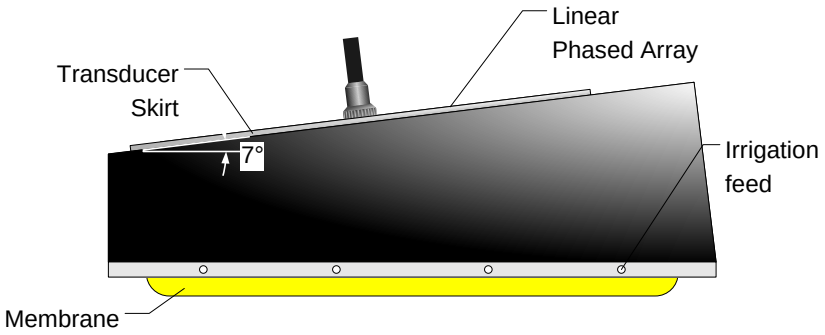

b.)

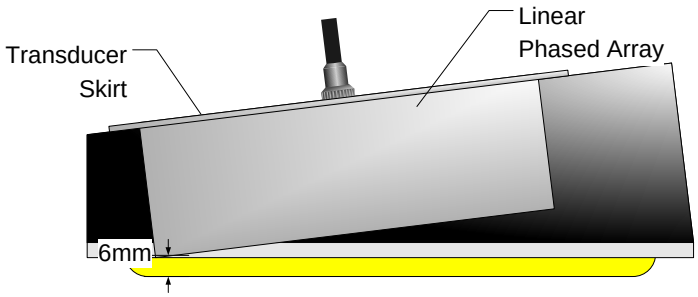

Figure 5-18 3rd generation membrane probe design, array has an approximate 6mm first element standoff height and angle of 7º.

The 3rd generation membrane coupled device has been designed to support the inspection of two flat plate welded test-pieces that are designed to representative of the target application component. In the welded test piece inspection a number of additional defects and inspection techniques will be considered. This will include a number of direct specular techniques; these techniques traverse the austenitic weld material and are commonly used to minimise the ultrasonic path length in noisy materials such as stainless steel. These techniques use longitudinal waves because this wave mode is less affected than vertically polarised shear waves by the material variations within the austenitic weld. The membrane coupled device design shown in Fig 5-18 is inappropriate for this type of inspection because the internal noise signal will overlap with the time period of interest. Two different designs were considered to address these inspections, in the first design a 20mm first element standoff and an array angle of 18º was implemented. This increased standoff delays the internal noise reflection in time, making it suitable for the direct specular inspection techniques. The array angle is selected to minimise the amount of steering required in each of the techniques used, thus optimising beam performance; this design is shown in the schematic diagram provided in Fig 5-19. The final design used a 6mm first element standoff and a 25º array angle and is shown in Fig 5-20. In this configuration the noise signal still occurs at an early time period, as in the 6mm standoff, 7º design, but

the amplitude was reduced significantly. However, as stated previously in section 5.3 the beam produced using this design has to be steered over a large angle in each of the inspections. This will potentially degrade the beam quality and limit the inspection performance. This was investigated experimentally and will be discussed in section 5.7.

a.)

b.)

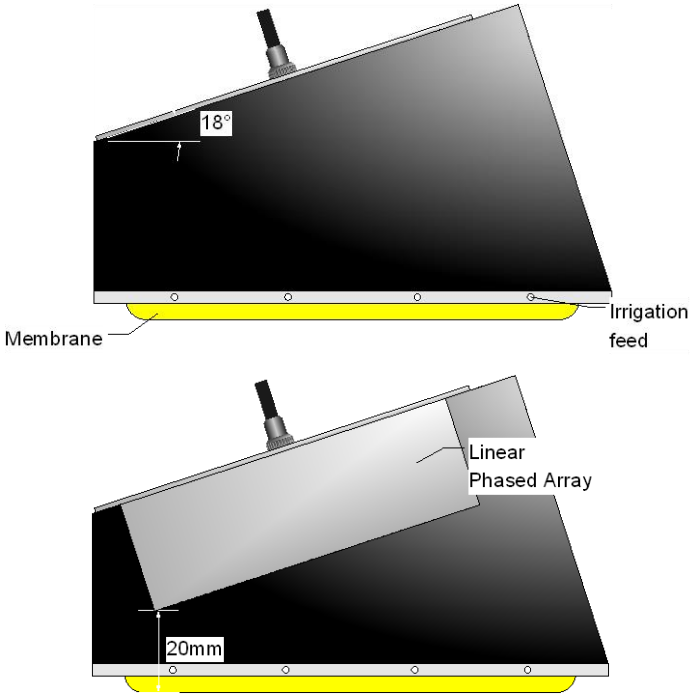

Figure 5-19 3rd generation membrane probe design, array has a 20mm first element standoff height and angle of 18º.

a.)

b.)

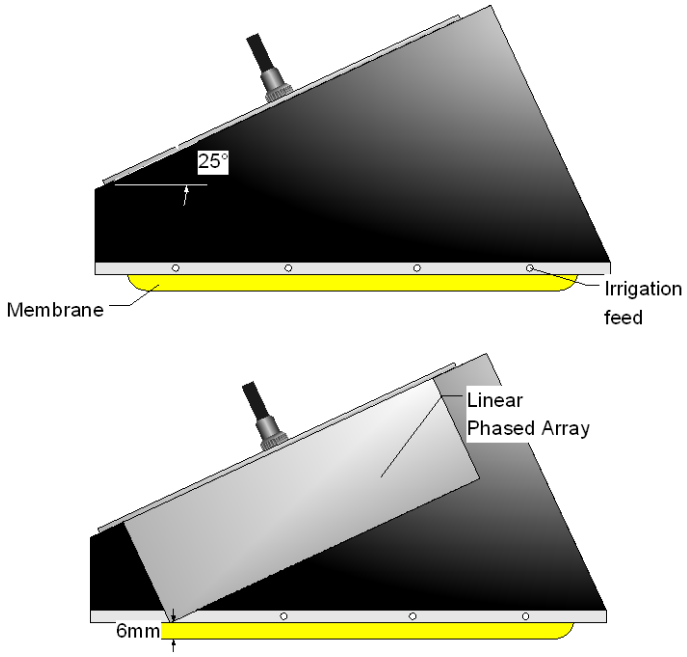

Figure 5-20 3rd generation membrane probe design, array has a 6mm first element standoff height and angle of 25°.

Imasonic were once again selected as the most appropriate vendor to manufacture the 128 element array. Through consultation with transducer design experts at Imasonic an element width of 15mm was chosen as most appropriate for the 3rd generation design to ensure good electrical impedance matching between the array controller and the transducer elements. This design maximises transducer sensitivity and minimises ringing. A 15mm width also ensures a suitably collimated beam is generated with minimal beam spread in the lateral dimension.

5.6. 3rd Generation Device Performance

5.6.1. Comparison of Irrigation and Immersion Inspection

All testing performed with the 80 element 2nd generation membrane coupled phased array device was performed in immersion. The 3rd generation probe was manufactured to include an irrigation system. This is required in most industrial inspection scenarios where it is impractical to complete testing in immersion. However, it is important to establish that the inspection performance of the device is not degraded by moving from an immersion technique to an irrigated approach. The

probe design had also been updated to include a layer of AptFlex F28 absorbent rubber (Precision Acoustics, Dorset, UK) on all of the internal faces of the probe housing. A comparison of the performance of the 6mm stand-off, 7º device was performed to understand any shifts in performance due to these design changes. This configuration was selected as the internal noise signal investigation discussed previously in this chapter had demonstrated that this approach was likely to deliver a high quality inspection for the flat plate, non-welded test-pieces. Three phases of testing were performed, immersion testing with the absorbent rubber, and irrigated testing with and without the rubber. All testing was performed on the two flat plate, non-welded test-pieces, these test-pieces and the inspection methods used to detect each of the embedded defects are discussed in chapter 3.

In order to make comparison possible, all FMC data was collected using a fixed gain of 45dB and in each case an aperture of 30mm was used; this corresponds to 40 elements in the 3rd generation array. A comparison of the results for defects 1-4 only has been performed and is presented below, because pitch-catch inspection of defects 5 and 6 is not performed with a single 128 element array. A comparison is performed of the maximum amplitude of each defect signal and of the localised SNR around the defect. This is similar to the approach that was taken previously and is discussed in chapter 3. However, in this comparison a single aperture of 30mm has been used to provide improved focusing at longer path lengths. Once again the FMC data has been processed to provide beam steering and fixed focal depth inspection. The results from this testing are summarised for defect 1-4 in Table 5-6 – Table 5-9 below.

Table 5-6 Summary of localised signal to noise ratio for the inspection of defect 1 using a 30 mm aperture with the 7º, 6mm membrane coupled device in immersion, irrigation with internal absorbing material and irrigation with no internal absorbing material.

Housing Design	Beam Steering Only		56mm Focal Depth	
	SNR (dB ± 1 dB)	Amplitude (A.U.)	SNR (dB ± 1 dB)	Amplitude (A.U.)
Immersion	24	94	27	140
Irrigation and absorbing material	25	104	31	204
Irrigation without absorbing material	26	128	28	164

Table 5-7 Summary of localised signal to noise ratio for the inspection of defect 2 using a 30 mm aperture with the 7º, 6mm membrane coupled device in immersion, irrigation with internal absorbing material and irrigation with no internal absorbing material.

Housing Design	Beam Steering Only		56mm Focal Depth	
	SNR (dB ± 1 dB)	Amplitude (A.U.)	SNR (dB ± 1 dB)	Amplitude (A.U.)
Immersion	11	34	15	54
Irrigation and absorbing material	14	28	18	50
Irrigation without absorbing material	12	32	17	57

Table 5-8 Summary of localised signal to noise ratio for the inspection of defect 3 using a 30 mm aperture with the 7º, 6mm membrane coupled device in immersion, irrigation with internal absorbing material and irrigation with no internal absorbing material.

Housing Design	Beam Steering Only		30mm Focal Depth	
	SNR (dB ± 1 dB)	Amplitude (A.U.)	SNR (dB ± 1 dB)	Amplitude (A.U.)
Immersion	13	22	13	19
Irrigation and absorbing material	12	19	13	21
Irrigation without absorbing material	15	26	15	27

Table 5-9 Summary of localised signal to noise ratio for the inspection of defect 4 using the 7º, 6mm membrane coupled device in immersion, irrigation with internal absorbing material and irrigation with no internal absorbing material.

Housing Design	Beam Steering Only		30mm Focal Depth	
	SNR (dB ± 1 dB)	Amplitude (A.U.)	SNR (dB ± 1 dB)	Amplitude (A.U.)
Immersion	5	10	10	14
Irrigation and absorbing material	4	9	10	16
Irrigation without absorbing material	6	10	14	16

A comparison of the results in Table 5-6 to 5-9 demonstrates that there are some differences between the results obtained using the three configurations of the 7˚, 6mm 3rd generation membrane coupled device. However, it is clear that the performance of the device is not significantly degraded by using the integrated irrigation system. There is no consistent variation in the results obtained and the performance of the inspection in both irrigation and immersion is comparable. There is also no significant degradation or improvement in the performance of the device when the attenuative rubber material is used. This indicates that the level of internal noise is relatively low; if large internal signals were reverberating around within the probe cavity the addition of the absorbent material would reduce the amplitude of these. The variation in the performance of the three different configurations is due to the repeatability of the inspection capability. Between each of these tests the probe has been completely removed from the device housing and the device has been reconfigured. This far exceeds normal use and it inevitably leads to the probe set-up being not identical on each occasion. All testing was performed from a single transducer position because scanned FMC inspection is not currently possible with the inspection set-up used. When reconfiguring the inspection system the position of the transducer relative to the defect therefore also changes slightly. When considering a small defect such as those in the flat plate, non-welded test-pieces this change in position can cause variation in the defect response. There is also some movement within the membrane device scanning jig that could contribute to further variability in the results. However, despite all of these sources of variability the localised defect SNR only changes by ±2dB and by only using a fixed gain no attempt has been made to compensate for changes in the device configuration through calibration. The reproducibility of the results is considered acceptable within an industrial NDE environment.

5.6.2. Comparison of Different 3rd Generation Membrane Device Designs

A comparison of the performance level of each of the three different 3rd generation membrane probe designs was also performed. Again testing was based on the inspection of the flat plate, non-welded test-pieces. This testing was performed to

provide a baseline of performance of each device. As discussed in chapter 3 there is no recognised FMC calibration procedure and so very accurate comparison between the results is not possible. Work to address this situation is ongoing as part of a second EngD project within Rolls-Royce Submarines (Duxbury, 2009). In order to make as accurate a comparison as possible all 3rd generation design testing was performed using the MicroPulse 5PA phased array controller. Once again all MicroPulse data was collected using a fixed gain of 45dB; this was found to provide suitable results for each probe design. This approach is valid because in each situation the same size aperture has been used and the attenuation of water is low, therefore small changes in array standoff have relatively little effect on the signal amplitude. The effect of beam spread is minimised by using a relatively large aperture of 30mm, which leads to a collimated beam.

The first comparison was performed between 0º longitudinal scans. This information can be used to highlight any discrepancies in the position and amplitude of the internal noise signal and the general level of background noise. In each case this data has been collected with the back edge of the phased array probe housing positioned approximately 165mm from the weld cap centre line, which corresponds to the optimum inspection position to detect defect 3 in the flat plate non-welded test-piece, this is shown in the schematic diagram in Fig 5-21. This configuration is used so that the weld cap geometry does not affect the result.

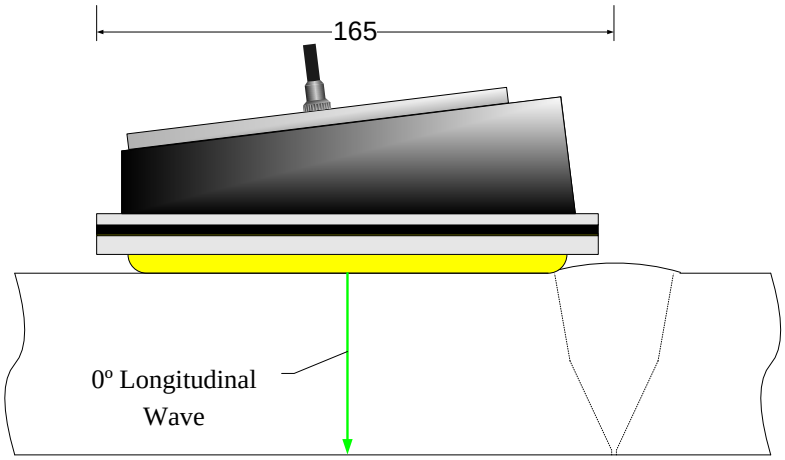

Figure 5-21 Schematic diagram of the experimental configuration used to generate a 0º longitudinal wave.

Results from the 0º longitudinal scans are shown in Fig 5-22; for comparison, a result from the 80 element 2nd generation array is shown in Fig 5-22(a). The A Scan gate start and end points used in each of the images in Fig 5-22 has been optimised for the theoretical position of the internal noise signal in each case. Therefore the B-Scan image shown in Fig 5-22 for each of the four different devices is not an identical size.

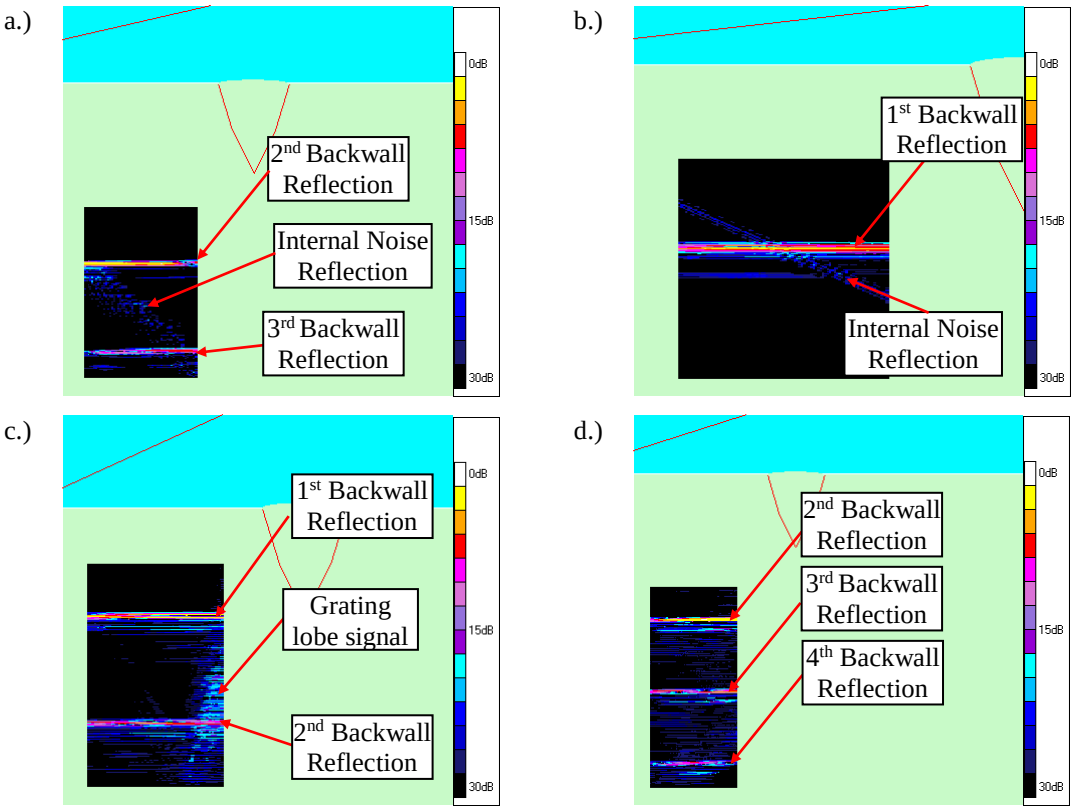

Figure 5-22 Comparison of the 0º scans generated with beam steering only when positioned to inspect defect 3 using a.) 80el device, b.) 6mm, 7º 128el device, c.) 6mm, 25º 128el device, d.) 20mm, 18º 128el device.

Each of the images in Fig 5-22 have been generated using beam steering only and are shown over a 30dB dynamic range. This approach allows side by side comparison of the data volume of interest using each approach. It is clear from Fig 5-22(b) that the 6mm stand-off, 7º probe configuration demonstrates a relatively strong internal reflection signal which corresponds in time with the first back-wall signal. This correlates well with the internal noise investigation performed using the 2nd generation configuration (Russell et al, 2008) and demonstrates that this signal occurs earlier than in the 2nd generation probe. This suggests that the 6mm stand-off, 7º probe configuration will provide good results when considering the non-welded

test-piece inspections and the equivalent inspections using the welded flat plate test-pieces. The internal noise signal with the 6mm stand-off, 25º device and 20mm stand-off, 18º device configurations are low amplitude and not readily observed in the results shown in Fig 5-22(c) and 5-22(d) respectively. This lower amplitude is expected, as is the increased level of general background noise. As discussed above, as the probe angle is increased, the intensity of the internal noise signal decreases but the shape of the main beam deteriorates, leading to the behaviour observed. The prominent noise signal seen in the 6mm stand-off, 25º probe is likely to be due to a grating lobe signal. In this device design, when steering the main beam to 0º, a forward facing grating exists at approximately 59º to the normal, which is allowed to interact with the internal front surface of the probe housing and may lead to this type of signal. However, when using a phased array in a practical inspection it is not necessary to steer a beam to 0º and this is not a limitation of the design. The increasing background noise observed in both of these steeper angle designs is also likely to be due to the deterioration in the beam generated over large steering angles. This effect is seen later when comparing performance of the three different designs for longitudinal wave inspection.

Changing the focal length of the beam produced by each of the arrays has a strong effect on the relative amplitude of the internal noise signal. By focusing close to the array the beam is increasingly divergent at longer time periods. The beam then no longer propagates normal to the component surface and multiple, high amplitude backwall signals are less likely to be observed. However, because the noise signal is due to an internal wedge reflection it still exists with a relatively high amplitude at all focal depths. This effect is also observed in the inspection of the flat plate target application test-pieces. Particularly when considering low amplitude defect signals, this effect can lead to limitations in the inspection capability.

Experimental testing was then performed with each of the three different probe configurations on defects 1-4 in the flat plate, non-welded test-pieces. All scans are generated using, where possible, identical setup parameters; this is the typical mode of operation that would be used in an actual inspection situation where specific defect locations and orientations are not known. The data generated using this approach is typically worse than the optimised results generated using prior knowledge of the

defect nature. Once again, although direct comparison between the performance of the three 3rd generation device designs is possible, quantitative comparison between the 2nd generation 80 element array and the three different 3rd generation, 128 element array results is not possible. This is because this data was collected at different times, and variations in the set up conditions have been used. In all comparison testing reviewed in this chapter of the thesis an aperture of 30mm has again been used. A summary of this comparison for defects 1-4 using the three different membrane coupled device designs is provided in Table 5-10 – 5-13. Results from the 7˚, 6mm device in irrigation with absorbing material have been used. This design is considered the most robust for a range of different inspections. It is also comparable to the set-up used in both the other configurations used in this testing.

Table 5-10 Summary of localised signal to noise ratio and signal amplitude for the inspection of defect 1 using the three different 3rd generation membrane device designs with a 30 mm aperture.

Housing Design	Beam Steering Only		56mm Focal Depth	
	SNR (dB ± 1 dB)	Amplitude (A.U.)	SNR (dB ± 1 dB)	Amplitude (A.U.)
7º, 6mm	25	104	32	204
25º, 6mm	26	143	31	254
18º, 20mm[1]	21	87	27	177

Notes

[1] Beam spread noise band obscures defect signal

Table 5-11 Summary of localised signal to noise ratio and signal amplitude for the inspection of defect 2 using the three different 3rd generation membrane device designs with a 30 mm aperture.

Housing Design	Beam Steering Only		56mm Focal Depth	
	SNR (dB ± 1 dB)	Amplitude (A.U.)	SNR (dB ± 1 dB)	Amplitude (A.U.)
7º, 6mm	14	28	18	50
25º, 6mm	11	27	15	44
18º, 20mm	7	19	13	32

Table 5-12 Summary of localised signal to noise ratio and signal amplitude for the inspection of defect 3 using the three different 3rd generation membrane device designs with a 30 mm aperture.

Housing Design	Beam Steering Only		30mm Focal Depth	
	SNR (dB ± 1 dB)	Amplitude (A.U.)	SNR (dB ± 1 dB)	Amplitude (A.U.)
7º, 6mm	12	19	13	21
25º, 6mm[1]	8	16	9	17
18º, 20mm[1]	6	18	6	17

Notes

[1] Beam spread noise band obscures defect signal

Table 5-13 Summary of localised signal to noise ratio and signal amplitude for the inspection of defect 4 using the three different 3rd generation membrane device designs with a 30 mm aperture.

Housing Design	Beam Steering Only		30mm Focal Depth	
	SNR (dB ± 1 dB)	Amplitude (A.U.)	SNR (dB ± 1 dB)	Amplitude (A.U.)
7º, 6mm	4	9	10	16
25º, 6mm	5	9	8	10
18º, 20mm[1]	6	9	10	16

Notes

[1] Beam spread noise band obscures defect signal

The results obtained for the inspection of all four defects using the 18º, 20mm device are typically worse than for the other two designs. In the case of the defect 1, 3 and 4 inspections, the location of the internal noise signal approximately corresponds to the defect signal. However, this device configuration is designed for direct specular inspection techniques and this limitation is expected. The results obtained using this design for the inspection of defects 2, 3 and 4 are also poor because the beam is being steered over a large angle to complete these inspections and being used in a non-ideal manner. This design is inappropriate for the four different inspection techniques used for the defects in the in flat plate non-welded test-piece. However, use of this design is appropriate for the detection of some defects included in the flat plate welded test-pieces. The inspection of these test-pieces is considered in greater detail in chapter 6.

A comparison of the performance of the 7˚, 6mm and the 25˚, 6mm design is more complex. When considering the inspection of defect 1 the localised defect SNR is comparable, but typically better using the 7˚, 6mm design. However, the signal amplitude is greater when using the steeper angled array. The difference in the SNR performance is because of the increased noise observed previously in the 25˚, 6mm design. However, the defect response is higher because the beam produced by this array is closer to its natural angle. When considering the inspection of defects 2-4, the 7˚, 6mm design out-performs both of the other configurations because of the low noise levels and the array is being used close to its natural angle. This high level of performance was expected from the experimental testing discussed in section 5.4 related to the optimised design of the 2nd generation device. It is clear from these results that although still highly effective, the performance of the 25˚, 6mm design is not as good as the other two configurations. The 25˚, 6mm device was not used in further testing of the flat plate welded test-pieces.

The results provided in Table 5-10 to Table 5-13 demonstrate that generally the inspection performance improves with the use of focusing. The amplitude of the defect response increases as the amount of energy impinging on the defect increases. The SNR of the defect response also increases when focusing is used. The background noise level expected in these test-pieces is low therefore all of the energy from a large aperture is incident upon the defect and a high quality signal response is observed.

The path length associated with the inspection of defect 3 is relatively long. It is only possible to focus a phased array within the near-field of the array aperture used. The inspection path length for defect 3 is beyond the maximum focal length of the 30 element aperture. This explains why the improvements in the inspection performance observed for the other three defects considered is not attained using this configuration for defect 3. A larger aperture must be used to provide the optimum performance for this type of inspection. Ideally a larger aperture size would also be used for the inspection of defect 4, but since the path length for the inspection of this defect is shorter than that for defect 3, some inspection performance improvement is still observed with the smaller aperture.

5.7. Internal Noise Signal Amplitude Variation

The amplitude of the internal noise band signal changes depending on the position of the array relative to the weld cap. This can clearly be seen in the 0º longitudinal wave scans performed using the 7º, 6mm stand-off device in Fig 5-23. In this comparison the device is positioned appropriately to detect defect 1 in Fig 5-23(a) and then moved back to a position appropriate for the inspection of defect 3 in Fig 5-23(b). In each of these figures a 30mm aperture with unfocused delay laws has been used. The internal noise signal occurs at a slightly different range in each of the images. This difference is caused by small variation in the ride height of the array. There is a large difference in the ultrasonic velocity in water and steel, therefore a small change in the ride height can have significant impact on the position of the internal noise signal. A schematic diagram of the set-up used in each case is shown in Fig 5-24. The effect of this variable amplitude internal noise signal is then shown for the inspection of defect 1 using this device in Fig 5-25.

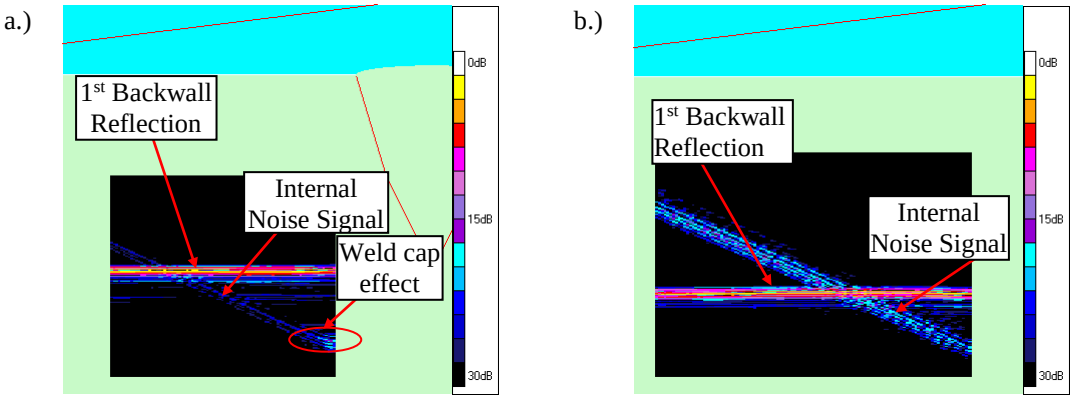

Figure 5-23 Comparison of the 0º scans generated with beam steering only when positioned to inspect a.) defect 1 and b.) defect 3.

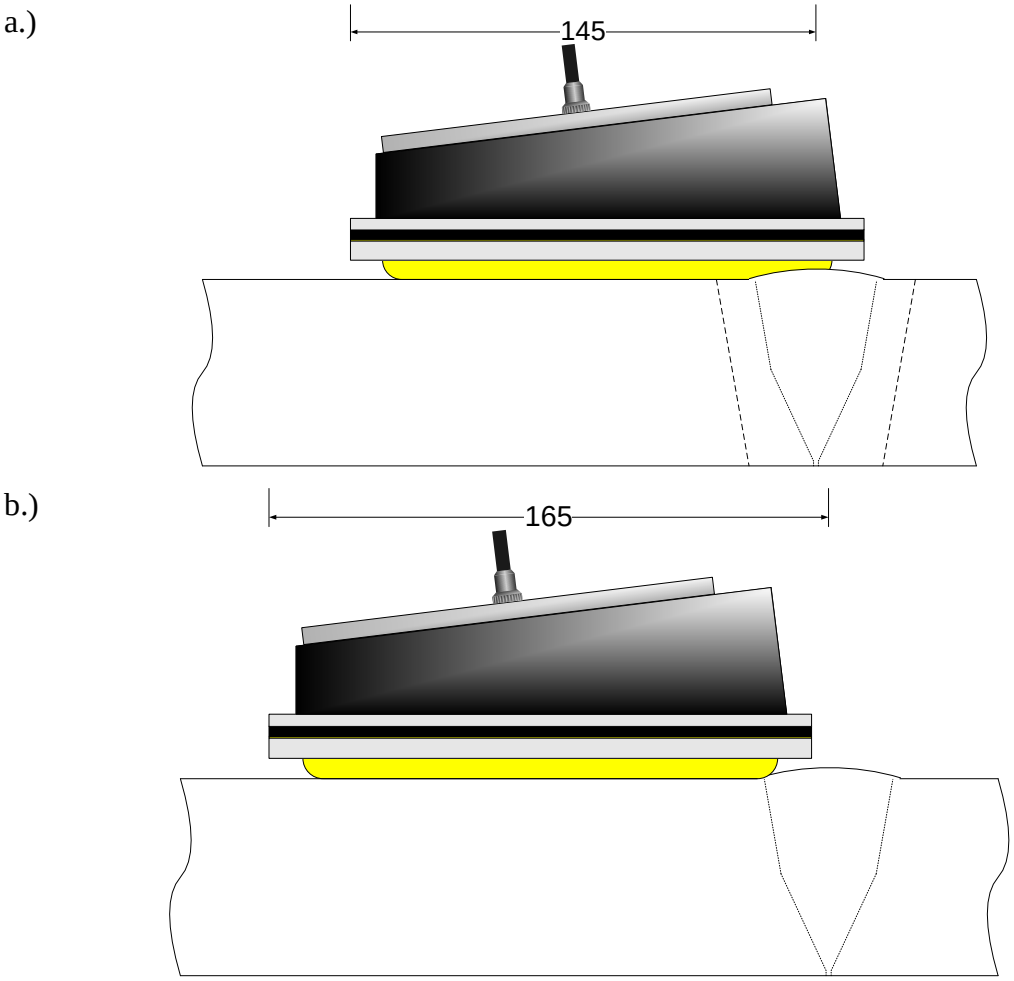

Figure 5-24 Schematic diagrams of the experimental set-up used to inspect a.) defect 1 and b.) defect 3.

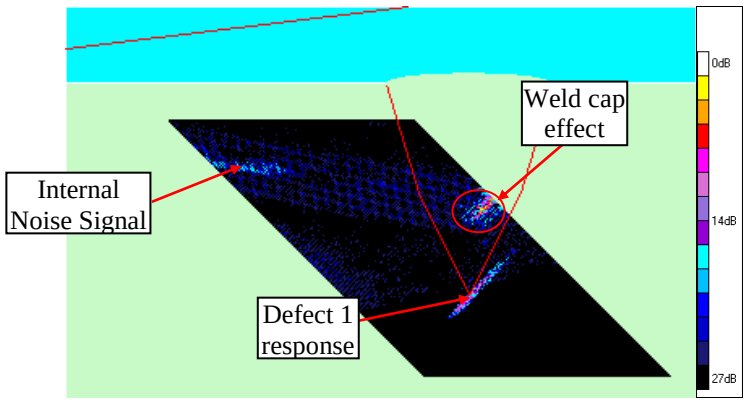

Figure 5-25 45º shear wave inspection of defect 1 showing variable amplitude. The defect response occurs over a broad arc due to beam spread.

When the transducer is positioned well away from the weld cap so that the entire array is over the flat region of the test-piece the internal noise signal has uniform amplitude. When the array is moved closer to the weld cap there is a localised increase in the amplitude of the internal noise signal. The amplitude of the internal noise signal in the region nearest to the weld-cap increases by approximately 4dB relative to the rest of this signal. As discussed previously the source of the internal noise signal is energy from the main beam impinging on the component outer surface and reflecting back to the transducer. Energy that propagates at an angle perpendicular to the front face of the transducer is then reflected back along the same path to the active aperture of the array. This path is shown in Fig 5-26(a) for the general case where the transducer is positioned over the flat component geometry. In this location it is energy at the edge of the beam which impinges on the component at the correct angle to generate the internal noise signal. The internal noise signal when the transducer is positioned over the weld cap profile is shown in Fig 5-26(b). In this situation some of the energy from the centre of the main beam is reflected at the correct angle to cause the internal noise signal. The intensity at the centre of the beam is significantly greater than at the edge which leads to an increase in the amplitude of the internal noise signal. The time associated with the beam spread internal noise signal can be controlled but this signal cannot be removed. Care must be taken when designing the transducer to complete a given inspection to ensure that the beam spread internal noise signal occurs at a time outside the region of interest. This is particularly important when scanning over the weld cap because as demonstrated here this can lead to a noise signal with increased amplitude which could obscure the response from an actual flaw.

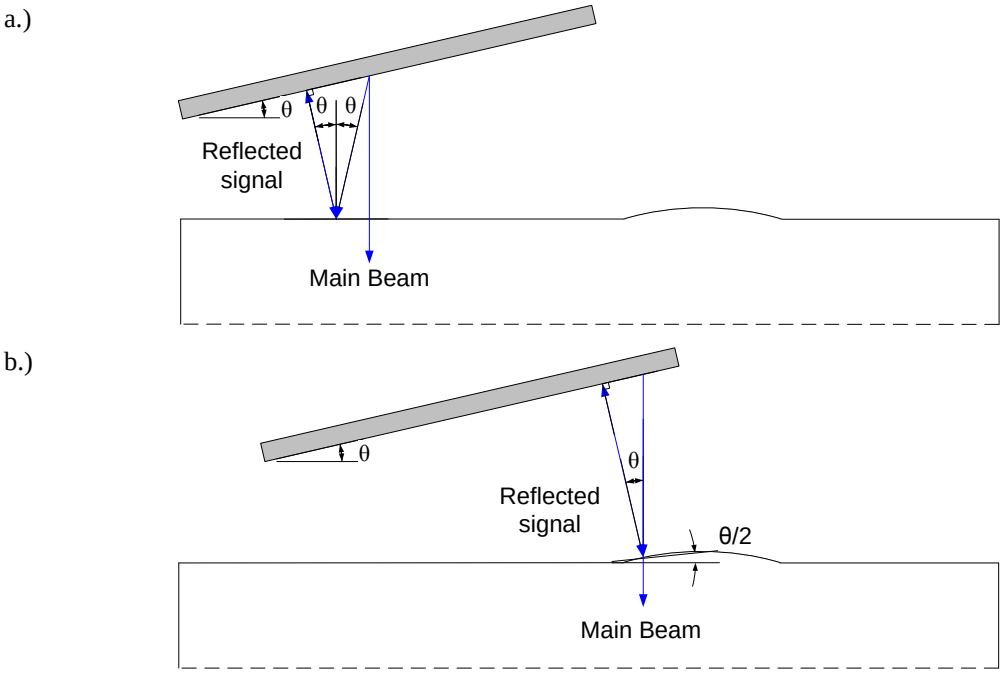

Figure 5-26 Schematic diagrams showing the source of internal noise within the membrane coupled phased array a.) on a flat surface, b.) on the rising face of the weld cap.

5.8. Summary

In the inspection of the two flat plate, non-welded test-pieces an internal noise signal within the 2nd generation membrane coupled phased array device led to a degradation in inspection performance. This chapter considers the investigation performed to understand the source of this internal noise signal and subsequent improvements to the membrane coupled device design. Two sources of noise are identified within the 2nd generation membrane coupled device, a grating lobe noise signal and a beam spread signal. The 2nd generation device was designed to have a large footprint to minimize the amount of axial scanning required. However, the maximum number of channels is limited and by increasing the footprint, the element pitch of the 80 element array had to be increased. This gave rise to a grating lobe signal within the 2nd generation device cavity. The beam spread internal noise signal occurs in all phased array wedges including conventional rigid wedges. The beam spread signal occurs when energy from the active aperture within the array reflects on the surface of the component under test back to the array. Energy impinging normally on the array is then reflected back along the same path to the active aperture where it is detected. The amplitude of the internal noise signal rapidly decreases as the angle of the array is increased relative to the outer surface of the component under test. The array angles

used with Perspex wedges are typically larger than when using water wedges, therefore the internal noise signal is a greater issue in water wedges than in Perspex. The internal noise signal is also higher in water wedges because of low attenuation and the large difference in ultrasonic velocity between water and steel causing a high proportion of the energy to be reflected at the interface.

A 3rd generation membrane coupled device has been designed. This device uses a 128 element, 0.75mm pitch 2MHz centre frequency array. The reduced element pitch still provides a relatively large footprint so that array scanning is minimized whilst also reducing the effects of grating lobes. Three different 3rd generation designs are considered, the first design uses a 6mm, 7º array which shortens the time associated with the beam spread noise. This device is designed for use in inspections with a relatively long path length. A 20mm, 18º device was also produced, in this design the beam spread signal occurs at longer path lengths making the device suitable for direct specular inspection techniques. Finally a 6mm, 25º device was designed; this was intended as a compromise between the other two devices for general use. Experimental testing demonstrated that the most appropriate approach to inspection of the target application component was to complete inspection using both of the first two designs. The 3rd generation device design incorporates an integrated irrigation system. Experimental testing was performed to demonstrate that the performance of the device was not degraded by using this irrigation system.

6. Flat Plate Welded Test-Piece Inspection

All of the experimental testing discussed previously using the membrane coupled phased array devices has been performed on two flat plate, non-welded test-pieces. The two flat plate non-welded test-pieces had weld metal deposited on their surfaces to produce a weld cap representative of the actual target application component. However, the target application for this technology is a section of stainless steel pipe-work that contains an austenitic weld. The presence of austenitic weld material introduces a number of ultrasonic inspection challenges. In order to demonstrate the performance of the membrane coupled phased array device in this application more representative test-pieces are required. Two flat plate welded test-pieces were produced, the test-pieces are made from representative stainless steel and both contain an austenitic weld with an undressed weld-cap.

In this chapter, the inspection of the two flat plate welded test-pieces representative of the target application component will be reviewed. In section 6.1 the design and manufacture of the two test-pieces will be discussed. This will be followed by an overview of the inspection process used to detect each of the embedded defects. The experimental results obtained from the inspection of the flat plate welded test-pieces using the 3rd generation membrane coupled device will then be presented. A theoretical study of the potential inspection speed improvements that can be achieved using the membrane coupled device has also been performed and this will be discussed in section 6.6.

6.1. Flat Plate Welded Test-Piece Design

The non-welded test-pieces described in section 3.1 did not contain an actual weld and only contained a subset of the range of possible flaws. The inspection of the non-welded test-pieces was restricted to a single inspection technique for each defect type. This earlier work demonstrated that the membrane coupled phased array provides an improved inspection capability over conventional techniques for this type of component. However, substantially more development was needed before the membrane device could be deployed. To develop the membrane probe inspection capability further, two flat plate, welded stainless steel test-pieces were designed and manufactured.

Stainless steel is used in NSRP components because it has high fracture toughness (Cui & Lundin, 2007), resistance to brittle fracture (Ford & Hudgell, 1987) and provides excellent resistance to corrosion and oxidation (Harker et al, 1990). The presence of austenitic weld material introduces a number of ultrasonic inspection challenges. The large columnar grain structure, typical of this type of weld, leads to scattering and beam steering of the ultrasound (Halkjær et al, 2000; Hudgell et al, 1989). The scattering effects occur from the grain boundaries, whereas the beam-steering is due to locally varying material properties across the different grains within the weld, which in turn leads to changes in the acoustic velocity (Connolly, 2009). To fully understand the membrane coupled device inspection capability when applied to the target application it was necessary to design and manufacture suitably representative test-pieces. Two flat-plate, welded test-pieces have been manufactured in order to limit the size and weight of the test-pieces and simplify the scanning process (Rolls-Royce, 2008a; Rolls-Royce, 2008b). The two welded test-pieces have a wall thickness and a surface roughness that is representative of the actual target application component.

The original intention of this work was to manufacture the welded test-pieces within Rolls-Royce. This approach would ensure that the weld composition and structure were fully representative of that found within the actual NSRP component. Manufacture of these test-pieces would also assist in the development of a Rolls-Royce capability to manufacture welded test-pieces that contained embedded flaws. Unfortunately due to resource constraints this approach could not be taken and the test-pieces were manufactured by Sonaspection (Lancaster, UK). Sonaspection have a defect inclusion process and a strong track-record in test-piece manufacture. However, Sonaspection were unable to produce a TIG welding process which was fully representative of that used on the target application component. In the two test-pieces an electric boat (EB) insert has been fused using a heating process without any weld filler metal, the bottom 6mm of the weld has then been produced using a manual metal arc (MMA) welding technique. The remainder of the weld has been built up using a representative TIG process. The welding process used in the manufacture of these test-pieces is likely to present a more challenging inspection than the actual target application weld, particularly in the root region. The intention of this development activity is focused on improving the membrane coupled device

capability. Further testing on a fully geometrically representative test-piece would be required before deploying this technology on the NSRP. Therefore differences in the weld composition are considered acceptable at this stage in development of the inspection capability.

Due to weld distortion in the actual target application component even when the weld cap has been removed some surface profile irregularity is still found (Rolls-Royce, 2001b). This surface profile irregularity further reduces inspection coverage when using conventional rigid wedge transducers. The weld cap on the two flat plate welded test-pieces produced by Sonaspection is representative of the pre-machined condition found on the actual target application. When the two flat plate welded test-pieces were manufactured, weld samples were also taken from each end of both test-pieces. A photograph of the cross-section from one of these weld samples is shown in Fig 6-1. The distortion of the upper surface is clearly visible in this photograph. The EB insert discussed above is also clearly visible in Fig 6-1. As in the actual target application the root region of the weld has also been left undressed. The complex geometry of the root region of the weld causes some additional inspection challenges when considering defects that occur within this region.

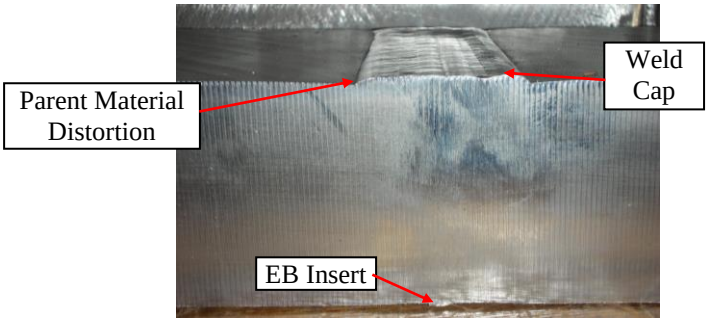

Figure 6-1 Photograph of the weld cross-section from the flat plate welded test-pieces.

The defects embedded in the two flat plate, welded test-pieces are described in Table 6-1. These defects are representative of all of the planar defects that are postulated could occur within the target application component. These test-pieces do not contain any intentional regions of porosity or inclusions; both of these types of defects are relatively small and are less of a concern than planar defects from a fracture mechanics perspective. By intentionally including defects during the welding

process it is possible to embed a far greater range of flaws than was achievable in the non-welded test-pieces. The six defect types included in the non-welded test-pieces have again been included in the welded test-pieces. However, a seventh mid-wall, mid weld defect normal to the backwall is also included. Two defects of each type have been included in the welded test-pieces. The first defect of each type is the same through-wall size as in the non-welded test-pieces; the second is twice this size. Two different size defects are included because accurate detection and characterisation of small defects is very difficult when the beam steering effects of austenitic weld are considered. Therefore, defects 8-14 are also included with a through-wall extent of 8mm. Defects 8-14 are still smaller than the validation defect size required in the current single element transducer inspection (Rolls-Royce, 2001a). Therefore if these defects can be reliably detected using the membrane coupled device, the performance of the inspection capability will exceed the minimum detectability requirements of the inspection. The two flat plate, welded test-pieces have been produced by welding two large sections of flat plate together. This allows the inspection of each defect from both scan directions. By using this approach during this development, it means that thorough characterisation of the membrane coupled device capability has been performed. This is a more cost efficient approach than manufacturing test-pieces that simulate single sided weld access.

Table 6-1 Defect Description for flat plate, welded test-pieces

Defect Number	Type of Defect	Location	Tilt	Skew
1	Lack of root fusion	Centreline of weld - inner surface breaking	0°	0°
2	Lack of sidewall fusion	Along lower weld fusion face - inner surface breaking	25°	0°
3	Lack of sidewall fusion	Along lower weld fusion face - at highest point of 25° prep angle from inner surface	25°	0°
4	Lack of sidewall fusion	Along upper weld fusion face - at lowest point of 10° prep angle from outer surface	10°	0°
5	Lack of sidewall fusion	Along upper weld fusion face - outer surface breaking	0°	0°
6	Structurally significant planar defect derived from LEFM[1]	Centreline of weld - under weld cap with ligament of 2-5mm to outer surface	10°	0°
7	Structurally significant planar defect derived from LEFM[1]	Centreline of weld - equidistant from inner and outer surfaces	0°	0°
8	Lack of root fusion	Centreline of weld - inner surface breaking	0°	0°
9	Lack of sidewall fusion	Along lower weld fusion face - inner surface breaking	25°	0°
10	Lack of sidewall fusion	Along lower weld fusion face - at highest point of 25° prep angle from inner surface	25°	0°
11	Lack of sidewall fusion	Along upper weld fusion face - at lowest point of 10° prep angle from outer surface	10°	0°
12	Lack of sidewall fusion	Along upper weld fusion face - outer surface breaking	0°	0°
13	Structurally significant planar defect derived from LEFM[1]	Centreline of weld - under weld cap with ligament of 2-5mm to outer surface	10°	0°
14	Structurally significant planar defect derived from LEFM[1]	Centreline of weld - equidistant from inner and outer surfaces	0°	0°

Notes

1. LEFM – Linear Elastic Fracture Mechanics

Each of the artificial defects described in Table 6-1 were introduced into the welded test-pieces during manufacture. As in the non-welded test-piece a best endeavour approach is taken to reproduce the postulated defect gape, however it is likely that the actual gape of each defect will again be approximately 300µm. The inclusion of realistic, elliptical defects is difficult; therefore rectangular defects of an equivalent area to the postulated elliptical defects have been included in both test-pieces. The through-wall dimension of the defect is the most critical in terms of generating a safety justification. Therefore the through-wall size of the artificial defect is maintained at 4mm for defects 1-7 and 8mm for defects 8-14. The length of the artificial defects is reduced to 6.3mm and 12.6mm for defects 1-7 and 8-14 respectively in order to maintain the cross-sectional area of the final defect. As with the non-welded test-pieces, all defects can be assumed to be ultrasonically smooth. The orientation of all of the flaws in the welded test pieces will be accurately known. These defects will cover a range of tilt angles at different points within the weld volume but all defects will have a nominal skew of $0^{\circ} \pm 5^{\circ}$, which corresponds to the Sonaspection manufacturing tolerance. The focus of the current research work is to further develop the membrane probe and to demonstrate its value in comparison to conventional rigid wedge techniques. This work is not intended to demonstrate detection of all possible defect types; therefore defects of different skews are not included in the test-pieces. Treatment of defects with different skews is being considered as an extension to this development activity and is due for completion in 2010. This additional development activity is beyond the scope of my doctorate studies and will not be discussed further in this document.

A photograph of the conformable phased array welded evaluation block 2 is provided in Fig 6-2, the configuration of this test-piece is essentially the same as for the welded evaluation block 1. The weld cap height and width dimensions are comparable to the actual component. The defects contained in evaluation block 1 are shown in the schematic diagrams in Fig 6-3 and the corresponding diagrams for block 2 are provided in Fig 6-4. The defects are positioned approximately 50mm apart along the weld to ensure that when the transducer is positioned in-line with the centre of the defect, only a single defect response is measured.

Figure 6-2 Photograph of conformable phased array welded evaluation block 2 (Rolls-Royce, 2008b).

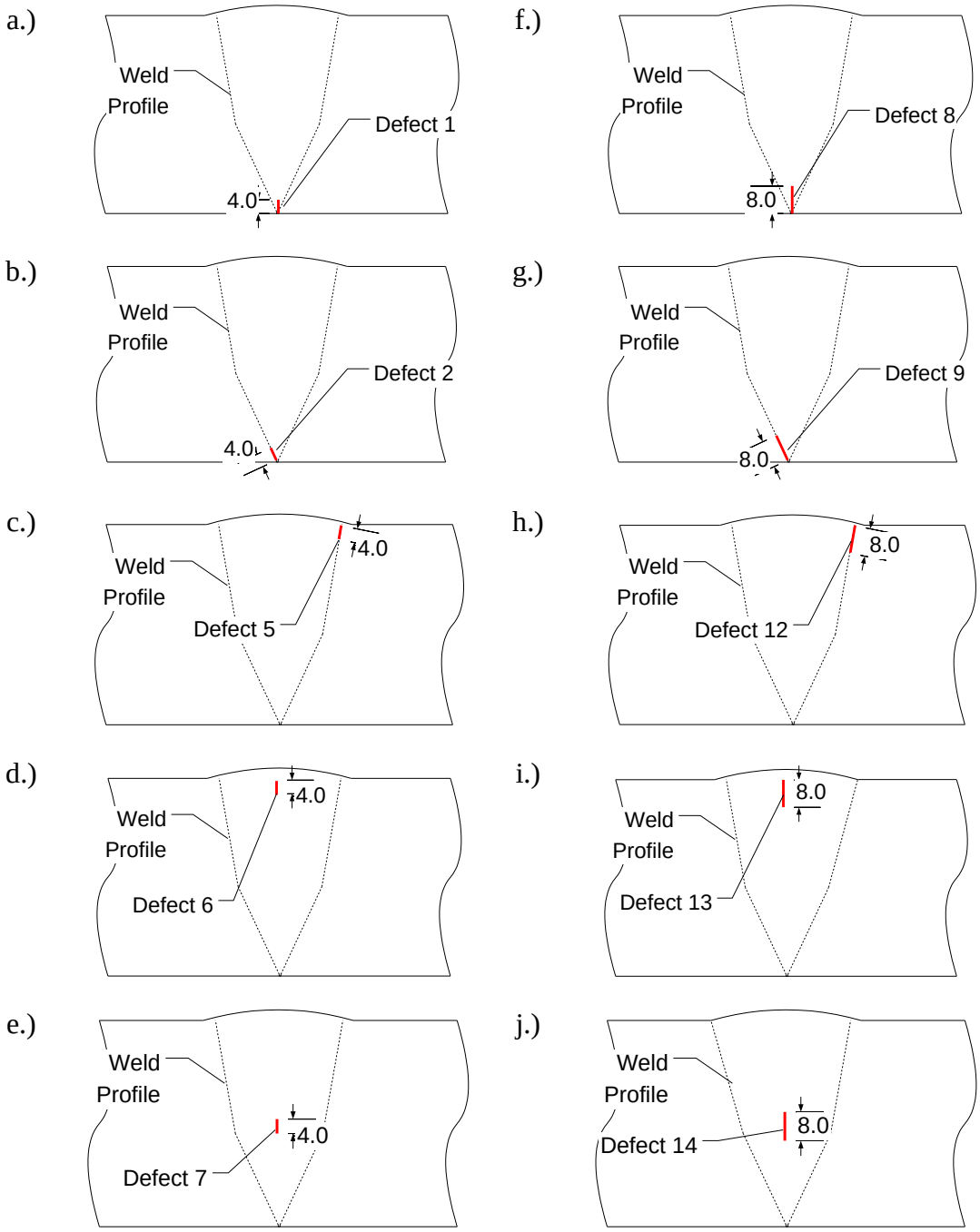

Figure 6-3 Schematic diagram of defects contained in the conformable phased array welded evaluation block 1, a.) defect 1, b.) defect 2, c.) defect 5, d.) defect 6, e.) defect 7, f.) defect 8, g.) defect 9, h.) defect 12, i.) defect 13, j.) defect 14.

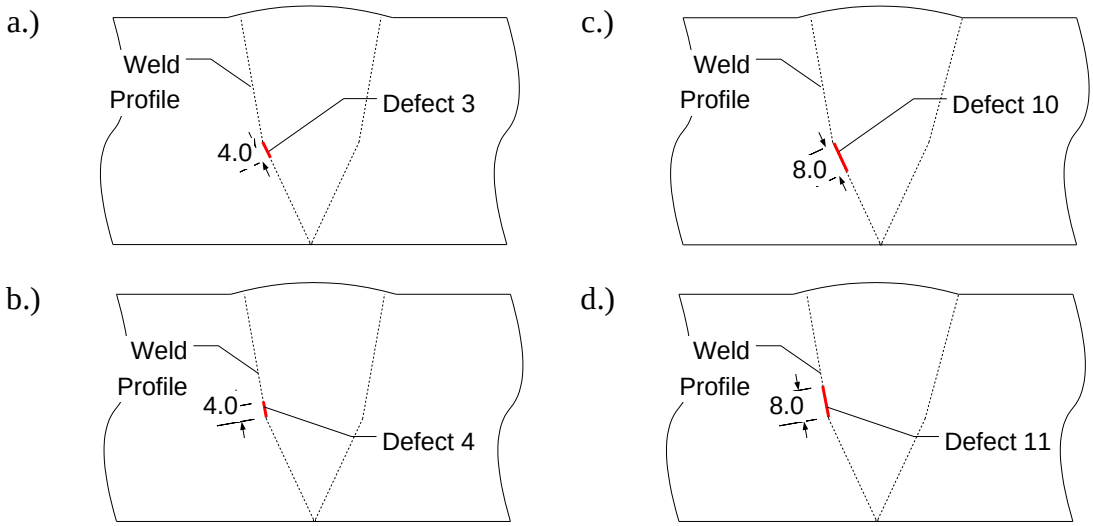

Figure 6-4 Schematic diagram of defects contained in the conformable phased array welded evaluation block 2, a.) defect 3, b.) defect 4, c.) defect 10, d.) defect 11.

6.2. Technique Description

The detection methods chosen in this work essentially represent five different UT inspection techniques:

a) Direct specular
b) Creep wave
c) Corner echo
d) Transverse-longitudinal (TL) skip
e) Transverse-longitudinal-longitudinal (TLL) skip

Three of these techniques were used in the inspection of the flat plate, non-welded test-pieces and have been discussed previously in chapter 3; these will only briefly be reviewed here. In the inspection of the flat plate, non-welded test-pieces, techniques that relied on a direct specular reflection from a defect through the weld region were not considered because of the absence of a representative weld. These techniques have been included in the inspection of the welded test-pieces and are discussed in detail below. Shear waves are strongly scattered and attenuated in austenitic weld material; therefore any techniques that traverse a large weld region are implemented using a longitudinal wave.

6.2.1. Direct Specular

Direct specular reflection occurs when the ultrasonic wave is incident upon a defect without first interacting with any other surface within the component under test. Typically specular detection of a planar defect requires the ultrasound to impinge on the defect at an angle within ± 10º to the normal of the defect. When this condition is met, a high amplitude response can be observed from the defect allowing accurate defect detection. Direct specular reflection of a defect is shown in the schematic diagram in Fig 6-5. This technique is used for the direct through weld inspection of defects within the flat plate, welded test-pieces.

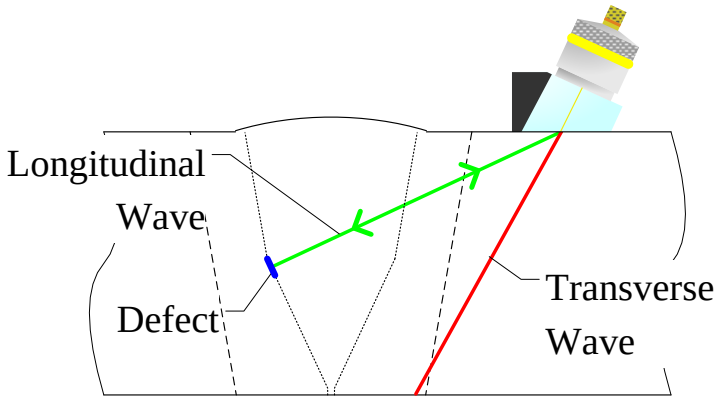

Figure 6-5 Schematic diagram of direct specular reflection.

6.2.2. Creep Wave

As the incident angle of the ultrasonic probe used in an inspection is increased, the resultant beam angle of the refracted waves also increases. Both longitudinal and transverse waves are generated until the first critical angle is reached. This critical angle corresponds to the point where the longitudinal wave is totally reflected within the probe. Immediately before the first critical angle is reached an outer-diameter (OD) creep wave is produced (Baby et al, 2003), in stainless steel this point is reached at approximately 75-80º and occurs with an associated shear wave at 32-33º. The creep wave has been reported in the literature with a number of different names, Langenberg et al use the descriptor subsurface longitudinal wave (Langenberg et al, 1990), Ermolov terms it a head wave (Ermolov, 2004) whereas Bray and Tang discuss

a critically refracted longitudinal wave (Bray & Tang, 2001). The creep wave travels at the same velocity as the longitudinal wave, the wave constantly mode converts to a shear wave, and this process radiates energy into the component under test. The shear wave generated in this process again occurs at approximately 32-33º. Due to this effect the creep wave is highly attenuated and relatively short lived. Assuming that the creep wave exists with sufficient amplitude it can be used to detect surface and slightly sub-surface defects on the component outer surface. To achieve this condition the transducer must be placed as close as possible to the defect location. A schematic diagram of the creep wave inspection is provided in Fig 6-6. It is challenging to generate this type of wave using a single element transducer and this technique was not used in the inspection of the flat plate non-welded test-pieces. Deployment of this type of technique on components with irregular surface geometries is not typically possible using rigid wedge transducers.

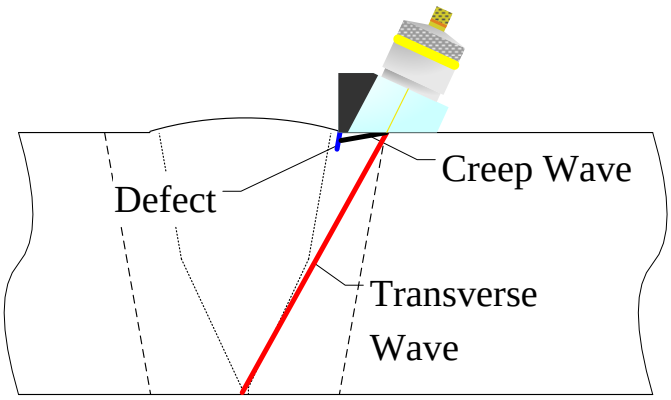

Figure 6-6 Schematic diagram of the creep wave inspection technique.

6.2.3. Corner Echo

The corner echo technique is used to detect surface breaking defects orientated normal, or near normal to the surface. The maximum amplitude corner echo response is achieved using a 45º shear wave (Krautkramer & Krautkramer, 1983) although other wave angles can also be used. The direct corner echo inspection technique is shown in Fig 6-7(a). This technique can also be used after reflection from the backwall and the skip corner echo technique is shown in Fig 6-7(b).

a.)

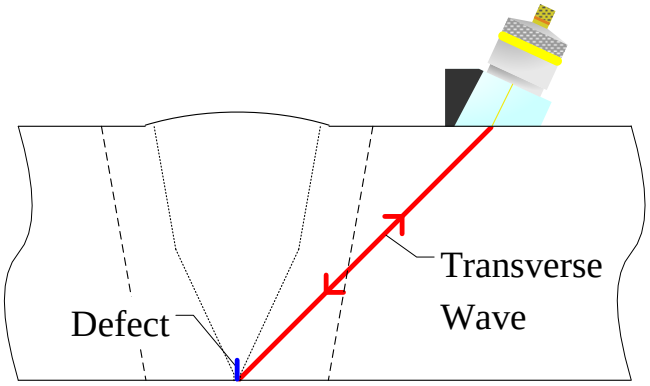

b.)

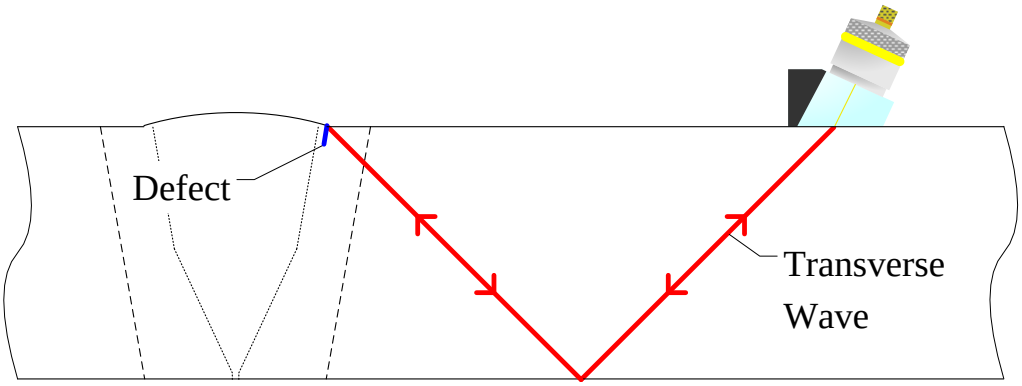

Figure 6-7 Schematic diagram of the a.) direct and b.) skip corner echo inspection technique.

6.2.4. Transverse-Longitudinal (TL) Skip

The Transverse-Longitudinal (TL) skip technique is a type of in-direct specular reflection. The technique involves a beam of ultrasound insonifying the defect specularly after a reflection with a surface within the component. In the inspection of both the non-welded and welded test-pieces this technique is used to achieve an in-direct specular defect reflection using a high angle longitudinal wave mode converted after reflection from the backwall. The TL skip technique is shown in the schematic diagram in Fig 6-8.

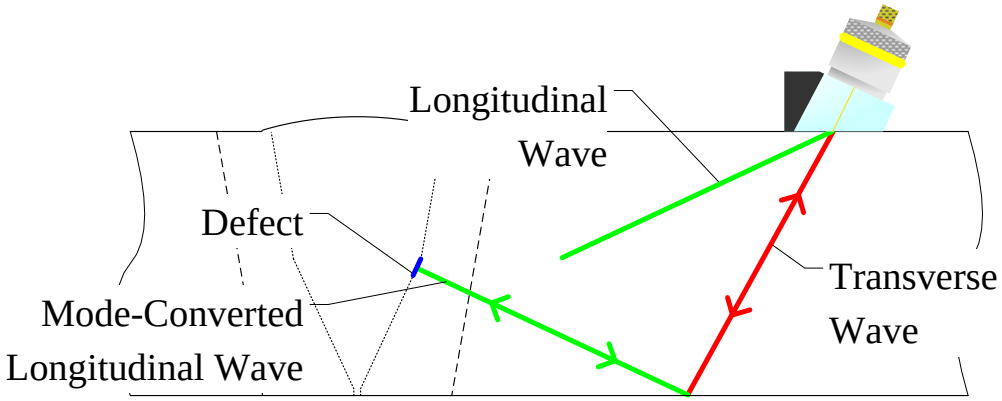

Figure 6-8 Schematic diagram of the Transverse-Longitudinal (TL) skip inspection technique.

6.2.5. Transverse-Longitudinal-Longitudinal (TLL) Skip

The Transverse-Longitudinal-Longitudinal (TLL) skip technique can be used to provide a suitable defect response from defects oriented with approximately ±10º tilt to the backwall normal. Depending on the depth of the defect to be detected and the angle of the beams used either a pitch-catch or self-tandem (ST) approach can be used. Both of these inspection techniques are shown in the schematic diagrams provided in Fig 6-9.

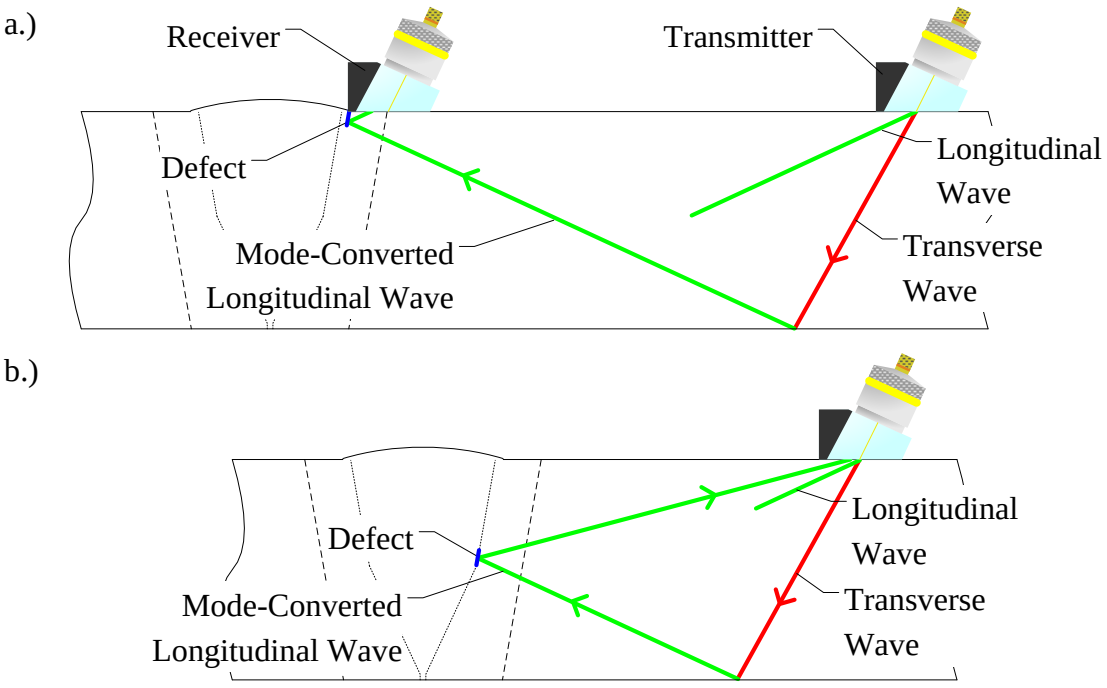

Figure 6-9 Schematic diagram of the Transverse-Longitudinal-Longitudinal (TLL) skip inspection technique, a.) pitch-catch and b.) self tandem (ST).

6.3. Chosen Inspection Techniques for Each Defect

A primary and secondary detection technique is used to detect each of the 14 artificial defects included in the flat plate, welded test-pieces when scanning from each direction either side of the weld cap. These techniques are summarised in Table 6-2. When a defect occurs in the centre of the weld, symmetrical inspection techniques are used. In order to distinguish between these directions, the through weld inspection is considered to be from the positive scan direction (i.e. left to right in Fig 6-3 and Fig 6-4) and near side weld inspection is considered as the negative scan direction. Each defect is therefore typically inspected using two different inspection techniques from each scan direction and is insonified from a number of different locations. This approach provides additional information regarding the nature of any defects found within a structure and allows the data interpretation engineer to postulate a possible cause of the defect. It also safeguards the inspection against potentially missing a defect because it occurs at a slightly different position or orientation to that expected. However, using this approach with conventional single element transducers is time-consuming. Reducing the time associated with this type of inspection provides some of the motivation for developing the membrane coupled device. The tests performed represent all of the main techniques used in the target application inspection. In the actual target application inspection further component scans with different focal lengths are carried out to provide complete through thickness inspection coverage. These tests are not required on the flat plate, welded test-pieces because defects are not included in these locations and a null defect response would be measured.

Table 6-2 Inspection technique summary for the flat plate, welded test-pieces.

I.D.	Defect Type	Length (mm)	Through-wall size (mm)	Ligament to ID (mm)	Tilt Angle (˚)	Through Weld Inspection Techniques		Near Side Inspection Techniques	
						Primary	Secondary	Primary	Secondary
1	Lack of root fusion	6.3	4	0	0	45 Shear (Corner Effect)	60 Shear (Corner Effect / Specular)	Mid-weld defect – symmetrical detection techniques	
2	Lack of side wall fusion	6.3	4	0.5	25	65 Comp (Specular)	65 Shear (Specular)	65 Comp (TL)	45 Shear (Corner Effect/TT)
3	Lack of side wall fusion	6.3	4	24.5	25	65 Comp (Specular)	60 Comp (Specular)	65 Comp (TL)	-
4	Lack of side wall fusion	6.3	4	28.5	10	65 Comp (TLL)	70 Comp (Specular)	65 Comp (TLL)	45 Comp (TLL)
5	Lack of side wall fusion	6.3	4	54	-10	65 Comp (TLL, pitch-catch)	OD Creep Wave	65 Comp (TLL, pitch-catch)	45 Shear (Skip - Corner Effect)
6	Mid-weld planar	6.3	4	54	0	65 Comp (TLL, pitch-catch)	OD Creep Wave	Mid-weld defect – symmetrical detection techniques	
7	Mid-weld planar	6.3	4	27	0	60 Comp (TLL, ST)	70 Comp (TLL, ST)	Mid-weld defect – symmetrical detection techniques	
8	Lack of root fusion	12.6	8	0	0	45 Shear (Corner Effect)	60 Shear (Corner Effect / Specular)	Mid-weld defect – symmetrical detection techniques	
9	Lack of side wall fusion	12.6	8	0.5	25	65 Comp (Specular)	65 Shear (Specular)	65 Comp (TL)	45 Shear (Corner Effect/TT)
10	Lack of side wall fusion	12.6	8	20.5	25	65 Comp (Specular)	60 Comp (Specular)	65 Comp (TL)	-
11	Lack of side wall fusion	12.6	8	28.5	10	65 Comp (TLL)	70 Comp (Specular)	65 Comp (TLL)	45 Comp (TLL)
12	Lack of side wall fusion	12.6	8	50	-10	65 Comp (TLL, pitch-catch)	OD Creep Wave	65 Comp (TLL, pitch-catch)	45 Shear (Skip - Corner Effect)
13	Mid-weld planar	12.6	8	50	0	65 Comp (TLL, pitch-catch)	OD Creep Wave	Mid-weld defect – symmetrical detection techniques	
14	Mid-weld planar	12.6	8	25	0	60 Comp (TLL, ST)	70 Comp (TLL, ST)	Mid-weld defect – symmetrical detection techniques	

The inspection technique used to identify the presence of each defect within the flat plate, non-welded test-pieces is again used for the inspection of the corresponding defects in the welded test-pieces. However, a number of other techniques are also used in the inspection of the welded test-pieces.

Defects 1 and 8 (lack of root fusion)

Defects 1 and 8 (see Fig 6-3a, f) occur approximately in the middle of the weld. This type of defect is detected using the same two techniques from both inspection directions, and both techniques rely on the corner echo response from this type of surface breaking defect. The two different wave angles used are selected to provide a suitable response from defects at slightly different tilts. A shear wave is used, despite the fact that the wave must propagate through a small region of weld material. This approach is taken because the corner echo response from shear waves is much higher than longitudinal waves (Krautkramer & Krautkramer, 1983). Hence, even if the wave is slightly attenuated by the weld, a strong response is likely to be observed because the amount of weld material that must be crossed is relatively small and the likely reduction in signal amplitude is small.

Defects 2 and 9 (lack of side wall fusion)

Defects 2 and 9 (see Fig 6-3b, g) occur at a tilt of 25º to the backwall normal, different techniques must therefore be adopted from each side of the weld. When scanning from the near side of the weld, this type of defect is equivalent to defect 2 in the non-welded test-pieces and the same primary inspection technique is used. This type of defect also produces a strong corner echo/transverse-transverse (TT) response and a 45º shear wave is used as a secondary inspection technique. Direct specular techniques are used for the through weld inspection of this type of defect. Suitably angled beams are generated to impinge on the defect at 90º to the defect surface; this approach is used to produce the maximum amplitude response. The primary inspection technique uses a 65º longitudinal wave because this is not likely to be excessively attenuated by the austenitic weld material. A 65º shear wave is used as in secondary inspection, the interpretation of the data obtained from this inspection is potentially simpler than from the primary inspection because only one wave mode

exists but the amplitude of the signal is likely to be lower because of higher levels of scattering through the weld.

Defects 3 and 10 (lack of side wall fusion)

The inspection of defects 3 and 10 (see Fig 6-4a, c) for the near side of the weld scan direction is equivalent to the inspection of defect 3 in the non-welded test-pieces. The 65º longitudinal wave TL mode conversion technique that has been described previously in chapter 3 is once again used to detect this defect. There are only limited techniques available to detect this type of defect and no secondary technique is used from this scan direction. Two different angled beams are used to detect this type of defect through the weld. It is expected that the defect occurs along the weld fusion face, so the highest amplitude response is anticipated to be produced by using a direct 65º longitudinal wave inspection. However, the ultrasonic beam is typically steered during this type of inspection (Bann, 2005). A secondary inspection is therefore performed using a 60º longitudinal wave as this was found to provide a suitable defect response. Shear wave inspection of defects of this type is not performed through weld due to excessive attenuation of the beam.

Defects 4 and 11 (lack of side wall fusion)

The primary inspection technique used for the detection of defects 4 and 11 (see Fig 6-4b, d) from both scan directions is the 65º longitudinal wave TLL mode conversion technique that was used for the inspection of defect 4 in the non-welded test-pieces. However, because the defect occurs on the fusion face, it is tilted and the beam path from each scan direction is slightly different. Therefore the relative positions of the transmit and receive paths are not identical. When this inspection is performed from the near side of the weld, a self tandem technique is used. However, when completing the inspection through the austenitic weld, there is a large offset between the transmit and receive paths. The secondary inspection from the near side of the weld also uses the TLL technique but a 45º longitudinal wave beam angle is used. Through weld inspection of this type of defect is relatively challenging. It is not possible to generate a high amplitude longitudinal wave that propagates normal to the defect surface. The highest angle longitudinal wave that can be reliably produced

is a 70º beam and this is used but it is recognised that the likely amplitude of the response will be low because of the mis-orientation of the beam.

Defects 5 and 12 (lack of side wall fusion)

Defects 5 and 12 (see Fig 6-3c, h) are outer surface breaking defects and occur along the upper fusion face. The near side inspection of both defects is equivalent to defect 5 in the flat plate non-welded test-piece. The same pitch-catch TLL primary inspection technique is once again used to detect this type of defect. Due to the position of the defect, there is a large separation between the transmit and receive paths and a pitch-catch configuration must be used. All of the pitch-catch inspection techniques implemented on the welded test-pieces use the same transducer configuration as in the non-welded test-piece inspection. The 2nd generation membrane coupled device and the 48 element rigid wedge transducer are used in all pitch-catch testing. A maximum of 128 elements can be addressed using the current Peak NDT MicroPulse 5PA array controller. It is therefore not possible to complete pitch-catch testing using the 128 element 3rd generation probe design. Defects 5 and 12 are surface breaking defects and will produce a strong corner echo response when using a suitably oriented beam. The secondary near side inspection technique used for this type of defect is a full-skip 45º shear wave technique. The primary inspection technique for the through weld inspection of defects 5 and 12 again uses the same pitch-catch 65º longitudinal wave TLL mode conversion technique as for the near side inspection. This inspection is challenging because the ultrasonic path passes through a large region of the austenitic weld. The secondary through weld inspection technique uses an OD creep wave.

Defects 6 and 13 (planar defect normal to the backwall)

Defects 6 and 13 (see Fig 6-3d, i) occur under the weld cap in the centre of the weld; the same two detection techniques are therefore used from both scan directions. This type of defect is equivalent to defect 6 in the flat plate, non-welded test-pieces and the same pitch-catch 65º longitudinal wave TLL mode conversion technique is once again used as the primary detection technique. This type of defect has a short ligament to the outer surface and will not produce a corner echo response. The OD creep wave is

therefore used as the secondary detection technique for this type of defect from both scan directions.

Defects 7 and 14 (planar defect normal to the backwall)

The mid-wall, mid-weld defect represented by defects 7 and 14 (see Fig 6-3e, j) was not included in the non-welded test-pieces. This type of defect cannot be introduced except during the welding process. This is a very challenging type of defect to detect and only a limited range of inspection techniques are available. Typically the main technique that can be used to detect this type of defect is the TLL technique (British Standards Institution, 2004a), depending on the beam angles used this can be a pitch-catch or a self tandem (ST) inspection. The beam angle that produces the highest amplitude response is dependent on the welding procedure used. It is therefore desirable to be able to consider the response from this inspection over a range of different beam angles. This cannot practically be achieved using conventional data acquisition techniques and only a limited range of angles can be considered. The primary inspection technique uses a 60º longitudinal wave and the secondary technique uses a 70º longitudinal wave. The defect occurs in the centre of the weld; therefore the same technique can be adopted from both scan directions.

6.4. Inspection Process

The footprint of the 3rd generation membrane coupled phased array is relatively large and it is possible to achieve complete coverage of the inspection volume from a limited number of transducer positions relative to the weld centre line. When processing inspection data from an aperture within the array, the A-Scan produced is plotted along a line projected from the centre of the aperture. A B-Scan image is then produced by "stacking" these A-Scans next to one another. The inspection coverage that can be achieved from a single transducer position is therefore dependent on the aperture size used to generate each A-Scan. The number of inspection positions required to achieve complete inspection coverage of the component under test is therefore dependent on the maximum aperture size to be used. Care must be taken to ensure that the entire inspection volume is covered when using all of the inspection techniques to be implemented on a component.

When designing a new inspection it is necessary to decide upon the maximum aperture size to be used. The maximum aperture size used will dictate the minimum scan pitch of the inspection. By using electronic scanning from a single probe position, a region in the component can be imaged. The size of the region is dictated by the aperture size used; as the aperture is increased the volume of the region inspected from that scan position reduces. In order to ensure that the entire component is suitably insonified, an appropriate mechanical scan pitch must therefore be selected. The mechanical scan pitch will also limit the algorithms that can be applied to the inspection data collected in the future. A compromise must be made between future proofing the inspection data and reducing time and limiting the overall amount of data collected during the inspection. Coverage of the entire target application inspection volume has been achieved by using the membrane device to complete six scans at different positions relative to the weld. This number of scans allows a suitably large aperture to be used for the inspection of all defects and provides some overlap of data from one scan position to the next.

The first scan of the target application component is performed with the membrane device directly over the weld cap. The FMC data gathered when the transducer is located in this position is then processed to provide a surface profile measurement of the weld cap region. In subsequent inspections when the membrane device is positioned partially over the weld, this information can then be used to update the delay laws used in each of these inspections. This approach is used because the most effective profile measurement technique is to position the transducer centrally on the weld cap and then to use a 0˚ longitudinal wave inspection (Long & Cawley, 2007). It is not possible to obtain sufficient information regarding the weld profile when steering the beam generated away from normal incidence because the reflected wave is no longer incident on the array. When using this approach it is essential that the position of the transducer is accurately known so that the correct surface profile information is used to update the delay laws.

A measured surface profile from the flat plate welded test-pieces is shown in Fig 6-10; this image has been produced using the 6mm, 7º device positioned directly over the weld cap. An aperture of 20 elements has been used and the data is displayed on a scale of 0-20dB although some variation does occur this image is representative

of the weld cap along the entire length of the test-pieces. The image clearly shows the distortion of the parent material either side of the weld as seen in the photograph in Fig 6-1.

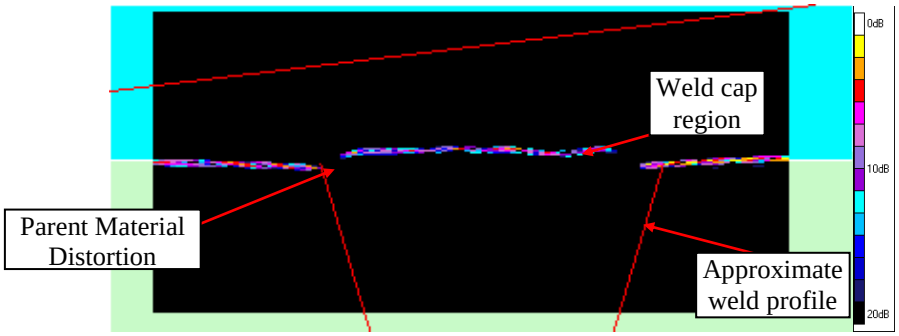

Figure 6-10 Weld cap profile of the flat plate welded test-pieces ultrasonically measured using the membrane device.

The optimum transducer position using the 3rd generation device for each of the different techniques to detect defects 1-7 is summarised in Table 6-3. The transducer positions used to detect defects 8-14 are identical to those used for the smaller defects. The optimum position for the central aperture of the probe to detect each of the defects is slightly different but as discussed, complete coverage is achieved using six scans. Each of the six scans performed is indicated by a different colour within Table 6-3. Inspection of the flat plate welded test-pieces has been performed using the 6mm, 7º design and the 20mm, 18º design. As discussed in chapter 5, these two designs are considered the most appropriate to provide complete inspection coverage of the test-pieces. The 6mm, 25º device has not been used due to the limited performance of this design.

Table 6-3 Membrane coupled device optimum inspection position for defects 1-7. Inspection of the entire volume of interest is performed from six transducer positions relative to the weld, each position is indicated by a unique colour. The colour coding used is discussed in Table 6-4.

I.D.	Defect Type	Length (mm)	Through-wall size (mm)	Ligament to ID (mm)	Tilt Angle (˚)	Approximate Optimum Aperture Centre Offset to Centre of Weld (mm)			
						Through Weld Inspection Techniques		Near Side Inspection Techniques	
						Primary	Secondary	Primary	Secondary
1	Lack of root fusion	6.3	4	0	0	58	100	58	100
2	Lack of side wall fusion	6.3	4	0.5	25	124	124	36	58
3	Lack of side wall fusion	6.3	4	24.5	25	64	52	106	-
4	Lack of side wall fusion	6.3	4	28.5	10	55	71	113	61
5	Lack of side wall fusion	6.3	4	54	-10	152	11	152	116
6	Mid-weld planar	6.3	4	54	0	152	11	152	11
7	Mid-weld planar	6.3	4	27	0	66	96	66	96

The colour coding adopted in Table 6-3 and how this relates to the position of both of the different 3rd generation probes used is provided in Table 6-4. The offset between the probe centre position provided in Table 6-3 and the probe reference point provided in Table 6-4 for the two different probe designs has been calculated by direct measurement from the engineering drawings of the two probe designs.

Table 6-4 Colour coding system used to position probe in membrane device inspections.

Probe centreline – weld centreline offset	Membrane probe reference point to weld centre line offset (mm)	
	7º, 6mm	18º, 20mm
0	79	76
30	109	106
60	139	136
90	169	166
120	199	196
Pitch-catch technique		

When the membrane coupled device is used to inspect the actual target application component it will be mechanically scanned in the circumferential direction and FMC data will be acquired every 2mm around the circumference of the pipe. This step size is used in the current single element transducer inspection as a compromise between inspection speed and accuracy. By using a linear array in the membrane probe design the lateral defect sizing performance is not affected (this dimension is referred to as the length of the defect in Table 6-3) so that this step size is again appropriate. As previously discussed in the inspection of the non-welded test-pieces it was not possible to acquire full encoded scan data using FMC with existing phased array controllers available within Rolls-Royce. Therefore in this comparison testing, data is once again collected from a single position for each defect and in each case the transducer is positioned approximately in-line with the defect centre line.

Although FMC data has been acquired in a large range of locations only the relevant data has then been processed to provide the required inspection image. Inspections based on FMC data acquisition are very versatile; by collecting a single FMC data set it is possible to subsequently process the data in a variety of different ways. In this

comparison the inspection data has been processed using different focal depths and aperture sizes. In order to baseline the performance of each technique, an unfocused test has been produced using an aperture of 12.5mm (17 elements). This is equivalent to the aperture used previously in the 2nd generation device inspection of the two flat plate, non-welded test-pieces reported in chapter 3. This technique is also representative of the likely performance that could be achieved using a conventional off-the-shelf single element transducer. This approach provides a baseline in performance for the inspection.

When using a phased array it is only possible to focus within the near field of the transducer. However, it is typically not possible to focus ultrasound either with an array or a mechanically focused single element transducer to a single point. In reality a given aperture will produce a beam with a finite width at all depths. Therefore a single aperture can be used to provide a high quality, reliable inspection over a range of different focal depths. A comparison of the beam characteristics when using a 17 element aperture and a 65 element aperture with the 3rd generation array is provided in Table 6-5. These results have been produced using CIVA to simulate the longitudinal wave produced with the array in immersion. A comparison of the unfocused beam produced by each aperture is provided in Fig 6-11. This comparison demonstrates that the beam shape produced by each aperture is very complex; however, it also demonstrates that the larger aperture has a longer near field length and can be used to provide a high degree of focusing over a long distance. The larger aperture produces a broad beam and the use of focused delay laws is essential to ensure that only a small region of the component is insonified during an individual inspection. Applying appropriate delay laws to focus the ultrasonic energy also has a far greater impact when using the larger aperture.

Table 6-5 Comparison of 6dB beam width and maximum amplitude obtained from a 17 element aperture and a 65 element aperture using the 3rd generation membrane device in immersion when using focused and unfocused delay laws.

Inspection Range (mm of water)	Aperture size (elements)	Beam Characteristics			
		Unfocused		Focused	
		6dB beam width (mm)	Maximum Amplitude (A.U.)	6dB beam width (mm)	Maximum Amplitude (A.U.)
50	17	12	12.4	4	20.5
50	65	46	12.2	2	47.3
100	17	9	16.1	7	18.1
100	65	46	17.8	2	55.8
200	17	24	9.5	17	9.9
200	65	38	15.9	3	35.6
400	17	33	4.3	33	4.4
400	65	68	4.1	18	7.9

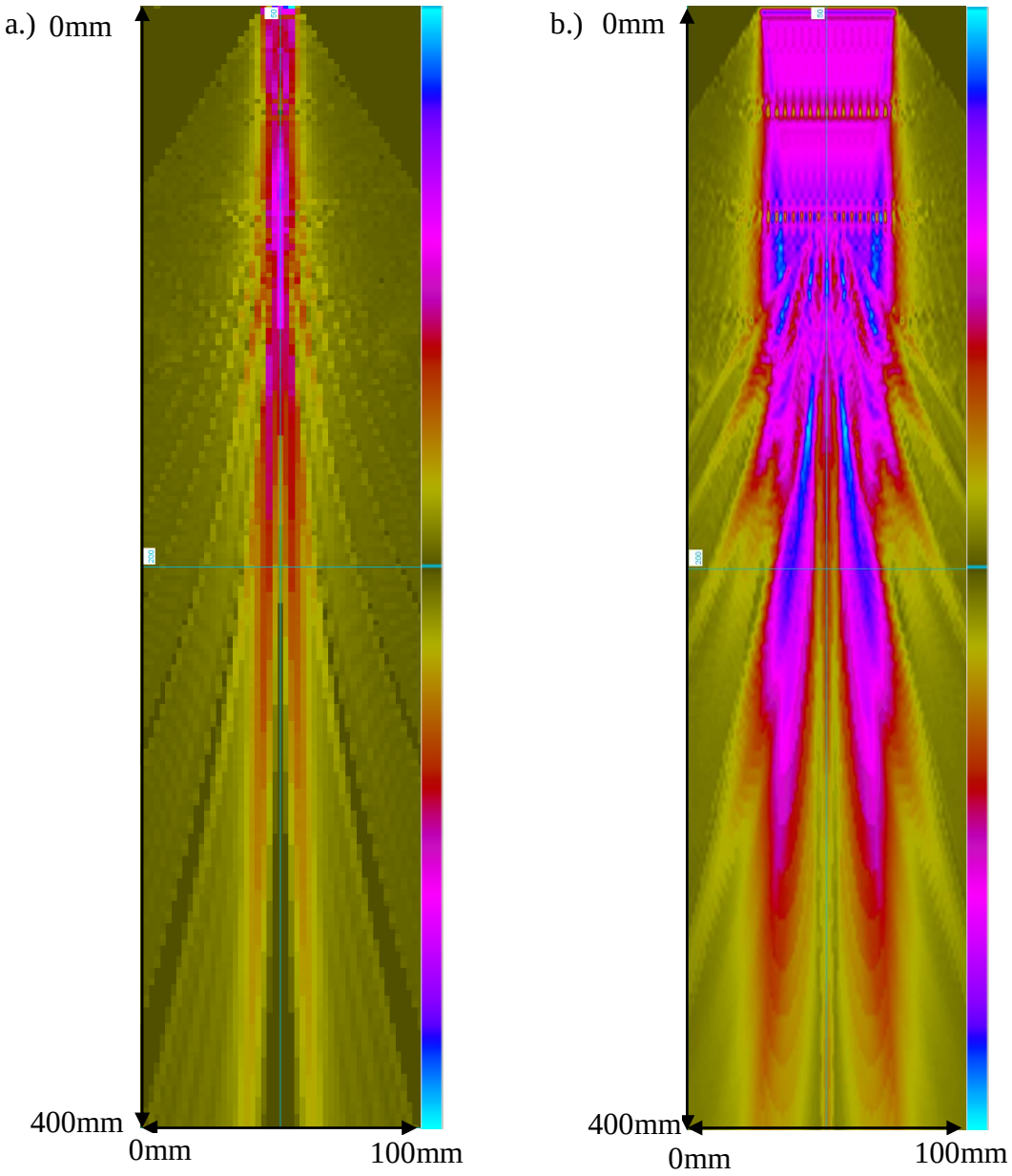

Figure 6-11 CIVA beam plots for 3rd generation membrane coupled array coupled to a water path using unfocused delay laws with a, a.) 17 element aperture and a, b.) 65 element aperture. Both images are shown over a 60dB dynamic range.

Calculation of the near field length with many of the complex techniques used in the inspection of the target application component is not straight-forward. An iterative approach was taken to determine the optimum aperture size to use for the focused beam inspection of each of the defects. As discussed above the aperture size used in a given inspection dictates the region of the component that is insonified from a single transducer position. Without mechanically scanning the transducer it is desirable to use the minimum possible aperture size to ensure that the largest possible region can be imaged from a given transducer position. Processing was initially performed with

a large aperture size to ensure that the defect was in the near field of the aperture used. A measurement of the defect through-wall extent was then performed from the B-Scan image obtained. This provided a measure of the maximum possible focusing that could be achieved. The aperture size was then gradually decreased until the measured through-wall size increased. This provided the minimum aperture size to achieve optimum defect detection. This approach is only acceptable when conducting an inspection on components with known defects such as the two flat plate, welded test-pieces. An alternative approach must therefore be developed before FMC based inspection can be deployed in industry. Work is ongoing to determine the optimum aperture size and delay laws for each inspection technique used and the best technique to combine the inspection data obtained. I lead this project within Rolls-Royce but this activity is beyond the scope of my doctorate and will not be reported in this thesis.

All of the experimental testing of the two flat plate, welded test-pieces was performed using an automated approach in a standard x-y scanning frame. As discussed in chapter 5 the 3rd generation membrane probe design has been updated to allow direct irrigation. Based on the comparison testing discussed previously, the membrane coupled device performs well when using this irrigation system and this approach has been used to provide the couplant required in all of the experimental testing performed in this inspection.

6.5. Experimental Results

Inspection of the flat plate, welded test-pieces has been performed using the 6mm, 7º and the 20mm, 18º, 3rd generation membrane coupled devices. Testing has also been performed using a pitch-catch arrangement; as discussed above the 80 element 2nd generation membrane device and the 48 element rigid wedge transducer were used to complete this testing. This configuration was used due to limitations in the total number of channels available within the MicroPulse 5PA phased array controller. The FMC data acquired from each of the 14 defects has been analysed using the range of different techniques listed in Table 6-2. A comparison of the SNR response from the defect using each of the different inspection techniques has then been performed.

A range of different focal regimes have been used in the welded test-piece inspection. When using a single depth of focus, the focal depth is optimised to detect the defect considered. Specific inspection techniques are used for the detection of surface breaking defects. Therefore when using this approach a single focal depth is appropriate and can be rapidly deployed. However, the depth of any embedded defects within the actual target application component is unknown and hence focusing throughout the inspection volume is required to provide complete inspection coverage. In an actual inspection multiple processing steps would be required at a range of focal depths and this is readily achievable with FMC data but processing this data would be time-consuming. An alternative approach is to use the ATFM algorithm, which produces a "fully-focused" B-Scan. Details of the ATFM algorithm are provided in section 2.2.

A very large amount of experimental data has been captured related to the inspection of the two flat plate welded test-pieces and it is inappropriate to review all of the results generated here. In sections 6.5.1 to 6.5.5 an overview of the performance of each of the main inspection techniques used will be provided. A comparison of the inspection performance when using the membrane device with delay laws to simulate a conventional off-the-shelf single element transducer inspection and the results obtained from the optimised inspection is then provided in section 6.5.6. This comparison quantifies the major improvements that can be achieved using the optimised inspection approach.

6.5.1. Direct Specular Through Weld Inspection

Direct specular through weld inspection is used to detect a range of defects within the target application component. A comparison of the inspection performance for all defects detected using this type of technique is shown in Table 6-6. When using an aperture of 17 elements and delay laws to simulate off-the-shelf single element transducer performance a beam steering only approach is used without any focusing. These results are shaded in yellow in Table 6-6. When using the optimised delay law inspection with variable aperture size ATFM focusing is used for all of the tests performed, these results have been shaded in blue in Table 6-6.

Table 6-6 A comparison of the inspection performance for all defects using a direct specular detection technique using single element (yellow shading) and optimised (blue shading) delay laws. Defects that are not detected are indicated by no value for the SNR.

Defect	Array	Aperture size (elements)	Beam Type	Primary / Secondary Technique	Inspection Performance SNR (dB ± 1 dB)
2	6mm, 7º	17	65º, Long	Primary	6
2	6mm, 7º	17	65º, Shear	Secondary	-
3	20mm, 18º	17	65º, Long	Primary	-
3	20mm, 18º	17	60º, Long	Secondary	-
4	20mm, 18º	17	70º, Long	Secondary	-
2	6mm, 7º	39	65º, Long	Primary	9
2	6mm, 7º	39	65º, Shear	Secondary	4
3	20mm, 18º	38	65º, Long	Primary	-
3	20mm, 18º	38	60º, Long	Secondary	-
4	20mm, 18º	31	70º, Long	Secondary	-
9	6mm, 7º	17	65º, Long	Primary	11
9	6mm, 7º	17	65º, Shear	Secondary	15
10	20mm, 18º	17	65º, Long	Primary	10
10	20mm, 18º	17	60º, Long	Secondary	9
11	20mm, 18º	17	70º, Long	Secondary	-
9	6mm, 7º	39	65º, Long	Primary	18
9	6mm, 7º	39	65º, Shear	Secondary	17
10	20mm, 18º	38	65º, Long	Primary	15
10	20mm, 18º	38	60º, Long	Secondary	15
11	20mm, 18º	31	70º, Long	Secondary	6

Through weld inspection of components containing an austenitic stainless steel weld is challenging and this is demonstrated by the number of defects that cannot be detected in Table 6-6. When using the direct specular inspection approach the transducer must often be located over the weld cap region. Therefore, without removing the weld cap or using a conformable array, particularly when using a large footprint array, it is not even possible to insonify the inspection region. Even when using a small array or a conventional single element transducer inspection coverage is limited. This is illustrated in the schematic diagram shown in Fig 6-12 for the through weld inspection of defect 3 using the 18º, 20mm device. This diagram indicates that

when using a similar size array with a rigid wedge for the inspection of this defect, the weld cap would have to be removed to provide suitable coupling.

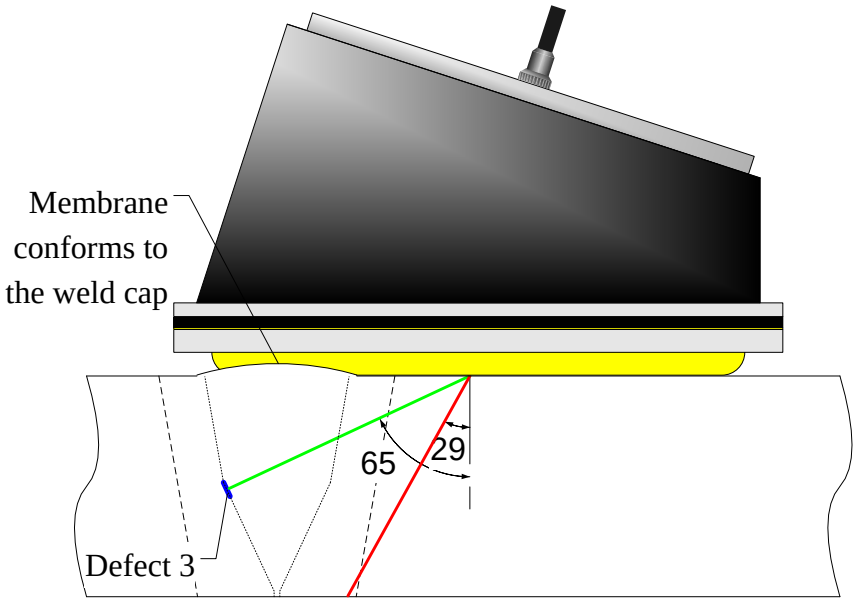

Figure 6-12 Schematic diagram to illustrate the through weld inspection of defect 3 using a direct 65º longitudinal wave inspection with the 18º, 20mm device.

Even when using the membrane coupled device technology to allow inspection through the weld cap region the anisotropic nature of the austenitic weld material makes inspection very difficult. This is a general limitation of through weld inspection and is not specific to the membrane coupled device approach. It was not possible to detect defects 3 and 4 using either the single element or optimised delay laws. However, as discussed previously these defects are significantly smaller than the validation defect size for the target application. Therefore, although desirable, the detection of this size of defect is not essential in this application.

Through weld inspection of defect 10 uses the same techniques as for defect 3 and uses the type of technique shown in Fig 6-12. The inspection of defect 10 was also challenging due to the presence of the austenitic weld material and the defect response is mis-placed within the weld volume due to the anisotropic nature of the weld. However, the inspection performance was also limited by an internal noise signal in the 18º, 20mm design. This issue was predicted with the low height profile design and hence this device was not used in the inspection but this issue was not expected in the 18º, 20mm device. The effect of the internal noise signal for the through weld

inspection of defect 10 using the 18º, 20mm device, can be seen in the B-Scan image provided in Fig 6-13. The image produced in Fig 6-13 has been generated using an aperture of 17 elements and unfocused delay laws to generate a 60º longitudinal wave. The SNR of the response from defect 10 provided in Fig 6-13 has been calculated by ignoring the effects of the internal noise signal. This approach has also been taken for all of the results provided in Table 6-6.

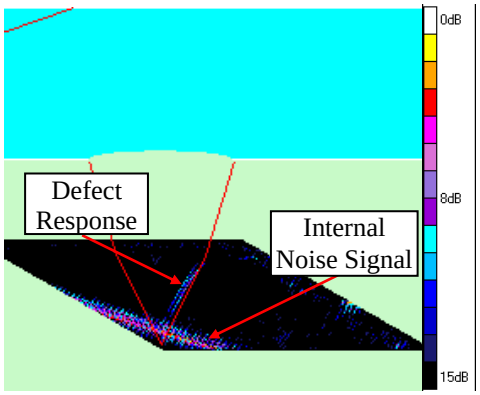

Figure 6-13 60º longitudinal wave B-Scan image obtained from the 17element aperture inspection of defect 10 through the weld using the 18mm, 20º device.

The presence of this noise signal in the inspection region of interest is due to a variation in the actual probe configuration from that expected. When completing an inspection using conventional rigid wedge transducers the transducer is forced into contact with the outer surface of the component under test. This ensures that appropriate coupling is maintained between the transducer and the component. Assuming that the component has a regular geometry then this approach also guarantees the height and angle of the transducer relative to the inspection surface. As discussed in section 3.3 this approach cannot be used when completing an inspection using the membrane coupled device. The array angle and height must be controlled by the scanning mechanism used so that the membrane can conform to the surface geometry of the component under test. The array can then be used to generate the surface profile of the component as shown in Fig 6-10.

During the non-welded test-piece inspection discussed in chapter 3, manual user intervention was used to optimise the inspection configuration for each of the embedded defects. When testing with the 3rd generation device, an approach which is more representative of that expected in industrial application has been used. In this

study a procedure has been developed to set-up the membrane device scanning jig. This process has been developed so that the probe angle and stand-off are as reproducible as possible and all probe positioning is relative to a single datum position. The flow of water couplant used in each measurement has been maintained at the same level using a standard peristaltic pump. Once the initial probe set-up has been performed there has been no further user intervention and scanning of the entire test-piece has been performed using a semi-automated approach. This proceduralised technique has allowed data collection to be performed by a number of Rolls-Royce employees. This has facilitated improved technology transfer into Rolls-Royce and helped to accelerate the commercialisation of membrane device approach and FMC based phased array inspection. However, this approach places additional challenges on the mechanical design of the scanning mechanism and further improvements to this design are required before a commercial membrane coupled device inspection can be developed. The required improvements will be considered when subsequent testing is performed on a fully geometrically representative test-piece in the future.

The variation in the array position can be compensated for by completing a measurement of the array position relative to the outer surface prior to subsequent processing of the experimental data. By completing this additional processing step it is possible to fully characterise the transducer position and optimise the performance of the inspection for each individual file. When using the current software this is a manual process, which increases the time associated with processing the data. Software development work is ongoing to automate this process but this will not be performed during the timeframe of my doctorate. This variation in the array position relative to the component is not a major limiting factor in the performance of the transducer because the actual height and angle can be readily measured. However, it does lead to some variation in the position of the internal noise signal which can potentially decrease the effectiveness of a given inspection.

As discussed in section 6.3 the direct specular through weld inspection of defects 4 and 11 is also limited because of the high degree of mis-orientation between the defect and the main beam angle. It was only possible to reliably and consistently detect defect 11 using this technique with the 18º, 20mm device. Unfortunately, the internal noise signal associated with this device that was seen to be an issue in the

inspection of defect 10 once again corrupted the B-Scan obtained. This is evident in the B-Scan obtained from this inspection using a 31 element aperture and a single focal depth of 26mm, shown in Fig 6-14. The defect SNR in the B-Scan provided in Fig 6-14 is approximately 6dB. Although the performance of this technique is limited, it does provide a useful confirmation of presence of the defect if detected using one of the other inspection techniques. This technique is also likely to provide a better quality defect response if the defect occurred with a slightly different tilt. The use of this technique as a secondary inspection is therefore valid but caution should be applied when using this approach.

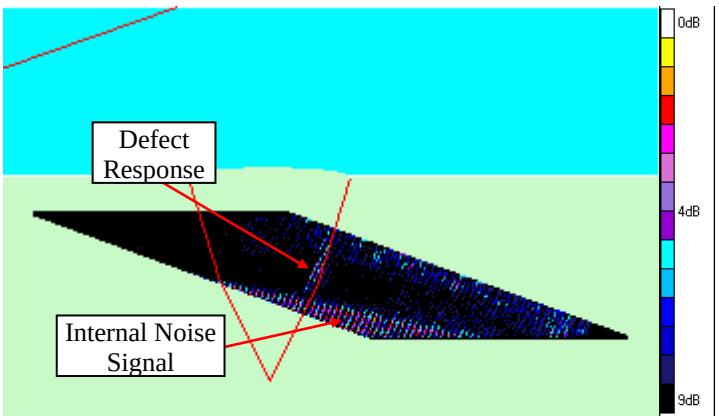

Figure 6-14 B-Scan image obtained using the secondary through weld scan direction inspection of defect 11 with the 18mm, 20º 3rd generation membrane device. Suitable delay laws have been used to produce 26mm focal depth from an aperture of 31 elements.

Due to the presence of the internal noise signal the through weld inspection performance for this type of defect is limited using both of the 3rd generation membrane coupled phased array designs. An attempt has been made to address this limitation through the design and manufacture of a twin crystal membrane coupled phase array device. In the twin crystal array there is a separate transmit and receive aperture, the beam spread internal noise signal is therefore not present and does not corrupt the B-Scan image. The twin crystal membrane coupled device is discussed in chapter 7.

6.5.2. Creep Wave Inspection

All of the testing performed using the creep wave technique used the 20mm, 18º, 3rd generation membrane device design. When using an aperture of 17 elements and

delay laws to simulate off-the-shelf single element transducer performance, a beam steering only approach is used without any focusing. When using the optimised delay law inspection an aperture of 40 elements was used along with delay laws to focus at 0 mm depth within the component. This type of technique can only be used to detect surface breaking, and near surface breaking defects so through thickness focusing is not required. Unfortunately it was not possible to detect any of the outer surface breaking defects using the creep wave inspection technique. When using this approach multiple signals were observed. Some of these signals were related to the weld cap geometry and it is possible that others were due to the defect itself. However, it was not possible to reliably distinguish the actual defect from these signals. As discussed previously the direct creep wave inspection of any near surface defects using a conventional pulse-echo transducer is an issue because of the dead-zone associated with the transducer. It is therefore possible that the creep wave inspection performance can be improved by using the twin crystal membrane coupled device. The design of this device is discussed in detail in chapter 7.

6.5.3. Corner Echo Inspection

The corner echo inspection technique is used to detect the surface breaking defects embedded within the welded test-pieces. A comparison of the inspection performance for all defects detected using this type of technique is shown in Table 6-7. Once again when using an aperture of 17 elements and delay laws to simulate off-the-shelf single element transducer performance a beam steering only approach is used without any focusing; and is shown shaded in yellow in Table 6-7. In this case when using the optimised delay law inspection with a variable aperture size, single depth focusing is used at a depth corresponding to the surface of the test-piece, these results are shaded in blue in Table 6-7. This focusing approach is suitable because a strong corner echo response is only obtained from surface breaking or very near surface breaking defects. The depth of the defect is therefore known and single depth focusing delay laws can be processed faster than the ATFM algorithm. Defects 1 and 8 occur centrally within the weld; therefore the convention adopted previously to describe the scan direction has been used, and scanning from left to right in Fig 6-3 is considered to be the through weld inspection direction. Although some small differences in inspection

performance from the two different directions are observed these are relatively small and are due to the non-symmetrical nature of the root region.

Table 6-7 A comparison of the inspection performance for all defects using the corner echo inspection technique using single element (yellow shading) and optimised (blue shading) delay laws.

Defect	Array	Aperture size (elements)	Beam Type	Primary / Secondary Technique	Scan Direction	Inspection Performance SNR (dB ± 1 dB)
1	6mm, 7º	17	45º, Shear	Primary	Through-Weld	13
1	6mm, 7º	17	60º, Shear	Secondary	Through-Weld	8
1	6mm, 7º	17	45º, Shear	Primary	Near side	8
1	6mm, 7º	17	60º, Shear	Secondary	Near side	9
2	6mm, 7º	17	45º, Shear	Secondary	Near side	16
5	20mm, 18º	17	45º, Shear (full-skip)	Secondary	Near Side	16
1	6mm, 7º	26	45º, Shear	Primary	Through-Weld	14
1	6mm, 7º	41	60º, Shear	Secondary	Through-Weld	10
1	6mm, 7º	26	45º, Shear	Primary	Near side	11
1	6mm, 7º	41	60º, Shear	Secondary	Near side	10
2	6mm, 7º	39	45º, Shear	Secondary	Near side	19
5	20mm, 18º	42	45º, Shear (full-skip)	Secondary	Near Side	18
8	6mm, 7º	17	45º, Shear	Primary	Through-Weld	21
8	6mm, 7º	17	60º, Shear	Secondary	Through-Weld	9
8	6mm, 7º	17	45º, Shear	Primary	Near side	8
8	6mm,	17	60º,	Secondary	Near side	11

	7º		Shear			
9	6mm, 7º	17	45º, Shear	Secondary	Near side	15
12	20mm, 18º	17	45º, Shear (full-skip)	Secondary	Near Side	20
8	6mm, 7º	26	45º, Shear	Primary	Through-Weld	22
8	6mm, 7º	41	60º, Shear	Secondary	Through-Weld	12
8	6mm, 7º	26	45º, Shear	Primary	Near side	10
8	6mm, 7º	41	60º, Shear	Secondary	Near side	16
9	6mm, 7º	39	45º, Shear	Secondary	Near side	24
12	20mm, 18º	42	45º, Shear (full-skip)	Secondary	Near Side	24

The corner echo inspection of defect 1 in the flat plate, non-welded test-pieces was very straight forward. In the non-welded test-pieces a simple notch defect was introduced into the parent material and a strong corner echo reflection was observed, with a high amplitude signal in comparison to the background noise. Inspection of the root region in real welds is much more challenging and this is clear from the results obtained for all of the root region defects in the welded test-pieces. The root region of the flat plate welded test-pieces has a relatively complex geometry because of the EB insert; as is shown in Fig 6-15. Even when no defect is present there are a number of possible paths that allow ultrasonic energy to return to the transducer. A schematic diagram of the main, non-defective, root signal for a 45º shear wave inspection is shown in Fig 6-15(a). Due to the curved nature of the EB insert this type of reflection can take place over a relatively wide range of aperture positions and beam angles. The EB insert signal can be compared to the signal that could be obtained from an actual defect using a corner echo is shown in the schematic diagram in Fig 6-15(b). Similar interactions can occur when considering the other corner echo inspection techniques used to detect root region defects.

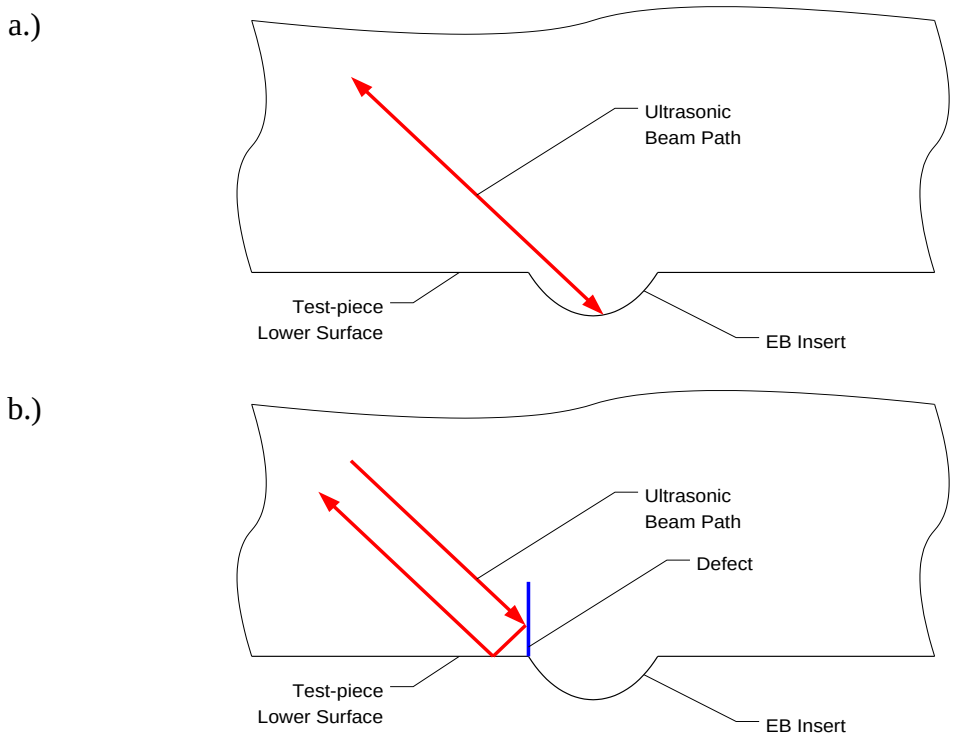

Figure 6-15 Schematic diagram of the inspection of a.) a non-defective root in the flat plate welded test-pieces and b.) a root defect.

The presence of these root signals makes correct interpretation of the inspection data critical. The non-defective root signals are distinguished from an actual defect signal by considering the inspection range and the relative amplitude of the two different signals. These differences in the measured ultrasonic signal can be quite subtle which makes accurate data display essential. However, some difference in range and a significantly reduced amplitude of the root signal can be readily observed for all four of the defects considered in this region of the test-piece. This allows all of the root region defects to be reliably detected using each of the techniques considered. The 45º shear wave corner echo provides a significantly higher amplitude signal and better SNR that the 60º technique. This is expected because the corner echo effect is strongest with 45º shear waves. The B-Scan image obtained from defect 8 using a 45º shear wave inspection from the positive scan direction is shown in Fig 6-16(a). This can be compared to the defect free case shown in Fig 6-16(b). This result illustrates the challenges in terms of data interpretation. In Fig 6-16(b) a root signal is observed, this signal occurs over a slightly broader range of times than the defect signal. The 6mm, 7º membrane configuration is more suitable for the inspection of the root region defects because the internal beam spread noise signal is well removed from the defect signal. The data shown in Fig 6-16 has been generated using the 6mm, 7º device with

an aperture of 12.5mm (17 elements) and processed to produce an unfocused shear wave. The amplitude of the response from defect 8 in Fig 6-16(a) is approximately four times greater than the defect free root response shown in Fig 6-16(b). This is indicated by the decrease in the SNR of the root signal relative to the background noise in comparison to the actual defect signal.

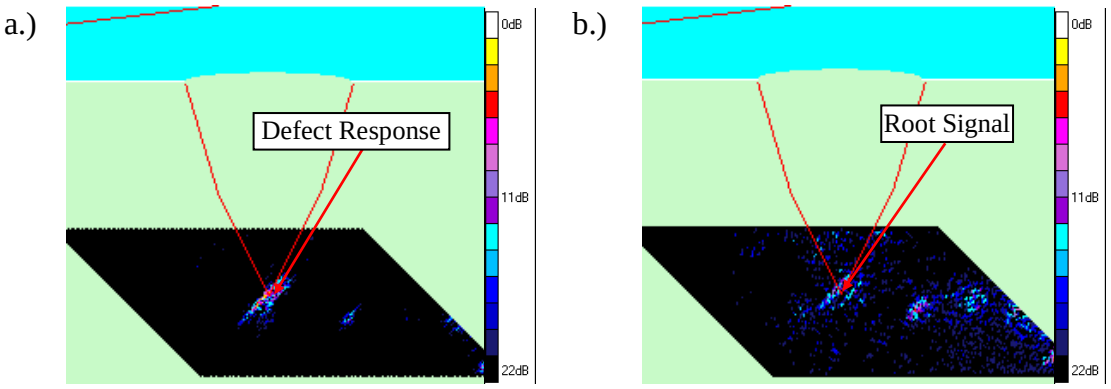

Figure 6-16 Comparison of the 45º shear wave B-Scan images obtained from a.) defect 8 and b.) a null defect region of the test-piece.

Detection of defect 5 and 12 using the full-skip 45º shear wave technique is relatively straightforward and a high amplitude signal is observed using both the single element and optimised delay laws. However, another strong geometrical feature is observed in the null defect case due to the toe of the weld cap. In a similar way to the inspection of the defects within the root region of the test-piece the data interpretation engineer must distinguish a defect signal from this geometrical response. Once again this is achieved by carefully monitoring the amplitude and the exact position of the signal. The interpretation engineer is typically provided with a detailed description of the component under test and would expect a signal from the toe of the weld. However, this is also one of the potential positions where the interpretation engineer is likely to anticipate a defect could occur. The 18 º, 20mm design is the most appropriate device to use for this inspection because it has a more optimised natural beam angle and hence provides a higher amplitude and better SNR than the low height profile design. A comparison of the response from defect 5 and a defect free region of the test-piece is provided in Fig 6-17. The images in Fig 6-17 have been generated using the 18 º, 20mm device with a 17 element aperture and unfocused delay laws. The amplitude of the response from defect 5 is double that observed from the defect free location and has a SNR 7dB higher than the defect free toe signal. The difference in the type of

response measured from a defect and a defect free region can also be clearly seen in Fig 6-17.

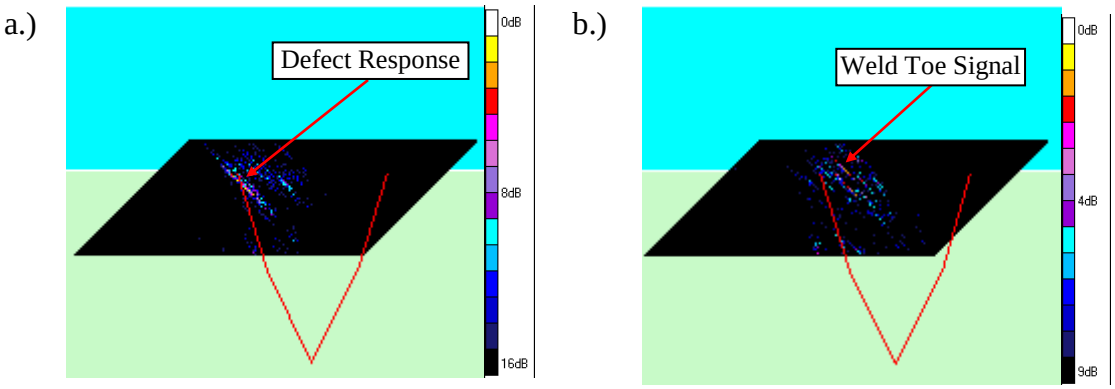

Figure 6-17 Comparison of the 45° full skip shear wave B-Scan images obtained from a.) defect 5 and b.) a null defect region of the test-piece. In each image an unfocused aperture of 17 elements is used and SNR is calculated relative to the background noise.

6.5.4. Transverse-Longitudinal (TL) Skip

The transverse-longitudinal (TL) skip technique is used to detect lack of side wall fusion defects on the 25º weld fusion face without the beam traversing the weld region. A comparison of the inspection performance for the four defects detected using this type of technique is shown in Table 6-8. In all cases the inspection is performed using the 6mm, 7º array with delay laws to generate a 65º longitudinal wave from the near side of the weld. When using an aperture of 17 elements and delay laws to simulate off-the-shelf single element transducer performance a beam steering only approach is used without any focusing. The optimised delay law inspection with a variable aperture size again uses the ATFM technique to provide through thickness focusing using a single set of delay laws. Results produced using the delay laws to simulate single element transducer inspection are shaded in yellow and the results produced using optimised delay laws are shaded in blue.

Table 6-8 A comparison of the inspection performance for the four defects detected using the TL skip technique using single element (yellow shading) and optimised (blue shading) delay laws.

Defect	Aperture size (elements)	Primary / Secondary Technique	Scan Direction	Inspection Performance SNR (dB ± 1 dB)
2	17	Primary	Near Side	14
3	17	Primary	Near Side	9
2	39	Primary	Near Side	18
3	65	Primary	Near Side	10
9	17	Primary	Near Side	17
10	17	Primary	Near Side	16
9	39	Primary	Near Side	19
10	65	Primary	Near Side	18

The TL inspection of these defects in the welded test-pieces is essentially identical to the inspection of defects 2 and 3 in the non-welded test-pieces and as would be anticipated the results are comparable. These results demonstrate that defects of this type can be reliably detected using the membrane coupled device. However, due to

the similarity between these results and those discussed in chapter 3 and chapter 5 this provided very limited additional information regarding the performance of this technology.

6.5.5. Transverse-Longitudinal-Longitudinal (TLL) Skip

As stated in section 6.2 the main inspection mechanism for the detection of mid-wall planar defects that occur approximately normal to the component surface is the transverse-longitudinal-longitudinal (TLL) technique. This technique is more complex to use than the techniques discussed above. A comparison of the inspection performance for all defects detected using this type of technique is shown in Table 6-9. All of the testing performed using this technique uses the 6mm, 7º 3rd generation membrane device design or a pitch-catch arrangement using the 80 element device along with the 48 element rigid wedge transducer. When using the pitch-catch inspection technique the membrane device is used as a receiver only and positioned directly above the weld cap as shown in Fig 6-18. In all inspections of this type the entire 48 element rigid wedge array is used to generate the transmitted plane wave. Different size apertures are then used with the membrane probe to compare the predicted single element transducer inspection performance to the optimised inspection. When using an aperture of 17 elements and delay laws to simulate off-the-shelf single element transducer performance a beam steering only approach is used without any focusing. Results obtained using these delay laws are shaded in yellow in Table 6-9. When using the optimised delay law inspection with a variable aperture size, ATFM is used to produce the results that are shaded in blue in Table 6-9. The use of ATFM based inspection ensures that the through thickness inspection capability is maintained. In order to distinguish between the two different scan directions when considering defects that occur in the centre of the weld the convention adopted previously has once again been used. Scanning from left to right in Fig 6-3 is considered to be the through weld inspection direction in the inspection results provided in Table 6-9.

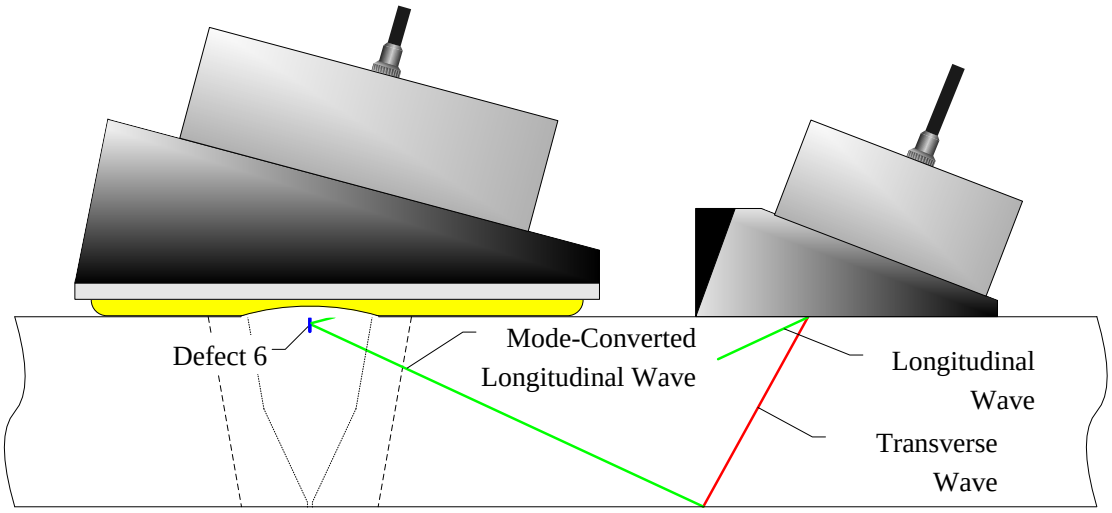

Figure 6-18 Schematic diagram of the pitch-catch TLL inspection setup.

Table 6-9 A comparison of the inspection performance for all defects using the TLL inspection technique using single element (yellow shading) and optimised (blue shading) delay laws. Defects that are not detected are indicated by no value for the SNR.

Defect	Array	Aperture size (elements)	Beam Type	Scan Direction	Primary / Secondary Technique	Inspection Performance SNR (dB ± 1 dB)
4	6mm, 7º	17	65º, Long	Through Weld	Primary	-
4	6mm, 7º	17	65º, Long	Near Side	Primary	8
4	6mm, 7º	17	45º, Long	Near Side	Secondary	9
5	Pitch-Catch	17	65º, Long	Through-Weld	Primary	-
5	Pitch-Catch	17	65º, Long	Near Side	Primary	5
6	Pitch-Catch	17	65º, Long	Through-Weld	Primary	6
6	Pitch-Catch	17	65º, Long	Near Side	Primary	-
7**	6mm, 7º	17	50º, Long	Through-Weld	Primary	-
7**	6mm, 7º	17	50º, Long	Near Side	Primary	6
4	6mm, 7º	46	65º, Long	Through Weld	Primary	-
4	6mm, 7º	46	65º, Long	Near Side	Primary	12
4	6mm, 7º	46	45º, Long	Near Side	Secondary	15
5	Pitch-Catch	17	65º, Long	Through-Weld	Primary	-
5	Pitch-Catch	17	65º, Long	Near Side	Primary	6
6	Pitch-Catch	17	65º, Long	Through-Weld	Primary	9
6	Pitch-Catch	17	65º, Long	Near Side	Primary	*
7**	6mm, 7º	44	50º, Long	Through-Weld	Primary	5
7**	6mm, 7º	44	50º, Long	Near Side	Primary	8
11	6mm, 7º	17	65º, Long	Through Weld	Primary	-
11	6mm, 7º	17	65º, Long	Near Side	Primary	10
11	6mm, 7º	17	45º, Long	Near Side	Secondary	11
12	Pitch-Catch	17	65º, Long	Through-Weld	Primary	7
12	Pitch-Catch	17	65º, Long	Near Side	Primary	9
13	Pitch-Catch	17	65º, Long	Through-Weld	Primary	10
13	Pitch-Catch	17	65º, Long	Near Side	Primary	7
14**	6mm, 7º	17	50º,	Through-	Primary	5

			Long	Weld		
14**	6mm, 7º	17	50º, Long	Near Side	Primary	7
11	6mm, 7º	46	65º, Long	Through Weld	Primary	-
11	6mm, 7º	46	65º, Long	Near Side	Primary	18
11	6mm, 7º	46	45º, Long	Near Side	Secondary	18
12	Pitch-Catch	17	65º, Long	Through-Weld	Primary	8
12	Pitch-Catch	17	65º, Long	Near Side	Primary	11
13	Pitch-Catch	17	65º, Long	Through-Weld	Primary	13
13	Pitch-Catch	17	65º, Long	Near Side	Primary	9
14**	6mm, 7º	44	50º, Long	Through-Weld	Primary	9
14**	6mm, 7º	44	50º, Long	Near Side	Primary	9

Notes
* Low level signal observed but inconclusive as to origin
** Optimum inspection of defect 7 and 14 uses a 50deg TLL technique with 34mm offset between transmit and receive paths

When using the TLL inspection technique there is often an offset between the transmit and receive paths. When completing the inspection using conventional single element transducers the offset between the two paths is controlled during the inspection planning phase and cannot be varied during the actual inspection. Typically two individual probes are used with a fixed stand-off between them, or as in the actual target application inspection, a bespoke probe is produced. A number of different probe separations must be used to provide complete coverage of the entire inspection volume. It is not practicably possible to provide a focused inspection with an optimised set-up for every possible defect position and orientation and hence the inspection performance can be compromised. Inspection coverage can be restricted further due to the presence of the irregular weld cap and typically it is once again only possible to detect some types of defect by mechanically grinding the weld cap off.

The membrane coupled conformable phased array device uses a large footprint array, and this approach minimises the amount of axial mechanical scanning that is required. Using this device in conjunction with the FMC data acquisition approach also allows a high degree of flexibility in terms of the exact inspection configuration used. It is possible to complete a wide range of TLL inspections using a self tandem (ST)

technique. When post processing the inspection data it is then possible to vary both the angle of the inspection and the offset between the transmit and receive paths to ensure that the optimum inspection configuration is used. By utilising the versatility of the membrane coupled device approach and optimising the delay laws for a given type of defect, it is possible to detect the mid-wall defects present in the welded test-pieces.

The inspection of defects 4 and 11 in the welded test-pieces using the TLL inspection with a 65º longitudinal wave from the near-side direction is equivalent to the inspection of defect 4 in the non-welded test-pieces. As expected, the inspection performance is comparable to the results obtained from the inspection of the non welded test-piece, which are reported in Chapters 3 and 5. The secondary inspection technique from the near side of the weld is very similar but uses a 45º longitudinal wave. When using this wave angle there is a separation between the transmit and receive paths and this must be accounted for during the processing of the FMC data. This can be readily achieved using the Imperial College FMC processing software and reliable detection of this type of defect is again possible using both sets of delay laws. The inspection performance improves significantly when using the large aperture with focused delay laws.

The through weld inspection of both defects 4 and 11 using the TLL inspection technique is much more challenging. As shown in the schematic diagram provided in Fig 6-19 for the inspection of defect 4, the mode-converted longitudinal wave must propagate through the austenitic weld material. The austenitic weld causes a large amount of scattering and beam steering and it is not possible to reliably detect this type of defect even when using the optimised delay laws. As discussed in section 6.5.1 the secondary through weld inspection technique for this type of defect is a direct specular reflection using a 70º longitudinal wave. Due to the slight mis-orientation of the defect to the beam it is only possible to detect defect 11 using this approach. Therefore, the through weld detection of defect 4 is not possible using either of the techniques considered. This is a limitation of the inspection technique used, however, defect 4 is smaller than the validation defect size for the actual target application inspection and as such is not essential for the safe operation of the plant.

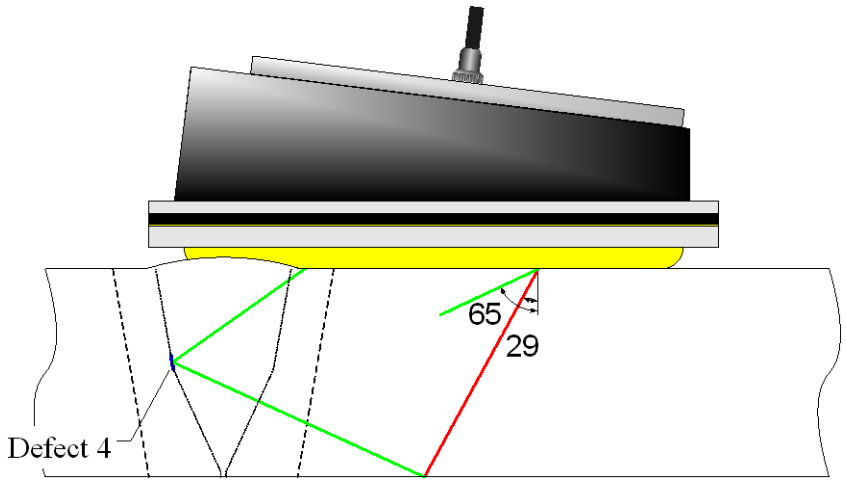

Figure 6-19 Schematic diagram of the through weld 65° longitudinal wave TLL inspection set for the inspection of defect 4.

In the inspection of outer surface breaking defects, the strong geometrical signal from the weld toe discussed in section 6.6.2 is once again observed. Due to the presence of this geometrical signal it is not always possible to reliably detect the presence of the defect. Detection of this type of defect is likely to be easier when processing of scanned data becomes possible. In the current approach comparison between the defect region and a single non-defective region is performed. However, when using scanned data, the interpretation engineer can monitor trends in the inspection data and is less reliant on point measurements.

Detection of defects 6 and 13 is extremely difficult when using conventional rigid wedge transducers and is only possible if the weld cap is removed. Due to the distortion of the parent plate even when the weld cap is removed this is still a very difficult inspection. Conversely, when using the membrane coupled device approach, detection of this type of defect can be reliably achieved with the weld cap in place. Defect detection is possible using both approaches used in this study. However, the inspection performance using the optimised delay laws demonstrated a significant improvement over the single element delay laws. When using the current, single point measurement technique, it is typically easier to detect mid weld defects than defects at the weld toe because the defect signal occurs well away from the high amplitude geometrical signals. Low level signals were observed in many of the inspections performed using the optimised delay laws. The origin of these signals is unclear and the presence of these signals prevents a reliable inspection from being

performed. Therefore both of the mid-weld outer surface defects were only reliably detected using the pitch-catch inspection techniques.

Defects 7 and 14 represent mid-wall, mid weld, planar flaws perpendicular to the component back-wall. It is only possible to artificially introduce this type of defect during the welding process and hence this type of defect was not included in the flat plate, non-welded test-pieces. The inspection techniques used to detect these defects are very similar to those used in the inspection of defects 4 and 11 but the inspection angles used are slightly different. When I designed the test program for the inspection of this type of defect I based the techniques used on the current inspection procedure (Rolls-Royce, 2002a). These techniques could be used to detect each of the two defects but the inspection performance was limited. When processing the data I found that the highest amplitude and best SNR signal could be obtained using a slightly different beam angle to that used in the current target application inspection. The actual inspection technique used to detect this type of defect is shown in Fig 6-20. This technique uses delay laws to generate a 50º longitudinal wave and an offset of 34 mm between the transmit and receive paths. The use of FMC data processing was essential in the identification of this optimum inspection technique and demonstrates the potential benefits that can be achieved by using this approach.

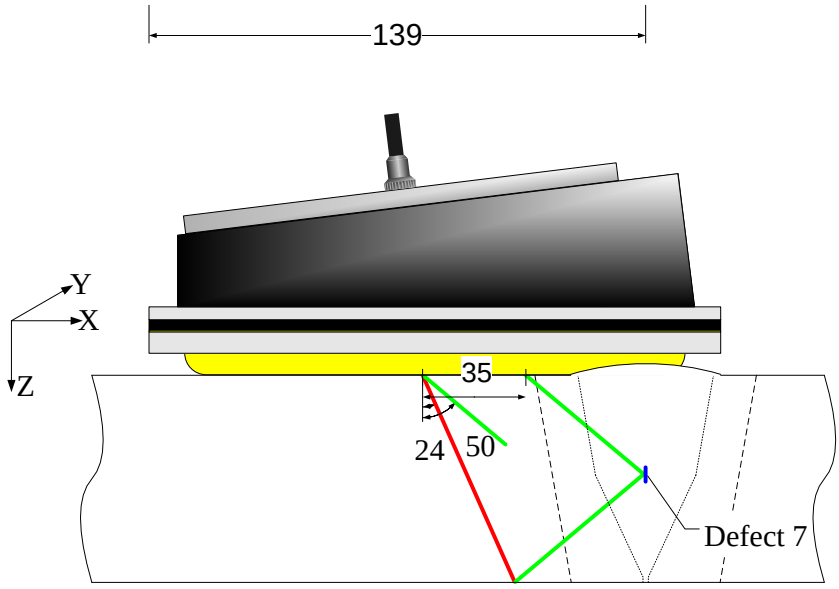

Figure 6-20 Inspection diagram to detect defect 7 using the 7º, 6mm 3rd generation 128 element membrane probe with a 50º TLL inspection from the positive direction.

The large separation between the transmit and receive paths means that the internal noise signal is not present within the B Scan generated from the data. Detection of the defect through the austenitic weld is challenging and the SNR of the defect response is relatively low. However, when using the inspection technique shown in Fig 6-20 it is possible to detect both defects 7 and 14. Both defects can be detected using the unfocused delay laws; however, inspection performance is improved by using the optimised delay laws with a larger aperture.

6.5.6. Inspection Summary

The inspection performance improvements that can be achieved by using the membrane coupled device with optimised delay laws in comparison to the small aperture, unfocused delay laws is significant in some cases. This is illustrated by the results provided in Table 6-6 to Table 6-9 and have been discussed in the preceding sections of this thesis. A summary of the inspection performance benefits that can be achieved using an optimised inspection is provided in Table 6-10. Critically the membrane device allows the reliable detection of some defects that are undetectable using delay laws which mimic the commercially available single element transducers. In Table 6-10 inspection techniques that can only be used to reliably detect a given defect using optimised delay laws are highlighted in green. Inspection techniques that can be used for defect detection using both approaches are highlighted in orange and techniques that do not provide a reliable inspection for a given defect using either approach are indicated in red. In many cases where a defect cannot be detected using a certain technique it is only the smaller defect of that type which cannot be reliably detected. The 4mm through wall defects embedded within the target application component are smaller than the current validation size defect within the actual target application component. These defects were included in the flat plate, welded test-pieces to discover the potential performance of the membrane device technology and detection of these defects is not essential for the safe operation of the component. The most common reason for inconclusive detection of the defects highlighted in red in Table 6-10 is the very challenging nature of through austenitic weld inspection. This is a general issue related to this type of inspection and it is not specifically associated with the use of the membrane coupled device. In situations where no

secondary inspection technique has been performed for a given defect this is shown in grey. An additional inspection technique may be considered for these specific defects in the future. When a defect occurs in the centre of the weld through weld inspection is considered to be from the positive scan direction (i.e. left to right in the images provided in Fig 6-3 and Fig 6-4) and near side weld inspection is considered as the negative scan direction. In all cases the SNR improvement that can be achieved when using the optimised delay laws is provided. The inspection performance can be improved for all defects, even when the defect can be detected using the single element transducer approach. These results graphically quantify the inspection performance improvement using the 3rd generation membrane coupled device with optimised delay laws.

Table 6-10 Table showing the SNR improvement when using an optimised delay law inspection in comparison to a 12.5mm aperture, unfocused inspection. Green shading indicates that it is only possible to detect a defect if optimised delay laws are used. Orange shading implies that a defect can be detected using both delay law approaches. Red shading is used to highlight defects that cannot be detected using a given technique and grey shading indicates where a specific test is not performed.

Defect	Inspection Technique SNR Performance (dB ± 1 dB)			
	Through Weld		Near Side	
	Primary Technique	Secondary Technique	Primary Technique	Secondary Technique
1	1	2	3	1
2	3	4	4	3
3	-	-	1	
4	-	-	4	6
5	-	-	1	2
6	3	-	-	-
7	5		2	
8	1	3	2	5
9	7	2	2	9
10	5	6	2	
11	-	6	8	7
12	1	-	2	4
13	3	-	2	-
14	4		2	

6.6. Membrane Device Inspection Speed Improvements

The reliable detection of a number of the defects within the two flat plate welded test-pieces requires the use of the conformable phased array membrane device. This is illustrated by the inspection technique diagrams shown for defect 3 in Fig 6-12 and

for defect 7 in Fig 6-20. These examples demonstrate that the complete inspection coverage of the target application component without the removal of the weld cap is only possible by using a conformable transducer. The experimental results reviewed in section 6.5 also indicate that it is only possible to reliably detect some of the defects that it is postulated could occur in the target application by using focused inspection techniques. This can only practically be implemented by using phased array transducers. The membrane coupled phased array device satisfies both of these requirements. The use of phased array transducers can also provide dramatic inspection speed improvements. I have performed a theoretical study to quantify the potential inspection speed improvement. This study considers the inspection of the actual target application component. At this stage in the development of the membrane coupled device inspection it is not possible to complete this study experimentally because a suitable geometrically representative test-piece has not been produced. However, an estimate of the time associated with the overall inspection can be accurately established based on knowledge of the required testing and the time required to complete smaller scale laboratory tests.

In the current single element transducer inspection, scans with five separate probe pans and 15 probe configurations must be performed. The technique document (Rolls-Royce, 2002b) provides details of the raster scan performed with each probe pan and these values have been used in this study. In the membrane device inspection it is anticipated that three different probe configurations are used and six circumferential scans are performed. In each probe configuration all of the 128 channels available on the MicroPulse 5PA will be used. The first probe configuration will use the low height profile linear array, the second will be based on the 20mm stand-off device, finally a pitch–catch scan using the 2nd generation membrane device and the 48 element rigid wedge transducer will be performed.

Accurate and repeatable calibration of the different probes used is critical to provide a high quality inspection. Calibration of the single element transducers is performed in line with BS EN 1713 (British Standards Institution, 1998a). There is currently no calibration standard for FMC phased array inspection, a technique is under development as part of the NPCT project but this needs further clarification (Duxbury, 2009). The current proposed FMC calibration process will characterise the

performance of the array on an element-by-element basis, the different beam requirements will then again be assessed by using the post-processing software. FMC calibration is likely to be more complex than calibration of conventional transducers and a conservative estimate of the time required to complete this process has been used.

A second comparison is also made where the "ultimate" membrane coupled device inspection is considered. This comparison assumes that the data transfer rate between the array controller and the host PC for FMC inspection is negligible. As computer processing speeds improve this condition will become more achievable. These conditions are also more likely to be met as controller architecture is optimised for FMC inspection.

6.6.1. Assumptions

In order to complete the theoretical study of the time required carrying out the inspection of the target application a number of assumptions have been made. These assumptions are summarized here:

- The target application component only allows single sided inspection access, therefore the full range of inspection techniques are required.
- When circumferentially scanning around the pipe a 2mm step size is used.
- All of the necessary mechanical movement of the transducer is performed at 5mm/s, in both the axial and circumferential directions and no allowance is made for acceleration and deceleration.
- A complete FMC scan is performed using the membrane coupled device at each scan position; inspection speed could be significantly improved by using half matrix capture and omitting duplicate scan data but this has not yet been validated for use within Rolls-Royce.
- In the single element transducer inspection the minimum amount of raster scanning is performed to provide the maximum possible inspection coverage.

- The time required for data transfer for the single element transducer inspection is assumed to be zero. This is likely to underestimate the inspection time, particularly when complex probe pans are considered.
- The time required to calibrate and setup each single element transducer scan is considered to be the same and is assumed to take approximately 1hour.
- The time required to calibrate and setup each membrane device scan is considered to be the same and is assumed to take approximately 2 hours.
- All phased array inspections are performed using FMC, the time required to complete this scan is based on experimental evidence using the MicroPulse 5PA array controller.
- All phased array inspections are performed using a 25 MHz sampling rate. This is a higher sampling rate than required to provide Nyquist sampling of the signal. However, the sampling rate is limited by the MicroPulse 5PA controller.
- For each membrane probe inspection two scans are performed, one with a 20µs gate length to record the surface profile. The second scan is to inspect for the defect and uses a 100µs gate.
- At this stage in the development process the manipulator set-up time can not be accurately estimated and therefore this effect is ignored. When using the membrane probe fewer probe changes are required and the manipulator setup process is significantly simpler than in the single element transducer case. This assumption is therefore likely to be highly conservative.
- The time required to analyze the data using each different transducer approach is the same, and is omitted from the speed calculation.
- Neither the single element nor the FMC data is averaged

A summary of the predicted inspection times for each of the three different approaches is shown in Table 6-12. This study demonstrates that in addition to the improved inspection coverage, SNR and increased inspection flexibility it is also possible to achieve significant speed improvements by using the membrane coupled phased array device.

Table 6-11 Summary of time required to complete the entire target application inspection.

	Single element transducer	Current membrane device performance	"Ultimate" membrane device performance
In-service inspection Time (hrs)	12.7	8.9	0.6
Calibration time (hrs)	23.0	6.0	6.0
Total in-service inspection time (hrs)	35.7	14.9	6.6
Improvement (%)	NA	58%	82%
Weld cap removal (hrs)	6.0	0.0	0.0
Pre-service inspection time (hrs)	41.7	14.9	6.6
Total improvement (%)	NA	64%	84%

To complete a thorough single element transducer inspection of the target application component the weld cap must be removed. The pre-service inspection time for the single crystal technique includes 6hrs that are estimated to be required to allow this removal process to be performed. The membrane coupled device allows complete inspection coverage to be performed without removal of the weld cap and this requirement is omitted from the inspection time. Based on the theoretical study performed the PSI time using the current device inspection equipment is almost three times faster than the equivalent single element transducer inspection. If the potential improvements that could ultimately be achieved are also included then the membrane probe PSI time can be reduced by well over 80%.

The single element transducer in-service inspection (ISI) time does not include the time required to remove the weld cap, it is assumed that this weld cap has been removed at manufacture. The single crystal ISI time is therefore less than the time required to complete the PSI. However, the membrane device approach can still

deliver significant inspection speed benefits. The current inspection capability is still predicted to reduce the ISI time by almost 60% and after improvements to the process of FMC data acquisition and processing a time reduction of over 80% could be achieved. These speed improvements can significantly help to improve the availability of the Submarine platform and reduce the cost of ownership to the MoD.

These inspection speed improvements are also likely to be an underestimate because the manipulator setup times have been omitted. The results also demonstrate that even for a large component such as the target application the time required to complete calibration of the equipment is significant. The calibration time estimate is also a source of potential error in these estimates. Finally the time required to complete the membrane probe inspection is strongly dependent on the data transfer speed from the controller to the host PC. Performance is only likely to approach the "ultimate" inspection speed if a powerful computer processor is used.

6.7. Summary

Two flat plate, welded test-pieces that contain a weld and weld cap that are representative of the target application component were designed and manufactured. These test-pieces contain a total of 14 defects at a range of different positions and orientations through-out of the weld region. These defects are designed to replicate all of the planar defects that it is postulated could occur within the actual target application component. A primary and secondary inspection technique from both sides of the weld has been designed. Implementation of these techniques on the welded test-pieces enable a thorough characterisation of the membrane coupled device inspection capability.

An inspection of the two welded test-pieces has been performed using three different membrane device transducer configurations. A proceduralised approach has been developed that has allowed experimental data to be gathered by a number of Rolls-Royce engineers. This approach has been adopted to accelerate the technology transfer process into Rolls-Royce and to rigorously assess the membrane device capability. The three different device configurations are complementary to one another and provide the optimum overall inspection coverage. By using this approach, coverage of the entire target application inspection volume, using each of

the primary and secondary defect detection techniques, can be achieved by carrying out six circumferential scans of the component. Completion of testing on the flat plate test-pieces demonstrates that all of the artificial defects embedded into the test-pieces can be detected by at least one inspection technique. FMC data acquisition is highly versatile and a single data set can be processed using a wide range of different inspection techniques. This allows the use of delay laws that are optimised for a given inspection. The results provided in this chapter demonstrate that these optimised delay laws provide an improved inspection performance in comparison to that achievable using delay laws to replicate conventional single element transducer inspection. The use of optimised delay laws provides an improvement in the SNR of the defect response in every inspection performed. However, in some cases the standard delay law inspection is already good and the level of improvement using optimised delay laws is limited. The use of ATFM provides a fully focused B-Scan image and reduces the overall amount of data processing required in comparison to completing multiple single focal depth processing steps. This approach will help to reduce the overall inspection time in industrial applications.

A theoretical study has been performed to assess the potential speed improvements associated with the membrane coupled device inspection. This study demonstrates that through the development of suitable software, currently available equipment can be used to reduce single element transducer inspection time of the target application component by over 60%. Improvement of the data acquisition and processing techniques would allow further reductions to be realised leading to a potential speed improvement of over 80% in comparison to conventional single element techniques.

7. Twin Crystal Membrane Coupled Device

Linear phased array probes offer a number of benefits over conventional single element transducers. These include inspection speed, and the ability to steer and focus the beam within a 2D region. However, in both single element and linear array transducers when the initial ultrasonic pulse impinges on the outer surface of the component under test a dead zone occurs. This dead-zone represents the region within the component under test where discontinuities cannot be reliably detected. The length of the dead zone can be reduced by selecting a high quality transducer with a short pulse duration and a suitable level of damping for the application (Krautkramer & Krautkramer, 1983). Another approach, often used within industrial NDE, is to use a transmit-receive longitudinal (TRL) or twin crystal transducer (Birks & Green, 1991).

The inspection of small lack of sidewall fusion defects and near surface defects within the flat plate non-welded and welded test-pieces has proved very difficult using the linear membrane coupled phased array device. In order to address this issue a twin crystal membrane coupled device has been designed and manufactured. In this chapter the use of twin crystal transducers is reviewed and the requirements of the twin crystal array inspection capability are briefly assessed. The design of the twin crystal membrane coupled device will then be discussed. Finally some preliminary results obtained using this device will be presented. The use of this type of membrane device was not originally envisaged at the start of this project and extensive testing and characterisation of the transducer has not yet been performed.

7.1. Twin Crystal Transducers

Twin crystal transducers use a separate transmitter and receiver that are positioned side by side in a single housing. A schematic diagram of a simple 0º longitudinal wave twin crystal probe is shown in Fig 7-1. This specific type of transducer is commonly used in industry for wall-thickness measurement (British Standards Institution, 2004b). The receiving element is unaffected by the ring down time associated with the transmitting element and near surface features can be detected. The transmit and receive elements are acoustically isolated from one another by introducing an absorbent material, such as cork between the two delay lines. Each

element is tilted at the "roof angle" of the transducer, this controls where the energy from the transmit and receive elements intersect. This beam crossing point provides a pseudo-focusing effect and the maximum sensitivity can be achieved at this point.

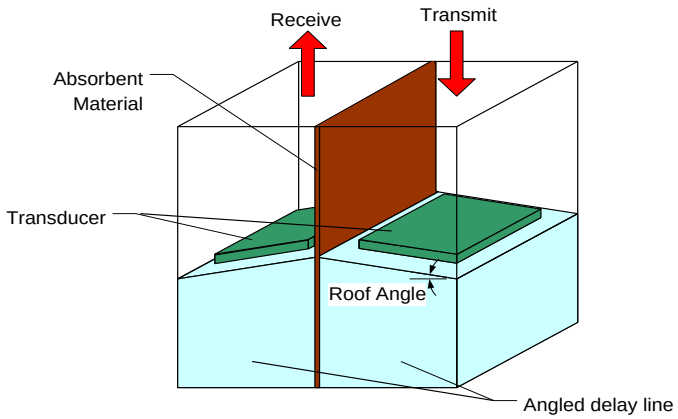

Figure 7-1. Schematic diagram of a single element 0º longitudinal wave twin crystal probe.

Angled twin crystal transducers can also be produced using both single elements and phased arrays. In this type of probe the angle of the ultrasonic energy produced is controlled by the tilt angle and the roof angle of the two transducers. A diagram of this type of transducer produced using the CIVA model is shown in Fig 7-2. Typically the roof angle and the tilt angle are fixed when the probe is manufactured and are the same for both the transmitter and the receiver. This type of probe design is more complex to manufacture and control than the simple linear transducers considered previously in this thesis.

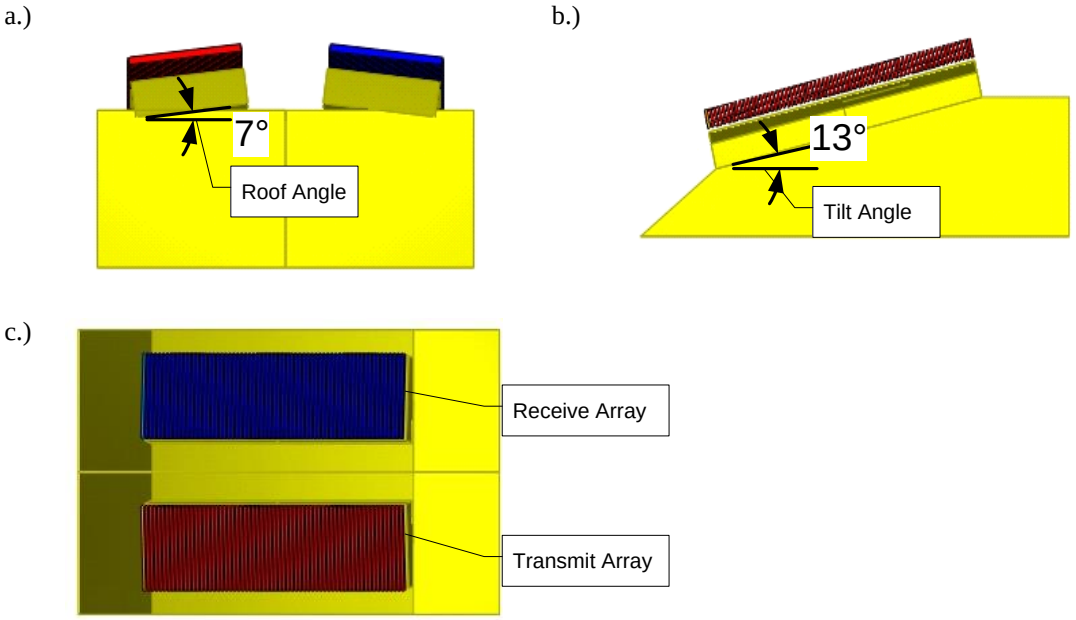

Figure 7-2. CIVA representation of an angled twin crystal array transducer a.) front view, b.) side view, and c.) plan view.

Angled twin crystal transducers have found application in industry, particularly for near surface and austenitic weld inspection. The use of twin single element transducers for near surface and through wall defect inspection is described by Edelmann (1981). This type of twin crystal transducer has been shown to provide SNR improvements in comparison to conventional single probe techniques (Dombret, 1991). Twin crystal single element and phased array transducers have been used to successfully detect SDH defects in austenitic stainless steel welds produced using different welding techniques (Dupond, 2006). Finally the use of CIVA to model twin crystal array inspection performance for coarse grained stainless steel components has been reported by Mahaut et al (2004).

7.2. Inspection Requirements

The membrane coupled phased array concept is very versatile and it is not limited to use with single linear arrays. A twin crystal linear phased array has been designed; specifically to address some of the limitations in the 3rd generation membrane coupled device inspection of the two flat plate welded test-pieces. The inspection results provided in chapter 6 demonstrate that the direct through weld inspection of the mid-wall lack of sidewall fusion defects was relatively poor. The use of a twin crystal

phased array is intended to improve the SNR performance in this type of inspection through austenitic weld material. Isolation of the transmitting array from the receiver array will also eliminate the issue of the beam spread internal noise signal within the membrane cavity.

The results in chapter 6 also demonstrate that the near surface defect inspection performance using the linear membrane approach is limited because it is not possible to generate an effective creep wave. Through suitable selection of the array tilt and roof angles, a twin crystal probe could also be used to generate this type of wave and improve the inspection of this type of defect. A twin crystal membrane device could therefore be used for the inspection of a range of defects within the target application and further improve the inspection capability associated with the conformable array approach.

The goal of this development work was to design a twin crystal transducer to provide satisfactory performance for the inspections detailed in Table 7-1. Only the defects that are currently being considered for detection with the twin crystal membrane coupled device have been included in Table 7-1. The eight defects within the flat plate, welded test-pieces that will be inspected have been discussed in detail in chapter 6, schematic diagrams of these defects are provided again in Fig 7-3. Only two different inspection techniques are currently being used in this inspection; direct through weld specular defect detection and the creep wave inspection technique. Details of these inspection techniques used are provided in section 6.2. The alternative inspections that were performed for the defects of interest will not be repeated with the twin crystal device. These alternative inspections are not included in Table 7-1 and are indicated by the grey shading.

Table 7-1 Inspection technique summary for the flat plate, welded test-pieces using the twin crystal membrane coupled phased array device. Grey shading indicates that additional inspection techniques are not deployed.

I.D.	Defect Type	Length (mm)	Through-wall size (mm)	Ligament to ID (mm)	Tilt Angle (˚)	Through Weld Inspection Techniques		Near Side Inspection Techniques	
						Primary	Secondary	Primary	Secondary
3	Lack of side wall fusion	6.3	4	24.5	25	65 Comp (Specular)	60 Comp (Specular)		
4	Lack of side wall fusion	6.3	4	28.5	10		70 Comp (Specular)		
5	Lack of side wall fusion	6.3	4	54	-10		OD Creep Wave		
6	Mid-weld planar	6.3	4	54	0		OD Creep Wave	Mid-weld defect – symmetrical detection techniques	
10	Lack of side wall fusion	12.6	8	20.5	25	65 Comp (Specular)	60 Comp (Specular)		-
11	Lack of side wall fusion	12.6	8	28.5	10		70 Comp (Specular)		
12	Lack of side wall fusion	12.6	8	50	-10		OD Creep Wave		
13	Mid-weld planar	12.6	8	50	0		OD Creep Wave	Mid-weld defect – symmetrical detection techniques	

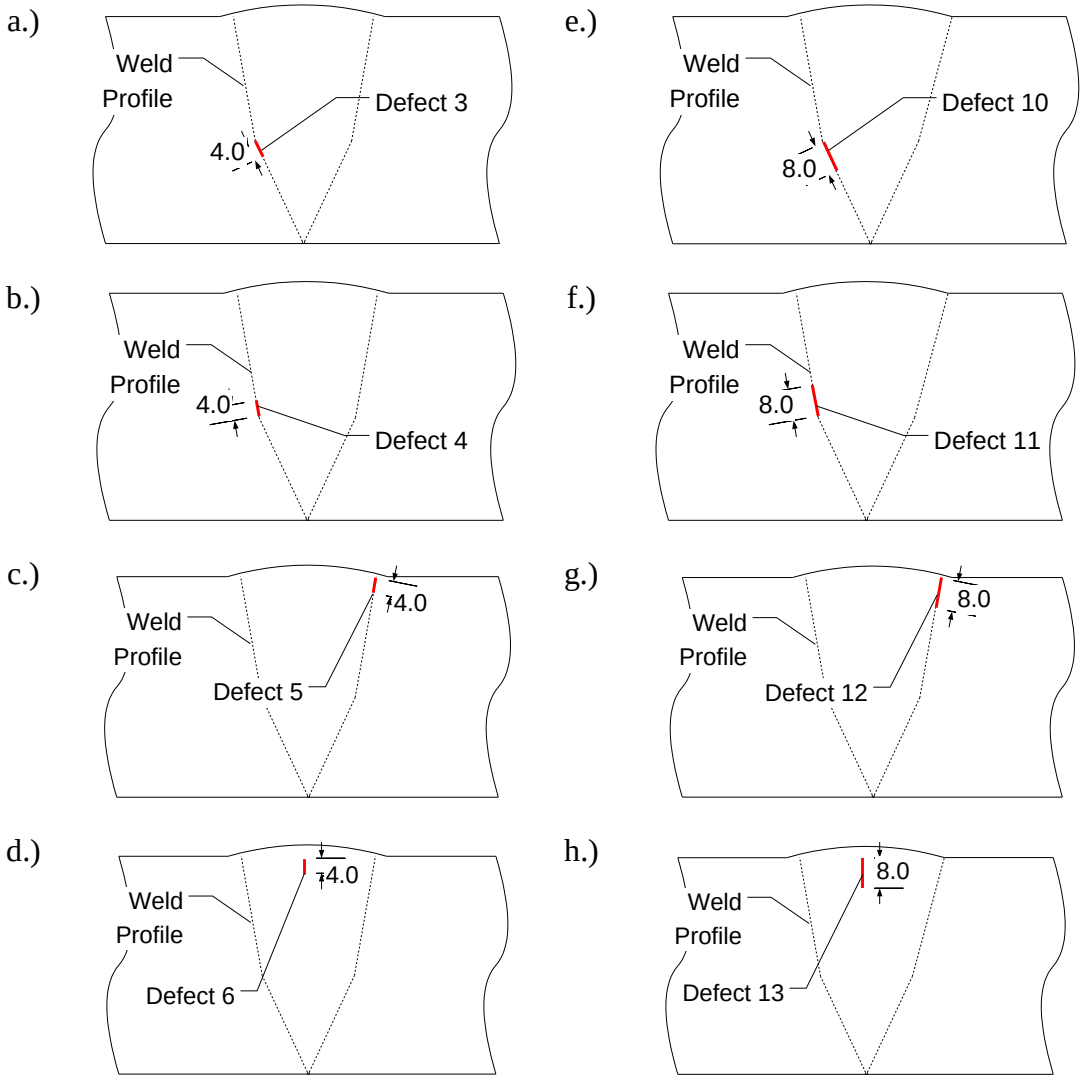

Figure 7-3 Schematic diagram of defects considered as part of the twin crystal membrane coupled phased array development activity , a.) defect 3, b.) defect 4, c.) defect 5, d.) defect 6, e.) defect 10, f.) defect 11, g.) defect 12, h.) defect 13.

7.3. Twin Crystal Membrane Coupled Device Design

The refraction angle of the ultrasonic energy produced by a conventional dual element twin crystal transducer is dictated by the tilt angle and also the roof angle of the wedge. However, in a phased array twin crystal transducer the refraction angle of the wave produced can also be varied by suitable control of delay laws. The roof angle of the twin crystal transducer controls the depth of the beam crossing point. This beam crossing provides a pseudo-focusing effect and the maximum sensitivity of the device corresponds to the point at which the two beams intersect. The sensitivity of this type of transducer decreases at depths less than and greater than the beam crossing point. Typically the performance of a twin crystal transducer is considered acceptable

between half and twice the beam crossing depth (Krautkramer & Krautkramer, 1983). The target application component has a relatively thick wall and it is clear from Table 7-1 that there is a large difference between the depth of the lack of sidewall fusion defects and the near surface defects. It is therefore not possible to design a single, fixed roof angle, twin crystal array that provides satisfactory complete through-thickness inspection performance.

There are a number of ways in which it is possible to effectively produce a variable roof angle twin crystal transducer. By using this approach a single transducer can be used to produce a range of refraction angle beams and different beam crossing points. One option to achieve this is to use a full 2D matrix transducer. A 2D matrix transducer uses a regular grid of elements which provides control of the ultrasonic beam within the 3D volume and hence a great deal of inspection flexibility. I lead a collaborative project between Rolls-Royce and University of Strathclyde to produce a flexible 2D matrix phased array (Harvey et al, 2009). This work is beyond the scope of my thesis and will not be discussed in detail here but the development of this device is focused on a different application where 2D conformability is required.

An alternative is to mount two 1.5D arrays onto a fixed angle wedge (Maes & Richard, 2008; Delaide & Dumas, 2005). A 1.5D array typically uses rectangular elements as shown in the schematic diagram produced using CIVA in Fig 7-4. The dimensions provided in Fig 7-4 provide an indication of the size of this type of transducer; however, the exact dimensions would be dependent upon the inspection application. The front and side elevations of this type of transducer are essentially identical to the standard twin crystal array transducer, shown in the schematic diagram in Fig 7-2. Therefore only the plan view of the 1.5D twin crystal array transducer is included in Fig 7-4. In this type of transducer a small fixed roof angle is typically used (Maes & Richard, 2008; Delaide & Dumas, 2005) to provide some mechanical control of the beam crossing point. The element delay laws are then controlled to further modify the beam crossing point and to change the refraction angle of the ultrasonic wave. The use of rectangular elements provides limited control of the effective roof angle but greater control of the tilt angle whilst maintaining the amount of ultrasonic energy that can be produced by the transducer. As discussed in chapters 2 and 5 in order to maintain the required steering capability and limit the production

of secondary maxima the element pitch used within the array must be relatively small. Defects can typically exist over a range of different tilt angles the ability to steer and focus the beam through-out the entire wall thickness of the component is therefore essential. Hence a large number of small elements is required to provide the necessary level of control. However, acceptable inspection performance can be achieved by using only a limited number of different beam crossing points. Therefore the roof angle must only be varied over a relatively small range of angles and only limited control of the beam in this direction is required. This allows a smaller number of relatively large, directional, elements to be used. Therefore the use of rectangular elements provides the best compromise in terms of overall array performance.

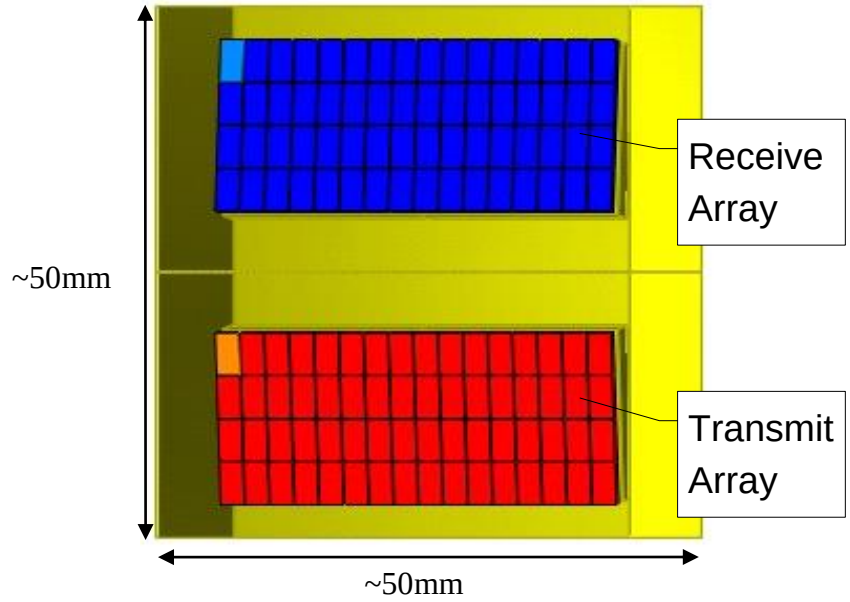

Figure 7-4 Plan view of the CIVA representation of a 1.5D phased arrays to generate a variable roof angle twin crystal transducer.

The fundamental issue with 2D matrix transducers and 1.5D twin crystal transducers that reduce their applicability to the target application inspection is that the overall size of the transducer is significantly reduced. This increases the amount of axial mechanical scanning that is required and increases inspection time. It also reduces the near field length of the transducer and limits the focal range. The results provided in chapter 6 demonstrate that the use of focusing is essential for optimum defect detection in the target application. The use of a small number of fixed roof angle

transducers optimized for through thickness beam steering and focusing is therefore necessary in the target application.

When using a twin crystal phased array the energy generated by each element within the array strikes the component outer surface at a compound angle. The propagation angle of the ultrasonic wave in the component under test is therefore more complex than in a simple linear array. The required tilt and roof angles of the two arrays for the detection of both the lack of sidewall fusion defects and the surface breaking defects have therefore been modelled using release 9.1 of the CIVA simulation package. This version of the CIVA platform does not accurately simulate creep wave propagation; it does however provide a notification if any of the beams produced by the array are approaching a critical angle. The accuracy of the CIVA model is therefore not guaranteed and caution must be exercised when using CIVA as a design tool for this type of application.

The Peak NDT MicroPulse 5PA phased array controller unit used in this development activity has 128 parallel data channels. Therefore the twin crystal design is limited to a maximum of 128 elements and simulation of two 64 element linear arrays was performed. The array element pitch and width used in the 3rd generation linear membrane device design has previously proved very successful and has once again been used in the design of the twin crystal device. Design of the twin crystal membrane coupled device was also performed in close collaboration with Lionel Reyes (Rolls-Royce, Senior Design Engineer) to ensure that the proposed twin crystal design could be manufactured.

When completing the design of the twin crystal, membrane coupled device a number of physical parameters describing the proposed transducer geometry were input into CIVA. The CIVA model was then used to understand the effect of changing these parameters on the resulting beam angle and the beam crossing point. This calculation is performed at a single emission point from the centre of the array. The exact beam characteristics will vary depending on the array aperture used because of the variable water path.

A CIVA screen capture is provided in Fig 7-5 showing the essential parameters that must be controlled to design the twin crystal membrane coupled device when using the CIVA modeling tool. These essential parameters are defined in Table 7-2 and where appropriate the values used within the CIVA simulation are provided. During the design phase the front and back length and the width (L1, L2 and L3 in Fig 7-5) of the transducer were set to relatively large values to ensure that no internal reflections would occur from either end of the transducer cavity. In addition the height of the transducer (L4) was fixed to ensure that the ride-height could be suitably controlled to allow the membrane device to conform to the weld cap geometry and that the device could be manufactured.

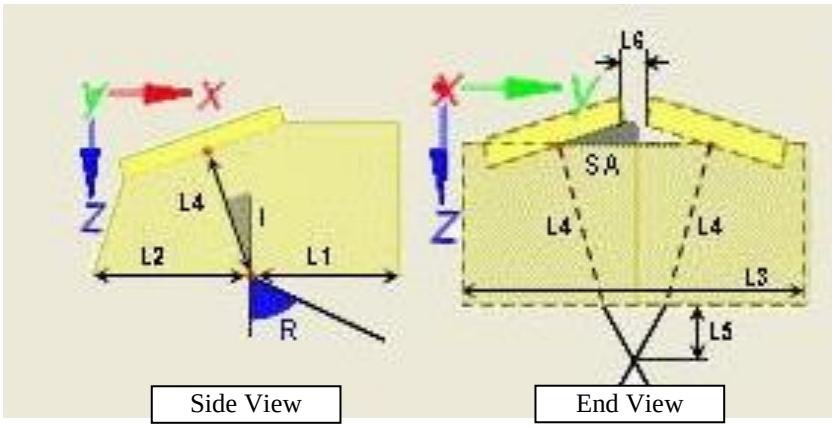

Figure 7-5 CIVA screen capture showing the essential parameters used to design the twin crystal membrane coupled device.

As discussed in section 7.1 the transmit and receive arrays must be physically separated using a high loss acoustic barrier. This design constraint limits the minimum separation (L6, in Fig 7-5) that can be achieved between the two arrays. I proposed to again use the AptFlex F28 attenuative rubber (Precision Acoustics Ltd) which was used in the 3rd generation device and was discussed in chapter 5. The twin crystal membrane device design was therefore performed to allow a 10mm thick piece of the rubber to be inserted between the transmit and receive arrays to minimise noise. To maintain manufacturability and allow this rubber material to be inserted between the arrays a fixed separation distance must be maintained. The distance between the centreline of the transmitting array and the centreline of the receiving array is controlled to be approximately 35mm, which corresponds to a value of 20mm for L6 within the CIVA model. The roof and tilt angles of the twin crystal transducer design

were then varied within the modelling environment to determine the different refraction angles and beam crossing points that could be produced.

Table 7-2 Definition of the essential parameters that must be controlled when using CIVA.

Parameter	Description	Value
L1	Front length – distance from array index point to front of the probe housing.	40mm
L2	Back length – distance from array index point to back of the probe housing.	40mm
L3	Width of probe – overall width of probe housing.	60mm
L4	Array height – perpendicular distance from the centre of the array to the outer surface of the component under test.	16mm
L5	Beam crossing depth – Vertical distance between the base of the probe and the beam crossing point.	Variable
L6	Minimum separation - distance between the transmit and receive arrays.	20mm*
R	Refraction angle – The beam angle produced by the probe.	Variable

Note

* Corresponds to a centre-to-centre separation of 35mm

As discussed in section 7.2, at this stage in the development of the twin crystal device two main designs are required to implement the two different inspection techniques being considered. The first probe design is for the detection of mid-wall, lack of sidewall fusion defects. The second design must be suitable for the creep wave detection of near surface defects. The inspection requirements listed in Table 7-1 show that a 60º longitudinal wave is the lowest angle beam that is required to complete both of these inspections. When considering a simple linear array, a water wedge tilt angle of 13º gives a refraction angle in steel of approximately 61º. This tilt angle was also successfully used in the 2nd generation membrane coupled device

described in chapter 2. Therefore a twin crystal membrane coupled device with a fixed tilt angle of 13º was designed.

Ultrasound produced by the transmitting array in the twin crystal probe impinges on the outer surface of the component under test at a compound angle. The effect of the tilt angle can be somewhat compensated for by suitable control of the delay laws, and hence a single tilt angle can be accommodated. However, the refraction angle of the longitudinal wave produced and the depth of the beam crossing point is very sensitive to small changes in the roof angle and this cannot be readily compensated for by varying the delay laws. The roof angle of the membrane coupled device must therefore be carefully controlled. An iterative approach was used to find the best roof angle for the inspection of each type of defect listed in Table 7-1. The most appropriate roof angle for the direct specular through weld inspection of the lack of side wall fusion defects is 4º. The ultrasonic beam produced from a 4º roof angle twin crystal membrane coupled device simulated in CIVA using null delay laws is provided in Fig 7-6a. The beam plot shown is calculated on a 2D plane along the centreline of the twin crystal device. The most appropriate roof angle for the generation of a creep wave for the inspection of the outer surface defects in the flat plate, welded test-pieces is slightly more complex. As previously discussed the version of CIVA being used to assist in the design of the twin crystal membrane coupled device does not accurately predict creep wave behaviour. The performance of the CIVA model in prediction of behaviour around the first critical angle is potentially limited. As the roof angle is increased it was found that near the first critical angle the predicted beam behaviour changed very rapidly. Therefore two different roof angles were predicted to be potentially appropriate; 7º and 7.5º. A CIVA beam plot using null delay laws for both roof angles is provided in Figure 7-6. Once again the beam plot is provided along the centreline of the twin crystal membrane coupled device. Experimental validation is required to assess which of these two designs is most appropriate for the inspection of the outer surface defects in the flat plate, welded test-pieces.

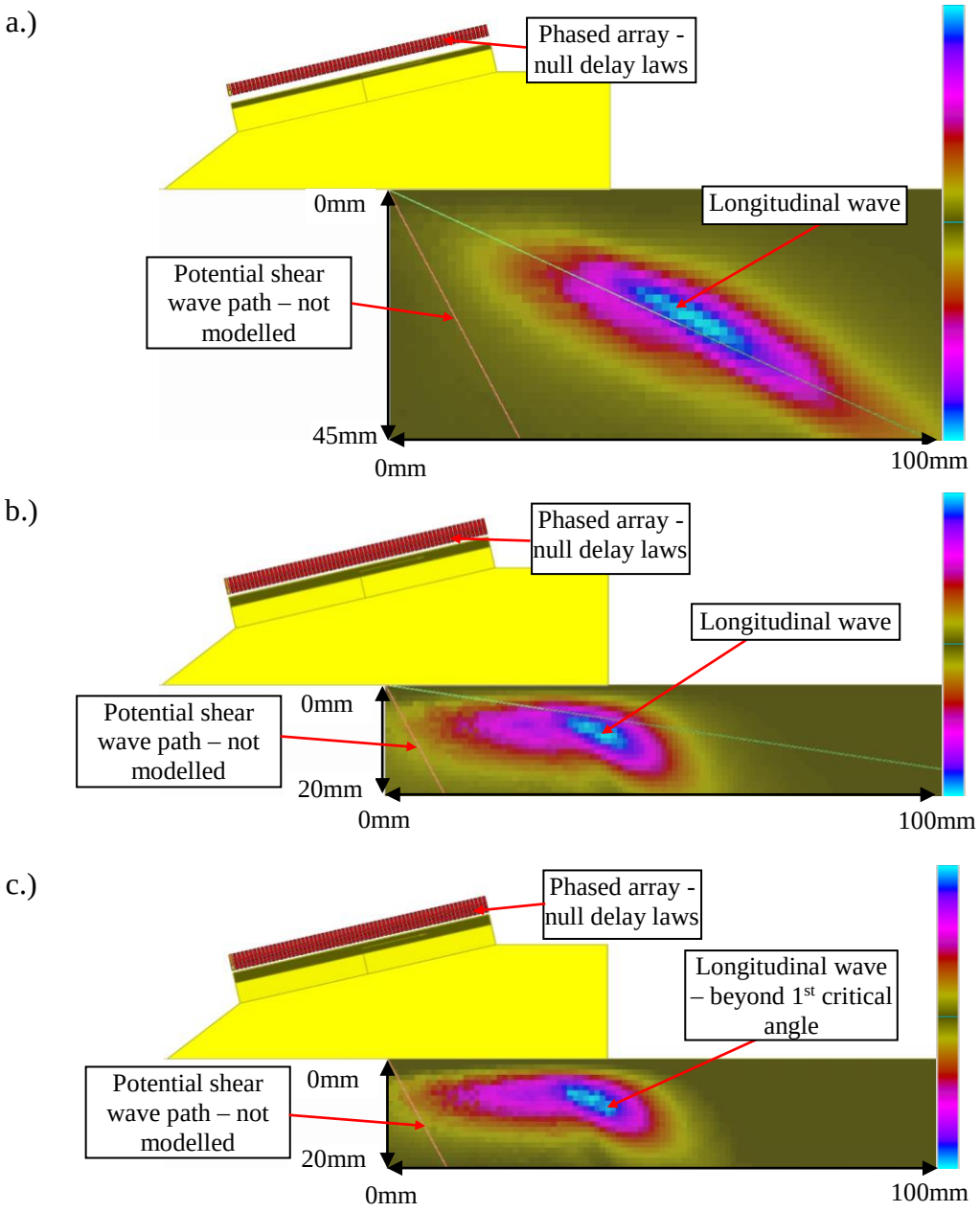

Figure 7-6 CIVA simulation of the beam produced using null delay laws by a 13º tilt angle twin crystal membrane coupled phased array device with a.) 4º roof angle, b.) 7º roof angle, c.) 7.5º roof angle. All images are shown over a 60dB range.

A comparison of angle of the refracted beam and the beam crossing point for twin crystal membrane coupled device predicted by CIVA with the three different roof angles considered is provided in Table 7-1. The results provided in Figure 7-6 and in Table 7-1 demonstrate that a twin crystal device with a 13º tilt angle can be used to generate the required beam angles and crossing points. The results provided correspond to the natural angle of the resultant beam in steel using the entire array

aperture. It may be possible to further optimise the performance of the twin crystal membrane device through the use of variable apertures and delay laws.

Table 7-3 Comparison of the longitudinal wave refraction angle and beam crossing point that can be produced using the twin crystal membrane coupled device design with the use of delay laws.

Roof Angle (º)	Longitudinal Wave Refraction Angle in Steel (º)	Beam Crossing Depth in steel (mm)
4.0	65	25
7.0	80	5
7.5	90	0

To improve the likelihood of producing a twin crystal membrane device that can be used to successfully produce a suitable beam angle, a variable angle design has been adopted. The three different transducer configurations can therefore be generated using a single array housing. A photograph of the twin crystal membrane device, showing the variable roof angle is provided in Fig 7-7. The twin crystal membrane coupled device has a non-parallel top surface; the roof angle can be altered with the angle adjustment bolt, labelled in Fig 7-7. Once a suitable roof angle has been selected the array is secured in place using the roof angle fixing bolt. This process is repeated for each of the two arrays independently, care must be taken to ensure that the final array configuration is symmetrical. The tilt angle of the device is fixed at 13º but the roof angle can be varied to control the actual beam angle produced. The design ensures that the emission point of the transmit array relative to the receiving array is fixed and that the roof angle can be varied between approximately 3º and 9º. Schematic diagrams of the 4º and 7º roof angle twin crystal membrane coupled devices are provided in Fig 7-8

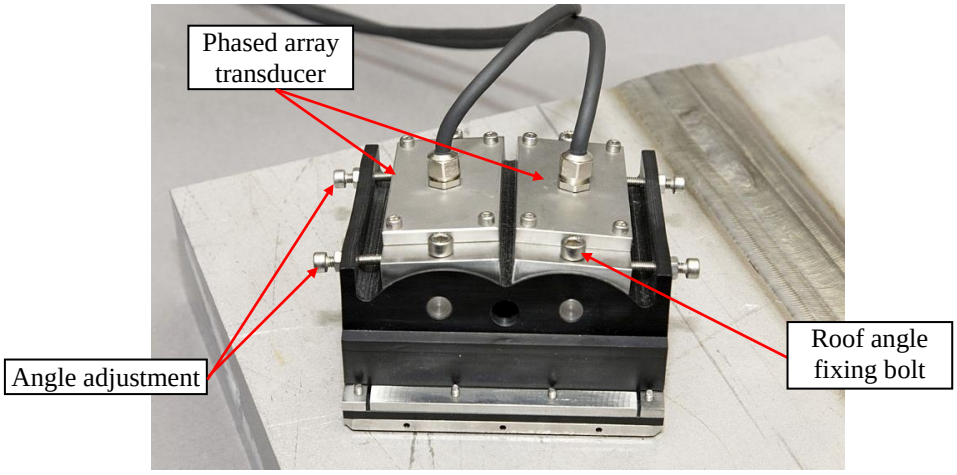

Figure 7-7 A photograph of the 4º roof angle configuration of the twin crystal membrane coupled device

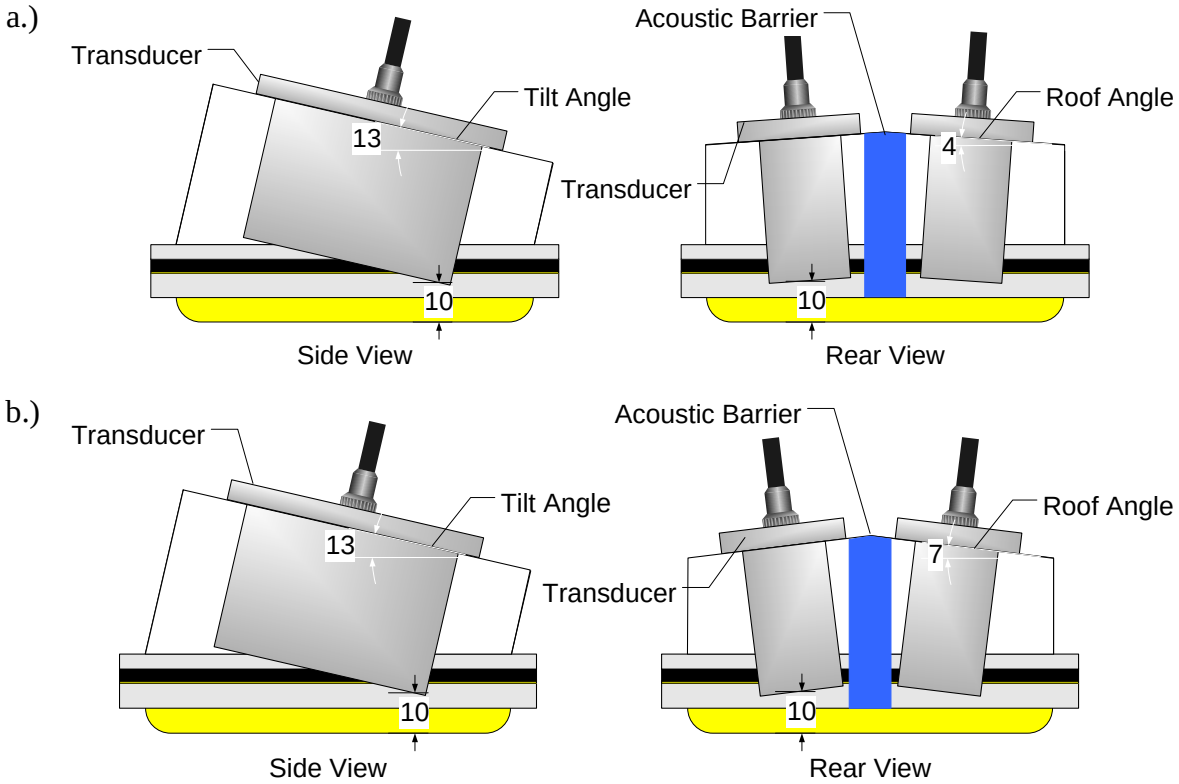

Figure 7-8 The twin crystal membrane coupled device a.) Schematic diagram of the 4º roof angle configuration, b.) Schematic diagram of the 7º roof angle configuration.

There is a potential crosstalk noise path within the twin crystal membrane coupled device. Ideally the AptFlex F28 absorbent rubber, which is used as an acoustic barrier to isolate the transmit and receive arrays, would be in contact with the outer surface of the component under test. The rear view of the both the 4º and 7º twin crystal membrane coupled devices provided in Fig 7-8 show that this is not the case. The

AptFlex F28 rubber is relatively rigid and it is not possible to use this material as an acoustic barrier and maintain conformability. The experimental results provided in section 7.5 indicate that this does lead to the presence of some background noise. However, through suitable control of the set-up parameters used this noise can be kept to an acceptable level. It may also be possible to alter the acoustic barrier material in future design iterations to reduce the level of this noise still further.

7.4. Inspection Deployment

When using the twin crystal membrane device it will still be necessary to update the delay laws used when scanning over components with complex surface geometries. Long and Cawley (2006) demonstrated that if the surface profile is known to ±0.25 mm the largest predicted loss in SNR is 3dB. The twin crystal membrane device is designed to minimise cross-talk between the transmit and receive arrays. Therefore it is not possible to measure the surface profile of the component under test by firing the transmitter and monitoring the response on the receiver. When using the twin crystal membrane coupled device with a low roof angle it is possible to use a single array in both transmission and reception; this is shown in the schematic diagram provided in Fig 7-9. When using the twin crystal device to measure the surface profile, measurements must be performed using both arrays individually to accurately map the surface profile for each inspection position. However, as the roof angle is increased less of the energy produced by the each individual array can be detected using the same array and an alternative approach is required. As discussed in section 6.4 it is possible to accurately map the surface profile of the component under test using the 3rd generation linear membrane coupled device. When using the 3rd generation device a proceduralised approach is used so that the first scan is performed with the membrane device directly over the weld cap surface. This information is subsequently used to update the inspection delay laws on later scans. The surface profile information gathered using the linear membrane coupled device can also be used to update the delay laws during the twin crystal membrane coupled device inspection. When using this approach it is once again essential that the position of the transducer is accurately known so that the correct surface profile information is used. Sufficiently accurate positioning of the transducer is readily achievable when using automated inspection techniques.

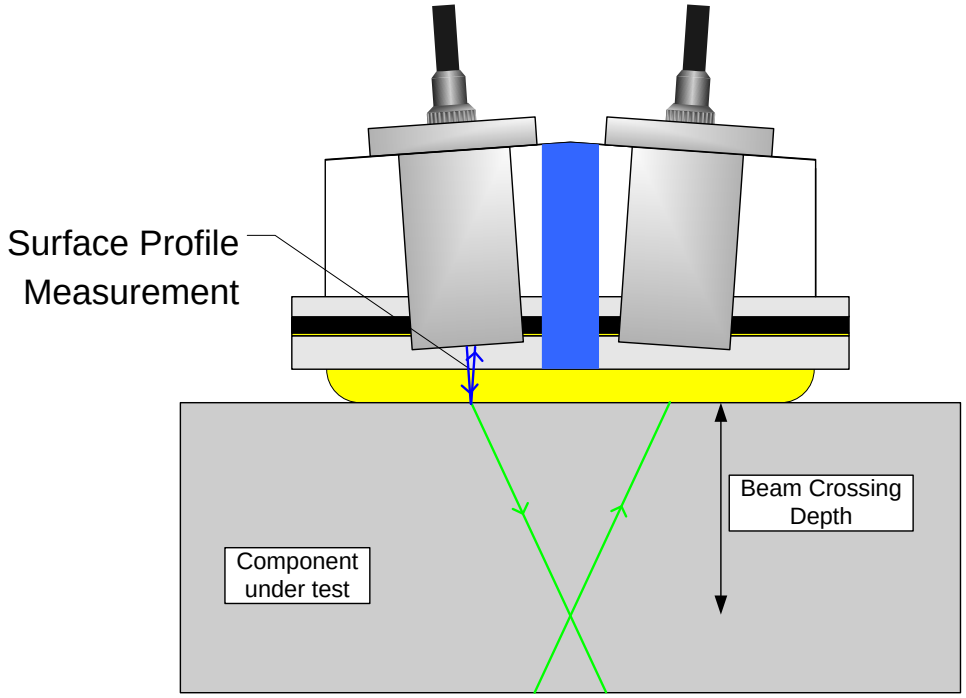

Figure 7-9 Schematic diagram of the surface profile measurement using the twin crystal membrane coupled device.

The twin crystal membrane device once again incorporates an integrated irrigation system. When designing the transducer housing the goal was to remove the tubes taking the irrigation feed and injecting coupling between the membrane and the component under test. The tubes used in the third generation device design are relatively long. There is a risk that these tubes could become caught and obstruct the movement of the membrane probe during scanning or become dislodged leading to a loss of couplant. The intention with the twin crystal design was to introduce irrigation channels into each side of the membrane housing and deliver couplant through the housing itself. This design is entirely possible but unfortunately due to the scanning frame design it was not possible to design the required irrigation channels in a cost effective way for manufacture of the prototype twin crystal device. The same irrigation system implemented on the 3rd generation device has therefore once again been used in the twin crystal transducer.

The height and angle of the twin crystal membrane coupled device is also once again controlled in the same way as that adopted with the 2nd and 3rd generation membrane coupled devices. The approach used is discussed in greater detail in section 3.3. In order to accommodate the larger footprint twin crystal device into the scanning frame

jig, it was necessary to complete some mechanical changes. These were performed with the assistance of Lionel Reyes (Rolls-Royce, Senior Design Engineer) and are shown in Fig 7-10. As with the 3rd generation device the twin crystal probe contains 128 elements, the 48 element rigid wedge transducer is used to control the ride height and angle of the array only and it is not electrically connected to the MicroPulse 5PA. The ride height of the array is controlled so that base of the picture frame on the array is approximately 6mm above the parent plate material using the procedure discussed in chapter 6.

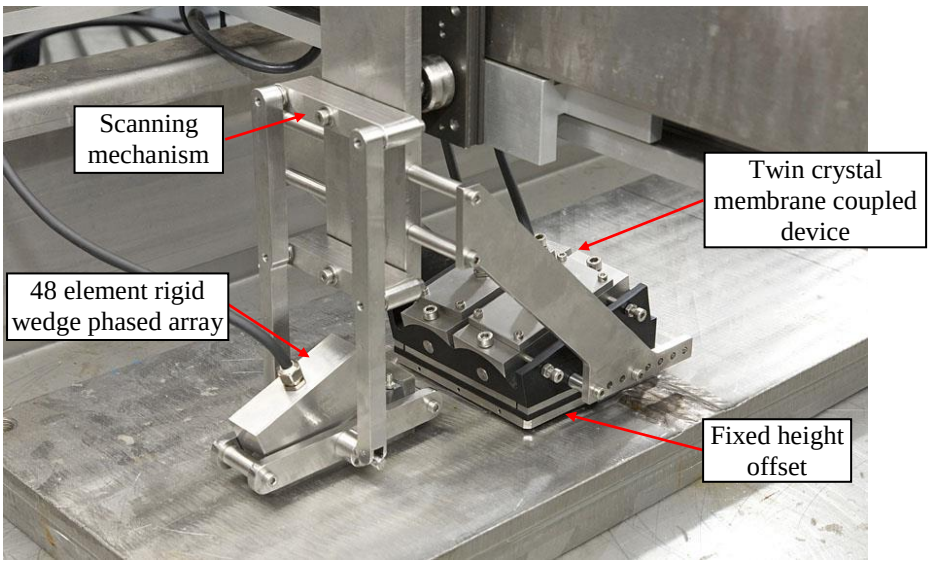

Figure 7-10 Photograph of the twin crystal membrane coupled device and the 48 element rigid wedge linear phased array.

7.5. Twin Crystal Membrane Device Experimental Results

The twin crystal membrane coupled device has initially been designed specifically for the inspection of a limited range of defects within the target application component. The defects and the inspection techniques to be considered are provided in Table 7-1. The use of all of the inspection techniques implemented with the 3rd generation membrane coupled device is therefore not required at this stage in the development of the twin crystal membrane device.

The development of the twin crystal device is still ongoing and limited experimental testing has been performed. The experimental testing performed at this time has focused on the through weld inspection of defects 3 and 10 using the direct specular technique with the roof angle of the transducer set to approximately 4º. A schematic

diagram of the inspection configuration used is provided in Fig 7-11, the same configuration is adopted in the inspection of both defects. Inspection of each defect is performed from a single location with the transducer positioned as shown in Fig 7-11 and approximately in line with the centre of the defect.

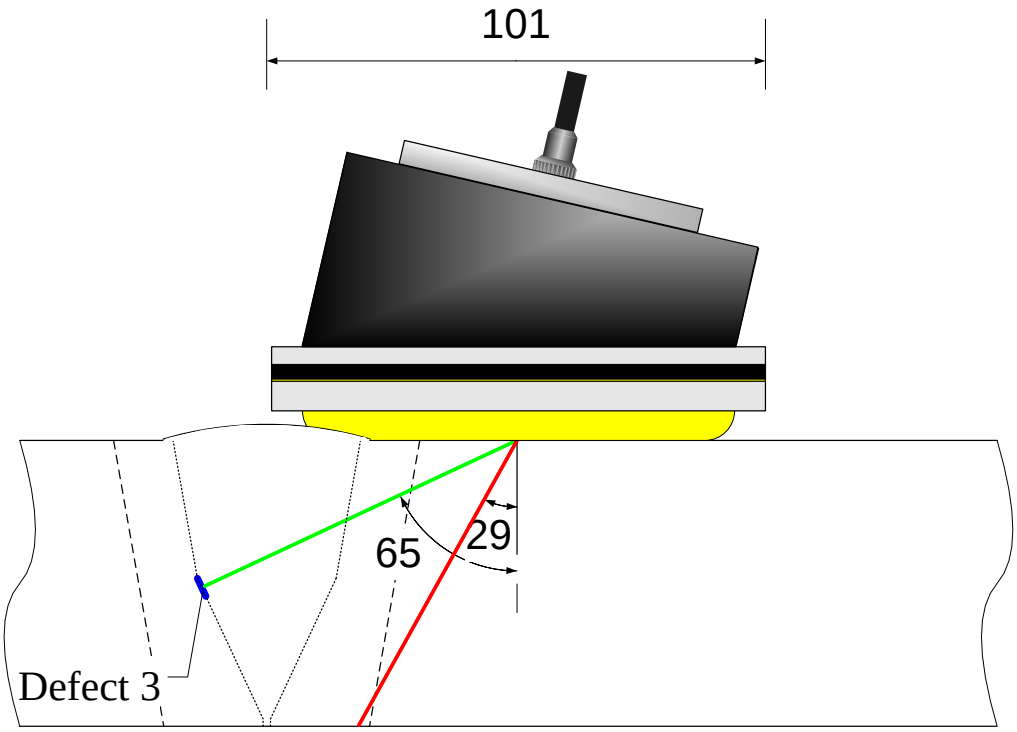

Figure 7-11 Schematic diagram of the experimental set-up used for the direct specular through weld detection of defect 3.

In order to process the FMC data acquired using the twin crystal device the Imperial College post processing software suite has been updated. I have worked with Dr Rob Long at Imperial College to implement these changes. I have determined the required techniques and Dr Long has been responsible for implementing these changes in the software. I have then performed some preliminary validation of these updates based on the experimental data acquired.

When using the configuration shown in Fig 7-11 it is possible to reliably detect defect 10 using the twin crystal membrane coupled device. The B-Scan image obtained from the direct specular 65º longitudinal wave inspection of defect 10 using the twin crystal device is shown in Fig 7-12(a). The inspection of defect 10 using the 18º, 20mm configuration of the 3rd generation linear membrane coupled device is

provided in Fig 7-12(b). The B-Scans provided in Fig 7-12 have been generated using an aperture of 17 elements (12.5mm) with unfocused delay laws. The result provided in Fig 7-12(a) using the twin crystal membrane device is very encouraging. The internal noise signal that is clearly evident in Fig 7-12(b) and which limits the performance of the linear membrane coupled device has been eliminated. A low amplitude ultrasonic cross-talk signal is observed but as discussed in section 7.3 the source of this noise is understood and can be reduced further by using a more appropriate acoustic barrier material to isolate the two arrays. The SNR of the defect response using the twin crystal device with unfocused delay laws is approximately 11dB which is comparable to the 10dB SNR obtained using the linear membrane coupled device. This indicates that the SNR performance of the two different approaches is very similar. However, the B-Scan obtained using the 3rd generation linear device, which is shown in Fig 7-12(b), has to be plotted on a different dynamic range because the internal noise signal appears at a higher amplitude than the defect signal.

a.)

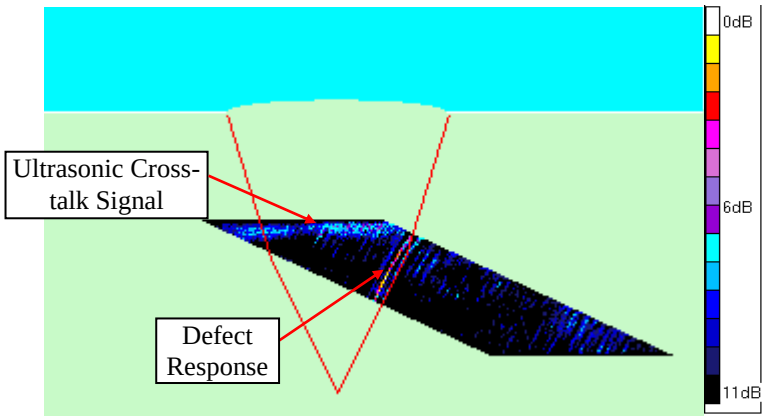

b.)

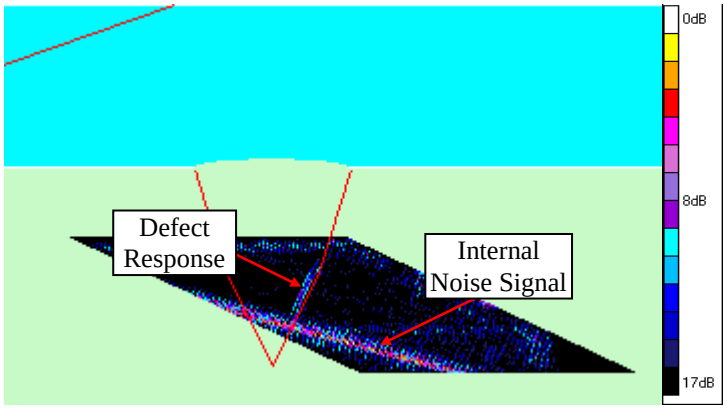

Figure 7-12 Comparison of the 65º longitudinal wave B-Scan images obtained using a 17element aperture with unfocused delay laws for the inspection of defect 10 through the weld using a.) the twin crystal membrane coupled device and b.) the 18mm, 20º 3rd generation linear membrane coupled device.

A complete comparison of the inspection performance for the through weld inspection of defects 3 and 10 using the 3rd generation 18º, 20mm linear membrane coupled device and the twin crystal membrane device is provided in Table 7-4. All of the results in Table 7-4 have been produced using an aperture size of 17 elements (corresponding to 12.5mm) and unfocused delay laws. The 3rd generation linear membrane coupled device results are highlighted using yellow shading and the twin crystal device results are shaded blue. The SNR performance of the 3rd generation device has been calculated by ignoring the effect of the internal noise signal. Even when this noise is ignored the twin crystal device provides some improvement in defect SNR. However, despite the removal of the internal noise signal it is still not possible to detect defect 3 through the austenitic weld using a small aperture with unfocused delay laws.

Table 7-4 A comparison of the inspection performance for the direct specular through weld inspection of defects 3 and 10 using the 3rd generation linear membrane device (yellow shading) and the twin crystal membrane device (blue shading). All inspections are performed using an aperture of 17 elements and unfocused delay laws. Defects that are not detected are indicated by no value for the SNR.

Defect	Array	Aperture size (elements)	Beam Type	Primary / Secondary Technique	Inspection Performance SNR (dB)
3	20mm, 18º	17	65º, Long	Primary	-
3	20mm, 18º	17	60º, Long	Secondary	-
3	Twin Crystal	17	65º, Long	Primary	-
3	Twin Crystal	17	60º, Long	Secondary	-
10	20mm, 18º	17	65º, Long	Primary	10*
10	20mm, 18º	17	60º, Long	Secondary	9*
10	Twin Crystal	17	65º, Long	Primary	11
10	Twin Crystal	17	60º, Long	Secondary	10

Note

* SNR performance of the 3rd generation linear device is calculated by ignoring the presence of the internal noise signal

As discussed in chapter 6, when completing the direct specular through weld inspection of defects 3 and 10 using optimised delay laws with the 3rd generation device an aperture size of 38 elements was used. Unfortunately due to the relatively short length of the twin crystal device it is not possible to duplicate this approach from

a single transducer location. In order to use a large aperture size and focused delay laws the twin crystal membrane coupled device would need to be scanned along the outer surface of the component under test. As discussed previously it is currently not possible to acquire scanned FMC data. This is a limitation of the current FMC inspection process and is being addressed through the development of a bespoke software suite within Rolls-Royce. However, this software suite is still under development and is beyond the scope of my doctorate. It is likely that when scanned inspection data can be acquired and suitably processed, that the twin crystal device can be used to provide further improvements to the through weld inspection performance. The performance of the twin crystal, membrane coupled device is very promising. The removal of the internal noise signal is a significant improvement and demonstrates the potential benefits of this approach.

7.6. Summary

The 3rd generation linear membrane coupled phased array device has been successfully used to detect a wide range of defects within the flat plate, welded test-pieces. However, the 3rd generation device design is not well suited to the through weld inspection of small lack of side wall fusion defects and the creep wave inspection of outer surface defects. The reliable detection of both of these types of defect is essential in the target application component and this provided the motivation for developing a twin crystal membrane coupled device. Rigid wedge single element and array twin crystal transducers have been successfully deployed within industry to detect this type of defect and the twin crystal membrane device is based on these standard transducers.

The CIVA modelling platform has been used to assess the most appropriate array tilt and roof angles to provide the required beam angles and beam crossing points. Based on this modelling, a twin crystal membrane coupled phased array has been designed with a fixed tilt angle of 13º and a variable roof angle. This design allows a single transducer housing to be used during the device development phase and to detect both defect types of interest. The initial focus for this development activity is to develop an improved through weld inspection capability for small lack of sidewall fusion defects.

A twin crystal membrane configuration using a roof angle of approximately 4º has been produced and shown to be capable of successfully detecting defect 10 through the weld within the flat plate welded test-pieces. The twin crystal membrane device eliminates the internal noise signal that limits the performance of the linear membrane coupled devices and provides an improved inspection capability. However, the acquisition of scanned inspection data is essential to allow the full potential of this inspection technology to be realised. Some further development work is also required to investigate the ability of the twin crystal transducer to generate a creep wave and to assess the performance of the device in the inspection of outer surface breaking defects.

8. Conclusions

The work presented in this thesis has reviewed a range of advanced ultrasonic NDE inspection techniques, discussed developments of each of these techniques and reviewed the framework for introducing these new technologies into the industrial environment.

In the concluding chapter of this thesis a brief summary of the research performed and the results obtained is provided. The main contributions of this work are then reviewed and the impact of this work on NDE within Rolls-Royce is discussed. Finally some suggested areas of future work are summarised.

8.1. Review of Thesis

In Chapter 1 I have outlined the structure of the EngD in NDE scheme. I have then introduced the industrial environment in which I have performed the research presented in this thesis and described the main motivations and objectives of this research and development activity. I have also discussed the project environment within Rolls-Royce and my role within this project. During the course of my EngD studies I have also taken on a range of additional responsibilities within Rolls-Royce beyond the scope of my studies. Although this work has not contributed to my research project it has helped to provide a thorough education in NDE and a solid foundation for a career in industry.

The basic principles and applications of conventional ultrasonic inspection are introduced in Chapter 2. Different types of ultrasonic phased arrays are then discussed and the benefits of this type of inspection such as improved speed and versatility are reviewed. One of the main motivations for this research is to improve the ultrasonic inspection of components with irregular surface geometry. Inspection of this type of component causes a number of specific challenges which currently limit the use of ultrasonic techniques on this type of component. This is a particular issue within the nuclear industry and it is a problem that Rolls-Royce has addressed by sponsoring this project. In many current inspections the component surface is machined during manufacture, however, this is expensive and time-consuming; it can lead to excessive wall thinning and can expose additional defects of concern. It is

therefore desirable to eliminate this machining process. Also in this chapter an array from the CEA is reviewed and evaluated. The first generation membrane coupled phased array device, developed by Dr Rob Long and Prof Peter Cawley at Imperial College is then discussed. The membrane coupled phased array device is designed to use FMC data acquisition techniques to measure the surface profile of the component under test. This measurement is then used to update delay laws and improve the performance of the inspection. Finally the basic design of the second generation membrane device, which was the first device with significant input from me and Rolls-Royce engineers, is introduced.

Chapter 3 discusses the early work performed to transfer the membrane coupled device technology from academia to Rolls-Royce. In order to continue the development of the membrane device approach and to make this research industrially relevant to Rolls-Royce, a thick-walled stainless steel section of pipe-work containing an austenitic weld was identified as a suitable target application. All further improvement of the membrane device has then focused on the development of techniques to thoroughly inspect this component. The first phase in this development process was to design two flat plate, non-welded test-pieces. An inspection procedure using the membrane coupled device with FMC data acquisition was then developed. The performance of the 2nd generation membrane device was assessed by comparing the inspection results obtained using the array and conventional rigid wedge transducers. This study demonstrates that the membrane probe was capable of providing complete inspection coverage from a limited number of scan positions. The membrane device could be used to detect all defects within the test-pieces, whereas the conventional techniques could only reliably detect four of the six defects.

Modelling is a key part of the inspection development and qualification process, it can be used to provide valuable insight into the performance of an inspection technique and aids the data interpretation process. Different modelling techniques have been used to support the further development of the membrane device and FMC based inspection. The basic modelling tools used in this research are introduced in Chapter 4. The CIVA modelling platform has been extensively used throughout this project to design and evaluate array configurations as well as to assist in inspection development. The appropriateness of CIVA to each of these applications is assessed.

The early part of my doctorate focussed on the development of FE modelling techniques for the inspection of large components with irregular geometry. The use of FE models and particularly absorbing boundaries to improve the efficiency of these models are then discussed. CIVA models and FE models were also generated for the inspection of each of the six defects. This work demonstrated the accuracy of both modelling approaches and provided an improved understanding of the detection mechanism.

Although the 2nd generation membrane device was capable of detecting all of the six defects within the flat plate, non-welded test-pieces there were some limitations to the performance of the device. In particular a strong internal noise signal was observed in some of the experimental results that corrupted the quality of the inspection. In chapter 5 the origin of this noise signal is explained. The subsequent redesign of the array configuration is then discussed and three 3rd generation designs are introduced. Results obtained using each of these designs to inspect four of the defects within the flat plate, non-welded test-pieces are then presented and the performance of each design is evaluated. The 3rd generation device design also incorporates an integrated irrigation system and testing to demonstrate the performance of the device is unaffected by using this approach is provided.

Testing of the flat plate, non-welded test-pieces was very successful, however, the inspection of these test-pieces is significantly simpler than the inspection of the actual target application component. The target application component contains an austenitic weld. Inspection through this weld is challenging due to the high noise levels and anisotropic nature of the grain structure within the weld. Two flat plate, welded test-pieces were designed and manufactured with, as far as possible, a fully representative weld. Inspection of these flat plate test-pieces was then performed with two different designs of the 3rd generation membrane coupled device. Two designs were used to provide optimum coverage and to remove the effects of the internal noise signal from the inspection image. Chapter 6 reviews the manufacture of these test-pieces and the design of the inspection techniques used to detect the embedded defects. The test-pieces contain seven different types of flaw; and two different sizes of each defect are included. The smaller defects are approximately 4mm through-wall which represents an extremely challenging defect to detect in a thick-walled stainless

steel structure. The larger defects are 8mm through-wall which, although less challenging, is still smaller than the validation size of the current inspection performed on this component. Results from the membrane device inspection testing are then reviewed and the performance of each device is assessed using a variety of inspection techniques. The experimental results demonstrate that complete inspection coverage of the flat plate test-pieces without removal of the weld cap can be achieved by using the conformable array transducer. Every defect is detected using at least one of the inspection techniques used and many of the defects are observed with a number of redundant beams. The inspection speed benefits associated with the use of the membrane coupled device in comparison to conventional single element transducer inspection are then reviewed. It is found that using existing controller technology and a desk-top PC, the scanning time can be improved by over 60%.

The flat plate, welded test-pieces contain a small number of defects that proved very difficult to detect using the 3rd generation linear membrane coupled device. The through weld inspection of small lack of sidewall fusion defects is not possible using the 3rd generation membrane device design due to the effects of the austenitic weld. The proposed inspection of a number of outer surface defects is to use a direct creep wave inspection technique. It was not possible to produce a reliable creep wave inspection using the 3rd generation linear membrane coupled design. A twin crystal membrane coupled phased array transducer has been designed and produced to address these limitations. In chapter 7, the use of twin crystal transducers for through weld and near surface defect detection is reviewed. The use of the CIVA modelling platform to assist in the design of the twin crystal membrane device is then discussed. The final design of the probe is then presented along with some preliminary results from the through weld inspection of the lack of sidewall fusion defects.

8.2. Outline of Main Contributions

The main areas of novel work associated with my doctorate relate to the adaptation and further development of academic research tools, and the application of these new technologies within Rolls-Royce. Much of this development has been a collaborative exercise with researchers at Imperial College. However, this project and my research specifically represent a major departure from existing practice within Rolls-Royce; transfer of this new capability into Rolls-Royce has been facilitated by my role as a

Research Engineer. The main contributions of this thesis are summarised in the following section. The areas of this research work that are unique have been presented at a range of national and international conferences and published in proceedings, these publications are summarised below:

- Lead Author:
    - Russell, J., Cawley, P., Drozdz, M., Lowe, M., Habgood, N. (2007) Finite Element Modelling of Elastic Wave Propagation and Defect Interaction in Large, Complex Components. In: Thompson, D.O. & Chimenti, D.E. (eds.) *Review of Progress in QNDE.* American Institute of Physics: Melville, New York, 27, pp. 99-106
    - Russell, J., Long, R., Cawley, P., Habgood, N. (2008) Inspection of Components with Irregular Surfaces Using a Conformable Ultrasonic Phased Array. In: Thompson, D.O. & Chimenti, D.E. (eds.) *Review of Progress in QNDE*, American Institute of Physics: Melville, New York, 28, pp. 792-799
    - Russell, J., Long, R., Cawley, P. (2009) Development of a membrane coupled conformable phased array. In: Bièth, M. & Whittle, J. (eds.) 7th International Conference on NDE in Relation to Structural Integrity for Nuclear and Pressurised Components. European Commission Joint Research Centre, Netherlands, 6, In Press.
    - Russell, J., Long, R., Cawley, P. (2009) Development of a membrane coupled conformable phased array inspection capability. In: Thompson, D.O. & Chimenti, D.E. (eds.) *Review of Progress in QNDE*, American Institute of Physics: Melville, New York, 29, In Press
- Co-Author:
    - Long, R., Russell, J., Cawley, P., Habgood, N. (2007) Non-Destructive Inspection of Components with Irregular Surfaces using a Conformable Ultrasonic Phased Array. In: Bièth, M. & Whittle, J. (eds.) 6th International Conference on NDE in Relation to Structural Integrity for Nuclear and Pressurised Components. European Commission Joint Research Centre, Netherlands, 6, pp 564-572.

- Long, R., Russell, J., Cawley, P., Habgood, N. (2008) Ultrasonic Phased Array Inspection of Flaws on Weld Fusion Faces using Full Matrix Capture. In: Thompson, D.O. & Chimenti, D.E. (eds.) *Review of Progress in QNDE*, American Institute of Physics: Melville, New York, 28, pp. 848-855.
- Long, R., Russell, J., Cawley, P. (2009) Ultrasonic phased array inspection of welded pipes using waves mode-converted at the inner surface of the pipe. In: Bièth, M. & Whittle, J. (eds.) 7th International Conference on NDE in Relation to Structural Integrity for Nuclear and Pressurised Components. European Commission Joint Research Centre, Netherlands, 6, In Press
- Long, R., Russell, J., Cawley, P (2009) Ultrasonic phased array through weld inspection using full matrix capture. In: Thompson, D.O. & Chimenti, D.E. (eds.) *Review of Progress in QNDE*, American Institute of Physics: Melville, New York , 29, In press.

8.2.1. Membrane Coupled Phased Array Device

A major part of my research work has been the further development of the membrane coupled phased array device. This novel technology provides a range of inspection benefits on components with irregular surface geometry and has not been successfully implemented before. I was involved in the design of the 2nd generation device. I also designed the flat plate, non-welded test-pieces that were used to evaluate the performance of this device. I then performed most of the experimental testing required to assess the performance of the 2nd generation device in the inspection of the two flat plate, non-welded test-pieces. I performed a substantial amount of data processing using the Imperial College FMC processing software. This work illustrated the potential benefits associated with the membrane device technology but also highlighted some of the limitations of the second generation design. I carried out the necessary modelling and experimental testing to understand the origin of the internal noise signals within the 2nd generation device and to remove this from the inspection image in subsequent designs. This investigation led to the design of the 3rd generation membrane devices.

I designed and purchased the 3rd generation membrane device probes. An initial assessment of the performance of the three different 3rd generation designs was then performed on the flat plate non-welded test-pieces. This testing demonstrated the improved performance that could be achieved using the 3rd generation devices. I designed and purchased two flat plate, welded test-pieces that contained a broad range of planar defects representative of those that could occur with the actual target application. A range of different inspection techniques based on the membrane coupled device technology were identified which provided complete and thorough inspection coverage of these welded test-pieces without the removal of the weld cap. I then performed some experimental testing of these test-pieces myself and trained others to use this inspection technology and lead the project to acquire the full range of experimental data.

The 3rd generation membrane coupled phased array device provides dramatic inspection improvements over conventional rigid wedge technology. When using a rigid wedge probe the transducer cannot be scanned over the irregular geometry of the weld cap, even with the weld cap removed the final surface profile is still irregular which limits inspection coverage and compromises performance. The membrane coupled phased array device provides complete inspection coverage with the weld cap in place. The membrane coupled device is used with FMC data acquisition which allows the surface profile of the component under test to be accurately measured. Delay laws are then applied in post-processing to compensate for the irregular surface profile and maintain inspection performance on components with an irregular surface. The use of this novel approach to inspection is essential to realise all of the benefits associated with the membrane coupled device technology.

The use of FMC also allows advanced algorithms to be used which cannot be implemented by using conventional data acquisition and processing. This provides an improved defect detection capability and future-proofs the inspection. The 3rd generation membrane coupled device utilises a large footprint phased array, this allows a large aperture to be used which provides excellent control over the beam angle and focal length. Processing of the inspection data was performed using two different approaches. Initial processing was performed using simple unfocused delay

laws, using this approach some of the defects could not be detected. Data processing was also performed using optimised delay laws with larger apertures and a range of different focal regimes. When using the optimised delay laws every defect within the welded test-pieces was successfully detected. This demonstrates that the membrane coupled device is highly effective and major improvements in defect detection that can be achieved by using this device. The use of a large footprint array also reduces the amount of mechanical scanning required so that inspection scanning time can be significantly reduced. The overall time required to complete the inspection scanning using the membrane coupled device is shown to be reduced by over 70% in comparison to conventional rigid wedge single element transducers.

Although every defect with the two flat plate, welded test-pieces could be detected using the 3rd generation membrane coupled device, some further inspection performance improvements are possible. The results of my testing using the membrane coupled device technology highlighted the specific inspections of concern. I then researched the alternative inspection techniques that could be used to address these limitations which led to the design of the twin crystal membrane coupled device. The twin crystal membrane coupled device is my design and I worked with the Rolls-Royce mechanical designers to generate suitable engineering drawings that have now been used to manufacture the probe. Preliminary data acquisition and processing has been performed using the twin crystal device to inspect the flat plate welded test-pieces. The results obtained illustrate that the internal noise signal that effects linear phased array devices has been removed leading to the improved through weld inspection of lack of side wall fusion defects. Further work is required to fully characterise the capabilities of the twin crystal array design and the collection of scanned FMC data is essential to realise the full potential of this technology.

8.2.2. Inspection Modelling

Prior to the start of my EngD Rolls-Royce inspection engineers used a very limited range of basic modelling tools. I introduced FE based inspection modelling techniques and demonstrated the use of these techniques on industrial applications. I also performed the initial study of using triangular elements and an automatically

generated mesh with ALID absorbing regions to rapidly and accurately model complex geometries. I have also introduced many aspects of the CIVA modelling platform to Rolls-Royce. I have worked with the NDE implementation engineers to introduce the use of CIVA into their inspection planning, qualification and data interpretation process.

8.2.3. FMC Based Phased Array Inspection

Phased array inspection techniques based on the acquisition of FMC data are very promising. However, they have not yet found application in industry. Through my research I have demonstrated the benefits associated with this type of inspection and established a framework within Rolls-Royce to implement this on industrial applications.

8.3. Future Work

8.3.1. Twin Crystal Membrane Device

The twin crystal membrane coupled device has been designed and manufactured, and some preliminary testing with this device has been performed. The results from this preliminary testing are very encouraging but further development is required. The internal noise signal that corrupts the B-Scan inspection image obtained using linear phased array transducers has been removed leading to improved defect detection. The performance of the twin crystal transducer has also been shown to be marginally better than the 3rd generation membrane coupled device for through weld inspection of lack of side wall fusion defects. In order to fully exploit all of the potential inspection improvements that can be achieved by using the twin crystal device the acquisition of scanned FMC data is essential. A bespoke software suite is currently under development within Rolls-Royce to address this requirement. When this is available complete validation of the FMC post processing algorithms using the twin crystal membrane coupled device will then be possible. An investigation of the through weld inspection of lack of sidewall fusion defects and of the creep wave detection of near surface defects will then be carried out.

8.3.2. Narrow Phased Array Membrane Device

In this work I have demonstrated that the current membrane coupled phased array device can be used to improve the detection of defects. The use of FMC data also allows a single data set to be processed in a variety of ways so that different inspection techniques can be used to accurately characterise a given defect. However the current approach does not provide any improvements in terms of the lateral sizing of defects. I have already performed preliminary modelling work on a new narrow phased array leading to a finalised design which has now been purchased. This array uses the same element pitch as the third generation array but the elements are much narrower. These elements produce a wide beam profile in the lateral dimension. By using this device and the synthetic aperture focusing technique (SAFT) it may be possible to improve lateral defect sizing. Further development of the FMC post-processing software will be required to facilitate this additional processing step.

8.3.3. FMC Inspection

Phased array inspection using FMC data acquisition is very versatile and it has great potential to radically improve automated array inspection techniques. However, it is still relatively immature and considerable further effort is required before this technique can be deployed within the nuclear industry. Many of these further developments have been touched on previously in this work but will also be briefly reviewed here. A recognised technique for the calibration of FMC data must be established. In order to achieve this, techniques for gathering and storing FMC data from an encoded scanning frame or manipulator are required. The quantity of data collected during a FMC inspection of a large, complex component such as those found in the nuclear industry is considerable. Techniques such as half matrix capture (HMC), which uses the theory of reciprocity to reduce the amount of inspection data to be collected and up-sampling of data must be investigated to minimise the data transfer requirements. Rolls-Royce is addressing each of these requirements with a view to commercialising phased array inspection using FMC in the near future.

8.3.4. Inspection Qualification and Implementation

The ultimate goal of this research work is to develop the advanced inspection tools to a sufficiently high level that they can be deployed in industrial applications. This is a complex process, particularly in the nuclear industry, however, a project plan has now been developed to progress the modelling work, the membrane coupled device and FMC inspection techniques to a sufficiently mature stage that they can go through inspection qualification and ultimately be used on industrial plant. The use of the membrane coupled device and FMC data acquisition represents a massive improvement in ultrasonic inspection capability. Rolls-Royce intends to utilise the potential benefits of this inspection capability to reduce the amount of radiographic inspection that must be performed during the manufacture of the target application component. The use of radiography leads to the requirement for large exclusion zones, this increases the time associated with the manufacturing process and increases cost. The membrane coupled device will allow ultrasonic inspection to be carried out without the need for subsequent machining of the component. The application of advanced delay laws to the FMC data acquired during the inspection will assist in replicating the current inspection sensitivity to small defects that cannot typically be detected using conventional ultrasonic inspection.

9. References

Achenbach, J.D., Gautesen, A., K. (1977) Geometrical theory of diffraction for three-D elastodynamics, J. Acoust. Soc. Am. Volume 61, Issue 2, pp. 413-421.

AGR Field Operations, Technology Design, Winsford, Cheshire, UK. www.technologydesign.co.uk.

Akhnak, M., Martinez, O., Ullate, L.G., Montero de Espinosa, F. (2002) 64 elements two-dimensional piezoelectric array for 3D imaging, *Ultrasonics*, 40, 139-143.

Alleyne, D.N. (1991) *The non-destructive testing of plates using ultrasonic lamb waves*. PhD thesis. University of London, Imperial College of Science Technology and Medicine.

Auld, B.A., (1973a) *Acoustic Fields and Waves in Solids - Volume 1* Chapters 4 and 8, Robert E. Krieger Publishing Company, Malabar FL.

Auld, B.A., (1973b) *Acoustic Fields and Waves in Solids - Volume 2* Appendix 4, Robert E. Krieger Publishing Company, Malabar FL.

Azar, L., Shi, Y., Wooh, S-C. (2000) Beam focussing behaviour of linear phased arrays, *NDT & E International*, 33, pp.189-198.

Baby, S., Balasubramanian, T., Pardikar, R.J. (2003) Ultrasonic study for detection of inner diameter cracking in pipeline girth welds using creeping waves. *International journal of Pressure Vessels and Piping*. 80, 139-146.

BAE Systems (1986) Orbital TIG Welding of Type 304L Stainless Steel Pipe with consumable Root Insert and wire Fill, PN 1217, DGS/GS/3003.

Bann, T. (2005) Presentation to the Stainless Steel Fabrication in the Nuclear Industry, Testing and Inspection of Stainless Steel Components.

Berkhout, J. (1986) The seismic method in the search for oil and gas: Current techniques and future developments, Proc. IEEE, 74, pp. 1133-1159. Birks, A.S., Green Jr, R.E. (eds.) (1991) Ultrasonic Testing. *ASNT Nondestructive Testing Handbook*, 7 Columbus, USA: American Society of Nondestructive Testing.

Bray, D.E., Tang, W. (2001) Subsurface stress evaluation in steel plates and bars using the L_{CR} ultrasonic wave. *Nuclear Engineering and Design*, 207, 231-240.

British Energy Group Plc, East Kilbride, UK, www.british-energy.com.

British Energy. (2002) GUIDE NT v1.13, Data Interpretation Guide Course Notes.

British Standards Institution (1998a) BS EN 1713:1998 *Non-destructive testing of welds - Ultrasonic testing - Characterization of indications in weld.* London: BSI.

British Standards Institution (1998b) BS EN 1714:1998, *Non-destructive testing of welds - Ultrasonic testing of welded joints*, London: BSI.

British Standards Institution (2001) BS EN 583-2:2001 *Non-destructive testing — Ultrasonic examination — Part 2: Sensitivity and range setting standard*. London: BSI.

British Standards Institution (2004a) BS EN 583-4:2002 *Non-destructive testing — Ultrasonic examination — Part 4: Examination for Discontinuities perpendicular to the surface standard*. London: BSI.

British Standards Institution (2004b) BS EN 14127:2004, *Non-destructive testing. Ultrasonic thickness measurement*, London: BSI.

British Standards Institution (2008) BS EN 583-5:2001 *Non-destructive testing – Ultrasonic examination - Part 5: Characterization and sizing of discontinuities*, London: BSI.

Calmon, P., Lhémery, A., Lecoeur-Tabi, I., Raillon, R., Paradis, L. (1998) Models for the computation of ultrasonic fields and their interaction with defects in realistic NDT configurations, *Nuclear Engineering and Design*, 180, pp. 271-283.

Calmon P., Leberre S., Sollier S., Benoist P. (2004) CIVA, an integration software platform for the simulation and processing of NDT data, Proceedings 16th World Conference on NDT.

Casula, O., Poidevin, C., Cattiaux, G., Dumas, Ph., (2006) Control of Complex components with smart flexible phased arrays, *Ultrasonics*, 44, pp. 647-651.

CEA List, Saclay, France, www-list.cea.fr.

CEDRAT Group, Meylan, France, http://www.cedrat.com.

Chapman R.K. (1984) *Ultrasonic scattering from smooth flat cracks: an elastodynamic Kirchhoff diffraction theory (main report)*, CEGB Report NWR/SSD/84/0059/R.

Chapman, R.,K. (1990) A system model for the ultrasonic inspection of smooth planar cracks. *Journal of Nondestructive testing*, Vol . 9, No. 2/3, 197-210.

Chatillon, S., Cattiaux, G., Serre, M., Roy, O. (2000) Ultrasonic non-destructive testing of pieces of complex geometry with a flexible phased array transducer. *Ultrasonics*, 38, 131-134.

Cheeke, J.D.N, (2002) *Fundamentals and Applications of Ultrasonic Waves*, CRC Press LLC.

Cinquin, M., Le Ber, L., Lonné, S., Mahaut, S. (2006) Results of 2006 UT modelling benchmark obtained with CIVA at CEA: beam modelling and flaw signal prediction. Thompson, D.O. & Chimenti, D.E. (eds.) *Review of Progress in QNDE*, American Institute of Physics, Melville, NY, 26, pp.1870-1877.

Connolly, G.D. (2009) *Modelling of elastic wave propagation in generally anisotropic media and austenitic steel welds.* PhD Thesis. University of London, Imperial College of Science Technology and Medicine.

Cui, Y., Lundin, C.D., (2007) Austenite-preferential corrosion attack in 316 austenitic stainless steel weld metals, Materials & Design **28(1),** 324-328.

Darmon, M., Calmon, P., Bele, B. (2003) Modelling of the ultrasonic response of inclusions in steel. In: Thompson, D.O. & Chimenti, D.E. (eds.) *Review of Progress in QNDE,* American Institute of Physics: Melville, New York, 23, pp 101-108.

Delaide, M., Dumas, Ph. (2005) Application of Piezocomposite Twin, Side by Side, Phased Array UT Probes for the Inspection of Stainless Steel, In: Thompson, D.O. & Chimenti, D.E. (eds.) *Review of Progress in QNDE,* American Institute of Physics: Melville, New York, 25, pp. 930-937.

Deschamps G.A. (1972) Ray techniques in electromagnetics, Proceedings of the I.E.E.E. Vol 60, pg 1022.

Dombret, Ph. (1991) Methodology for the ultrasonic testing of austenitic stainless steel, *Nuclear Engineering and Design*, 131, (3), 279-284.

Drinkwater, B.W., Wilcox, P.D. (2006) Ultrasonic Arrays for Non-Destructive Evaluation: A Review, *NDT&E International*, 39, 525-541.

Drozdz, M., Moreau, L., Castaings, M., Lowe, M.J.S., Cawley, P. (2005) Efficient numerical modelling of absorbing regions for boundaries of guided wave problems. In: Thompson, D.O. & Chimenti, D.E. (eds.) *Review of Progress in QNDE*. American Institute of Physics: Melville, New York, 25, pp.126-133.

Drozdz, M. (2006) *Efficient numerical modelling of ultrasound reflection from cracks and corrosion.* Transfer report. University of London, Imperial College of Science Technology and Medicine.

Drozdz, M., Skelton, E., Craster, R.V., Lowe, M.J.S. (2007) Modelling bulk and guided waves in unbounded elastic media using absorbing layers in commercial FE packages. In: Thompson, D.O.& Chimenti, D.E. (eds.) *Review of Progress in QNDE*. American Institute of Physics: Melville, New York, 26, pp. 87-94.

Drury, J.C. (1983) *Ultrasonic Flaw Detection for Technicians*, Salesbury Press Ltd, UK.

Drury, J.C. (2005) Ultrasonics, part 3: refraction and mode conversion, Insight, 47(1), 44-46.

Dupond, O., Chassignole, B., Doudet, L. (2006) Welding Process Effect on Ultrasonic Testing Austenitic Stainless Steel Welds, In: Bièth, M. & Whittle, J. (eds.) 5th International conference on NDE in relation to structural integrity of Nuclear and Pressurised components, European Commission Joint Research Centre, Netherlands, 5, pp 1041-1050.

Duxbury, D., (2009) A calibration routine for Full Matrix Capture (FMC), RRMP34160.

Edelmann, X. (1981) Application of ultrasonic testing techniques on austenitic welds for fabrications and in-service inspection, *NDT International*, 14, (3), 125-133.

EPRI (2004) Evaluation of Flexible Arrays for Ultrasonic Examination of Piping Welds with Uneven Surfaces: Interim Report, 1009643.

Ermolov, I.N. (2004) Progress in the theory of ultrasonic flaw detection problems and prospects. *Russian Journal of Nondestructive Testing*, 40, (10), 655-678.

Ford, J., Hudgell, R.J. (1987) A final report on the performance achieved by non-destructive testing of defective butt welds in 55mm thick type 316 stainless steel, NDT Development & Applications Department, Risley Nuclear Power Development Laboratories.

Gengembre N., Lhémery A. (2000) Pencil method in elastodynamics: application to ultrasonic field computation, *Ultrasonics*, 38, pp. 495-499.

Gubernatis J.E., Domany, E., (1977) The Born approximation in the theory of the scattering of elastic waves by flaws, *J. Appl. Phys.* Vol 48, Issue 7, pp. 2812-2819.

Halkjær, S., Sørensen, M.P., and Kristensen, W.D. (2000) The propagation of ultrasound in an austenitic weld, *Ultrasonics*, Vol 38, pp. 256-261.

Harker, A.H., Ogilvy, J.A., Temple, J.A.G. (1990) Modeling Ultrasonic Inspection of Austenitic Welds, Journal of NDE **9(2/3):** 155-165.

Harvey, G., Gachagan, A., Mackersie, J.W., McCunnie, T., Banks, R. (2009) Flexible Ultrasonic Transducers Incorporating Piezoelectric Fibres, *IEEE Trans. Ultrason. Ferroelec. Freq. Contr.*, 56, pp. 1999-2009.

Henneke II, E., Chimenti, D., Papadakis, E. (eds.) (1991) Fundamental Principles of Ultrasonic Wave Propagation Nondestructive Testing Handbook, 7 Columbus, USA: American Society of Nondestructive Testing.

Holmes, C., Drinkwater, B., Wilcox, P. (2005) Post-processing of the full matrix of ultrasonic transmit–receive array data for non-destructive evaluation. *NDT & E International*, 38, 701-711.

Hudgell, R.J., Worral, G.M., Ford, J., Gray, B.S. (1989) Ultrasonic characterisation and inspection of austenitic welds, *Int. J. Pressure Vessels & Piping*, Vol 39, pp 247-263.

Hunter, A.J., Drinkwater, B.W., Wilcox, P.D. (2009) Ultrasonic Imaging using a Flexible Array: Improvements to the Maximum Contrast Autofocus Algorithm. In: Thompson, D.O.& Chimenti, D.E. (eds.) *Review of Progress in QNDE*, American Institute of Physics: Melville, New York, 29, In press.

Imasonic, Besançon, France. www.imasonic.com.

JRC Petten (1999) EUR 19071 EN, ENIQ Recommended Practice 6: The use of modelling in inspection qualification. ENIQ Report No. 15.

JRC Petten (2007) EUR 22906 EN, European Methodology for Qualification of Non-Destructive Testing, ENIQ Report No. 31.

Kapranos, P.A. and Whittaker, V.N., "Ultrasonic inspection of fatigue cracks in austenitic 316 and 347 weldments," Brit. J. NDT 24(3): 129-134 (1982).

Keller, J.B. (1957) Diffraction by an Aperture, J. Appl. Phys., 28, 426.

Kirchoff, G.R. (1891) Vorlesung uber Mathematische Physik vol II (Leipzig: Tueber).

Kishore, N.N., Sridhar I., Iyengar N.G.R. (2000) Finite element modelling of the scattering of ultrasonic waves by isolated flaws. *NDT&E International*, 33, 297-305.

Krautkramer, J., Krautkramer, H. (1983) *Ultrasonic Testing of Materials*, 3rd Edition. London, Springer-Verlag.

Langenberg, K.J., Fellinger, P., Marklein, R. (1990) On the Nature of the So-called Subsurface Longitudinal wave and/or the surface Longitudinal "Creeping" Wave. *Research in Nondestructive Evaluation*, 2, 59-81.

Lemaitre, P., Koble, T. D., Doctor, S., (1996), Summary of the PISC round robin results on wrought and cast austenitic steel weldments, part II: wrought-to-cast capability study, *Int. J. Pres. Ves. & Piping*, 69, pp. 21-32.

Liu, G.R. & Quek Jerry, S.S. (2003) A non-reflecting boundary for analysing wave propagation using the finite element method. *Finite Elements in Analysis and Design*, 39, 403-417.

Long, R., Cawley, P. (2006) Phased Array Inspection of Irregular Surfaces In: Thompson, D.O. & Chimenti, D.E. (eds.) *Review of Progress in QNDE*. American Institute of Physics: Melville, New York, 26, pp. 814-821.

Long, R., Cawley, P., (2007a) Further Development of a Conformable Phased Array Device for the Inspection of Irregular Surfaces. In: Thompson, D.O. & Chimenti, D.E. (eds.) *Review of Progress in QNDE*. American Institute of Physics: Melville, New York, 27, pp. 754-761.

Long, R., Russell, J., Cawley, P., Habgood, N. (2007b) Non-Destructive Inspection of Components with Irregular Surfaces using a Conformable Ultrasonic Phased Array. In: Bièth, M. & Whittle, J. (eds.) 6th International Conference on NDE in Relation to Structural Integrity for Nuclear and Pressurised Components. European Commission Joint Research Centre, Netherlands, 6, pp 564-572.

Long, R., Drozdz, M., Lowe, M., Cawley, P., Wilcox, P., Drinkwater, B., Thomas, R., Gaghagan, A., Mackersie, J., (2007c) Improved Inspection of Reactor Components Using Ultrasonic Arrays, ICRR AR 04-2007.

Long, R., Russell, J., Cawley, P., Habgood, N. (2008) Ultrasonic Phased Array Inspection of Flaws on Weld Fusion Faces using Full Matrix Capture. In: Thompson, D.O. & Chimenti, D.E. (eds.) *Review of Progress in QNDE,* American Institute of Physics: Melville, New York, 28, pp. 848-855.

Long, R., Russell, J., Cawley, P (2009) Ultrasonic phased array through weld inspection using full matrix capture. In: Thompson, D.O. & Chimenti, D.E. (eds.) *Review of Progress in QNDE,* American Institute of Physics: Melville, New York, 29, In press.

Lonné S. de Roumilly, L., Le Ber, L., Mahaut, S., Cattiaux, G. (2006) Experimental validation of CIVA ultrasonic simulations. In: Bièth, M. & Whittle, J. (eds.) 5th International conference on NDE in relation to structural integrity of Nuclear and Pressurised components, European Commission Joint Research Centre, Netherlands, 5, pp 356-363.

Lowe, M.J.S., *Plate Waves for the NDT of Diffusion Bonded Titanium* Chapter 2 (PhD thesis, Mechanical Engineering Department, Imperial College of Science, Technology and Medicine, London UK, 1992).

Lowe, M.J.S., Hansen, U. (2008) Finite Element Analysis Short course for EngD Research Engineers.

Mitsui Babcock, (2005) Replacement of Radiography by Ultrasonic Inspection**,** *Health and Safety Executive Research Report*, 301.

Maes, G., Richard, D. (2008) On the Use of Advanced UT Phased Array Methodology and Equipment, Proceedings 17th World Conference on NDT.

Mahaut, S., Godefroit, J-L., Roy, O., Cattiaux, G. (2004) Application of phased array techniques to coarse grain components inspection, *Ultrasonics*, 42, 791-796.

Martinez, O., Akhnak, M., Ullate, L.G., de Espinosa, F.M. (2003) A small 2D ultrasonic array for NDT applications, *NDT&E International*, 36, pp. 57-63.

Mondal, S., Wilcox, P.D., Drinkwater, B.W. (2005) Design of two-dimensional ultrasonic phased array transducers, *ASME-J Pressure Vessel Technology*, 127, pp. 336-344.

Norton, S.J. (1992) Annular array imaging with full-aperture resolution, *J Acoust Soc Am*, 92, pp. 3202-3206.

Ogilvy, J.A., (1991) Theory of wave scattering from random rough surfaces, IoP Publishing, UK.

Pavlakovic, B.N. (1998) *Leaky Guided Ultrasonic waves for NDT*. PhD thesis. University of London, Imperial College of Science Technology and Medicine.

Peak NDT, Derby, UK, www.peakndt.com.

Precision Acoustics Ltd. (n.d.) *AptFlex F28*. [Online] Available from: http://www.acoustics.co.uk/products/aptflex-f28 [Accessed on 20/11/09].

Rajagopal, P., Drozdz, M., Lowe, M.J.S. (2008), Towards Improved Finite Element Modeling of the Interaction of Elastic Waves with Complex Defect Geometries, In: *Review of Progress in Quantitative NDE*, D.O.Thompson and D.E. Chimenti (eds.), American Institute of Physics: Melville, New York, 28, pp. 49-56.

RD Tech (2004) Introduction to Phased Array Ultrasonic Technology Applications. Canada, Olympus NDT.

Rolls-Royce (2001a) Confidential Document.

Rolls-Royce (2001b) Confidential Document.

Rolls-Royce (2002a) Confidential Document.

Rolls-Royce (2002b) Confidential Document.

Rolls Royce (2006a) *Conformable Phased Array Evaluation Block 1*. Rolls Royce Drawing number: 55053/DT/064685.

Rolls Royce (2006b) *Conformable Phased Array Evaluation Block 2* Rolls Royce. Drawing number: 55053/DT/064689.

Rolls-Royce (2006c) Confidential Document.

Rolls Royce (2008a) *Conformable Phased Array Welded Evaluation Block 1*. Rolls Royce Drawing number: SUB3000032.

Rolls Royce (2008b) *Conformable Phased Array Welded Evaluation Block 2*. Rolls Royce Drawing number: SUB3000033.

Rolls-Royce (2009) Confidential Document.

Roy, O., Mahaut, S. & Casula, O. (2002) Control of the ultrasonic beam transmitted through an irregular profile using a smart flexible transducer: modelling and application. *Ultrasonics,* 40, 243-246.

Russell, J.D. (2006a) Engineering doctorate in non-destructive evaluation 6 month report.

Russell, J.D. (2006b) Engineering doctorate in non-destructive evaluation 12 month report.

Russell, J.D (2007a) Engineering doctorate in non-destructive evaluation 18 month report.

Russell, J.D. (2007b) Engineering doctorate in non-destructive evaluation 24 month report.

Russell, J.D. (2007c) Conformable Phased Array Target Application Non-Welded Test-piece Design Basis Document.

Russell, J., Cawley, P., Drozdz, M., Lowe, M., Habgood, N. (2007) Finite Element Modelling of Elastic Wave Propagation and Defect Interaction in Large, Complex Components. In: Thompson, D.O. & Chimenti, D.E. (eds.) *Review of Progress in QNDE.* American Institute of Physics: Melville, New York, 27, pp. 99-106.

Russell, J.D. (2008a) Engineering doctorate in non-destructive evaluation 30 month report.

Russell, J.D. (2008b) Engineering doctorate in non-destructive evaluation 36 month report.

Russell, J., Long, R., Cawley, P., Habgood, N. (2008) Inspection of Components with Irregular Surfaces Using a Conformable Ultrasonic Phased Array. In: Thompson,

D.O. & Chimenti, D.E. (eds.) *Review of Progress in QNDE*, American Institute of Physics: Melville, New York, 28, pp. 792-799.

Russell, J., Habgood, N. (2008) Advanced Array NPCT Project Plan.

Schmerr Jr, L.W. (1998) *Fundamentals of Ultrasonic Non-Destructiev Evaluation – A Modelling Approach*, Plenum Press, New York

Schmid. (1997) *Ultrasonic testing of austenitic and dissimilar metal welds.* [Online] Available from: http://www.ndt.net/article/pow1297/schmid/schmid1.htm [Accessed 20/11/09].

Schmitz, V., Langenberg, K.J., Kappes, W., Kroning, M., (1995) Inspection procedure assessment using modelling capabilities, *Nuclear Engineering and Design*, 157, pp. 245-255.

Serco Technical and Assurance Services, Risley, UK, http://www.serco.com/.

Shipp, R., Schneider, C., Bird, C., Nageswaran, C. (2008) *Handbook for Qualification of Ultrasonic Phased Array Inspection*. TWI Report 17575/1/08.

Shung, K.K., (2002) Technical Note: The Principle of Multidimensional Arrays, *Eur J Echocardiography*, 3, pp. 149-153.

Silk, M., (1980) Ultrasonic Techniques for Inspecting Austenitic Welds, Research Techniques in NDT, Academic Press, London **4(11):** pp. 393-449.

Simulia. (2006) *ABAQUS v6.6 Analyis User's Manual.* [Online] Available from: http://www.simulia.com/support/documentation.html [Accessed 20/11/09].

Sonaspection International, Lancaster, UK, http://www.sonaspection.com/index.html.

Swanson Analysis. (1992) ANSYS user's manual for revision 5.0. Houston, TX: Swanson Analysis Systems.

Toft, M.W., (1987) Experimental Studies of ultrasonic reflection from various type of misorientated defect, CEGB report number: OED/STN/87/20060/R, PWR/MWG/NDT/P(86)39.

Velichko, A., Wilcox, P.D. (2009) Modeling Elastodynamic Scattering Using Finite Elements In: Thompson, D.O. & Chimenti, D.E. (eds.) *Review of Progress in QNDE*, American Institute of Physics: Melville, New York, 29, *In Press.*

Wilcox, P.D., Holmes, C., Drinkwater, B.W., (2007) Advanced Reflector Characterisation with Ultrasonic Phased Arrays in NDE Applications, *IEEE Trans. Ultrason. Ferroelec. Freq. Contr.*, 54, pp. 1541-1550.

Wooh, S-C., Shi, Y. (1999) Optimum Beam Steering of Linear Phased Arrays. *Wave Motion*, 29, 245-265.

Ying C.F., Truell R. (1956). Scattering of a plane longitudinal wave by a spherical obstacle in an isotropically elastic solid, *J. Appl Phys.* 27, pp. 1086-1097.

Zetec Inc, Snoqualmie, WA, USA: www.zetec.com.